A reference-free mill monitoring method based on the inter-insert periodic correlation in angular domain

Xiaowen Zhu

N°d'ordre NNT : 2022ISAL0078

THESE de DOCTORAT DE L'INSA LYON, membre de l'Université de Lyon

Ecole Doctorale N° ED 162
Mécanique, Energétique, Génie Civil, Acoustique

Spécialité/ discipline de doctorat :
Génie Mécanique

Soutenue publiquement le 19/09/2022, par :
Xiaowen ZHU

A reference-free mill monitoring method based on the inter-insert periodic correlation in angular domain

---

Devant le jury composé de :

FROMENTIN Guillaume	Professeur des Universités	ENSAM-Cluny	Président
RITOU Mathieu	Maître de Conférences HDR	IUT Nantes	Rapporteur
SERRA Roger	Maître de Conférences HDR	INSA Centre Val de Loire	Rapporteur
CHANAL Hélène	Maître de Conférences HDR	SIGMA Clermont	Examinatrice
GUILLET François	Professeur des Universités	Université Jean Monnet	Examinateur
KAFTANDJIAN-DOUDET Valérie	Professeur des Universités	INSA-Lyon	Examinatrice
ANTONI Jérôme	Professeur des Universités	INSA-Lyon	Directeur de thèse
GIRARDIN François	Maître de Conférences	INSA-Lyon	Co-directeur de thèse

Département FEDORA – INSA Lyon - Ecoles Doctorales

SIGLE	ECOLE DOCTORALE	NOM ET COORDONNEES DU RESPONSABLE
CHIMIE	**CHIMIE DE LYON** **https://www.edchimie-lyon.fr** Sec. : Renée EL MELHEM Bât. Blaise PASCAL, 3e étage secretariat@edchimie-lyon.fr	**M. Stéphane DANIELE** C2P2-CPE LYON-UMR 5265 Bâtiment F308, BP 2077 43 Boulevard du 11 novembre 1918 69616 Villeurbanne **directeur@edchimie-lyon.fr**
E.E.A.	**ÉLECTRONIQUE, ÉLECTROTECHNIQUE, AUTOMATIQUE** **https://edeea.universite-lyon.fr** Sec. : Stéphanie CAUVIN Bâtiment Direction INSA Lyon Tél : 04.72.43.71.70 secretariat.edeea@insa-lyon.fr	**M. Philippe DELACHARTRE** INSA LYON Laboratoire CREATIS Bâtiment Blaise Pascal, 7 avenue Jean Capelle 69621 Villeurbanne CEDEX Tél : 04.72.43.88.63 **philippe.delachartre@insa-lyon.fr**
E2M2	**ÉVOLUTION, ÉCOSYSTÈME, MICROBIOLOGIE, MODÉLISATION** **http://e2m2.universite-lyon.fr** Sec. : Bénédicte LANZA Bât. Atrium, UCB Lyon 1 Tél : 04.72.44.83.62 secretariat.e2m2@univ-lyon1.fr	**Mme Sandrine CHARLES** Université Claude Bernard Lyon 1 UFR Biosciences Bâtiment Mendel 43, boulevard du 11 Novembre 1918 69622 Villeurbanne CEDEX **sandrine.charles@univ-lyon1.fr**
EDISS	**INTERDISCIPLINAIRE SCIENCES-SANTÉ** **http://ediss.universite-lyon.fr** Sec. : Bénédicte LANZA Bât. Atrium, UCB Lyon 1 Tél : 04.72.44.83.62 secretariat.ediss@univ-lyon1.fr	**Mme Sylvie RICARD-BLUM** Institut de Chimie et Biochimie Moléculaires et Supramoléculaires (ICBMS) - UMR 5246 CNRS - Université Lyon 1 Bâtiment Raulin - 2ème étage Nord 43 Boulevard du 11 novembre 1918 69622 Villeurbanne Cedex Tél : +33(0)4 72 44 82 32 **sylvie.ricard-blum@univ-lyon1.fr**
INFOMATHS	**INFORMATIQUE ET MATHÉMATIQUES** **http://edinfomaths.universite-lyon.fr** Sec. : Renée EL MELHEM Bât. Blaise PASCAL, 3e étage Tél : 04.72.43.80.46 infomaths@univ-lyon1.fr	**M. Hamamache KHEDDOUCI** Université Claude Bernard Lyon 1 Bât. Nautibus 43, Boulevard du 11 novembre 1918 69 622 Villeurbanne Cedex France Tél : 04.72.44.83.69 **hamamache.kheddouci@univ-lyon1.fr**
Matériaux	**MATÉRIAUX DE LYON** **http://ed34.universite-lyon.fr** Sec. : Yann DE ORDENANA Tél : 04.72.18.62.44 yann.de-ordenana@ec-lyon.fr	**M. Stéphane BENAYOUN** Ecole Centrale de Lyon Laboratoire LTDS 36 avenue Guy de Collongue 69134 Ecully CEDEX Tél : 04.72.18.64.37 **stephane.benayoun@ec-lyon.fr**
MEGA	**MÉCANIQUE, ÉNERGÉTIQUE, GÉNIE CIVIL, ACOUSTIQUE** **http://edmega.universite-lyon.fr** Sec. : Stéphanie CAUVIN Tél : 04.72.43.71.70 Bâtiment Direction INSA Lyon mega@insa-lyon.fr	**M. Jocelyn BONJOUR** INSA Lyon Laboratoire CETHIL Bâtiment Sadi-Carnot 9, rue de la Physique 69621 Villeurbanne CEDEX **jocelyn.bonjour@insa-lyon.fr**
ScSo	**ScSo*** **https://edsciencessociales.universite-lyon.fr** Sec. : Mélina FAVETON INSA : J.Y. TOUSSAINT Tél : 04.78.69.77.79 melina.faveton@univ-lyon2.fr	**M. Christian MONTES** Université Lumière Lyon 2 86 Rue Pasteur 69365 Lyon CEDEX 07 **christian.montes@univ-lyon2.fr**

*ScSo : Histoire, Géographie, Aménagement, Urbanisme, Archéologie, Science politique, Sociologie, Anthropologie

Acknowledgement

This Ph.D. thesis was undertaken in the Laboratoire Vibrations Acoustique (LVA) of the Institut national des sciences appliquées de Lyon (INSA Lyon), under the co-direction of Prof. Jérôme ANTONI and Asst. Prof. François GIRARDIN.

This work was funded by French government fellowships and was carried out within the framework of the LABEX CeLyA (ANR-10-LABX-0060) of Université de Lyon and the program *Investissements d'Avenir* (ANR-11-IDEX-0007) operated by the French National Research Agency (ANR). I am grateful for the opportunity to work in this interesting area of tool condition monitoring.

First of all, I would like to express my appreciation to François GIRARDIN for his valuable experience and advice and for his regular encouragement and supervision. He helped me in many ways, especially with the scientific approach, organization, and experimental aspects of this work. As a foreigner, I also received his care and attention in my daily life, especially during the lockdown of the epidemic. I would also like to extend my deep thanks to Jérôme ANTONI for his willingness to share his research knowledge and for his constructive proposals and comments on my work. They have both been great mentors, always sparing time from their busy schedules for the guidance I have received. The influence of your great scientific culture and human qualities on me is priceless.

I also wish to convey my sincere appreciation to Mr. RITOU Mathieu, Maître de Conférences HDR at IUT Nantes, and Mr. SERRA Roger, Maître de Conférences HDR at INSA Centre Val de Loire, for agreeing to report on my thesis. I would also like to thank Mr. FROMENTIN Guillaume, Professor at ENSAM-Cluny, Mrs. KAFTANDJIAN-DOUDET Valérie, Professor at INSA Lyon, Mr. GUILLET François, Professor at Université Jean Monnet, Mrs. CHANAL Hélène, Maître de Conférences HDR at SIGMA Clermont, for having accepted to participate in the jury. Thank you for taking your valuable time to read, judge, and criticize this work.

The experimental part of my thesis was performed with the help of Alexandre Zelez and Thibaut Chaise, and I would like to warmly thank them for their technical instruction and operational support. I also want to thank Nathalie LORIOT, the secretary of the lab, whose good management helped me to solve administrative problems.

And a special thank to all my "Ph.D." friends, with whom I shared very pleasant moments. My sincere thanks go to Adrien MARSICK, Alice DINSENMEYER, Sanae SERBOUT, Nicolas PONCETTI, Yasmine HAWWARI, Corentin GUILLON, Yaqiang JIN, Xavier PLOUSEAU-GUÉDÉ, Nicolas AUJOGUE, Matthieu DECAUX, Valentin MIQUEAU, Achilleas ACHILLEOS, Florent DUMORTIER, Luc LAROCHE, Zijian NIU, Giorgio PULVIRENTI, etc.

Eventually, I wish to thank my family and my friends for their love and help during these years. Gratitude goes as well to my fiancé, Zhaofeng, who was also working on his Ph.D., for the very challenging days we have had together and for the emotional support we have provided to each other.

19 September 2022, in Lyon, France
Xiaowen ZHU

Abstract

Based on the tendency of Industry 4.0, this thesis targets the tool condition monitoring (TCM), which is the terminal process of flexible production. The aim is to detect the abnormal tool behavior as early as possible to improve the surface quality of workpieces and to prevent subsequent losses from serious tool failures.

In this context, a methodology for monitoring the wear of end mills in real-time production based on the inter-insert correlation is presented. The approach takes advantage of the angular domain characteristics to segment the signal into periodic cycles of the same angular duration, which are then amenable to correlation analysis. Under high rotational speeds, the external working environment experienced by the individual teeth can be considered quasi-equivalent. Through the correlation analysis, the impact of the non-stationary operation on the monitored signal is effectively reduced. From a wide range of correlation algorithms, singular value decomposition (SVD) is selected to proceed with the analysis, and an ordered separability index with latent correlation characteristics is extracted to assess the current condition of the tool. The feasibility of the proposed indicator was valid and evaluated via the simulated signal and a series of experimental data collected by designed milling patterns.

The results demonstrate the promising development of this method in forming an efficient TCM system. The proposed approach is more independent of the cutting conditions (changes in speed or direction) than the traditional teach-in method and does not require a trial run. It partially fills the gap of tool monitoring demand in flexible manufacturing for customized small batch production. At the same time, inter-insert correlation is also seen as part of a broader framework for monitoring and maintaining rotating machinery. It has great potential to be applied to the analysis

of different signals generated by other mechanical components with a rotating nature.

Keywords: Condition monitoring, Milling tool, Wear, Correlation, SVD.

Résumé

Chapitre 1 - Introduction

Dans le contexte de l'industrie 4.0, les machines-outils à commande numérique sont, d'une part, considérées comme un élément vital dans l'établissement de systèmes de production intelligents et flexibles, en raison de leur bonne base industrielle et de leurs caractéristiques automatiques. D'autre part, la surveillance de l'état des outils (TCM) est restée un obstacle au cours de la dernière décennie.

Puisque l'outil se trouve à la fin de la chaîne de production, son état a un impact direct sur la qualité de la surface de la pièce. Il peut entraîner un temps d'arrêt involontaire avec une diminution de l'efficacité ou, pire encore, endommager la broche en raison des contraintes supplémentaires. Par conséquent, la TCM en temps réel est devenue une nécessité.

Les difficultés de la TCM résident principalement dans le fait que :

- l'outil est un article consommable de taille relativement petite et aucun capteur ne peut être attaché directement ;
- l'environnement de travail est compliqué et présente une visibilité/accessibilité limitée en raison de la présence de liquide de refroidissement et de copeaux métalliques ;
- l'opération subit toujours des changements rapides à une vitesse de rotation élevée ;
- les trajectoires de fraisage varient selon les différentes tâches et ne présentent pas de schéma fixe.

Cette recherche se situe dans ce contexte et vise à développer une nouvelle méthode basée sur la corrélation inter-insert utilisant la décomposition en valeur singulière

(SVD) pour surmonter les difficultés mentionnées ci-dessus. Les innovations de l'approche proposée portent sur les aspects suivants :

- Elle est fondée sur l'échantill- onnage ou le rééchantillonnage du signal dans le domaine angulaire, ce qui permet de segmenter le signal en unités de dent de coupe.

- Les multiples inserts d'un même outil sont considérés comme des individus en interaction. Sous des vitesses de rotation élevées, l'environnement de travail externe subi par les dents individuelles peut être considéré comme quasi-équivalent. Grâce à l'analyse de corrélation, l'impact du fonctionnement non stationnaire sur le signal surveillé est réduit de manière efficace.

- Il n'est pas nécessaire d'organiser des essais ou de former un grand nombre de données pour obtenir des signaux de référence.

- Cette méthode peut être considérée comme versatile, et peut être appliquée à une large gamme de sources de signaux provenant de machines tournantes.

À la connaissance des auteurs, aucune recherche similaire n'existe et la méthode proposée est originale ainsi qu'innovante.

La thèse est organisée dans les 5 chapitres suivants. Le contexte théorique nécessaire à l'étude est passé en revue dans Chapitre 2. Chapitre 3 construit le modèle général et discute des questions spécifiques. Chapitre 4 présente le dispositif expérimental et les conditions opérationnelles. Les résultats d'analyse les plus importants sont présentés dans Chapitre 5. Enfin, Chapitre 6 clôt la thèse par une conclusion et quelques perspectives.

Chapitre 2 - L'état de l'art

L'histoire du développement de la TCM est d'abord retracée et les efforts qui ont déjà été faits par la communauté académique sur ce sujet important sont explorés. Ensuite, une revue de la littérature divisée en trois sections spécifiques : les caractéristiques des opérations de fraisage, la construction du système de surveillance de l'état des outils et l'algorithme de corrélation pertinent.

Le type d'usinage contrôlé visé par ce travail est précisé comme étant le fraisage en bout et ses caractéristiques opérationnelles correspondantes, les types d'usure et

la durée de vie de l'outil sont analysés. La revue montre que l'usure en dépouille est le type d'usure le plus dominant sur les fraises en bout. Après l'usure initiale, l'usure augmente à un taux assez constant pendant la majeure partie de sa durée de vie. Finalement, elle atteint une zone d'usure exponentiellement accélérée, qui marque la fin de sa vie opérationnelle. Ensuite, le processus de formation du copeau est discuté plus en détail dans des conditions normales et d'usure. Le modèle de force de fraisage est construit sur la base de la formation de copeaux. En combinant les caractéristiques de durée de vie de l'outil mentionnées ci-dessus avec le modèle de force de coupe en cas d'usure, l'interaction entre les dents de l'outil a été saisie comme base de la corrélation inter-insert.

Sur cette base, les trois éléments qui constituent le système TCM sont configurés : la perception sensorielle, l'extraction de caractéristiques et la prise de décision. Après avoir considéré la rentabilité et les applications des capteurs existants, ainsi que la disponibilité de l'équipement dans le laboratoire, les forces de coupe ont été sélectionnées comme signal cible pour l'analyse ultérieure.

La revue indique que les méthodes actuellement disponibles commencent généralement par extraire les caractéristiques pertinentes, puis analysent l'état de l'outil sur la base de la comparaison entre les données de surveillance en temps réel et une référence prédéterminée. Cette référence standard peut être obtenue par un simple essai ou par des paradigmes cognitifs. Cependant, à part le gaspillage de matériel, les résultats obtenus à partir des essais ne font pas autorité. En particulier dans les opérations non stationnaires (fraisage avec charge variable et trajectoire complexe), la référence peu fiable peut entraîner de fausses alarmes et des arrêts non souhaités. D'autre part, la référence conclue par le paradigme cognitif, bien que relativement stable, a rencontré des difficultés dans la formation des données en raison de ses coûts élevés d'acquisition de données et du développement insuffisant de la technologie de stockage et de transmission.

En outre, la revue a noté l'émergence progressive des méthodes de traitement du signal dans le domaine angulaire. La fraise, en tant que mécanisme rotatif, présente naturellement une régularité d'échantillonnage dans le domaine angulaire. Cet avantage du signal angulaire est exploité pour réduire l'instabilité due aux variations de vitesse et pour effectuer une meilleure segmentation du signal en fonction des dents. Ainsi, le concept de surveillance de l'outil dans le domaine angulaire en utilisant les corrélations inter-insert est présenté. Enfin, la courbe ROC (receiver operating

characteristic) est présentée comme un outil d'aide à la décision.

Après une recherche documentaire approfondie, quelques études pertinentes basées sur les corrélations ont été trouvées, mais elles diffèrent encore des idées présentées dans cette thèse. Une fois l'originalité du concept confirmée, des méthodes spécifiques pour effectuer une analyse de corrélation sur les segments ont été discutées. Comme le nombre de dents d'un outil est généralement supérieur à 2, l'analyse de corrélation est envisagée en conjonction avec une analyse multivariée. Quatre exigences ont été proposées comme critères pour trouver l'algorithme de corrélation des segments à base de dents :

- le modèle doit être capable d'analyser plusieurs variables simultanément et de produire un résultat complet ;
- le modèle doit être capable d'extraire les caractéristiques qui reflètent l'état de l'outil, tout en fournissant l'interprétation appropriée dans un sens physique ;
- le modèle peut réduire la taille de l'information originale tout en capturant les caractéristiques principales ;
- le modèle n'est pas obligé de distinguer les variables indépendantes et dépendantes.

Finalement, après une discussion approfondie sur l'analyse en composantes principales (PCA), la SVD a été identifié comme l'algorithme pour la TCM basée sur la corrélation inter-insert.

Chapitre 3 - Modélisation générale du comportement des mécanismes de rotation

Après avoir lu la littérature et identifié l'algorithme spécifique pour la corrélation inter-insert, ce chapitre se concentre sur l'applicabilité de la méthode proposée. Le type de signal ciblé par la corrélation inter-insert doit présenter les caractéristiques suivantes :

- le signal doit contenir des événements récurrents ;
- ces événements doivent correspondre au même nombre de points d'échantillonnage avec troncabilité ;

- il doit y avoir une interaction entre ces segments.

Sur cette base, un modèle général du comportement des machines rotatives est développé pour l'expansion future de la méthodologie. En ce qui concerne le processus de fraisage en bout étudié dans ce cas, un angle de trajectoire a été introduit pour rectifier le problème de la variation de trajectoire pendant les tâches d'usinage non stationnaires afin de mieux s'adapter à ce modèle général. Le modèle de force de coupe mentionné dans le chapitre précédent est incorporé dans ce processus général comme base théorique pour la validation expérimentale. Parallèlement, la vitesse angulaire instantanée (IAS) est incluse comme signal de simulation plus pratique pour l'analyse préliminaire de faisabilité. Elle est conforme aux trois caractéristiques requises mentionnées ci-dessus et démontre que la corrélation inter-insert peut être largement utilisée pour les signaux générés par les machines tournantes.

D'autre part, la segmentation du signal, qui est une étape préalable importante de la corrélation inter-insert, est présentée en détail. Sur cette base, la stratégie de réalisation de l'analyse de corrélation entre les segments de signaux est spécifiquement discutée. Trois méthodes, dont l'extraction globale, l'extraction par dent et l'extraction par révolution, ont été analysées. Compte tenu de l'efficacité du taux de mise à jour pour la surveillance en ligne et du volume de données calculé en temps réel, il a été déterminé que la matrice cible était générée par la méthode basée sur les révolutions.

Chapitre 4 - Plan d'expérience et prétraitement des données

Après avoir déterminé l'algorithme spécifique, la matrice cible et le signal de simulation, ce chapitre décrit l'acquisition et le prétraitement des données expérimentales. La machine-outil DECKEL MAHO DMC 635 V a été utilisée pour les tests expérimentaux. Un dynamomètre 3 axes Kistler 9257A a été vissé sur son banc d'opération, délivrant des forces de coupe mesurées dans trois directions orthogonales $(\vec{x}, \vec{y}, \vec{z})$. En combinaison avec les informations de déplacement en $\vec{x}, \vec{y}$ fournies par le banc et les informations angulaires θ provenant du codeur rotatif intégré à la broche, un total de six signaux sont collectés simultanément et transmis à l'analyseur de signaux dynamiques Oros R35.

Après avoir déterminé le montage expérimental et les paramètres des conditions de coupe pour l'opération, quatre trajectoires de fraisage différentes ont été conçues.

Le contour carré contient quatre coupes en ligne droite et est utilisé pour établir la condition de travail stationnaire. La trajectoire en forme de losange vise à vérifier la compatibilité des coordonnées angulaires utilisées dans la méthode proposée et les coordonnées cartésiennes du système de la machine-outil. La trajectoire en forme de carré arrondi contient des trajectoires courbes, conçues pour tester des régimes non stationnaires. L'objectif de la courbe désignée est d'observer comment la corrélation inter-insert est affectée par l'enroulement du matériau autour de l'outil, lorsque la fraise passe respectivement par les contours intérieur et extérieur. Sur cette base, en ajoutant des trous à la courbe désignée, celle-ci est utilisée pour tester le comportement de l'indicateur lorsque l'outil rencontre un tel changement soudain.

Le prétraitement préalable à la corrélation inter-insert comprend le rééchantillonnage du signal dans le domaine angulaire, la correction de la direction de fraisage, la troncature, la segmentation, le centrage sur le zéro, etc. Les résultats obtenus à partir du prétraitement des données expérimentales montrent que les étapes de rééchantillonnage dans le domaine angulaire et de correction de la direction clarifient efficacement les composantes du signal correspondant à chaque dent, ce qui améliore l'opérabilité de la segmentation et fournit une base prometteuse pour la corrélation inter-insert.

Chapitre 5 - Caractérisation de l'état de l'outil par SVD

Après les étapes de prétraitement décrites dans le chapitre précédent, les signaux obtenus dans différentes conditions de coupe sont prêts pour la corrélation inter-insert. Ce chapitre détaille les résultats du traitement des algorithmes SVD pour les matrices cible, qui est le contenu central de la corrélation inter-insert pour la TCM.

Le signal simple et idéalisé de simulation IAS a d'abord été pris comme source pour la SVD, et la signification physique des composants correspondants a été explorée dans les scénarios en ligne droite et en courbe. La matrice unitaire gauche $\mathbb{U}$ extrait la forme d'onde partagée normalisée des segments en préservant le déphasage dû à la trajectoire incurvée ; la matrice des valeurs singulières $\mathbb{\Sigma}$ peut être considérée comme le facteur d'échelle déterminant la contribution des séquences de décomposition au signal original ; et la matrice unitaire droite $\mathbb{V}$ contient l'évolution proportionnelle dans les segments. L'indice de séparabilité $\alpha_{k,1}$ présente la capacité de

la valeur singulière de premier ordre à se rapprocher des données originales. Lorsque les segments de la matrice cible présentent une similitude extrêmement élevée, $\alpha_{k,1}$ affichera un état dominant proche de 1, et en cas d'usure de l'insert, $\alpha_{k,1}$ diminuera de manière sensible.

Ensuite, la méthode SVD est appliquée aux données expérimentales pour vérifier que les résultats sont cohérents avec la simulation. Les résultats montrent que la corrélation inter-insert gère avec succès les données réelles complexes. Parallèlement, la comparaison entre les différents groupes expérimentaux révèle que la méthode est bien compatible avec les coordonnées angulaires et cartésiennes et qu'elle est indépendante de la profondeur radiale de coupe. Une analyse de sensibilité a ensuite été réalisée, et la plage de sensibilité Δ_{WS} a été obtenue. Sur cette base, deux indicateurs sont dérivés respectivement de l'indice de séparabilité $\alpha_{k,1}$ et de la plage de sensibilité Δ_{WS}. Ces deux indicateurs sont en fait deux expressions d'un même principe. L'indicateur $\alpha_{k,1}$ a l'avantage d'une réponse rapide et d'une facilité de calcul, mais la correction de la direction du chemin est nécessaire pour obtenir une plus grande précision. L'indicateur Δ_{WS}, quant à lui, ne nécessite pas de correction préalable de la trajectoire, mais présente une charge de calcul plus importante. Le flux de travail est résumé dans la figure suivante.

En fonction de la disponibilité de l'équipement, la stratégie appropriée peut être sélectionnée de manière flexible. Le signal de l'outil d'usure a été utilisé pour tester ces deux indicateurs. Finalement, les courbes ROC (receiver operating characteristic) donnent des AUC (area under curve) de 0,87 et 0,96 respectivement.

La corrélation inter-insert pour la TCM peut réduire efficacement l'influence des facteurs externes sur le processus d'analyse et est donc indépendante des changements de profondeur de coupe et des changements de trajectoire. Cette méthode sans référence comble en partie les besoins de surveillance des outils dans la production de petits lots personnalisés. Parmi les perspectives prometteuses, certaines limites sont également identifiées. La méthode proposée a du mal à maintenir un état stable dans certaines situations qui peuvent provoquer un déséquilibre de la quantité de coupe entre les plaquettes, comme le passage sur un trou, le fraisage d'un contour extérieur à faible rayon, etc. Cela pose un nouveau défi pour les développements futurs.

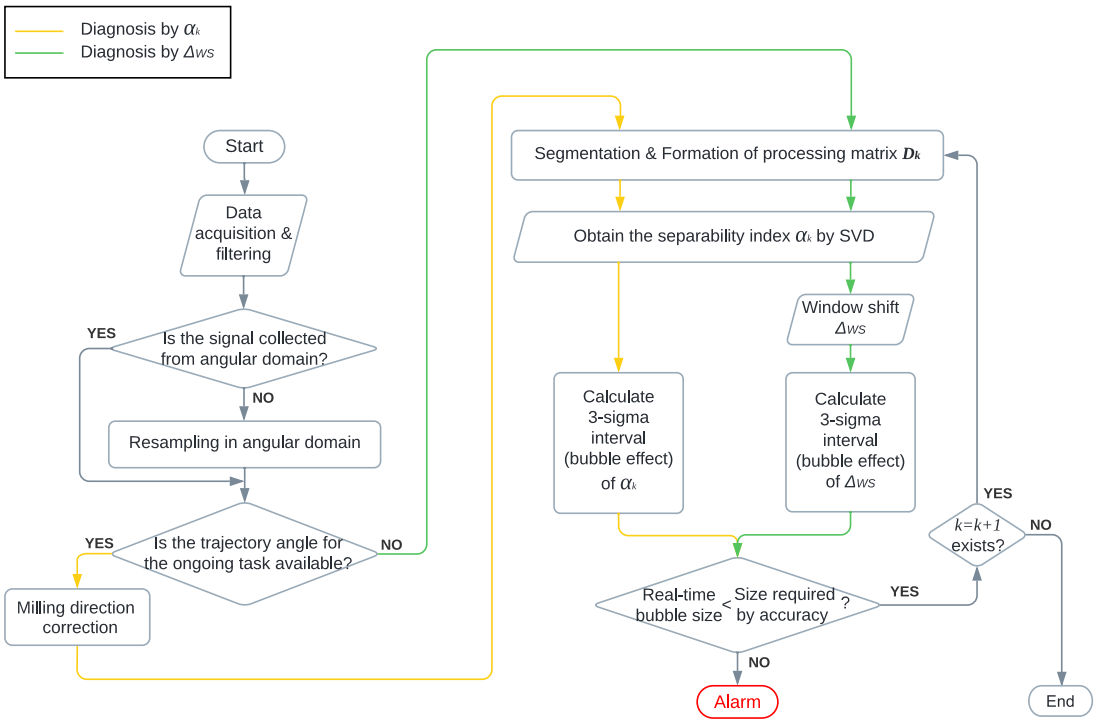

Fig. 1: General flowchart of TCM system based on the inter-insert correlation using SVD

Chapitre 6 - Conclusion générale

Ce travail a proposé une solution TCM sans référence pour la fabrication flexible. Les principales contributions peuvent être conclues comme suit :

- Le comportement des signaux de rotation est exploré plus avant dans le domaine angulaire, ce qui crée une base stable pour la segmentation des signaux correspondant à chaque insert de l'outil.

- Le concept d'exploitation de la corrélation inter-insert pour surveiller l'état de l'outil est proposé. La dérivation théorique et l'analyse expérimentale sont justifiées de manière préliminaire avec des résultats très prometteurs.

- Parmi les nombreuses méthodes de corrélation, un traitement spécifique utilisant la SVD est identifié. Chacune de ses composantes de décomposition a une signification physique correspondante, tout en étant efficace en termes de

calcul. Sur cette base, l'indice de séparabilité des ordres pour évaluer l'état de fonctionnement actuel de l'outil est introduit et deux stratégies dérivées pour la détection des défauts sont proposées.

- Par rapport à la prise de décision par *Teach-in & Comparaison* utilisée dans le système de surveillance le plus, la méthode proposée dans ce manuscrit présente les avantages de la commodité, de l'intuitivité et de la flexibilité pour s'adapter aux différentes trajectoires de fraisage (conditions cyclostationnaires et cyclo-non-stationnaires). Comme il n'est pas nécessaire de procéder à des essais ou à une formation au gros des données pour obtenir un seuil de référence standard pour chaque tâche de fraisage, il est très facile à personnaliser à la demande dans la production ainsi que dans la production en petites quantités.

Les perspectives d'avenir de cette recherche résident dans deux aspects. Le premier consiste à établir une correspondance plus précise entre les exigences de précision et l'indicateur proposé. Cela nécessitera une série d'expériences pour déterminer les critères spécifiques à appliquer, mais il ne concerne que les caractéristiques de l'outil (matériau, angle d'hélice, etc.), indépendamment des conditions de coupe. Comme son principe de fonctionnement est basé sur l'analyse de corrélation d'événements répétés sur la base de révolution, il peut être considéré comme faisant partie d'un cadre plus large pour la surveillance et la maintenance des machines tournantes. On peut donc s'attendre à ce qu'une autre direction soit prise, à savoir l'exploration de son potentiel dans le diagnostic d'autres structures périodiques, telles que les engrenages et les roulements.

Glossary

Scalars are written as italic letters, such as a.

Vectors are written as bold italic letters, such as $\boldsymbol{a}$.

Matrices are written as hollow upper-case letters, such as $\mathbb{A}$.

Notations relating to general cutting conditions:

V_c	cutting speed (m/min)
N	rotation frequency (rpm)
ω	instantaneous angular speed (rad/s)
Ω	passing speed during the curve (rad/s)
n_z	number of teeth of the tool
f_z	tooth feed (mm/tooth/rev)
V_f	feed rate (mm/min)
MRR	material removal rate (mm^3/min)
a_e	radial depth of cut (mm)
a_p	axial depth of cut (mm)
R	radius of the tool (mm)
R_c	curvature radius of the cutting trajectory (mm)
i	subscript indicating the tooth counts ($i = 1, 2, \ldots, n_z$)
θ_i	angular position of the teeth (rad)
Θ	trajectory angle (rad)
ϑ	unified angle (rad)

Notations relating to cutting force:

VB	width of the wear land on the flank (mm)
Vb	reduced length of the tool tip due to flank wear (mm)
h_c	instantaneous nominal cut thickness in general case (mm)
h_c*	instantaneous nominal cut thickness in worn case (mm)
F	resulting force (N)

F_s	shear force (N)
τ_{s}	shear stress (N/m)
ϕ_{c}	shear angle (rad)
β_{a}	friction angle (rad)
α_{r}	angle between the rake face and the normal to the work plane (rad)
F_t	tangential force (N)
F_r	radial force (N)
K_{tc}, K_{te}, K_r	constants of the force model related to tool–workpiece pair
F_{basic}	standard milling force (N)
$\overline{F}$	average force (N)
Ψ_F, Ψ_F	shape of the force and corresponding matrix (N)
$\Delta F, \Delta F$	part of the cutting force increased or decreased due to wear and corresponding matrix (N)

Notations relating to SVD:

d	sample point
$\boldsymbol{d_{k,i}}$	segment of tooth i in the k^{th} revolution
$\overline{d_{k,i}}$	average value of segment $\boldsymbol{d_{k,i}}$
$\mathbb{D}_{\mathbb{seg}}$	segmented data presented as a matrix
$\overline{D_{seg}}$	average value of matrix $\mathbb{D}_{\mathbb{seg}}$
$\mathbb{D}_{\mathbb{e}}$	extraction matrix
$\mathbb{D}_{\mathbb{k}}$	revolution-based data matrix
$\sigma, \mathbb{\Sigma}$	singular value and corresponding matrix
$\boldsymbol{u}, \mathbb{U}$	left singular vector and corresponding matrix
$\boldsymbol{v}, \mathbb{V}$	right singular vector and corresponding matrix
α_{ki}	separability index of the i^{th} order for the k^{th} revolution
m	constant presenting the number of data in one segment
n	constant presenting the total segments
i	subscript indicating the tooth counts before SVD and the order counts after SVD ($i = 1, 2, \ldots, n_z$)
j	subscript indicating the sample counts ($j = 1, 2, \ldots, m$)
k	subscript indicating the revolution counts ($k = 1, 2, \ldots, \frac{n}{n_z}$)
e	subscript indicating the extraction counts ($e = 1, 2, \ldots,$ final extraction)
L	execution number of shift
l	overlap number in the shifting processing
Δ_{WS}	sensitivity range
μ_{qp}	average value of α_{k1} from $(q-p)^{th}$ to q^{th} revolution
σ_{qp}	standard deviation of α_{k1} from $(q-p)^{th}$ to q^{th} revolution

Acronyms:

AAS	Average Angular Speed
AE	Acoustic Emission
AFNOR	Association Française de Normalisation
AI	Artificial Intelligence
AISI	American Iron and Steel Institute
APT	Automatically Programmed Tool
AR	Auto-Regressive
ARMA	Auto-Regressive Moving Average
AUC	Area Under Curve
CAD	Computer-Aided Design
CAM	Computer-Aided Manufacturing
CCA	Canonical Correlation Analysis
CIRP	Collège International pour la Recherche en Productique
CNC	Computer Numerical Control
CNS	Cyclo-non-stationary
COT	Computed Order Tracking
CS	Cyclostationary
CS1	First-Order Cyclostationary
CS2	Second-Order Cyclostationary
CWT	Continuous Wavelet Transform
DWT	Discrete Wavelet Transform
EFFRA	European Factories of the Future Research Association
FA	Factor Analysis
FFT	Fast Fourier Transform
FMS	Flexible Manufacturing System
FoF	Factories of the Future
FP	False Positive
GSA	Generalized Synchronous Average
IAS	Instantaneous Angular Speed
IBM	International Business Machines corporation
IC	Integrated Circuits
ICT	Information & Communication & Technology
IoT	Internet of Things
IR	Industrial Revolution
ISO	International Organization for Standardization
MA	Moving Average
MANOVA	Multivariate Analysis of Variance
NC	Numerical Control
NF	Normalisation Française

OEE	Overall Equipment Effectiveness
PC	Principal Components
PCA	Principal Component Analysis
PHM	Prognostics and Health Management
RMS	Root Mean Square
ROC	Receiver Operating Characteristic
SA	Synchronous Averaging
SAE	Society of Automotive Engineers
SVD	Singular Value Decomposition
TCM	Tool Condition Monitoring
TP	True Positive
TPM	Total Productive Maintenance
TTL	Transistor-Transistor Logic
WPT	Wavelet Packet Transform
WT	Wavelet Transform

List of Tables

Tab. 2.1 Monitoring and maintenance history overview 18
Tab. 2.2 Scenarios for points generation 27
Tab. 2.3 Time domain features and descriptions 44
Tab. 2.4 Frequency domain features and descriptions 46
Tab. 2.5 List of correlation coefficients [Zha+13] 55

Tab. 4.1 OROS OR35 analyzer input data recording 85
Tab. 4.2 General parameters of milling experiments 87

Tab. 5.1 Parameters for straight-time simulation signal 104
Tab. 5.2 Parameters for curve-time simulation signal 109
Tab. 5.3 Experimental parameters of the data sets involved in the following analysis 112

Tab. A.1 The characteristics of DECKEL MAHO DMC 635 V machine center 146
Tab. A.2 The characteristics of Kistler 9257A dynamometer 147
Tab. A.3 The characteristics of OROS OR35 Analyzer 149

List of Figures

Fig. 1.1 Maintenance strategies: (a) Derived subordination; (b) corrective maintenance; (c) pre-determined maintenance; (d) predictive maintenance. 5

Fig. 2.1 Tool geometry elements of a four-tooth milling cutter 20
Fig. 2.2 Cutting condition in milling 21
Fig. 2.3 Tool deterioration phenomena [Ano89]: (a) flank wear; (b) crater wear; (c) catastrophic failure. 23
Fig. 2.4 Tool life (T) curves: variation of flank wear (Vb) land with operation time. 24
Fig. 2.5 Chip formation in general case 26
Fig. 2.6 Tool cut thickness 27
Fig. 2.7 Chip formation with flank wear 30
Fig. 2.8 Forces during milling process: (a) general preview; (b) partial zoom [Alt12]. 33
Fig. 2.9 Force behavior in different tool conditions: (a) relatively healthy state at the 1^{st} revolution; (b) severe worn state at the 98^{th} revolution. 34
Fig. 2.10 Basic process flow of TCM in milling processes 35
Fig. 2.11 Kistler 3-component force dynamometer[Kisb] 38
Fig. 2.12 Sensor application versus level of precision 41
Fig. 2.13 Typology of signals 48
Fig. 2.14 ROC curves: (a) AUC=1; (b) 0.5 <AUC <1; (c) AUC=0.5 [MAT22]. 52
Fig. 2.15 Schematic diagram of the PCA principle 58
Fig. 2.16 Visualization of the SVD [Str93] 62

Fig. 3.1 End milling preset trajectory model 69

Fig. 3.2 Segmentation of signal: (a) the signal of the force divided by two red dotted lines corresponds to a segment; (b) illustration of the reshaping process. 72

Fig. 3.3 Simulation result comparison 75

Fig. 3.4 Example diagram of curved path milling (top view) 76

Fig. 3.5 Curve-line simulation signal 77

Fig. 3.6 Re-expression of components of $\mathbb{D}_{\Phi}$ 80

Fig. 4.1 Experimental setup 85

Fig. 4.2 Tool initial condition: (a) end mill inspection display; (b) the tool diameter including 1^{st}, 3^{rd} or 4^{th} tooth is 31.770 mm; (c) the tool diameter including 2^{nd} tooth is 31.830 mm. 86

Fig. 4.3 Trajectory display for contour of square 88

Fig. 4.4 Trajectory display for contour of square 89

Fig. 4.5 Trajectory display for contour of rounded square 90

Fig. 4.6 Trajectory display for contour of designed curve 91

Fig. 4.7 Trajectory display for contour of designed curve with holes . . . 92

Fig. 4.8 Demonstration of Hilbert transformation: (a) composition of the analytic signal; (b) representation of phase information corresponding to the rotational angle of the spindle. 94

Fig. 4.9 Schematic diagram for data acquisition under different domains with variable rotational speed ($\omega_1 < \omega_2 < \omega_3$) 95

Fig. 4.10 Comparison before and after resampling in angular domain of the average value of each segment $\overline{d_{k,i}}$: (a) sampling in time domain; (b) resampling in angular domain (θ) 95

Fig. 4.11 Comparison before and after trajectory correction by average value of each segment $\overline{d_{k,i}}$: (a) angle of reference (θ) without correction; (b) angle of reference ($\theta + \Theta$) with correction. 96

Fig. 4.12 Truncation 98

LIST OF FIGURES

Fig. 5.1 Simulation signal for SVD components demonstration: (a) the simulated amplitudes $K = [5, 5, 10, 1]$ correspond respectively to segments of each normal revolution cycle; (b) the simulated amplitudes $K_{change} = [1, 5, 10, 15]$ correspond respectively to segments of the tenth revolution with sudden change caused by the tooth wear; (c) a full view of the simulated signal. 103

Fig. 5.2 Demonstration of decomposed components by SVD: (a) left singular matrix $\mathbb{U}$; (b) ordered singular matrix $\mathbb{\Sigma}$; (c) right singular matrix $\mathbb{V}$. 105

Fig. 5.3 The result of combined decomposed components $\mathbb{\Sigma V}^\top$ represents the amplitude of the signal being processed. 106

Fig. 5.4 SVD analysis by revolution for straight-line simulation signal: (a) the extracted waveforms for revolutions (the 1^{st}-order of $\mathbb{U}$); (b) the extracted amplitudes for revolutions (the 1^{st}-order of $\mathbb{\Sigma V}^\top$). 108

Fig. 5.5 SVD analysis by revolution for curve-line simulation signal: (a) the extracted waveforms for revolutions (the 1^{st}-order to 3^{nd}-order of $\mathbb{U}$); (b) the extracted amplitudes for revolutions (the 1^{st}-order to 3^{nd}-order of $\mathbb{\Sigma V}^\top$). 110

Fig. 5.6 Separability index of the curve-line simulation signal 111

Fig. 5.7 SVD results for healthy tool: (a) left singular vector $\boldsymbol{u_k}$ of SVD as a function of revolutions presents a basic waveform of signal; (b) ordered singular value σ_k times transposed right singular vector $\boldsymbol{v_k}^\top$ presents the corresponding value of force. 113

Fig. 5.8 Separability index for each order with respect to samples 114

Fig. 5.9 Hierarchical presentation of signal by order: (a) the 1^{st}-order component occupied dominant contribution at the beginning of tool wear; (b) when a tooth is severely worn, the 1^{st}-order is not enough to express the signal signature, thereby the proportion of the 2^{nd}-order increases. 115

Fig. 5.10 Fundamental verification: **Contour of square** - (a) 1^{st}-order of $\mathbb{U}_\Bbbk$; (c) 1^{st}-order of $\mathbb{\Sigma V}^\top$; (e) Separability index; **Contour of rhombus** - (b) 1^{st}-order of $\mathbb{U}_\Bbbk$; (d) 1^{st}-order of $\mathbb{\Sigma V}^\top$; (f) Separability index. . . . 116

Fig. 5.11 The results with and without the step zero-centering: (a) 1^{st}-order of separability index for central data; (b) 1^{st}-order of separability index for original data. 117

Fig. 5.12 The influence of the tool's radial engagement: (a) **Test #1_10** with a_e =3.2 mm; (b) **Test #1_12** with a_e =12 mm; (c) **Test #2_6** with a_e =11 mm. 118

Fig. 5.13 Types of Bootstrapping 121

Fig. 5.14 Decomposition for random selection P 122

Fig. 5.15 Separability index for random selection P 122

Fig. 5.16 Decomposition for random selection CR 123

Fig. 5.17 Separability index for random selection CR 123

Fig. 5.18 Sensitivity analysis based on bootstrap before and after trajectory correction: (a) angle of reference (θ) without correction; (b) angle of reference ($\theta + \Theta$) with correction. 124

Fig. 5.19 Sensitivity analysis Δ_{WS} of separability index α_{k1} before and after trajectory correction are almost the same: (a) angle of reference (θ) without correction; (b) angle of reference ($\theta + \Theta$) with correction. 126

Fig. 5.20 Status information of the data used for validation: (a) surface condition of machined workpiece; (b) final condition of inserts. 128

Fig. 5.21 Fault detection based on separability index α_{k1} (blue line) with upper (purple line) and lower (yellow line) limit of 3-sigma interval: (a) tool in good condition; (b) tool in worn condition. 129

Fig. 5.22 Fault detection based on sensitivity range Δ_{WS} (blue line) with upper (purple line) and lower (yellow line) limit of 3-sigma interval: (a) tool in good condition; (b) tool in worn condition. 131

Fig. 5.23 General flowchart of TCM system based on the inter-insert correlation using SVD 132

Fig. 5.24 Receiver operating characteristic curves of proposed two TCM methods 133

Fig. 5.25 Demonstration of the milling trajectory and corresponding stages of tool states 135

LIST OF FIGURES

Fig. 5.26 Limitation: **Contour of designed curve** - (a) 1^{st}-order of $\mathbb{\Sigma V}^{\top}$; (c) fault detection based on separability index α_{k1}; (e) Fault detection based on sensitivity range Δ_{WS}; **Contour of designed curve with holes** - (b) 1^{st}-order of $\mathbb{\Sigma V}^{\top}$; (d) fault detection based on separability index α_{k1}; (f) Fault detection based on sensitivity range Δ_{WS}. 136

Fig. A.1 Display of DECKEL MAHO DMC 635 V machine center 145
Fig. A.2 Display of Kistler 9257A dynamometer 146
Fig. A.3 Working principle of the rotary encoder: (a) for each revolution, the photosensitive sensor receives the light information passing through the slits, and then produces a reference signal and two sinusoidal analogue signals with a phase difference of 90°; (b) the three signals from the rotary encoder are converted into a TTL signal, which triggers one acquisition of the high-frequency pulse clock for each of its rising edges. 148
Fig. A.4 The characteristics of APX3000R325M16A end mill 149
Fig. A.5 FFT of spindle: (a) spectral representation of initial signal; (b) spectral representation after filtering. 151

Fig. B.1 The result of traditional correlation analysis by expansion of PCC: (a) **Test #1_10**; (b) **FG #120915**. 154
Fig. B.2 Correlation between each pair of the inserts: (a) Upper triangular part of the matrix $\mathbb{R}_{\mathbb{k}}$; (b) Eigenvalues of the matrix $\mathbb{R}_{\mathbb{k}}$. 156

Fig. C.1 **Results of square contour Test #1_4 ($a_e = 8mm$)** - (a) illustration of the cut; (b) 1^{st}-order of $\mathbb{U}$; (c) 1^{st}-order of $\mathbb{\Sigma V}^{\top}$; (d) fault detection based on separability index α_{k1}; (e) Fault detection based on sensitivity range Δ_{WS}. 158
Fig. C.2 **Results of rhombus contour Test #1_18 ($a_e = 8mm$)** - (a) illustration of the cut; (b) 1^{st}-order of $\mathbb{U}$; (c) 1^{st}-order of $\mathbb{\Sigma V}^{\top}$; (d) fault detection based on separability index α_{k1}; (e) Fault detection based on sensitivity range Δ_{WS}. 159
Fig. C.3 **Results of designed curve Test #2_8 ($a_e = 3.2mm$)** - (a) illustration of the cut; (b) 1^{st}-order of $\mathbb{U}$; (c) 1^{st}-order of $\mathbb{\Sigma V}^{\top}$; (d) fault detection based on separability index α_{k1}; (e) Fault detection based on sensitivity range Δ_{WS}. 160

Contents

Acknowledgement **v**

Abstract **vii**

Résumé **ix**

Glossary **xix**

List of Tables **xxiii**

List of Figures **xxv**

1 Introduction **1**
1.1 General context 2
1.2 Problematic and objectives 7
1.3 General strategy and innovations 10
1.4 Organization of the thesis 11

2 State of the art **13**
2.1 Introduction 14
2.2 A brief history of machining monitoring 14
2.3 Characteristics of operation 18
2.3.1 Tool geometry 19
2.3.2 Tool cutting condition 20
2.3.3 Tool wear and tool life 21
2.3.4 Chip formation behaviors 25
2.3.5 Milling force model 31
2.4 Constructive elements of TCM system 35
2.4.1 Selection of the sensor system 37
2.4.2 Feature extraction 42
2.4.3 Action for decision making 51
2.5 Correlation-based monitoring 52
2.5.1 Relationships between variables 54
2.5.2 Multivariate correlation analysis 56
2.5.3 Singular value decomposition (SVD) 61

2.6 Conclusion 64

3 General modeling of the rotational machinery behavior 65
3.1 Introduction 66
3.2 Required signal features for inter-insert correlation 66
3.3 Trajectory change and unification of the angle 68
3.4 General modeling of rotational machinery behavior 70
3.4.1 Segmentation 71
3.4.2 In case of milling force 73
3.4.3 In case of instantaneous angular speed (IAS) 74
3.5 Correlation strategies 77
3.6 Conclusion 81

4 Experiment design and data pre-processing 83
4.1 Introduction 84
4.2 Experimental setup 84
4.3 Milling parameters and trajectories 87
4.3.1 Different trajectories cases 88
4.4 Data pre-processing 92
4.4.1 Hilbert transformation 93
4.4.2 Resampling 94
4.4.3 Milling direction correction 96
4.4.4 Truncation & Segmentation & Zero-centering 97
4.5 Conclusion 98

5 Characterization of tool state by SVD 101
5.1 Introduction 102
5.2 SVD components 102
5.2.1 Straight-line simulation signal 107
5.2.2 Curve-line simulation signal 108
5.3 Analysis of results 112
5.3.1 Validity verification of SVD analysis with experimental data . 113
5.3.2 Fundamental verification 115
5.3.3 Sensitivity analysis 119
5.4 Fault detection 127
5.4.1 TCM based on separability index $\alpha_{k,1}$ 128
5.4.2 TCM based on sensitivity range Δ_{WS} 131
5.4.3 Summary and evaluation 131
5.5 Limitation 134
5.6 Conclusion 137

6 General conclusion 139
6.1 Conclusion 140
6.2 Principal contributions 142

6.3 Further works 143

A Appendix A - Experimental equipment **145**

B Appendix B - Two attempts of correlation-based TCM **153**

C Appendix C - Relevant results **157**

References **161**

Chapter 1

Introduction

Summary

1.1 General context 2
1.2 Problematic and objectives 7
1.3 General strategy and innovations 10
1.4 Organization of the thesis 11

1.1 General context

With globalization, a clear international division of labor has been formed between developed and newly industrialized countries. More than 80% of low-value-added production lines have been transferred to developing regions. In the 1980s, the United States had overemphasized the importance of the tertiary industry, further contributing to the decline of its manufacturing sector for a time. But in the post-COVID19 era, the significance of domestic manufacturing to the health of the national economy has been reconfirmed, in which traditional machining occupies a very essential position.

After entering the 20^{th} century, the means of production and productivity held by mankind have grown exponentially, and the pace of technological development continues to accelerate [Han01]. To meet the surging consumer demand stimulated by social development, the machining process is streamlined, standardized, and globalized. Fordism is one of the typical successful cases with high efficiency and low cost and provided numerous products for the seller's market society at that time. However, this mode of production came at the expense of a reduction in product diversification. As the economy developed, the competitive advantage of companies evolved, and it no longer manifested itself in simple rivalries on quality, price, and quantity, but rather in a demand for innovative and even customized production. At the same time, with the high rate of technological iteration, the fixed processes of mass production, represented by Fordism, cannot be adapted swiftly. It is therefore difficult to keep up with the shifting trends of the market, which ultimately leads to redundancy and waste of large amounts of inventory. To survive in the current ever-changing and unpredictable market environment, companies have to face three major challenges in the production of customized on-demand goods:

- How to target market fronts and meet customized needs?
- How to minimize the prohibitive price of one-off products made on order?
- How to quickly restructure production lines for early delivery?

Flexible Manufacturing System (FMS) is seen as the main answer to these

questions. In general, an FMS system consists of three main units: **a central control computer** to govern the manufacturing parameters, **a programmed working center** (usually an automated computer numerical controlled (CNC) machine, robot or 3D printer), and **a material handling system** to optimize the production workflow [Kos+21]. It provides firms a proactive and strategic manufacturing foundation to adapt to the dynamic trend of consummation. Its flexibility involves following three main aspects [Tol09]:

- **Design flexibility**
  The conception, modification, and development of the product could be modeled and simulated before manufacturing through computer-aided design (CAD) software. Customers can participate in the early design stage to ensure the final product will meet their requirements.
- **Machine flexibility**
  The machining process is divided into multiple independent operations, whose sequence and type are allowed to be changed and combined by pre-programmed codes to produce new product categories without expensive expenses.
- **Routing flexibility**
  The process routing is composed of a variety of machines to achieve a one-stop production mode from raw material to packaging. A wide range of machinery options and high interface compatibility between machinery can adapt to production scale changes, such as in volume, capacity, or capability, and enable faster implementation of a product transition.

Flexibility is a latent competence of a system rather than an actual behavior. It is usually interpreted as reactive sensitivity to three factors:

- **Scope**
  Long-term flexible production involves process improvements and innovations. The system is structurally reconfigurable, reusable, and scalable. The larger the range of adaptation, the greater the flexibility.
- **Time**
  The time required to switch between different working states. The shorter the time, the greater the flexibility.

- **Cost**
  The cost required to switch between different working states. The lower the cost, the greater the flexibility.

FMS works on an on-demand basis following the market trends, thus reducing inventory backlogs, increasing machine efficiency, improving labor productivity, minimizing manufacturing costs, and making companies more competitive. However, the development of FMS is slower than anticipated, despite all the advantages mentioned above. The effectiveness of an FMS depends to a large extent on the automation level in other areas of the entire organization. It can operate with limited manpower, but various support equipment is needed. Therefore, some companies are hesitant to introduce such a sophisticated system because of **the heavy initial investment** required and **the subsequent maintenance expenses** associated with it [TTV09].

However, in the context of fierce global competition, companies must constantly make technological advances in order to maintain the competitiveness of their production systems. For this reason, many companies make a compromise choice by building FMS systems on top of their existing equipment — CNC machining centers. Since the CNC machining center was one of the first automation technologies to be introduced in the business, it already has a good industrial base with low subsequent retrofitting costs compared to implementing emerging technologies.

The CNC machining center is a computer-controlled motorized platform, where high-performance microprocessors and programmable logical controllers work in a parallel and coordinated manner. It is equipped with a range of tools in different sizes and materials, such as drills, flat end mills, ball nose mills, etc., which can be called up in accordance with CAD/CAM codes for different operations and automatically perform subtractive manufacturing. At the same time, in contrast to additive manufacturing (3D printer), the high-speed operation of CNC machining dictates a high productivity ceiling, which allows the system to shift freely from small customized batches to efficient mass productions [BM85].

Alongside the evolution of techniques, technologies, and strategies for industrial production, other aspects are also advancing in parallel. The hardness levels of materials were previously unthinkable. In addition to the need for diversification, social demands are at the same time placing higher requirements on product precision and

structural complexity. In order to pass the strict quality control session, companies need to pay a high fee to safeguard the FMS services.

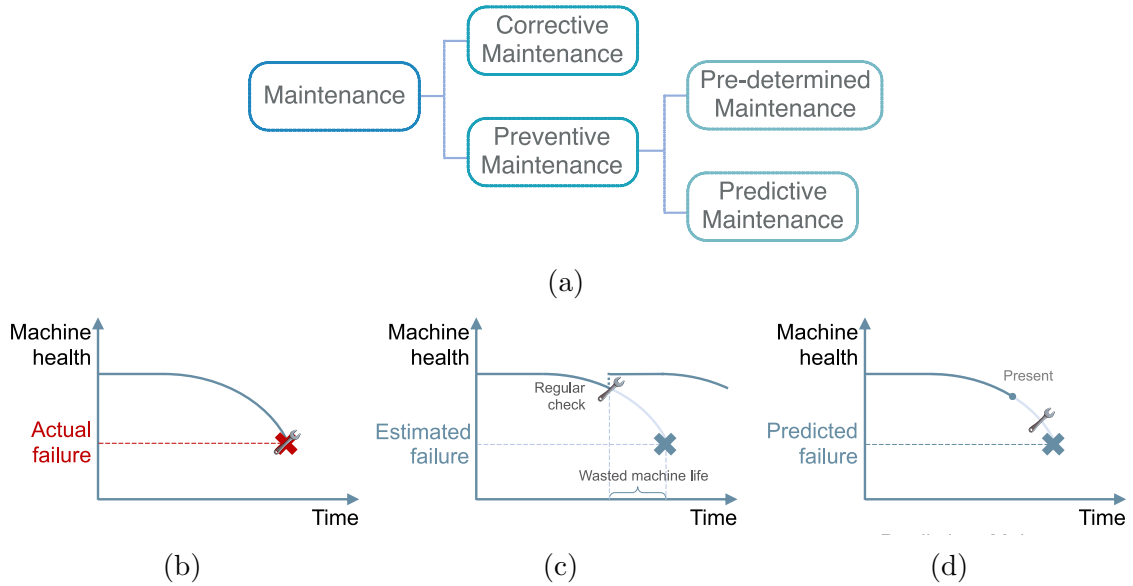

Fig. 1.1: Maintenance strategies: (a) Derived subordination; (b) corrective maintenance; (c) pre-determined maintenance; (d) predictive maintenance.

According to the AFNOR standard NF X60-000 (April 2016), maintenance is a collection of actions including all technical, administrative, and management behaviors within the life cycle of an asset, intended to maintain or restore it to a state in which it can perform the required function [AFN16]. Basically, there are two different maintenance strategies available, depending on the circumstances and level of maintenance, as shown in Fig. 1.1. **The corrective maintenance** (reactive maintenance) is acceptable when dealing with simple situations, such as changing a light bulb. Equipment can be repaired or replaced after it has worn out, malfunctioned, or broken down as it has no serious subsequent effects. However, once a sophisticated system with certain expensive components is involved, it is very risky to simply leave the machine running until it fails completely. The consequences are not only high repair costs, but also involve significant safety issues. At present, **the preventive maintenance** (proactive maintenance) is implanted in most actual manufacturing, which means that the parts are maintained or replaced at predetermined planning according to the standards provided by the supplier (operating hours, number of units produced, number of movements carried out, etc.), thereby minifying the probability of system failure. Compared with traditional corrective maintenance, regular and

routine checks are more systematic and assure. However, it does not make full exploitation of the service life of the components, which can be considered redundancy and waste.

Facing challenges and competition, maintenance is not stagnated. It has also evolved over the years to support the transformation of the industrial world. A more advanced method based on condition monitoring, called the **predictive maintenance**, has been derived from preventive maintenance [For11]. It refers to a sensor-based system that will determine the health of equipment by observing real-time data collection and will only take action when maintenance is truly required. In contrast to simply planned maintenance, predictive maintenance enables a significant degree of prioritization and optimization over maintenance resources. Ideally, predictive maintenance could minimize spare parts costs and increase productivity, as well as ensure product quality.

Extensive instrumentation of equipment with specialized analysis tools has led to a development trend in recent years. For a discrete-event system such as a box packing line, the execution of predictive maintenance is simple. The next task only will be proceeded when the sensors confirm that the previous task has been completed correctly. Due to the independence between each task and the slow operation speed of the work-line, the above treatment will not cause excessive subsequent losses. However, the predictive maintenance for material removal manufacturing on CNC machines is a totally different story.

The sensor-assisted monitoring system is already installed in most CNC machining centers to proceed with in-process milling monitoring during unmanned machining operations as much as possible [Alt12]. By integrating different sensors, such as position sensors, dynamometers, rotary encoders, etc., current CNC centers allow simultaneous servo-position, velocity control of all the axis, monitoring of the controller, and vibration performance. However, the prognosis of tool conditions in predictive systems is a bottleneck that has plagued the entire manufacturing industry for the past decade.

1.2 Problematic and objectives

With steady developments on the other side, difficult-to-monitor tool wear as a weak point in machining has limited the industry's progress. According to statistics, among all factors, cutter breakage has become one of the main causes of downtime, which accounts for approximately 6.8% causes of unwanted stoppage [RJO05].

Although most CNC machining centers are equipped with sensor-based monitoring systems, they can only monitor the general condition of the machine. Due to the consumable nature of the cutter and its overly small size, there are currently no sensors that can be directly attached to it. On the other hand, the remote sensors do not have good accessibility and visibility to monitor the tool condition as the coolant and constant chip generation during the operation. The cutting tool is like the fingernail, working hard without any painful sensation even when it is already injured, which unfortunately is a fairly common case.

In fact, the aforementioned 6.8% only refers to situations where the tool is seriously damaged. In most cases, the tool has no visible cracks but is already excessively worn. During steady production, the excessive wear that appeared prior to scheduled tool replacement will introduce cutting conditions change including enormous chip heating, cutting speed change, chattering, etc. Using a dull cutter will produce ripples on the machined surface, and the quality of the workpiece will be immeasurably reduced. Especially when the machined products are high added value parts, if the problem cannot be discovered in time, the consequences and losses will be extremely significant.

Excessive tool wear also has a high risk of triggering periodic overloads at the cutting edge, which might accelerate the tool damage as chipping or accidental breakage of the insert and even put dangerous stresses on the spindle and other parts of the machine. In the event of an incident, sufficient stoppage must be taken quickly to limit the damage and the resulting additional costs. Such a shutdown accident not only wastes time and diminishes efficiency, but also may cause irreparable damage to the machine (mostly to the spindle).

Therefore, under the trend of a lightly staffed or fully automated machining en-

vironment, the monitoring of the real-time status of the tool has become an essential issue. **Tool condition monitoring** has therefore been abbreviated to TCM as a term specifically for the study of tool diagnosis and prognosis. The data predict that an accurate and reliable TCM system can allow scheduled maintenance, which may save 10% to 40% of the cost of production projects [Lam+14].

As mentioned earlier, in order to adapt to the diverse social requirements, the generated milling paths and selected operating parameters vary according to the customer's needs. In the context of flexible manufacturing, **the main difficulties for real-time TCM** can be summarized as follows:

(i) The cutter is a consumable item with a relatively small size, to which no sensors can be directly attached.

(ii) The working environment has limited visibility and accessibility due to the presence of coolant and metal chips.

(iii) The condition of the tool may undergo rapid changes at a high rotational speed.

(iv) The milling trajectories are complex and vary from the different tasks with no fixed pattern.

(v) The sources of vibration signals are extremely sophisticated.

Among these obstacles, the difficulties (i) and (ii) place demands on acquisition techniques. After decades of development, countless researchers have proposed many different TCM methods at this stage. Generally, TCM can be divided into 2 ways, direct and indirect, to monitor the type and amount of wear [Lau+14]. The direct TCM usually requires a high-frequency acquisition camera [Lau+13; DPS16] or uses optical methods such as laser measurement to directly obtain vision data [RMK98; TG08]. It not only tries to capture data on the surface but also seeks the information with the cutting edge or even the geometry of the chip [Ayk+07]. However, due to the practical limitation of accessibility, the lack of illumination, and the presence of coolant liquid, etc., it is very difficult to use in real-time monitoring [Shi88]. The indirect TCM is based on various indirect parameters output from the machine, such as cutting force [KK97; Kar07], vibration [Sev+15; Yuq+15], motor current [Sev+11; Lee99], acoustic emission [MA08; Ren+14], temperature [OC01; SS12], etc. It involves the collection and analysis of indirect signals to deduce the current work

status of an in-service tool in order to predict possible failures.

Current available methodologies usually start with features extraction by signal processing techniques, such as statistical analysis in the time or frequency domain [Nou+15; Moh+19], FFT [Ver+09; MA08], wavelet analysis [ZSH09], etc., and then follow *Teach-in & Comparison* principle to diagnose the tool status: the assessment is based on the comparison between the real-time monitoring data and a predefined reference. This standard reference can be obtained with a simple trial run or by cognitive paradigms, such as neural networks [SMP19; HA03; SÖ16], fuzzy logic [SÖ16; CK17], genetic algorithms [ABB00; Ach+02], etc. However, apart from wasting material, the results obtained from test runs are not authoritative. Especially when it comes to cyclo-non-stationary operations (milling with variable load and complex trajectory), which is the most common task in the industry, the unreliable reference may lead to false alarms and unnecessary stoppages. On the other hand, the reference concluded by the cognitive paradigm, although relatively stable, has encountered challenges in data training due to its high costs of data acquisition and insufficient development in storage and transmission technology [Zho+22; Zhu+21]. Therefore, neither of the two are suitable for monitoring small batch or customized on-demand production.

This thesis comes into this context aiming to design and demonstrate a new TCM method to overcome the difficulties (iii) and (iv) and reliably detect tool states during real-time operations. To accomplish this overall aim, several objectives are listed as follows:

- The first objective is to identify the suitable indirect signal characteristics that can be used to describe the condition of the machining process.
- The second objective is to consider non-stationarity issues of the regime introduced by factors such as trajectory changes, variable loads, etc.
- The third objective is to confirm that the diagnostic tool can handle the massive volume of data that is generated by rapid machining.
- The fourth objective is to ensure that the method can identify fault conditions from sensor data without the need for data training.

Delivering these goals contributes to minimizing the frequency and severity of downtime, and reducing the manual interventions that are common in today's manufacturing.

1.3 General strategy and innovations

The kinematic excitation of rotating mechanisms is often synchronized with the shaft. This kind of physical nature determines that most of their output signals are cyclostationary (CS), i.e., they exhibit periodic statistical characteristics [Ant+04].

Instead of comparing the real-time signal with a rigid reference object, the similarities and the differences inside the signal are explored. Combining the several stages of the typical tool life curve, the inserts will gradually show different degrees of wear from the initial similar state and the correlation between them will continuously decrease. Therefore, this research proposed to take advantage of **the inter-insert correlation** as the general strategy.

Milling is a continuous long-term assignment in a high-speed and high-temperature working environment. The process involved multiple external interferences including ambient vibration noises, coolant influx, etc., as well as the internal condition changes, such as a tool passing through curved paths, etc. Considering the fact that the disturbance is formed much slower than the high-speed rotation of the tool, therefore, the different teeth can be seen as subject to quasi-equivalent influences in one revolution. After correlation analysis, the results focus on the differences between the tool inserts. This method is suitable to reveal weak fault signatures from strong and sophisticated environmental noises. It thus can analyze the end mill state under both cyclostationary (operation with constant speed, load, and straight trajectory) and cyclo-non-stationary conditions (operation with variable speed, load, and complex trajectory).

The innovations of the proposed approach are embodied in the following aspects:

(i) It is founded on sampling or resampling of the signal in the angular domain, which allows the signal to be segmented in units of cutting tooth. Few works

cover the signal in the angular domain. The research in this paper is developed based on the previous work of Girardin et al. [GRR10] on the instantaneous angular speed;

(ii) The multiple tool inserts on the same tool are considered as interacting individuals, and the real-time continuous signal is divided into corresponding segments for self-comparison;

(iii) The inter-insert correlation analysis can eliminate the external cyclo-non-stationary factors and focus only on the state of the tool. The high rotational speed characteristic, which is originally seen as the monitoring difficult point (iii), reversely helps to approximate the external working environment of each tooth to be quasi-equivalent, and thus contributes to a better correlation result;

(iv) There is no need to arrange the trial runs or a large amount of data training to obtain reference signals;

(v) More importantly, this method can be considered versatile, which has the potential to be applicable to a wide range of signal sources from rotating machinery.

After a literature review, it appears the current researches mostly emphasize the correlation between the proposed indicator and the mechanical state [Sen+12; Dut+13b; NL19], or compare the real-time signal with a known template [RSJ06; SJ07; Niu+21]. As far as the authors know, there is no similar research and the proposed method is original as well as innovative.

1.4 Organization of the thesis

This thesis is divided into 6 chapters.

In Chapter 1, the thesis is started with a general introduction, including current trends in machining and existing maintenance strategies. We locate the position of this work and delineate its problem and objective. A general strategy is equally set with the declaration of innovation of this study.

In Chapter 2, the theoretical background required for the study is reviewed through three aspects: the milling operation, the construction of tool condition mon-

itoring system, and the correlation relevant algorithm. Through the analysis, the source and processing method used to analyze the signals are selected.

In Chapter 3, specific problems are modeled and strategies for correlation analysis are discussed in detail as well as the scope of application.

In Chapter 4, we state the experimental design and implementation details, containing multiple milling trajectories. The data collected through the experiments are pre-processed.

In Chapter 5, the processing results of simulated and experimental data are presented, including the physical significance corresponding to each decomposed component, the validity, and sensitivity analysis of the indicator proposed, and the workflow for fault detection.

In Chapter 6, we seal the thesis with a conclusion and some perspectives.

Chapter 2

State of the art

Summary

2.1 Introduction . . . 14
2.2 A brief history of machining monitoring . . . 14
2.3 Characteristics of operation . . . 18
2.3.1 Tool geometry . . . 19
2.3.2 Tool cutting condition . . . 20
2.3.3 Tool wear and tool life . . . 21
2.3.4 Chip formation behaviors . . . 25
2.3.4.1 General case . . . 25
2.3.4.2 Case including consideration of the tool defects . . . 30
2.3.5 Milling force model . . . 31
2.4 Constructive elements of TCM system . . . 35
2.4.1 Selection of the sensor system . . . 37
2.4.2 Feature extraction . . . 42
2.4.2.1 Time domain analysis . . . 42
2.4.2.2 Frequency and time-frequency domain analysis . . . 44
2.4.2.3 Angular domain analysis . . . 46
2.4.3 Action for decision making . . . 51
2.5 Correlation-based monitoring . . . 52
2.5.1 Relationships between variables . . . 54
2.5.2 Multivariate correlation analysis . . . 56
2.5.3 Singular value decomposition (SVD) . . . 61
2.6 Conclusion . . . 64

2.1 Introduction

Tool monitoring has been used throughout the development of the modern industry to avoid issues such as poor machining surface quality and noisy operations. Section 2.2 provides a brief history of machining monitoring and highlights the necessity for the subject today.

Section 2.3 clarifies the types of monitored machining targeted by this work and analyzes the corresponding operational characteristics, wear types, and tool life. The chip forming process is further discussed under both normal and wear conditions, and the corresponding milling force model is summarized.

Based on this, Section 2.4 analyzes each of the three elements of the TCM system: sensorial perception, feature extraction, and decision making. The signal acquisition methods as well as the performance and applications of existing sensors are investigated. Then feature extraction proceeding from the time domain, frequency domain, and angular domain classification is compared. Finally, the receiver operating characteristic (ROC) curve is introduced as a tool to aid decision-making. Based on this, an inter-insert correlation-based tool condition monitoring concept is proposed.

Section 2.5 further delves into the specific methods of correlation and multivariate analysis to support the implementation of the proposed methodology.

2.2 A brief history of machining monitoring

The late 18^{th} century was a historical turning point in the modernization of human society. Since the first Industrial Revolution (IR), marked by James Watt's invention of the steam engine in 1765, production methods were gradually mechanized. The weavers' looms greatly increased the efficiency of their labor and can be seen as representative of the embryonic industrialization of manufacturing [Kos+21]. In this period, the concept of monitoring did not yet exist. Because the machines were elementary in construction, no specialist thus was required to take care of the maintenance. It can be said that in those days it took less time and money to do

nothing than to schedule a detailed maintenance program. People naturally used the machines until they broke down and then repaired them.

Following the first wave of the IR, society entered a phase of rapid standardization. With the emergence and spread of many important inventions, such as electrification, motors, turbines, and large assembly lines, manual production began to be gradually replaced by mass mechanized production in the late 1870s. In turn, the increased mechanization required more metallic parts (made of cast or wrought iron), which boosted the development of machine tools, creating a healthy cycle. Among enough builders, it is difficult to say exactly who 'invented' the milling machine, but Henry Maudslay was the unquestioned leader in the development of machine tools [Roe16]. He is the first to build a functional lathe using an innovative combination of known screws, sliding frames, and variable speed gears. The workshops established by him trained a generation of people dedicated to the design and manufacture of machine tools based on his works. Machine tools, including milling machines, turning machines, etc., were developed from the early 20^{th} century as an important manufacturing tool in workshops.

As technology continues to evolve, the range of products expands, which brings an unparalleled level of complexity to the supply chain. Alongside the closer links in industry, a machine breakdown in any single sector can lead to numerous (and costly) subsequent problems. At this point, attention began to be paid to the health of machines, and the idea of repairing equipment in advance before it broke down was put forward. However, the technology at the time was not yet adequate to enable real-time monitoring. Henry Ford, one of the pioneering managers, advised in *Ford T Series Manual (1919)* [Com19]: *"Frequently inspect the running gear. See that no unnecessary play exists in either front or rear wheels and that all bolts and nuts are tight. Make a practice of taking care of every repair or adjustment as soon as its necessity is discovered. This attention requires little time but may avoid delay or possible accidents on the road."* This is undoubtedly the kind of preventive maintenance mentioned in Section 1.1.

After then, WWI, WWII, and the Cold War became the driving force behind the development of machine tools. An American technology-focused defense, intelligence, security, and infrastructure engineering firm called Parsons Corporation was founded in 1944 in Centreville, Virginia. It was committed to developing rotor blades for the

aerospace sector, which is a very challenging task due to the complexity of the shapes and the precision required. Parsons' executives were very farsighted in realizing that by linking up with new emerging IBM computers, it was possible to produce accurate contour lines, which had until then been hard to calculate manually. Within a short period, Parsons signed a contract with the US Air Force to supply automatic contour cutting machines for large wing sections of aircraft [UKE18]. In collaboration with the MIT Servomechanisms Laboratory, the first computer-controlled continuous path CNC milling machine was successfully developed in the early 1950s to produce parts demanded by the aerospace industry [MIT04]. In 1955, IBM developed an automatic device for tool replacement.

With the advancement of transistor technology, 80% of the wiring connections in machine tools were reduced by using integrated circuits (IC). Subsequently, the laboratory's Computer Application Group, led by Douglas T. Ross, developed the Automatically Programmed Tool (APT) Language, which removed the last major technical barrier to the large-scale use of NC in manufacturing and solved once and for all the problems of whether NC could be economically viable based on the cost of programming [Rei91]. The APT language was adopted as the international standard for CNC machine programming in 1978. During the 1980s, commercial CAM/CAD systems gained in maturity and graphics-based 3D modeling systems have been gradually integrated. The main feature of this period was the boom in electronics and information technology, which was brought into production to drive machine automation.

During the same time frame (1967-1969), the British company Molins developed the *System 24* automated workshop for the first time based on the basic concept of FMS proposed by D.T.N. Williamson (US Patent 4621410). With six multiprocess machine tools working in a modular structure, the tentative goal is to achieve 24/7 continuous processing services under unattended conditions [Int85]. Although it was not completed due to economic and technical difficulties, it brings together ideas such as high-speed milling, cell-based production, computer control (but not CNC in the modern sense), transfer, and storage of workpieces in an attempt to achieve efficient production under automation. By this time, downtime was already having a major impact on production. In the 1970s, Total Productive Maintenance (TPM) has been developed by Seiichi Nakajima in Japan, as a method of physical asset

management focused on optimizing equipment performance with the aim of increasing the economic efficiency of production. It emphasized the higher priority of condition monitoring, integrated maintenance into the company's basic strategy, and involved system-wide employees in maintenance activities [PNR13].

Over the same period, numerous studies on the use of sensors to monitor manufacturing activity state began to be carried out by the academic community [MKV76]. As transistors continued to shrink as predicted by Moore's Law, computer technology gradually possessed the hardware capability to implement online analysis of production data. Sensors are progressively being exploited in laboratory environments to measure and collect data. Real-time monitoring became possible by combining the experience gained from previous conventional maintenance with data-driven analysis statistical models. This allowed asset failure to be predicted/prevented before problems occurred and helped to enable process optimization at a later stage.

M. Weck et al. [WEC+80] published the article *Concept of integrated data processing in computer controlled manufacturing systems* in 1980. It concerns a flexible and automated manufacturing processes method, which has been successfully demonstrated in an aerospace machining application at the University of Aachen. The application of sensors in CNC machine tools steadily expanded during the late 20^{th} century, replacing manual monitoring of production processes and eliminating personnel costs while improving product quality and minimizing downtime. As the general aspects of maintenance strategy and technology have improved, the diagnostic challenges of tools have come to the fore and been noticed.

In January 1993, CIRP established a framework within the context of the Working Group on Tool Condition Monitoring (TCM WG), to investigate the international state of the art, technological challenges, and growing trends in TCM both from a research perspective and from within the manufacturing industry [Byr+95]. It focused on catastrophic tool failures, collisions, progressive tool wear, and tool chipping/fracture during machining processes (including milling, turning, drilling, etc.). A further issue of the TCM WG was *A Review of Tool Condition Monitoring Literature Data Base* published by Teti et al. in 1995, which is continuously updated until 2006 with 500 new publications comprising more than 1000 classified references [RST08]. In 2010, the same author presented a keynote paper in CIRP Annuals [Tet+10], which summarized the developments in sensor systems, advanced signal processing, mon-

itoring scopes, etc. A large number of citations over several decades demonstrates the continuing interest and significance of the subject for the manufacturing sector.

With the rapid advancement of the Internet, diagnostic and maintenance technology is witnessing and participating in the revolution of Industry 4.0 (IR4). A wide range of predictive maintenance systems consists of sensors, cyber-physical systems, the Internet of Things (IoT), big data analysis, cloud computing, web and artificial intelligence, mobile networks, etc. [PŽB19; CST18], and the TCM is a crucial element for the operational practice. In 2009, a research program called Factories of the Future (FoF) was launched by the European Factories of the Future Research Association (EFFRA). It was a recovery plan after the economic crisis in 2008, for rebooting the industry competitiveness with newly developed high-value-adding manufacturing. In the roadmap proposed by EFFRA, it highlighted the necessity of monitoring the actual state of the machine/tool in a continuous mode [CRI13].

From January 2014 to December 2015, the EU Commission carried out a project to develop an advanced monitoring technology to track tool wear with a budget over 1,245,000 euros [EI15]. In 2020, European Horizon 2020, the biggest EU Research and Innovation program ever, reiterated the call for *Factories of the Future* to emphasize the condition monitoring as a key development theme of the day [EI20].

Timeline	1760s-1830s	1870s-1910s	1940s-1980s	1980s-Present
Technology development characteristics	Mechanization, steam power, weaving loom	Mass production, assembly lines, electrical energy	Computers, electronics, automation	Cyber systems, Internet of things, sharing cloud
Monitoring means	Visual inspection	Instrumental inspection	Sensor monitoring	Predictive analysis
Type of maintenance	Corrective maintenance	Planned maintenance	Productive maintenance	Predictive maintenance
Staff requirements	Trained craftsmen	Inspectors	Engineers	Data scientists

Table 2.1: Monitoring and maintenance history overview

2.3 Characteristics of operation

Among the many types of machining, the studied case of this thesis is based on conventional milling, which is one of the most important branches in the family tree of the material removal process. Milling is usually performed as a secondary process, following the basic process, such as casting or batch deformation (forging,

drawing, etc.), to determine the final parameters of the geometry and dimensions of the workpiece. The tool is in direct contact with the workpiece to complete the finishing process. Therefore, the condition of the tool is critical to the final quality of the product.

2.3.1 Tool geometry

For a more precise description to be followed, some terms of tool geometry are introduced here first. The corresponding illustrations are in Figure 2.1.

The cutting tool in milling is called a milling cutter. The milling cutter interacts directly with the material, but it is not as one piece with the machine spindle. Between these two components, the tool holder provides a critical interface, which mounted and tightened the cutter to ensure that it moves or vibrates as little as possible during the milling process. The cutting edges are known as the teeth in general conversation, whereas the real action part is the screw-tightened replaceable coated insert. The cutting tool inserts are widely used in practical production due to their significant economical nature. Each insert contains several cutting edges. It allows the tool equipped with a brand new milling edge by adapting simply three steps — un-clamp, rotate the insert to the next available edge, and re-clamp. When all the edges are worn out, the insert has then attended to its full potential and is ready to be discarded and replaced. However, it is always a difficult task to determine if the cutting edge is in a sufficient state to continue the productive work, which is also the targeted subject of this research.

Most milling tools are multi-edge tools (single-edge tools are mostly found in turning; and in a very rare case, a single-edge milling tool called fly-cutter might be used). During the milling process, the tool performs a discontinuous cutting operation in a rotational manner. This implies that the teeth of the tool enter and exit the workpiece during each revolution. Such an intermittent action is surely accompanied by significant force impacts and thermal shocks on the rotational basis. Therefore, the tool must be made of a material that is harder than the workpiece and designed by geometry to ensure that it can withstand the harsh working conditions.

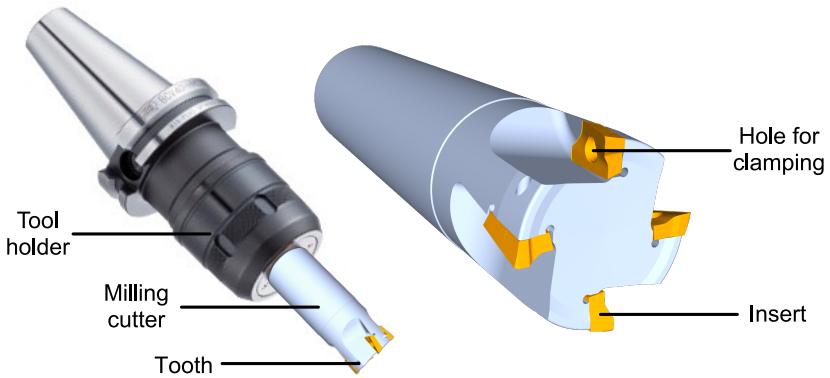

Fig. 2.1: Tool geometry elements of a four-tooth milling cutter

2.3.2 Tool cutting condition

During the milling process, a desired relative motion is achieved between the workpiece and the tool to form chips and remove them from the workpiece. In most circumstances, this relative motion is generated by a motion known as the cutting speed V_c in conjunction with an operation known as the feed f_z. The rotation axis of the cutting tool is perpendicular to the direction of the feed. Figure 2.2 illustrates a basic milling operation. The rotation frequency N (rpm) in milling is defined from V_c (m/min) and the radius of the cutter R (mm) as

$$N = \frac{1000 \cdot V_c}{2\pi R}. \tag{2.1}$$

The instantaneous angular speed ω (rad/s) is also equivalent to N as well as V_c; it can be expressed by converting the units as

$$\omega = \frac{2\pi N}{60} = \frac{1000 V_c}{60 R}. \tag{2.2}$$

The feed rate V_f (mm/min) of the tool is the speed of the relative motion between the cutter and the workpiece. It can be calculated by the feed per tooth f_z (mm/tooth), the teeth number n_z and rotational frequency N as

$$V_f = f_z \cdot n_z \cdot N. \tag{2.3}$$

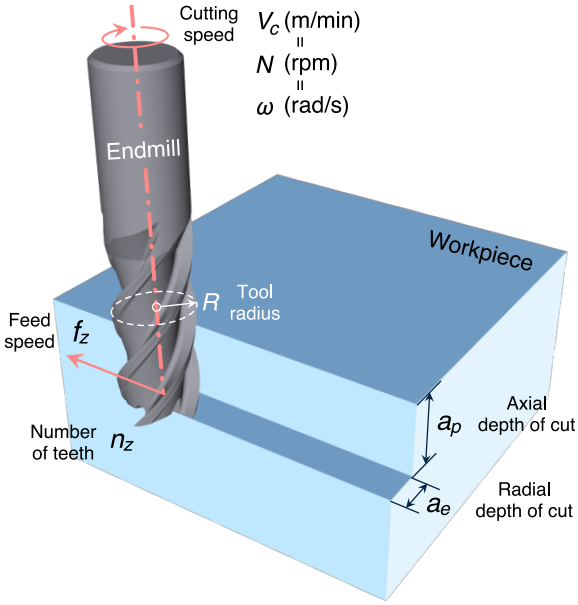

Fig. 2.2: Cutting condition in milling

The material removal rate MRR (mm^3/min) in milling is determined by multiplying the cross-sectional area of the cut and the feed rate V_f. Hence, if the milling operation involves a radial depth of cut a_e (mm) and an axial depth of cut a_p (mm), then the material removal rate is

$$MRR = a_e \cdot a_p \cdot V_f. \tag{2.4}$$

2.3.3 Tool wear and tool life

The tool can only be put into operation when its cutting edges are able to produce the part with specified surface finish and dimensional tolerances. Tool life is defined as the duration of cutting time after which the tool is no longer usable. In actual milling, there are several modes of tool failure, as listed below [Gro10]:

(i) **Fracture failure**

This failure mode commonly behaves in the form of brittle fracture and is most frequently seen at the tool point where the cutting force is overly high. Possible solutions are switching to a more ductile tool material or adjusting the milling parameters, For example, reducing the feed rate or the depth of cut, increasing the nose radius, etc.

(ii) **Temperature failure**

Temperature failure occurs often when the cutting temperature is too high. The material of the tool point is softened by the heat, which leads to the plastic deformation of the originally sharp cutting edge. The common way to prevent this kind of failure is to reduce the cutting speed and use coolant appropriately.

(iii) **Progressive wear**

During the milling process, the tool works intermittently, and the teeth periodically interact with the workpiece. As the cutting edge enters the workpiece, it is heated; and as it exits the workpiece, it begins to cool. At the same time, the cutting force on the tool varies periodically with the thickness of the chip. Such cycling of temperature and stresses produces alternating compression and tension on the tool, which leads to gradual fatigue and progressive wear.

If neither of the above two cases leads to a tool failure, then the cutting edge will eventually come to the end of its life due to continuous wear. Although some measures, such as proper use of lubricants, development of higher wear-resistant materials, etc., can be taken to slow down this failing process, the tool wear is always an inevitable phenomenon, as a gradual loss of tool material in the contact zone between the tool and the workpiece.

Of the three failure modes mentioned above, the first two need to be avoided as far as possible. In addition to significantly reducing the tool life, they can also cause sudden tool failure. As a result, the surface quality of the workpiece may be damaged, which might lead to the requirement of further rework or even possible scrapping of the whole workpiece. Ideally, therefore, tools should fail in a progressive wear pattern to achieve the theoretical maximum service life and the corresponding economic advantages.

The two main locations where progressive wear occurs on the cutter are the flank and the top rake face. The two common types of wear accordingly are the flank wear as shown in Figure 2.3(a) and the crater wear as shown in Figure 2.3(b) [Ano89]. It is necessary to note that if the insert is not replaced in time when these two above types of wear reach a certain level, the catastrophic deterioration will happen as shown in Figure 2.3(c).

Crater wear is a cavity in the leading edge surface caused by the friction of

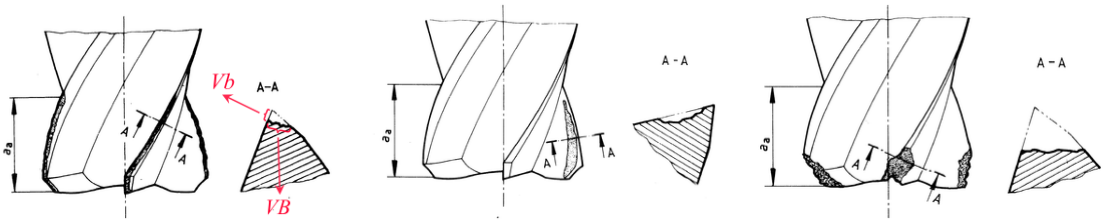

(a) (b) (c)

Fig. 2.3: Tool deterioration phenomena [Ano89]: (a) flank wear; (b) crater wear; (c) catastrophic failure.

continuous chip removal under heavy loads and high temperatures. Its severity can be assessed by measuring the depth or area of the crater. Flank wear, on the other hand, is caused by the friction between the rake face of the tool and the surface of the machined workpiece. As the flank wear increases, the area of contact between the tool and the workpiece becomes larger, which further causes a stronger rubbing between the two. The flank wear can be measured primarily as the width of the wear land on the flank VB, as shown in Figure 2.3(a). It is worth noting that the direct effect of tool wear on cut thickness comes from the length of the working part of the tip Vb in Figure 2.3(a), rather than VB. But the values of Vb and VB always remain proportional (the coefficient is related to the fixed angle of the cutting edge) and share the same wear trend. Since this manuscript is mainly concerned with the parameter affecting the chip in the calculation, the term flank wear is used to refer to Vb in the following discussion.

Flank wear occurs at the expense of losing a portion of the sharp cutting edge, which influences greatly the quality of the product and also is the most frequent situation in practice. Therefore, it is more important to control the flank wear than the crater wear.

Through extensive experience, a typical tool life curve has been concluded, as illustrated in Figure 2.4. Here, the relationship shown is concerned with flank wear, but the same trend holds for the crater wear as well.

A typical flank wear growth curve with milling time can be classified into three regions [Alt12]:

(i) **Initial wear zone**

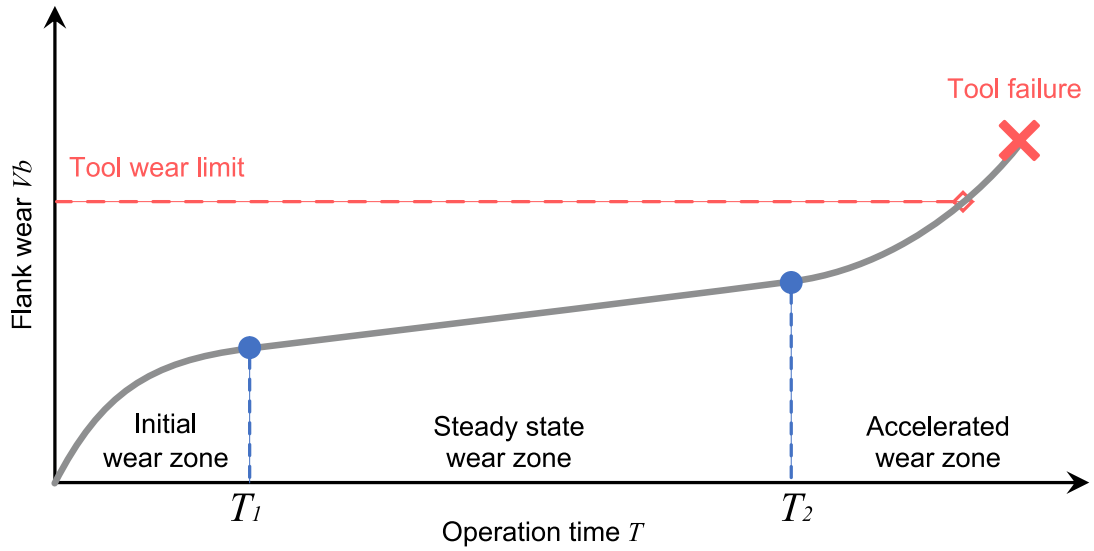

Fig. 2.4: Tool life (T) curves: variation of flank wear (Vb) land with operation time.

The first zone occurs at the very beginning of the cut and is a break-in period that may last only a few minutes. The brand new, extremely sharp cutting edge will undergo a rapid wear during this period until the friction between the tool and workpiece reaches a relative steady balance.

(ii) **Steady state wear zone**

Following the initial wear region, the flank wear on the second stage behaves at a fairly constant rate. Although in practice, the tool wear sometimes might deviate from the theoretical line shape, in approximation, the steady state wear phase can be depicted as a linear function of time for most cases. The slope of this function will be influenced by the workpiece material (e.g. hardness, ductility, etc.) and the cutting conditions (e.g. cutting speed, feed rate and depth of cut, etc.).

(iii) **Accelerated wear zone**

As the flank wear accumulates to a certain level, the slope of the curve increases exponentially. This marks the tool service has entered the failure zone. At this point, both the overall efficiency and quality of the milling process begin to decrease, accompanied by a significant increase in cutting temperature. The tool must be replaced before it reaches its critical limit to prevent catastrophic

tool deterioration.

On this basis, F.W. Taylor was the first to propose a calculation method for modelling tool life, as

$$T_t = C_t \cdot V_c^{-p'} \cdot (n_z \cdot f_z)^{-q'}, \tag{2.5}$$

where T_t (min) presents the estimation of tool life; C_t, p' and q' are constants depending on the given tool-workpiece material pair, the preset milling operation condition (e.g. feed rate, cutting speed, depth of cut, radial engagement of the cut, etc.) and the tool life criterion required.

Since the above constants rely on numerous conditions and immeasurable realistic factors may arise in practice, the industries cannot afford to take such a huge risk and apply the T_t simply as the time point for tool replacement. Hence, the Taylor equation can only be used as a reference. It is more important to monitor the current state of the tool in real-time, ensuring the quality of the machined piece as well as the full exploration of the tool life, which is also the topic of ongoing research in this thesis.

2.3.4 Chip formation behaviors

2.3.4.1 General case

The most direct and obvious reflection of the current tool condition is the corresponding chip formation on the workpiece. In the general case, it is assumed that each tooth produces a similar cut thickness.

Figure 2.5 uses an end mill (down milling) as an example, illustrating the tooth path in the material removal process. Since it does not involve oblique cutting, its three-dimensional motion is simplified to a two-dimensional orthogonal model. It appropriately omits certain unnecessary geometric complexities while retaining an efficient description of the machining mechanism.

The wedge-shaped cutting edge is perpendicular to the direction of cutting speed V_c. When the tool is forced into the material by the spindle, the workpiece at the tip

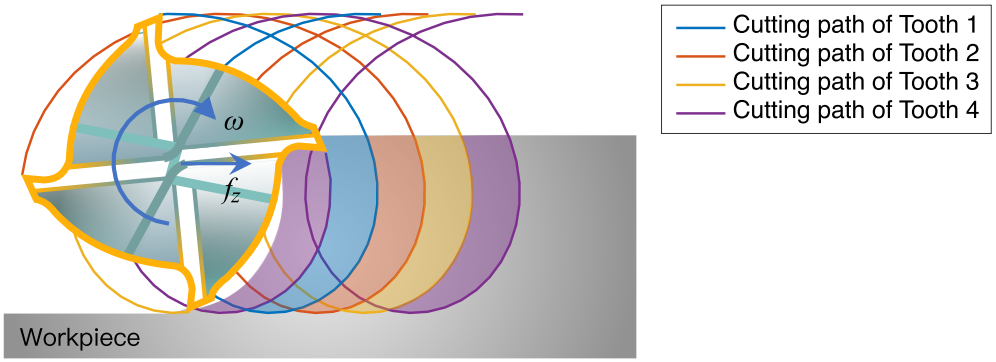

Fig. 2.5: Chip formation in general case

of the tool experiences material failure under the effect of shear deformation. With the further forces of shear, the failed partial material is completely separated from its parent material and is discharged as chips. In general, the typical geometry shape produced by milling is a plane surface. However, as it can be seen from the bottom of the curves, the resulting plane is actually formed by the tangents of multiple curves. Therefore, it is necessary to be careful about the match between the feed rate and cutting speed in order to avoid overly sparse curves, which might lead to ribbed leftover material on the surface of the workpiece.

In Figure 2.5, four trochoid-like curves present the paths traversed by the four teeth during the feeding. The painted areas with the corresponding colors on the workpiece are the chips produced as the teeth pass by. It can be observed that the cut thickness is not a constant, but varies in the radial direction of the tool. It will be designated as h_c. The cut thickness h_c appears to be thickest at the beginning and then gradually thins out.

Figure 2.6 specifies which distance geometrically corresponds to the cut thickness and the scenarios for points generation are summarized in Table 2.2. The exact value of the varying h_c can be solved by establishing a system of curve equations.

Assuming that the tool is rotating at a constant speed ω (if not, then integrate to calculate θ), and the rotational angle of the tool at a given moment t is

$$\theta = \omega t. \tag{2.6}$$

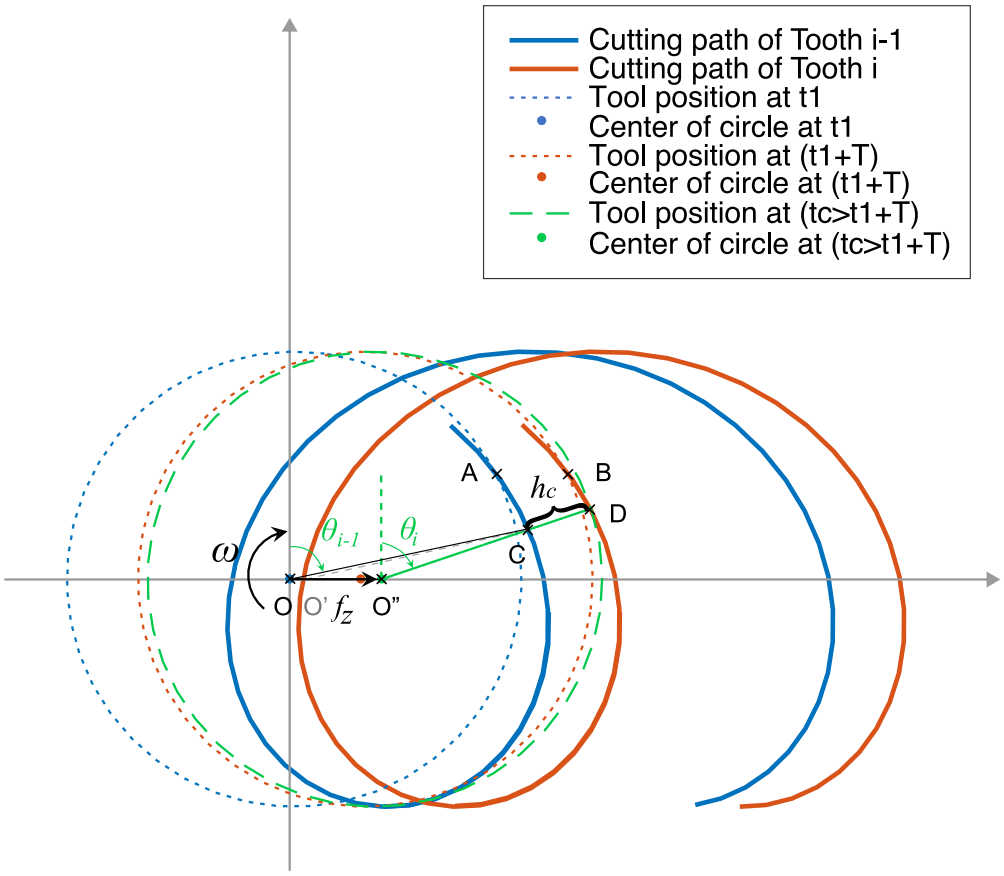

Fig. 2.6: Tool cut thickness

Point	**A**	**C**	**B**	**D**	**O**	**O'**	**O"**
Subject	Tooth $(i-1)$	Tooth $(i-1)$	Tooth i	Tooth i	Shaft	Shaft	Shaft
Time	t_1	t'	t_1+T	t_c	t_1	t'	t_c
	$(t_1 < t' < t_1+T < t_c)$						

Table 2.2: Scenarios for points generation

Taking the vertical upward direction as the standard rotation start, then the instantaneous immersion angle of the i^{th} teeth can be presented as

$$\theta_i(t) = \theta - \frac{2\pi}{n_z}(i-1), \tag{2.7}$$

where i is the subscript indicating the tooth counts $(i = 1, 2, \ldots, n_z)$. By splitting the tool movement into the superposition of its own rotation and feed motion, and with

the reference of the cycloid or trochoid modeling, the path of teeth can be represented as

$$\begin{cases} x_i(t) = \frac{n_z \cdot f_z \cdot \theta(t)}{2\pi} + R\sin\theta_i(t), \\ y_i(t) = R\cos\theta_i(t). \end{cases} \tag{2.8}$$

The blue solid curve and the red solid curve in Figure 2.6 were created in MATLAB from the above equations, representing the paths of the $(i-1)^{th}$ and i^{th} tooth, respectively. The blue dashed circle stands for the position of the cutter at the moment $t = t_1$, while the $(i-1)^{th}$ insert is at point A. As for the red dashed circle, it represents the position of the tool when $t = t_1 + T$, where T corresponds to the time of one tooth passage, defined as

$$T = \frac{2\pi}{n_z \cdot \omega}. \tag{2.9}$$

At this moment ($t = t_1 + T$), the i^{th} tooth is in the position of point B, which is the same location of the $(i-1)^{th}$ tooth on the tool circumference at $t = t_1$, but superimposed with the translation of the feed. When the process continues to a certain time t_c ($t_c > t_1 + T$), the i^{th} insert follows the red solid curve passing from point B to point D. The corresponding tool position at $t = t_c$ is the green dashed circle, whose circle center is marked as point O". The intersection of the line O"D to the path of the $(i-1)^{th}$ insert is noted as point C, which corresponds to the position of the $(i-1)^{th}$ tooth at the moment t', and the center of the circle of the tool at t' is noted as O'. The distance of CD is the cut thickness formed by the i^{th} tooth at $t = t_c$. The coordinates of the point O", point D and point C can be express as

$$\begin{cases} x_{\mathrm{O"}} = \frac{n_z f_z \cdot \theta(t_c)}{2\pi}, \quad y_{\mathrm{O"}} = 0, \\ x_{\mathrm{D}} = \frac{n_z f_z \cdot \theta(t_c)}{2\pi} + R\sin(\theta_i(t_c)), \quad y_{\mathrm{D}} = R\cos(\theta_i(t_c)), \\ x_{\mathrm{C}} = \frac{n_z f_z \cdot \theta(t')}{2\pi} + R\sin(\theta_{i-1}(t')), \quad y_{\mathrm{C}} = R\cos(\theta_{i-1}(t')). \end{cases} \tag{2.10}$$

Since the point O", D and C are in the same straight line, the corresponding equation can be formulated as

$$\frac{x_{\mathrm{C}} - x_{\mathrm{O"}}}{y_{\mathrm{C}} - y_{\mathrm{O"}}} = \frac{x_{\mathrm{D}} - x_{\mathrm{O"}}}{y_{\mathrm{D}} - y_{\mathrm{O"}}}. \tag{2.11}$$

Substituting Equation 2.10 into Equation 2.11, it can be simplified as

$$\frac{n_z f_z(\theta(t') - \theta(t_c))}{2\pi}\cos(\theta_i(t_c)) + R\sin(\theta_{i-1}(t') - \theta_i(t_c)) = 0. \tag{2.12}$$

Since Equation 2.12 contains both trigonometric and algebraic terms (transcendental equation), the only unknown t' in the equation can be solved with high precision by approximation algorithms, such as the bisection method or the Newton–Raphson method. This enables the calculation of the cut thickness as

$$h_c = \sqrt{(x_\mathrm{D} - x_\mathrm{C})^2 + (y_\mathrm{D} - y_\mathrm{C})^2}. \tag{2.13}$$

Although the numerical method is accurate, the closed-form cut thickness model provides an approximate solution for ease of use and better physical understanding of the milling process. By applying the cosine law to the triangle $\triangle$OO"C, the cut thickness can be geometrically presented as

$$\begin{aligned} h_c &= \overline{O"D} - \overline{O"C} \\ &= \overline{O"D} + \overline{O'O"} \cdot \sin\theta_i - \sqrt{\overline{O'C}^2 - \overline{O'O"}^2\cos^2\theta_i}, \end{aligned} \tag{2.14}$$

where

$$\overline{O"D} = \overline{O'C} = R; \tag{2.15}$$

$$\overline{O'O"} \approx \overline{OO"} = f_z. \tag{2.16}$$

For traditional milling, the tool radius is usually much larger than the feed ($2\pi R \gg n_z f_z$), where the distance between OO' can be neglected and the actual distance between OO", noted as f_{real}, can be simply replaced by f_z [MAR41; CC13]. Then the cut thickness can be approximated as [MAR45]

$$h_c \approx f_z \sin\theta_i + R - \sqrt{R^2 - {f_z}^2\cos^2\theta_i} \tag{2.17}$$

$$\approx f_z \sin\theta_i \qquad \text{if } -\frac{17}{36}\pi < \theta_\mathrm{i}(\mathrm{t}) < \frac{17}{36}\pi. \tag{2.18}$$

For micro-end-milling, a similar equation using precise feed per tooth f_{real} can

be rewritten as [KZ13]

$$\begin{aligned} h_c &= f_{real}\sin\theta_i + R - \sqrt{R^2 - f_{real}^2\cos^2\theta_i} \\ &\approx f_z\sin\theta_i - \frac{n_z {f_z}^2\cos\theta_i\sin\theta_i}{2\pi R + n_z f_z\cos\theta_i} + R - \sqrt{R^2 - \left(\frac{2\pi R f_z\cos\theta_i}{2\pi R + n_z f_z\cos\theta_i}\right)^2} \end{aligned} \quad (2.19)$$

2.3.4.2 Case including consideration of the tool defects

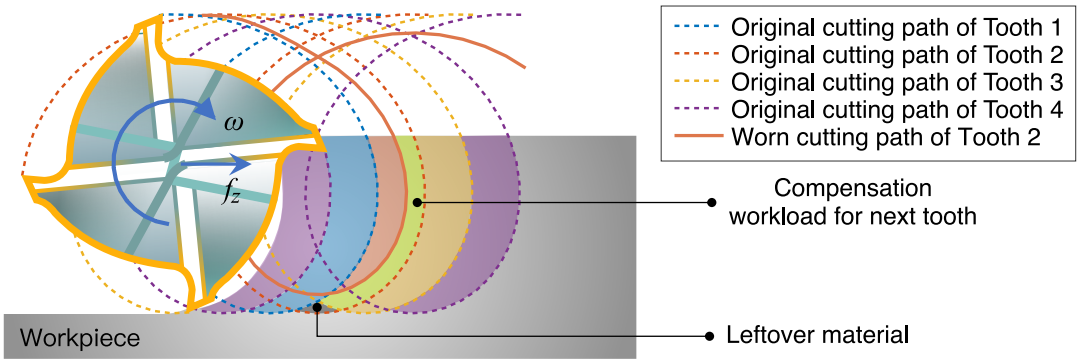

Fig. 2.7: Chip formation with flank wear

Theoretically, each tooth of the cutter is supposed to chop the same amount of material as shown in Figure 2.5. However, in practice, the tool can easily have defects that change the cut thickness like the illustration in Figure 2.7. The dashed line corresponds to the trajectory of the tooth movement under the normal condition in Figure 2.5, where the trajectory of the 2^{nd} tooth is marked with a red solid line after it has become worn. It can be seen that due to the flank wear, the chips of the 2^{nd} tooth (red-colored zone) become thinner and the part of the undone workload that it left (green-colored zone) is piled up to the next tooth. The 3^{rd} insert carries the extra burden of the additional work, but it can not fully compensate for the error caused by the 2^{nd} tooth. For each revolution afterward, a small strip of ribbed material (black colored zone) will be left on the machined surface.

The defect of the cutter might refer to the tool's runout, whose teeth lengths are unequal in the first place. Another possible defect is that the teeth are distributed

in an uneven angular position on the circumference of the tool. All of the above are inborn defects brought about by limited manufacturing precision, which are considered minor and controllable compared to the subsequent flank wear or even the break of the insert.

When considering the flank wear phenomenon of the tool, the wear amount of the current i^{th} tooth Vb_i and the previous $(i-1)^{th}$ tooth Vb_{i-1} needs to be aggregated into the cut thickness model. The condition mentioned in Equation 2.15 is changed to

$$\overline{O"D} = R - Vb_i \quad \text{and} \quad \overline{O'C} = R - Vb_{i-1}. \tag{2.20}$$

With the expansion using Taylor series, the cut thickness includes wear condition is

$$h_c* = f_{real} \sin\theta_i + (R - Vb_i) - (R - Vb_{i-1}) \cdot \sqrt{1 - \left(\frac{f_{real}\cos\theta_i}{R - Vb_{i-1}}\right)^2} \tag{2.21}$$

$$\approx f_{real} \sin\theta_i + Vb_{i-1} - Vb_i + \frac{f_{real}^2 \cos^2\theta_i}{2(R - Vb_{i-1})}. \tag{2.22}$$

In some severe worn cases, if $Vb_i > h_c + Vb_{i-1}$, then h_c* is numerically negative, which means the tooth i does not experience the chip load at all. Depending on the scenarios and the requirements, the feed with diverse accuracy (Equation 2.13 - 2.19) can be chosen to solve the equation. In the studied case, Equation 2.21 can be approximated as

$$h_c* \approx f_z \sin\theta_i + Vb_{i-1} - Vb_i. \tag{2.23}$$

2.3.5 Milling force model

It is already known that different flank wears make the material to be removed unevenly distributed between the teeth. From the inverse deduction method, the parameters related to the cut thickness variation can be considered as logical external expressions for the cutting state. Since it is difficult to detect the cut thickness in real-time, the signals closely related to the chip formation, such as cutting forces and instantaneous angular velocities, etc., can be used as a reasonable source for the analysis of the tool condition. It possesses the potential to be a versatile method for related mechanisms, and the total cutting force is chosen here as an example.

Merchant established an orthogonal cutting model by assuming the shear zone is a very thin plane [Mer45]. The resulting force of the tool on the chip is noted as $\boldsymbol{F}$, whose vector composition can be interpreted into three deconstructions from different aspects, as listed below [Gro10]:

(i) $\boldsymbol{F} = \boldsymbol{F_s} + \boldsymbol{F_n}$
$\boldsymbol{F}$ can be decomposed into a shear force $\boldsymbol{F_s}$ along the shear plane and a normal force to shear $\boldsymbol{F_n}$. These two explain how the material is failed and discards the chips under the shear deformation. The angle between the shear plane and the work plane is designated as the shear angle ϕ_{c}.

(ii) $\boldsymbol{F} = \boldsymbol{F_u} + \boldsymbol{F_v}$
$\boldsymbol{F}$ can also be decomposed into a friction force $\boldsymbol{F_u}$ along the rake face of the tool and a normal force to friction $\boldsymbol{F_v}$, both of which describe the process of chip flow along the rake face causing the crater wear. The angle between the rake face and the normal to the reference plane is α_{r}, and the angle formed by the vector triangle of $\boldsymbol{F}$, $\boldsymbol{F_u}$, $\boldsymbol{F_v}$ is denoted as the friction angle β_{a}.

(iii) $\boldsymbol{F} = \boldsymbol{F_r} + \boldsymbol{F_t}$
$\boldsymbol{F}$ can likewise be decomposed into a tangential force $\boldsymbol{F_t}$ along the direction of the instantaneous cutting speed and a radial force $\boldsymbol{F_r}$ perpendicular to $\boldsymbol{F_t}$. Both of these can be seen as the tooth tip rubbing against the newly machined surface, which has a significant effect on flank wear.

As the cutting forces diagram illustrated in Figure 2.8(b), the resulting force F can be numerically expressed as

$$F = \frac{F_s}{\cos\left(\phi_{\mathrm{c}} + \beta_{\mathrm{a}} - \alpha_{\mathrm{r}}\right)} = \frac{\tau_{\mathrm{s}} \cdot a_p \cdot h_c}{\sin\phi_{\mathrm{c}} \cdot \cos\left(\phi_{\mathrm{c}} + \beta_{\mathrm{a}} - \alpha_{\mathrm{r}}\right)}, \tag{2.24}$$

where τ_{s} is the corresponding shear stress on the shear plane.

Since only the geometry of the tool is known beforehand, and the friction angle and shear angle are not enough to be accurately predicted. Hence, it is customary to define the cutting forces mechanistically as a function of the cutting conditions and

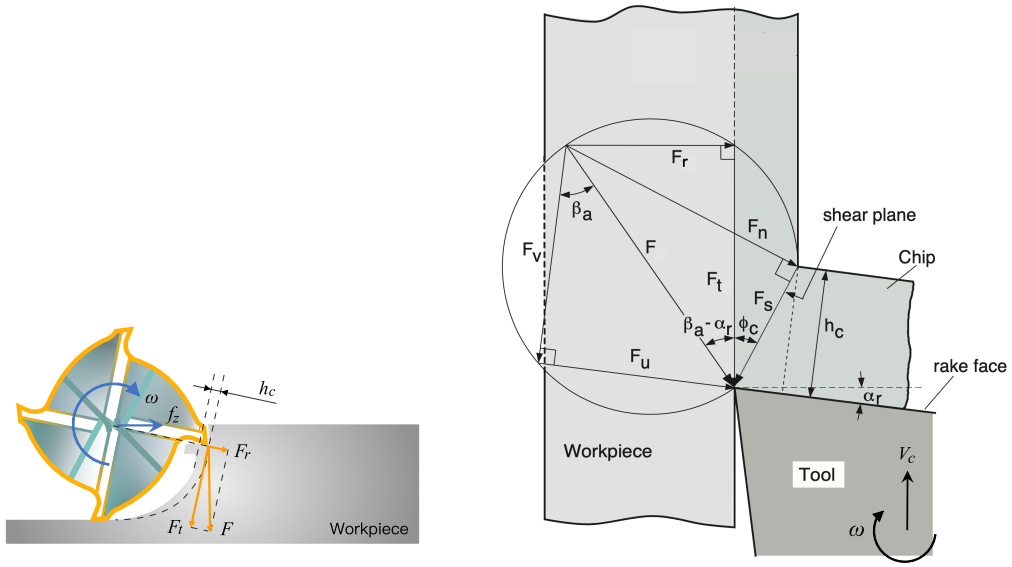

(a) (b)

Fig. 2.8: Forces during milling process: (a) general preview; (b) partial zoom [Alt12].

the cutting constant as [Rit+14; KDL82]

$$\begin{cases} F_t = K_{tc} \cdot a_p \cdot h_c + K_{te} \cdot a_p; \\ F_r = K_r \cdot F_t, \end{cases} \tag{2.25}$$

where

$$\begin{cases} K_{tc} = \frac{\tau_s \cdot \cos(\beta_a - \alpha_r)}{\sin \phi_c \cdot \cos(\phi_c + \beta_a - \alpha_r)}; \\ K_r = \tan(\beta_a - \alpha_r). \end{cases} \tag{2.26}$$

The radial force F_r is proportional to the tangential force F_t. K_{tc} and K_r are the cutting constants contributed by the shearing action in tangential and radial directions, respectively, and K_{te} is the edge coefficient that does not contribute to the shearing and is directly calibrated from metal cutting experiments for a tool-workpiece pair [Alt12; FDK84].

Taking the flank wear into account on this basis, by substituting the above

equations, the total cutting force corresponding to the i^{th} tooth can be derived as

$$\begin{aligned} F(\theta_i) &= \sqrt{[F_r(\theta_i)]^2 + [F_t(\theta_i)]^2} \\ &= a_p \cdot h_c * \cdot K_{tc} \cdot \sqrt{{K_r}^2 + 1} + a_p \cdot K_{te} \cdot \sqrt{{K_r}^2 + 1} \\ &= a_p \cdot h_c * \cdot K_c + a_p \cdot K_e \\ &= a_p \cdot (f_z \cdot K_c \cdot \sin\theta_i + K_e) + a_p \cdot K_c \cdot (Vb_{i-1} - Vb_i) \\ &= F_{basic}(\theta_i) + \Delta F(\theta_i), \end{aligned} \tag{2.27}$$

where

$$F_{basic}(\theta_i) = \overline{F} + \Psi_F(\theta_i) = a_p \cdot K_e + a_p \cdot K_c \cdot f_z \cdot \sin\theta_i. \tag{2.28}$$

and

$$\Delta F(\theta_i) = a_p \cdot K_c \cdot (Vb_{i-1} - Vb_i). \tag{2.29}$$

The term $F_{basic}(\theta_i)$ stands for the standard milling force, with $\overline{F}$ corresponding to the constant force and $\Psi_F(\theta_i)$ representing the shape of the force during the cutting. ΔF_i embodies the part of the cutting force increased or decreased due to wear. The term $(Vb_{i-1} - Vb_i)$ actually emphasizes the similarities and differences between two adjacent teeth, which will make the subsequent process easier and also makes the results more intuitive.

To observe the state and corresponding behavior of the tool in milling, two periods of signals presenting the 1^{st} and the 98^{th} rotation cycles respectively are extracted and displayed in Figure 2.9.

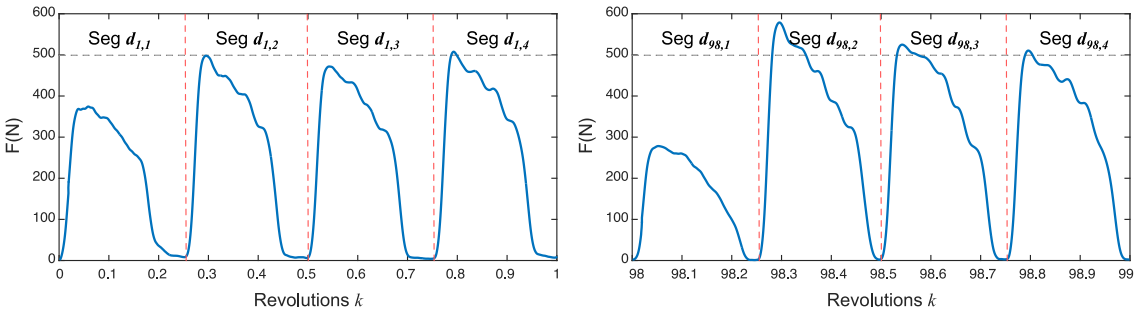

(a) (b)

Fig. 2.9: Force behavior in different tool conditions: (a) relatively healthy state at the 1^{st} revolution; (b) severe worn state at the 98^{th} revolution.

Since the tool used to collect the data was not a brand-new cutter, there were

already varying degrees of slight wear between the cutting inserts at the beginning. Combined with the typical tool life curve in Section 2.3.3, the tool in the period presented by Figure 2.9(a) has passed the initial wear stage and is in the stable wear state. Besides Figure 2.9(b) shows significant degradation of the 1^{st} tooth. Although it still maintains the characteristic waveform of down milling (the tooth experiences the maximum chip load at entry, and then the load gradually decreases), its value drops significantly compared to Figure 2.9(a). In contrast, the cutting force of the 2^{nd} insert increased remarkably, and in the meantime, there was also a small rise for the 3^{rd} tooth.

This is due to the fact that when the previous tooth wears or breaks, the cutting conditions of the corresponding process often tend to be modified. The next insert will be subjected to compensatory overload. The most intuitive change is between two consecutive teeth, but it may also affect a third or other subsequent teeth. Such a performance matches both the modeling of chip generation in Section 2.3.4 and the cutting forces in Section 2.3.5, establishing a good basis for the subsequent analysis.

2.4 Constructive elements of TCM system

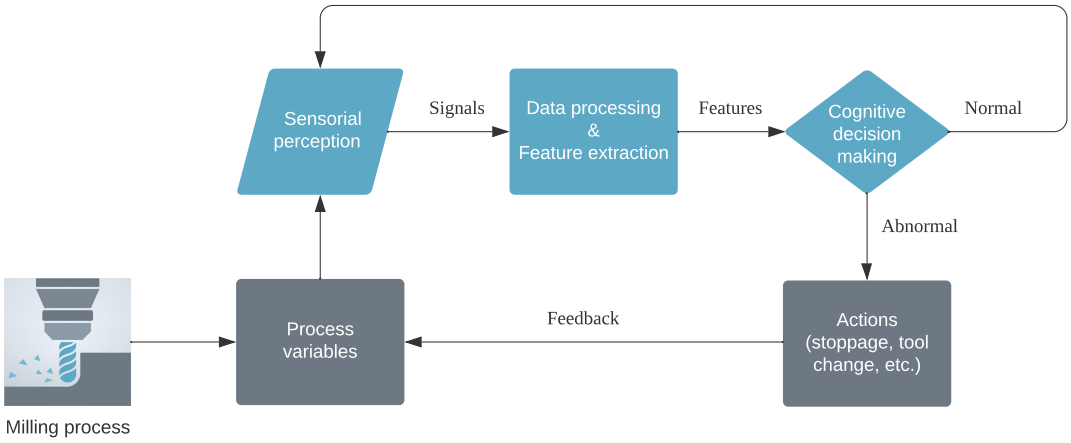

Fig. 2.10: Basic process flow of TCM in milling processes

The evaluation of the cutting tool condition discussed in this thesis refers to the identification during the machining process rather than under the standstill condition.

Hence, it is a challenging task as each manufacturing operation exhibits nonlinear time-varying characteristics. Rehorn et al. [RJO05] discuss the TCM system in terms of different types of cutting processes (turning, face milling, drilling, end milling, etc.). With the development of sensors, Teti et al. [Tet+10] then breaks the discussion of monitoring into sections and outlines the unit components and general structure for composing a sensor-based TCM system.

A typical machining process is considered to operate according to the following principles. Process variables in the cutting area, such as cutting force, angular velocity, vibration, temperature, etc., are influenced by the state of the cutting tool. Appropriate physical sensors can be used to acquire these potentially effective data for monitoring the machining process. The measured signals are conditioned and processed, either analogically or digitally, with the aim of extracting or generating characteristic signatures related to the tool state or material removal process. Such real-time features are then evaluated by a cognitive decision system and provide the final diagnosis in order to advise the operator or directly perform the appropriate optimization or correction actions. The entire workflow is shown in Figure 2.10.

Many later publications followed the same logic of discussion. For example, Zhou et al. [ZX18] described a similar process and supplemented it with a number of decision models from the rapid advancement of deep learning in recent years; while Lauro et al. [Lau+14] focused more on summarizing the development of sensor and signal acquisition processing. With the growth of ICT infrastructures based on manufacturing domains, this set of analytical logic has been formally incorporated into PHM (Prognostics and Health Management) standards, such as the ISO 13374 series [Ano17], to respond to industrial needs.

The three basic elements for tool state supervision [Gar+13] are: the correct choice of sensors for recording the signal in the monitoring environment, the accurate data manipulation and characterization, and the reliable decision-making models with minor/low prediction of errors. They will be discussed in the following three subsections.

2.4.1 Selection of the sensor system

According to Teti et al. [Tet+10], measurement techniques used for TCM are traditionally divided into two types:

- Direct measurement: where laser [RMK98; TG08] and optical [Lau+13; DPS16] sensors are often applied to capture data with high accuracy on the machining surface, the cutting edge, or even the geometry of the chips. These methods are commonly only implemented in laboratories due to environmental constraints such as illumination and coolant usage in practical production and their high expense.

- Indirect measurement: where the actual wear value is subsequently deduced based on various related inputs, such as cutting force [KK97; Kar07], vibration [Sev+15; Yuq+15], motor current [Sev+11; Lee99], acoustic emission [MA08; Ren+14], temperature [OC01; SS12], collected by different sensors. It is less accurate than the direct method but is also less complex and more suitable for practical applications.

Based on this background, four major categories of sensors that are relatively mature and widely used in today's TCM systems [AR10] are explored in detail: dynamometers, accelerometers, acoustic emission (AE) sensors, and current sensors.

Dynamometers

Dynamometer is a device that can measure the cutting forces transmitted by the rotating shaft of the CNC machine center. The cutting forces, which are very sensitive to the conditions of the cutter, are deemed to be the best responding variable of the milling process [PA04; Don+06] (other signals such as vibration, acoustic emission, etc. are caused by cutting force). In fact, force measurement occupies a large part of the TCM literature. Kim et al. [KK97] describe cutting force as two parts:

- Static part: which presents the average value of the cutting force.

- Dynamic part: which corresponds to the superimposed fluctuation of the cutting force.

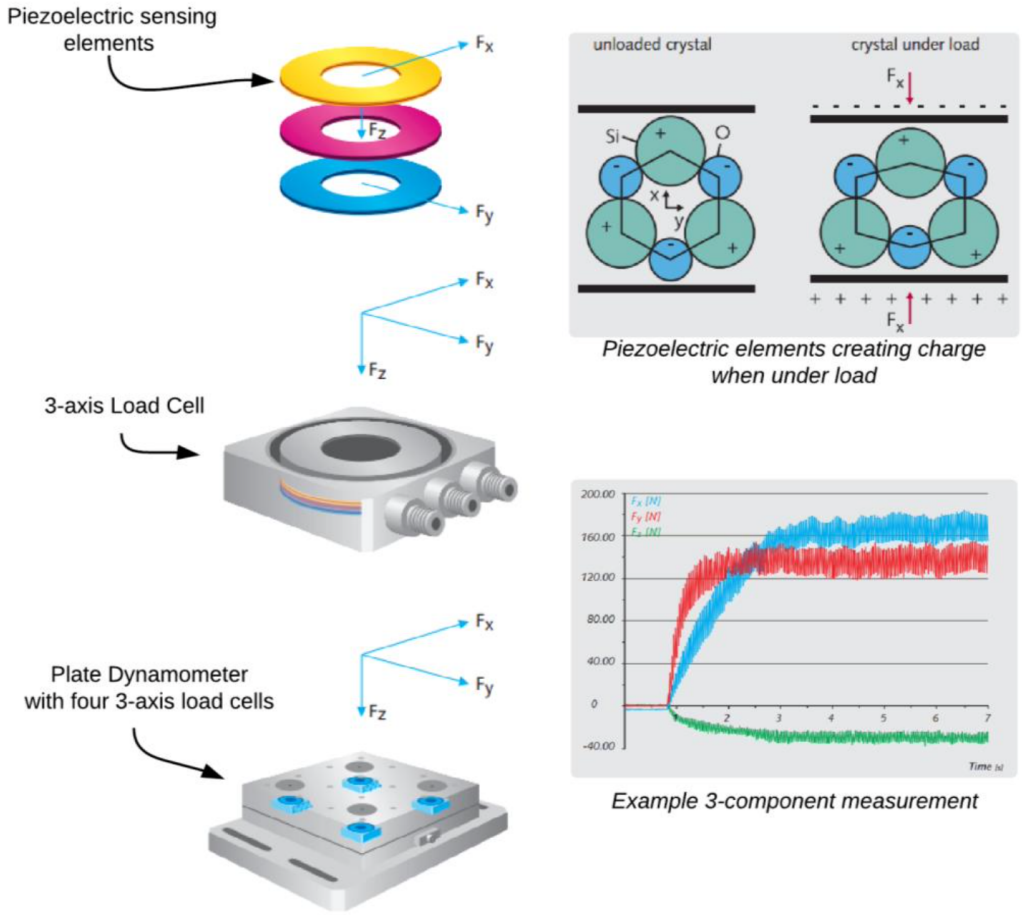

Fig. 2.11: Kistler 3-component force dynamometer[Kisb]

The measurement of the static part already provides an effective feedback on tool conditions during milling. Tansel et al. [Tan+00] reported that when cutting tools continuously lose their sharp edges, the wear of the tool flank will lead to an increasing contact area between the cutting edge and the workpiece, thus causing a gradual rise in the average values of friction and cutting forces. The dynamic part, on the other hand, can further satisfy the need for higher monitoring accuracy [SMR19]. Liang et al. [LHL04] pointed out that when a substantial breakage of the insert occurs, there is a dynamic process in which the cutting force increases instantaneously and then falls back. The magnitude of this drop depends on the reduction of the cutting chip volume due to partial breakage. Kim et al. [KK97]

developed a combined-type tool dynamometer that can measure the static cutting force and the dynamic cutting force together by use of strain gauges and a piezo-film accelerometer. Given the growing need for measuring dynamic response and the increasing stiffness of processing devices, piezoelectric sensors have been preferred over strain gauges in recent years. As shown in Figure 2.11, Kistler's three-component plate dynamometer has several 3-axis force load piezoelectric cells evenly distributed in the plate. These piezoelectric sensing elements produce a charge proportional to the load in the direction of measurement [Kisb]. Huang et al. [HMK15] detected the tool breakage in end milling operation based on the cutting forces obtained by the piezoelectric dynamometer.

The measurement accuracy has made the multi-axis dynamometers desirable for laboratories. But their mounting characteristics, which would limit the size of the workpiece, as well as their high cost, cause an uncommon use of them in commercial applications [Sta+16; Gha+11].

Accelerometers

Vibration measurements acquired by accelerometers are often used for chatter detection and are also widely published in TCM. This is because the vibration signatures satisfy the conditions of robustness, reliability, and applicability. Meanwhile, the accelerometers are inexpensive and easy to install [Dim02]. Since vibration is originally caused by the cutting forces, under ideal conditions, it can provide a periodic signal shape similar to the cutting forces for the diagnosis of tool wear [Sev+15]. During machining, the wear of the insert initially increases the elastic deformation of the workpiece material, causing frictional damping that reduces the vibration to a small extent. When the flank wear exceeds a certain threshold, the increased cutting force due to strong friction on the contact surface becomes dominant and excites an increase in vibration amplitude [EKT03].

Many studies have demonstrated the feasibility of using vibration signals for TCM in the milling process. Wang et al. [Wan+14] conducted milling experiments on Ti6Al4V alloy. Vibration signals corresponding to four tool wear states are collected. Their features are extracted in the time and frequency domains for TCM analysis. Hsieh et al. [HLC12] demonstrated that when coupled with appropriate

feature extraction and classifiers, spindle vibration signals can distinguish the different tool conditions in the micro-milling process. Bisu et al. [Bis+12] decomposed the vibration sources and proposed the vibration envelope method to perform a complete dynamic analysis of various components characterizing the machine tool. However, at the same time, they emphasized that vibration signals are the result of mixing different sources, making it difficult to identify the damage state of a specific component.

In fact, there are indeed many issues in the practical application of monitoring vibration levels to assess tool conditions. In particular, forced vibrations caused by machine components, such as unbalanced rotating parts, inertial forces in reciprocating parts, etc., are not related to the state of the cutter [Lau+14]. Despite the advantages of accelerometers such as cheapness and ease of installation, the vibration source diversity, complexity, and difficulty of filtering make it hard to target the desirable measurements [CK17].

AE sensors

Acoustic emission is the phenomenon of radiation of elastic waves in solids. The accumulated elastic energy is rapidly released when the internal structure of material undergoes irreversible changes due to aging, temperature gradients, or external mechanical forces [AR10]. The released energy is generally in the range of 1 kHz to 1 MHz and creates acoustic emission in the form of mechanical waves [Chi+00].

Many research has shown interest in the application of AE measurement to TCM during milling processes. On the one hand, the AE signal can take into account the primary (due to chip formation), secondary (due to friction between tool and chip), and tertiary (due to friction between tool flanks and workpiece) cutting zones [Lu08]. On the other hand, the AE technique has a superior signal-to-noise ratio and higher sensitivity compared to other sensors as shown in Figure 2.12. Marinescu et al. [MA08] reported the possibility of using AE sensory measures to monitor the surface integrity of tools and workpieces, and compared it with conventional monitoring methods. In reference [Li02], Li inventories and reviews a range of issues concerning AE generation, classification, signal processing, and several methods for estimating tool wear using AE sensors.

Although AE sensors are inexpensive and easy to install, Jemielniak [Jem00] noted that the range of cutting operations must be tested in advance in order to adjust the amplifier gain and avoid signal distortion due to sensor overload. According to Zhou et al. [ZX18], intermittent cutting leads to the appearance of AE signal spikes, which complicates the analysis. Other studies have argued that the use of AE sensors for tool wear is controversial and that they are better suited as additional sensors for increased reliability, as they are more sensitive to noise and changes in cutting conditions than to the condition of the tool itself [ZV14].

Current sensors

Current sensors can sense changes in cutting force indirectly through the torque output from the spindle motor. Compared to dynamometers, current sensors do not require extensive wiring and have no limitations on the size of the workpieces, making them simpler and more economical to apply [Lau+14]. However, due to the inertia of the motor rotor, the sensing bandwidth of current sensors is limited, it cannot observe the high-frequency component of the cutting force, and is only suitable for monitoring low-speed events. With the development of high-speed machining, current sensors are more and more considered as a complementary information for diagnosing tool wear [Gho+07; AR10].

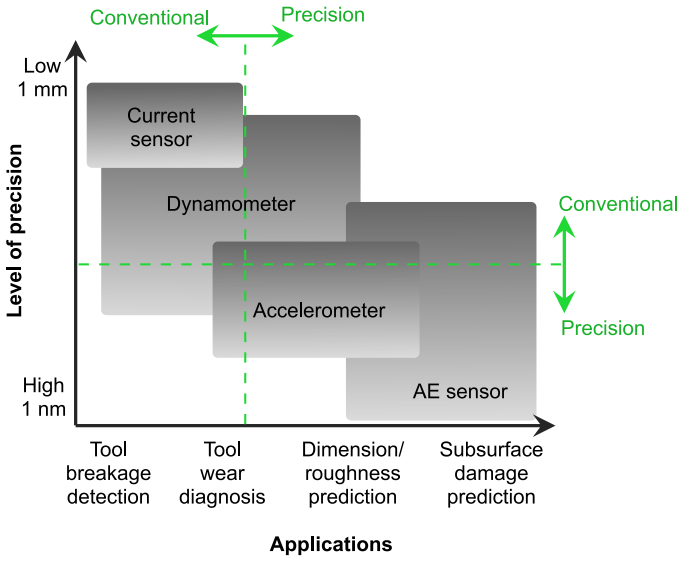

Fig. 2.12: Sensor application versus level of precision

Combining the results of Ertekin [EKT03] using three different types of materials to test dynamometer, AE sensor, and accelerometer, along with the information above, the application and robustness of the different sensor signal characteristics are summarized in Figure 2.12. Considering that the focus of this thesis is on the analysis of tool wear/breakage, and the data acquisition is performed in the laboratory, as well as the accuracy, reliability, and response speed of the signal sources, the cutting force based on a dynamometer is finally selected for taking the measurements. For the next step in the future, it is appropriate to use signals closer to actual production to validate the indicators.

2.4.2 Feature extraction

After the sensor is selected, the acquired analog signal will normally be pre-processed, such as digital conversion, low-pass/band-pass filtering, etc., for preparation of the feature extraction. The signals need to be converted into adequately characterized descriptors, for two reasons. One is to closely represent the tool condition, and the other is to significantly reduce the dimensions of the original information.

Many research works have been done to study various feature extraction approaches in the time, frequency, and angular domains. The descriptor output from the feature extraction module will become the input of the monitoring model module and thus construct the TCM system.

2.4.2.1 Time domain analysis

Time domain analysis refers to a display of response parameters as a function of time. The signal obtained by equal time measurements is univariate and can present an overall picture of the time series under study. A measuring signal $x(t)$ containing N samples can be generally described as

$$x_j = x(t_0 + (j-1)\Delta t), \tag{2.30}$$

where $j = 1, 2, ..., N$; t_0 is the start time point; Δt is the sampling interval. To prevent or reduce aliasing, the Nyquist-Shannon theorem states that a sufficient condition

for signal reconstruction requires a sampling frequency greater than twice the signal bandwidth.

Time domain features usually necessitate minimal computation, because they can be extracted directly from any time-record based data. The most commonly used time domain features are summarised in Table 2.3, which include (1) the arithmetic mean, the average value, the magnitude; (2) the root mean square (RMS); (3) the variance (or standard deviation); (4) the skewness; (5) the kurtosis; (6) the signal power; (7) the peak-to-peak or peak-to-valley amplitude; (8) the crest factor [Tet+10; CBA10]. These features serve as statistical summaries reflecting the grand picture of the targeted signal. In the TCM aspect, time domain features are mostly established for AE and cutting force signals [Moh+20].

Wang et al. [WGY13] calculated five indicators containing RMS, variance, peak-to-peak value, kurtosis, and skewness from force signals as feature vectors to depict the time domain characteristic for TCM. Kuljanic et al. [KST08] reported a chatter indicator based on the standard deviation of the signal in time. Mohanraj et al. [Moh+19] adopted vibration signatures in the time domain as representatives to analyze the tool condition under optimum process parameters utilizing various coolants. The results show that the arithmetic mean and the skewness rise continuously with increasing flank wear.

Besides the statistical features, the more advanced feature generating approach in the time domain is time series modeling. The main techniques of time series analysis frequently used in TCM are the auto-regressive (AR), moving average (MA), and auto-regressive moving average (ARMA) models [BSM07]. Due to the high computing load inadequate for online process monitoring, the 1^{st} or the 1^{st} and the 2^{nd} orders of AR, MA or ARMA coefficients are often used as the feature representatives [Don+06]. Nouri et al. [Nou+15] proposed an effective algorithm based on MA from cutting force data to estimate the tool wear in face milling. Chelladurai et al. [CJV08] applied ARMA analysis to validate the emulation differences between actual and created artificial flank wears.

The features extracted in the time domain have corresponding well-defined physical meanings and generally present linear characteristics, which are sufficient for stationary machining like turning [ZSH09]. Yet it is not suitable for non-stationary

Features	Description	Comments
Mean	$\bar{x} = \frac{1}{N}\sum_{j=1}^{N} x_j$	Arithmetic mean of the signal.
Root mean square	$x_{\mathrm{RMS}} = \sqrt{\frac{1}{N}\sum_{j=1}^{N} x_j^2}$	Statistical measure of the intensity of the signal.
Variance	$\sigma^2 = \frac{1}{N-1}\sum_{j=1}^{N} (x_j - \bar{x})^2$	Non-negative value indicating the spread of the signal data around its mean value. Equal to the standard deviation squared.
Skewness	$Sk = \frac{1}{N}\frac{\sum_{j=1}^{N}(x_j-\bar{x})^3}{\sigma^3}$	A measure of the asymmetry of the probability distribution of the signal.
Kurtosis	$Ku = \frac{1}{N}\frac{\sum_{j=1}^{N}(x_j-\bar{x})^4}{\sigma^4}$	A measure of the "peakedness" of the probability distribution of the signal. Higher kurtosis means more of the variance is the result of infrequent extreme deviations, as opposed to frequent modestly sized deviations.
Signal power	$P = \frac{1}{N}\sum_{j=1}^{N} x_j^2$	Equivalent to the square of the RMS value.
Peak to peak amplitude	$x_{\mathrm{pk-pk}} = \max(x_j) - \min(x_j)$	The difference between the maximum amplitude and minimum amplitude of the signal.
Crest factor	$x_{\mathrm{CF}} = \frac{\max(x_j)}{x_{\mathrm{RMS}}}$	x_{CF} provides a value of the peak amplitude relative to the signal RMS.

Table 2.3: Time domain features and descriptions

machining, which is however the most common situation in industrial plants, including end milling, as discussed in this thesis.

2.4.2.2 Frequency and time-frequency domain analysis

Through fast Fourier transform (FFT), the time domain data can be transferred into the frequency domain for the investigation of frequency structure and harmonic

components of the signal. The main advantage of carrying signal processing in the frequency domain over the time domain is its capacity for spectrum display, which allows the easy reorganization and segregation of the interest frequency components. Similar to the study in the time domain, data that have been converted to the frequency domain can also provide frequential statistics. A power spectrum $s(f)$ calculated by the square of FFT magnitude of $x(t)$ can be written as

$$s_j = s(f_0 + (j-1)\Delta f), \tag{2.31}$$

where $j = 1, 2, ..., N$; f_0 is the beginning frequency of the corresponding spectrum; Δf is the sampling spacing. The general statistical features are listed in Table 2.4 [CBA10; Bin+09].

Vibration and sound signals are usually the object for feature extraction in frequency domain analysis. Lu and Kannatey-Asibu [LK02] use audible sound generated from the cutting process as analyzing source for monitoring tool wear during turning. Through the observation of the microphone and accelerometer power spectrum, the energy distribution for sharp and worn tools is easily discernible from the sound and vibration signals. However, when confronted with nonstationary signals whose frequency varies with time, frequency-domain methods focus only on the feature information of the spectrum perspective and can lose sight of the temporal information of the data.

To overcome the shortcomings mentioned above, many researchers turned to the time-frequency domain analysis based on wavelet transform (WT) for feature extraction in TCM for milling processes [ZYN15]. Wavelet transform enables the decomposition of signals into various components in various time windows and frequency bands using scale and mother wavelets, which can achieve adaptive time-frequency analysis. Since Tancel et al. [Tan+93] first applied WT for tool wear monitoring, the algorithm has also derived a series of optimizations. Continuous WT (CWT) can extract the feature pattern from both stationary and non-stationary signals, but it is computationally intensive, which led to the development of discrete WT (DWT) [Kwa06]. However, Hong et al. [Hon+16] indicated that DWT has information loss for high frequency signals, and they proposed wavelet packet transform (WPT) to enhance the resolution for high-frequency band signals. More details about WT can be found in the literature [ZSH09] for references.

Features	Description	Comments
Mean of total band power	$\bar{s} = \frac{1}{N}\sum_{j=1}^{N} s_j$	Arithmetic mean of the frequency power for a selected band of the frequency spectrum.
Variance of band power	$\sigma_s^2 = \frac{1}{N-1}\sum_{j=1}^{N}(s_j - \bar{s})^2$	Non-negative value indicating the spread of the frequency magnitude data.
Skewness of band power	$Sk_s = \frac{1}{N}\frac{\sum_{j=1}^{N}(s_j-\bar{s})^3}{\sigma_s^3}$	A measure of the asymmetry of the probability distribution of the spectra.
Kurtosis of band power	$Ku_s = \frac{1}{N}\frac{\sum_{j=1}^{N}(s_j-\bar{s})^4}{\sigma_s^4}$	A measure of the "peakedness" of the probability distribution of the spectra.
Peak amplitude	$s_{pk} = \max(s_j)$	Peak of power spectrum in a specific frequency band that is expressed by the energy level (W/Hz).
Peak frequency	f_{pk}	Relative frequency that corresponds to the highest amplitude.
Spectral crest factor	$s_{\mathrm{CF}} = \frac{s_{pk}}{\bar{s}}$	Also termed as relative spectral peak.

Table 2.4: Frequency domain features and descriptions

2.4.2.3 Angular domain analysis

Although most of the TCM studies have been conducted in the time domain, frequency domain, or time-frequency domain, research based on the angular domain has gradually gained attention in recent years.

The angular signal is defined on the basis of constant angular intervals $\Delta\theta$, which can be described in the same format as the time domain signal as

$$x_j = x(\theta_0 + (j-1)\Delta\theta), \tag{2.32}$$

where $j = 1, 2, ..., N$; t_0 is the initial angle. Angle-based recording data bring the possibility to yield the stationarity in the angular view regardless of the speed variation. It also provides the potential to detect angular periodicity by involving kinematic relationships on the rotating machine under consideration [Ren+10].

In order to acquire such an angular signal, two classes of solution are distinguished:

(i) **Angular sampling**
Angular sampling is a direct measurement, whose signal acquisition is automatically synchronized with the impulses of a tachometer/encoder [ADG02]. But it is currently considered difficult to set up, both in terms of financial and technical concerns. Therefore, the scientific community often chooses to resample the time signal into the angular domain for obtaining samples and further exploring the subject.

(ii) **Signal resampling**
Signal resampling is a means of converting a time signal to an angle signal by means of analog calculations. It is performed with the help of a tachometer/encoder working in parallel for phase estimation to determine the correspondence between time and angle of the target signal [Wan+19]. Generally, the tachometer provides one impulse per revolution, while the encoder can supply multiple impulses, which affords a better angular resolution. On this basis, the computed order tracking (COT) algorithm assumes that the rotating part has a constant speed in the section between the two impulses, and then resamples the time signal at constant angular increments by interpolation [DBP18].

More detailed steps and notes on obtaining angular signals can be found in the literature [RM05; And+10].

In the field of condition monitoring, the rise of research in the angular domain is due to the recent recognition that the cyclostationary process fits the properties of most rotating machine signals and that it can therefore be used to design new processing tools. In fact, Antoni et al. [Ant+04] demonstrated that almost all rotating machine signals can be considered as being cyclostationary, as long as the proper viewpoint is taken.

Cyclostationarity

The construction of the cyclostationary theory first originated in the field of communications during the 1980s, when it was recognized that the process of modulating signals for Hertzian transmission naturally led to a cyclostationary behavior [Ant09]. W. A. Gardner foresaw on this basis, the applicability of the cyclostationary signals to the description of periodic physical phenomena, and laid the relevant theoretical foundations with terminological specifications [Gar86].

It is clear that stationary signals are defined as those with constant statistical characteristics or moments (e.g. mean, variance, etc.) along the time axis. In contrast, the statistics of cyclostationary signals vary cyclically with respect to the period T (also known as the "cycle") on the function of certain variables. As shown in Figure 2.13, it is classified under the category of non-stationary signals [GNP06]. The cyclostationary signals include generally all non-stationary signals generated under a constant regime by periodic mechanisms. At the same time, periodic signals and stationary random signals are considered to be the two important special cases whose cycle equals to zero [AAX16].

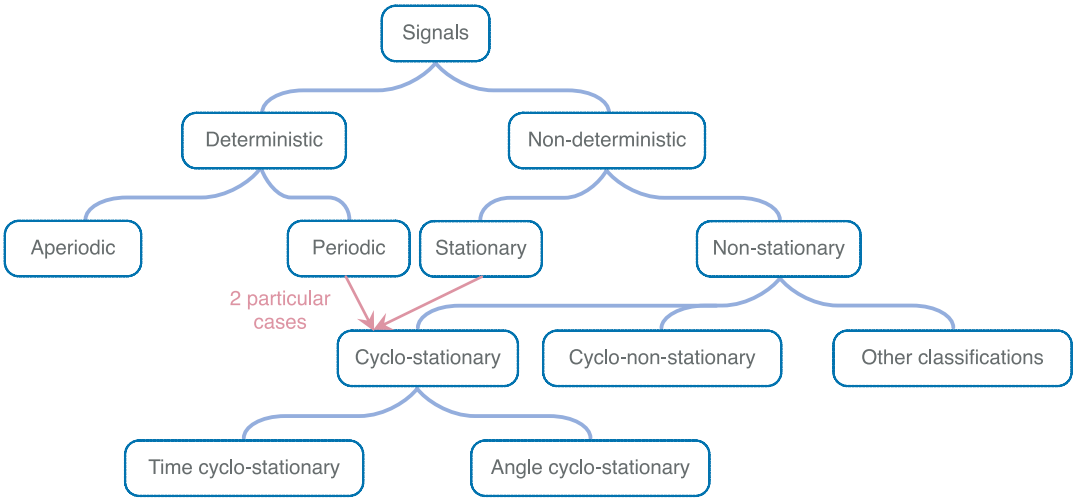

Fig. 2.13: Typology of signals

Cyclostationary signals have two subordinations as illustrated in Figure 2.13, according to the sampling variable that defines the cyclic period, either time $T(t)$ or angle $T(\theta)$. For rotating subjects, since its kinematic variables are all dependent on the

rotation angle θ, the rotating machine signals are essentially considered to be angle cyclostationary rather than time cyclostationary [Ant+04]. Consequently, the condition monitoring in the engineering machinery field involving rotating mechanisms, such as bearings [AR02], gears [SH05] and internal combustion engines [DBP18], etc., gradually started to perform signal processing based on the angular domain to preserve the cyclostationarity of the collected data.

Based on the consistent rotational mechanical characteristics, Lamraoui et al. [LTB14] explored the chatter conditions of Al 7075-T6 aluminum alloy based on angular domain in high speed milling. Through the comparison of analysis in time, frequency, and time-frequency domains, they confirmed that the angle cyclostationary process can facilitate the observation of the cutting force behaviors as well as the investigation of the system stability information. It provided an undoubted advantage in rotating machining operations that have pioneered a new way of using it in tool wear/breakage detection.

Under the assumption of cycloergodicity [Ant+04], angle synchronous averaging (SA) is considered as the best way to estimate the first-order cyclostationary (CS1) signatures, which is characterized by the periodic mean value of the signals. With the pre-knowledge of the desired components, angle SA processes the angular signal into segments that are equal in length to the period $T(\theta)$, and then averages them to extract the periodic waveform from the noisy signal. Compared to the time SA, each period of the angle SA contains a constant number of angular increments, which facilitates the operation of averaging. Ritou et al. [Rit+14] used the cutting force signal collected by the eddy current sensor as a signal source to detect the tool condition by angle SA analysis. The proposed method has been implemented in an industrial case of a pocket machining operation and validated very promising results.

By subtracting the periodic waveform extracted with angle SA from the original signal, the residual signal can be obtained [Ser+05]. It contains second-order cyclostationary (CS2) components and higher-order components. Only CS1 and CS2 are discussed here, because these two are already sufficient to cover the vast majority of practical purposes in mechanical engineering applications. The most common description for CS2 signal processing is the synchronous autocovariance function, which can be easily estimated by calculating the autocorrelation of the residual signal [Cas+18]. Feng et al. [Fen+21] developed an identification procedure that can

track the evolution of fatigue pitting and abrasive wear of gears by investigating the correlation between vibration-based CS2 signals and the tribological features of the two wear phenomena.

Cyclo-non-stationarity

Since the CS paradigm was adopted in the exploration of TCM, its application has always been limited to stationary machine regimes. Although angle-CS can relax these restrictions to some extent, it is still not sufficient to handle the large fluctuations in the operating conditions [AAX16]. Therefore, cyclo-non-stationary (CNS) signals have been recently introduced to extend the cyclostationarity to cases where a signal still conserves short-term cyclic patterns related to the angular rotation, but at the same time is (strongly) non-stationary on a long-term basis [Abb+16b].

In the milling context, the typical situation can occur in the following machine regimes:

- Start-up and shut-down periods, where the tool experiences dramatic rotational speed variation;
- Direction changing periods, where the tool steers according to preset non-linear trajectory and encounters the change in chip volume.

The signal generated at this time is still based on the periodic rotation, but the former is subject to amplitude modulation, while the latter is affected by phase modulation. Such distortions can jeopardize the effectiveness of numerous processing methods. Stander et al. [SH06] improved the previously mentioned angle SA by performing phase correction prior to the averaging operation. Abboud et al. [Abb+16a] proposed generalized synchronous average (GSA), which redefined the angle averaging to account for the speed dependence and accommodate for the induced changes in the signal. It is also worth noting that without constant rotational conditions, the conversion between the time-CS and angle-CS is ambiguous and incomplete. Literature [Ant+04] discussed the conditions for the equivalence of their conversion. On the other hand, there are also attempts [Abb+15; AAB14] to address the problems from a joint angle-time vision.

Overall, performing TCM from the angular domain is a newly developed technique in about the last 10 years. Many of the methods have not yet reached a very mature stage, especially for the CNS signal processing whose definition in our case remains controversial [Abb+16b]. But there is no denying that angular domain analysis does have an attractive potential. This thesis also seeks to follow this direction, drawing on the strengths of angular analysis while simplifying the feature extraction process to facilitate industrial implementations.

2.4.3 Action for decision making

Once the features are extracted, appropriate criteria need to be set to determine the condition of the tool and whether to make an alert. A large number of schemes, techniques, and paradigms are used to develop decision-making support systems. The objective is to find a balance between good detection probability and false alarms based on the data features.

Receiver operating characteristic (ROC) curve is introduced for the purpose of assessing the developed feature as well as locating an adequate threshold for actions. It works based on the probabilities calculated by the confusion matrix. By plotting the true positive rate (TPR) versus the false positive rate (FPR), the curve shows the trade-off in the TPR and the FPR for the varying value of that threshold. There will always be a point in (0,0) where every case is classified as normal. Similarly, every case is classified as abnormal at point (1,1). The area under the curve (AUC) is a metric for the evaluation of the feature classifier. Figure 2.14 demonstrated three types of performances for ROC curves. An ideal feature for classifier is like Figure 2.14(a) with AUC=1. It may imply the presence of the threshold perfectly labeled for each detection in the test data [MAT22]. At the same time, it is also important to check if the amount of data is insufficient or the classifier is over-fitted. In most cases, the ROC curve does not reach such an ideal state, but rather looks like the shape of Figure 2.14(b) (0.5 <AUC <1). Sometimes the curve may present jaggedness, which commonly comes with the gap in the test data. If the curve is a straight line from the bottom left to the top right as shown in Figure 2.14(c)(AUC=0.5), the performance does no better than a random guess. It's better to reconsider the model or engineer some better features.

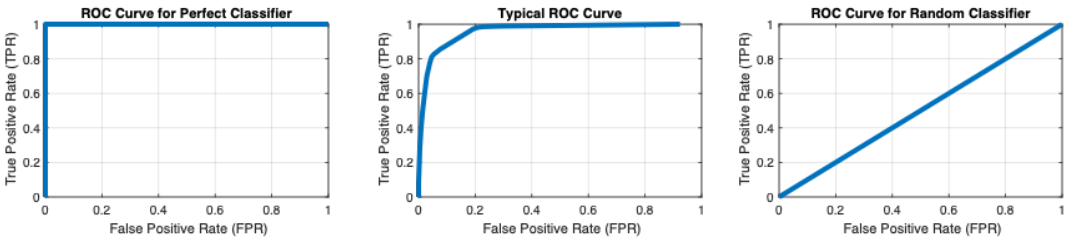

(a) (b) (c)

Fig. 2.14: ROC curves: (a) AUC=1; (b) 0.5 <AUC <1; (c) AUC=0.5 [MAT22].

In Chapter 5, ROC curves are employed to validate the validity of the proposed features. Since the research is mainly concerned with feature extraction rather than decision making, the thesis will not carry out the extension about the AI algorithms for TCM here. More details including neural networks, fuzzy logic, genetic algorithms, etc. can be found in the literature [Moh+20; Tet+10].

2.5 Correlation-based monitoring

Through the analysis of the end milling operation behaviors in Section 2.3 and the study of the TCM process in Section 2.4, the following facts were brought to our attention:

- The structure of the tool generally contains multiple teeth with interactive characteristics.
- The most concerning wear type for end mill is flank wear. The wear value Vb exhibits linear under the normal conditions and increases exponentially as the tool approaches the service life (referring back to Figure 2.4).
- The condition of the teeth affects the chips formation, which in turn is reflected in the indirect signals.
- The end mill, as a tool functioning in a rotary manner, has the advantage of inherent periodicity. The implementation of the study in the angular domain can avoid to a certain extent the irregularities in the time domain due to the speed variation. However, few studies are devoted to this direction.

- The signals generated by the rotating tool are CS signals during the stationary operations and CNS signals during the non-stationary regime (speed or trajectory changes).

Based on the above facts along with the investigation of the background and development trend of machining in Chapter 1, a concept of tool condition assessment using inter-insert correlation is tentatively proposed. While treating the tool as a whole, the concept also strives to consider multiple inserts as interacting individuals. The correlation analysis among them can eliminate as much as possible the external non-stationary factors and gather the focus on the condition of the tool. When the cutter undergoes variation in speed, all the inserts can be seen as being similarly affected. At the same time, the operating mode of high rotational speed with low feed rate makes the trajectory changes experienced by individual cutting edges tend to be similar. Especially the high-speed machining can better approximate the external working environment of each tooth as quasi-equivalent, thus contributing to more accurate correlation results.

After an extensive literature search, some relevant correlation-based studies were found. Most of the methodologies aim to establish the correlation between flank wear and some specific parameters (vibrations [KDK19], cutting forces [ZZW13], temperature [Wan+05], surface texture [Dut+13a], etc.) in order to perform condition monitoring.

Other studies [HWG17; KS17; Che+15] try to start with the establishment of the working standard in good condition as a reference, then follow *Teach-in & Comparison* principle to diagnose the tool status: the assessment is based on the correlation between the real-time monitoring signal and the pre-defined standard. A common method of obtaining this reference in current manufacturing is to perform a trial cut at the same working parameters. However, as described in chapter 1, it is not financially acceptable for the trend towards flexible customized production in small quantities and is not robust as well, especially when non-stationary operations are involved. The cognitive paradigm is another way to pre-acquire the reference, which although relatively stable, has encountered challenges in data training due to its high costs of data acquisition and insufficient development in storage and transmission technology [Zho+22].

Prasad and Babu [PB17] tried to find a better solution in terms of cost. They proposed a 3D finite element simulation model in their study of dry turning to replace the actual test cut as a standard for correlation analysis. However, compared to turning, milling is more complex on the trajectory, its simulation is more challenging and the reliability is yet to be verified. Furthermore, it is also a complicated work to re-simulate different milling conditions (speed and trajectory variations) for each machining task.

With the purpose of excluding the influence of external operating factors on the TCM, Fong et al. [Fon+21] used the original tool image as a benchmark and developed an offline monitoring system by cross-correlating the worn tool image with the initial one. Such an intuitive approach is indeed independent of different milling conditions, but the accessibility of the machine is always a restriction, limiting its development from offline to online monitoring.

The methods mentioned above are all correlation-based but still differ from the ideas presented in this thesis. To the authors' knowledge, such a study using inter-insert correlation as the detection feature proposed in this work has not been published in the field of TCM.

For the concrete implementations of the proposed simple concept, the segmentation previously used in the angle SA is drawn upon for separating the signal corresponding to its unit of teeth. The specific way in which these segments are correlated is worth exploring.

2.5.1 Relationships between variables

Relevant relationships between variables can be subdivided into parallel and dependent relationships. Correlation analysis is appropriate for the former, while the latter needs to be processed by regression analysis [CC18]. In the context of the present discussion, it is clear that the teeth of the tool are considered as being on an equal footing. Therefore, the correlation method to be employed should be free of any distinction between dependent and independent variables.

In order to measure the degree of correlation, several correlation coefficients

were derived and defined to numerically assess the relevance between two variables. Depending on the type of variable requiring comparison (such as continuous variables, nominal variables indicating on/off state, etc.), the appropriate correlation coefficient is suggested for each combination as listed in Table 2.5 [Zha+13]. Since the targeted segments in this study are continuous signals, the Pearson correlation coefficient (PCC) is selected.

Types of variables		A		
		Nominal (binary)	**Ordinal**	**Continuous**
B	**Nominal (binary)**	Phi	Rank-biserial	Point-biserial
	Ordinal	Rank-biserial	Polychoric, Spearman rank, Kendal rank	Polyserial
	Continuous	Point-biserial	Polyserial	Pearson

Table 2.5: List of correlation coefficients [Zha+13]

Pearson correlation coefficient

PCC is the most frequently used correlation calculation. It is a measure of the linear dependence between two sets of random variables $\boldsymbol{A}$ and $\boldsymbol{B}$, and can be defined as

$$R(\boldsymbol{A}, \boldsymbol{B}) = \frac{\mathrm{Cov}(\boldsymbol{A}, \boldsymbol{B})}{\sigma_A \sigma_B}, \tag{2.33}$$

where $\mathrm{Cov}(\boldsymbol{A}, \boldsymbol{B})$ represents the covariance of $\boldsymbol{A}$ and $\boldsymbol{B}$, and σ_A and σ_B are relatively the standard deviation of $\boldsymbol{A}$ and $\boldsymbol{B}$. As its foundation is the normalization of the covariance of A and B, the correlation result will always be between -1 and 1, where 1 is total positive linear correlation, 0 is no linear correlation, and -1 is total negative linear correlation [RN88].

However, the traditional correlation analysis like Pearson coefficient is always a pairwise correlation method, which can only provide a statistical relationship between two random variables [ASG06]. The tooth number n_z of the common end-mill is often 2 to 6 or more. The study first attempted to extend the Pearson coefficient to correlate with multiple sets of variables at the same time. But the results showed obvious limitations. The concerned processing with specific experimental data can be found in Appendix B.

Correlation matrix

The correlation matrix is the first method that comes to mind as it is the nature transition for correlation analysis from two variables to multiple variables. Suppose there are n segments, then the correlation matrix is

$$\mathbb{R} = \begin{bmatrix} R_{1,1} & R_{1,2} & \cdots & R_{1,n} \\ R_{2,1} & R_{2,2} & \cdots & R_{2,n} \\ \vdots & \vdots & \ddots & \vdots \\ R_{n,1} & R_{n,2} & \cdots & R_{n,n} \end{bmatrix}, \tag{2.34}$$

containing the Pearson correlation coefficients calculated from the combination of any two segments. $\mathbb{R}$ is a symmetric matrix and the elements on the diagonal are equal to 1, representing the self-correlation. Corresponding to the combinations of the segments, the matrix has C_2^n coefficients that do have the ability to reflect the inter-insert relationships, but are very trivial and cannot provide a simple and comprehensive expression. The concerned processing with specific experimental data can be found in Appendix B.

Therefore, the direction of the literature review gradually tapped into multivariate analysis, trying to combine it with correlation.

2.5.2 Multivariate correlation analysis

A wide variety of multivariate analysis methods are available in scientific research. The choice of the most appropriate method depends on the type of data and problem as well as the objectives that the analysis is expected to achieve. As a result, four requirements were proposed as criteria for finding a suitable multivariate analysis model for correlating the tooth-based segments:

- The model needs to be able to analyze multiple variables simultaneously and produce a comprehensive result.
- The model should be capable of extracting features that reflect the tool condition while providing the appropriate interpretation in a physical sense.
- The model could reduce the size of the original information while capturing the main characteristics.

- The model is not required to distinguish the independent and dependent variables.

Among the common models, cluster analysis and discriminant analysis are targeted at classification problems. Multivariate analysis of variance (MANOVA) requires a distinction between the independent and dependent variables. And canonical correlation analysis (CCA) is an extension of multiple regression analysis, for summarising the joint variation in two sets of variables [CC18]. Based on the evaluation of the above criteria, principal component analysis (PCA) is considered to be the more appropriate model for current needs.

It is worth noting that factor analysis is often mentioned alongside principal component analysis, as they both simplify the function of the data by analyzing correlations between variables. However, FA is more oriented towards identifying the latent structure among the variables and estimating the loading on each factor of individual variables. According to [CC18], it has several limitations. A large number of assumptions have to be made in setting up the FA model. Besides, the number of factors is unknown and needs to be obtained by complex sequential tests or external consideration based on the proposed assumptions. The loading of the factors will change as the number of factors changes. PCA, on the other hand, is dedicated to finding the principal components of the best linear combination of variables. It requires neither the specification of any underlying statistical model to account for the residual error nor any assumptions about the probability distribution of the original variables. The components derived in PCA are unique (except where there are equal eigenvalues) and so stay the same as one varies the number of components that are thought to be worth including.

Principal component analysis (PCA)

PCA can be traced back as far as 1901 to the work of Pearson. It was gradually popularised during the 20^{th} century and is widely applied since then for describing complex multivariate problems [JM+60].

PCA is a variable-oriented technique, with no distinction between independent and dependent variables, and is suitable for situations where variables are generated on an equal footing. The general aim of PCA is to construct overall indicators after

analyzing correlations between multiple variables, uncovering the dominant combinations of features that describe as much of the data as possible.

To achieve the aforementioned objectives, its main technical thrust lies in transforming the observed set of n correlated variables (each variable has m observation samples) into a new set of uncorrelated variables, also referred to as principal components (PCs) [BK19]. These new variables are linear combinations of the original variables and are arranged hierarchically in decreasing order of importance. If the original variables are highly correlated, the first few components may already have the potential to represent most of the variations in the original data. With minimal loss of the original information, extracting the first few components as the overall indicators representing the original variables can lower the dimension of the problem, thereby saving the amount of subsequent data manipulation amount and facilitating its storage. On the other hand, if the original variables are barely correlated, then PCA may seem pointless.

When $n = 2$, the principle of PCA can be interpreted in a geometric way illustrated in Figure 2.15. All data points are plotted using variable 1 and variable 2 as

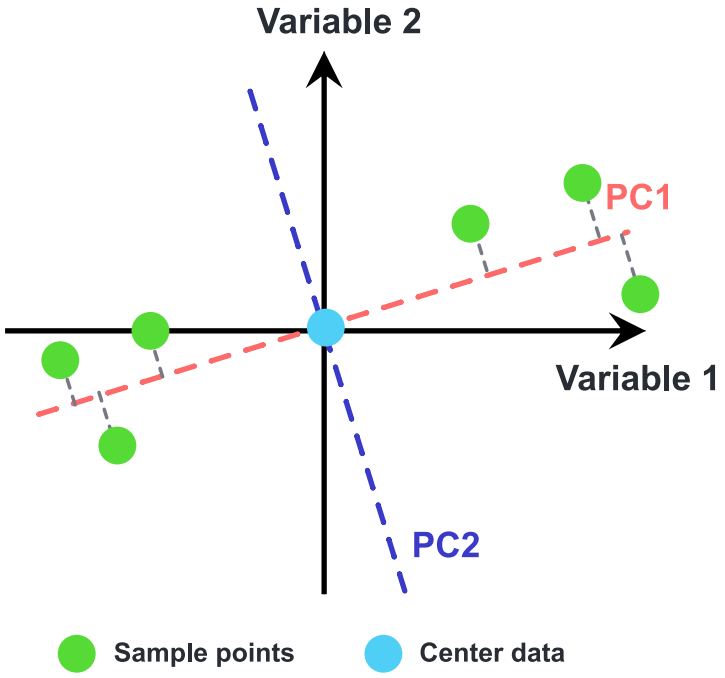

Fig. 2.15: Schematic diagram of the PCA principle

coordinates. Then the average of the variable 1 and variable 2 sequences needs to be calculated as the center of data. To facilitate the computation, all data points are shifted so that the center is on top of the origin in the graph, as shown in Figure 2.15. If it is desired to represent two-dimensional data points in one dimension, the work required is to locate a line going through the origin and minimize the sum of distances from the data to that line. Since the distance from the data point to the origin remains constant, according to the Pythagorean theorem, requiring the minimum sum of the distances from the data to the line is equivalent to requiring the projections of the sample points on this line to be as separate as possible. This level of dispersion can be expressed mathematically as the variance of the sample points. Suppose the mean-subtracted sample matrix is

$$\mathbb{X} = \begin{pmatrix} a_1 & a_2 & \cdots & a_m \\ b_1 & b_2 & \cdots & b_m \end{pmatrix}, \tag{2.35}$$

then the variance of the projections of the sample points on this basis can be expressed as

$$\mathrm{Var}(a) = \frac{1}{m}\sum_{j=1}^{m} a_j^2 \tag{2.36}$$

For a two-dimensional problem, it is sufficient to find the direction that maximizes the variance. Intuitively, in order for the different PCs to represent as much of the original information as possible, duplicate information should be avoided, i.e. no (linear) correlation between the PCs. Mathematically, the correlation between two variables can be expressed in terms of their covariance. With a zero mean, the covariance of two variables is expressed as their inner product divided by the number of elements m. The theoretical covariance can be empirically approximated as

$$\mathrm{Cov}(a, b) \approx \frac{1}{m}\sum_{j=1}^{m} a_j b_j. \tag{2.37}$$

The covariance matrix of the data

$$\mathbb{C} = \frac{1}{m}\mathbb{X}\mathbb{X}^\top = \begin{pmatrix} \frac{1}{m}\sum_{j=1}^{m} a_j^2 & \frac{1}{m}\sum_{j=1}^{m} a_j b_j \\ \frac{1}{m}\sum_{j=1}^{m} a_j b_j & \frac{1}{m}\sum_{j=1}^{m} b_j^2 \end{pmatrix} \tag{2.38}$$

can be employed to conclude these two requirements. In order to satisfy the constraints, this covariance matrix needs to be diagonalised. Let $\mathbb{Y} = \mathbb{P}\mathbb{X}$, then

$$\mathbb{Z} = \begin{pmatrix} \lambda_1 & & & \\ & \lambda_2 & & \\ & & \ddots & \\ & & & \lambda_n \end{pmatrix} = \frac{1}{m}\mathbb{Y}\mathbb{Y}^\top = \frac{1}{m}(\mathbb{P}\mathbb{X})(\mathbb{P}\mathbb{X})^\top = \mathbb{P}\left(\frac{1}{m}\mathbb{X}\mathbb{X}^\top\right)\mathbb{P}^\top = \mathbb{P}\mathbb{C}\mathbb{P}^\top, \tag{2.39}$$

where $\mathbb{C}$ is the original covariance matrix, the matrix $\mathbb{Z}$ is obtained after diagonalization, whose non-diagonal elements are all zero. The optimisation objective of PCA now becomes finding a matrix $\mathbb{P}$ that satisfies $\mathbb{P}\mathbb{C}\mathbb{P}^\top$ is a diagonal matrix and the diagonal elements are arranged hierarchically in descending order. Each row of $\mathbb{P}$ is the eigenvector of $\mathbb{C}$, corresponding to the eigenvalue in the diagonal of $\mathbb{Z}$ arranged in descending order. Depending on the required precision, the percentage variance

$$\alpha = \frac{\sum_{j=1}^{z} \lambda_j}{\sum_{j=1}^{n} \lambda_j} \tag{2.40}$$

can be used to determine the first z dimensions that need to be retained from the n-dimensional data volume.

The traditional calculation of PCA described above is based on the eigendecomposition of the covariance matrix, which squares the condition number, i.e. the digits lost by the roundoff errors will be doubled. When confronted with the continuously updating large input matrix, it could cause problems. Therefore, singular value decomposition (SVD) is introduced in this context. The SVD algorithm typically works by bidiagonalization or similar methods that avoid forming the covariance matrix, and thus provides higher numerical precision [LLM16].

2.5.3 Singular value decomposition (SVD)

SVD is one of the most well used and general-purpose practical tools in numerical linear algebra for data reduction processing. It can help reducing high dimensional data into the key features that are necessary for analyzing, understanding, and describing [WRR03].

A matrix data set

$$\mathbb{X} = \begin{bmatrix} | & | & & | \\ \boldsymbol{x_1} & \boldsymbol{x_2} & \cdots & \boldsymbol{x_n} \\ | & | & & | \end{bmatrix} \in \mathbb{R}^{m \times n}, \tag{2.41}$$

can be seen as a collection of a certain set of experiments. Each column vector $\boldsymbol{x_i} \in \mathbb{R}^{m \times 1}$ $(i = 1, 2, ..., n)$ presents a group of measurements of the physical system state that is evolving in time from experiments with m data points. Whether n is greater than m or m is greater than n (assuming $n < m$ in the following discussion), the SVD always has a unique matrix decomposition that exists for every input matrix $\mathbb{X}$. The data set can be decomposed into three parts as

$$\begin{aligned} \mathbb{X} &= \mathbb{U}\mathbb{\Sigma}\mathbb{V}^\top \\ &= \begin{bmatrix} | & | & & | \\ \boldsymbol{u_1} & \boldsymbol{u_2} & \cdots & \boldsymbol{u_m} \\ | & | & & | \end{bmatrix} \cdot \begin{bmatrix} \sigma_1 & & \\ & \ddots & \\ & & \sigma_n \\ - & - & - \\ & 0 & \end{bmatrix} \cdot \begin{bmatrix} - & \boldsymbol{v_1}^\top & - \\ - & \boldsymbol{v_2}^\top & - \\ & \vdots & \\ - & \boldsymbol{v_m}^\top & - \end{bmatrix}, \end{aligned} \tag{2.42}$$

where $\mathbb{U} \in \mathbb{R}^{m \times m}$ and $\mathbb{V} \in \mathbb{R}^{n \times n}$ are unitary matrices, and $\mathbb{\Sigma} \in \mathbb{R}^{m \times n}$ is a matrix with real, non-negative entries on the diagonal and zeros off the diagonal. The two-dimensional geometric interpretation of the SVD operation is illustrated in Figure 2.16.

SVD can provide systematic interpretations in terms of correlations among the columns of object matrix $\mathbb{X}$ and correlations among the rows of $\mathbb{X}$. When the decomposed components are substituted into the correlation matrix among the columns of $\mathbb{X}$, the result obtained corresponds to the definition of eigendecomposition, as

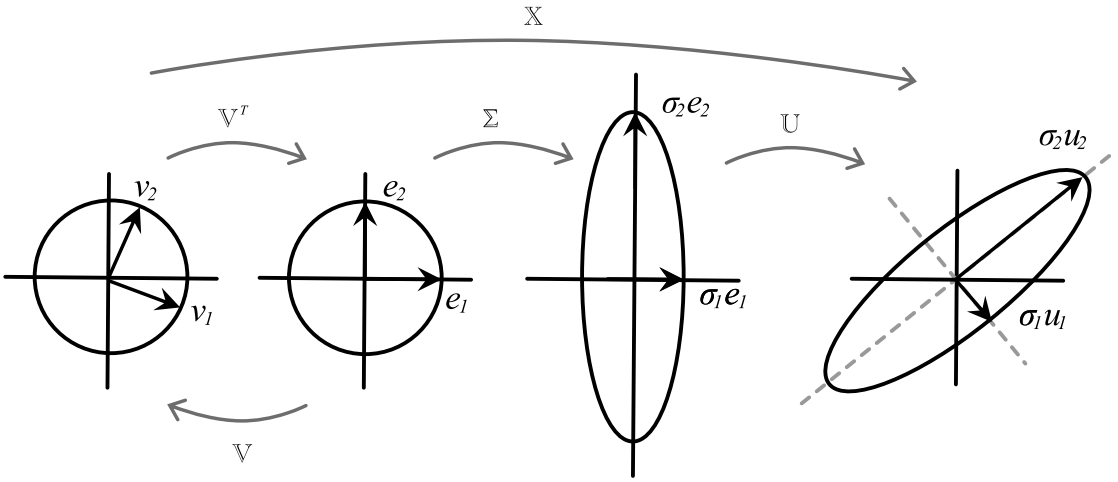

Fig. 2.16: Visualization of the SVD [Str93]

expressed below :

$$\mathbb{X}^\top \cdot \mathbb{X} = \mathbb{V}\mathbb{\Sigma}^\top \mathbb{U}^\top \cdot \mathbb{U}\mathbb{\Sigma}\mathbb{V}^\top = \mathbb{V}\mathbb{\Sigma}^2\mathbb{V}^\top \Rightarrow (\mathbb{X}^\top \cdot \mathbb{X}) \cdot \mathbb{V} = \mathbb{V}\mathbb{\Sigma}^2. \tag{2.43}$$

It means $\mathbb{V}$ and $\mathbb{\Sigma}^2$ contain the eigenvector and eigenvalue of the column-wise correlation matrix $\mathbb{X}^\top \cdot \mathbb{X}$. Similarly, $\mathbb{U}$ and $\mathbb{\Sigma}^2$ contain the eigenvector and eigenvalue of the row-wise correlation matrix $\mathbb{X} \cdot \mathbb{X}^\top$.

If taking this decomposition into a physical explanation without looking at the specific application scenarios, then $\mathbb{U}$ is the hierarchically arranged "eigen" information about the measurements, and $\mathbb{V}$ is essentially the "eigen" time series that stands for how each mode $\mathbb{U}$ evolves in the duration of the process. The eigenvalues in $\mathbb{\Sigma}$ represent the amount of energy that each of these column vectors captures, hierarchically arranged in order of importance [BK19].

For a better understanding, one can simplify Equation 2.42 in the following way:

$$\mathbb{X} = \sigma_1 \boldsymbol{u_1} \boldsymbol{v_1}^\top + \sigma_2 \boldsymbol{u_2} \boldsymbol{v_2}^\top + \ldots + \sigma_n \boldsymbol{u_n} \boldsymbol{v_n}^\top. \tag{2.44}$$

Here, σ_i are the ordered singular values, $\boldsymbol{u_i}$ is an m-dimensional column vector, and $\boldsymbol{v_i}$ is an n-dimensional column vector. The matrix $\mathbb{X}$ is decomposed by SVD

into a weighted, ordered sum of separable matrices $\sigma_i \boldsymbol{u_i} \boldsymbol{v_i}^\top$. Those matrices can be considered as n-order superposition arranged by their ability to approximate the original input matrix. This is the so-called **SVD separable model**.

Although the first singular value occupies the dominant position, the second, third, and even higher order singular values, as long as they are non-zero, also have a certain meaningful value, such as the representation of noise in the measurement, etc.

For estimating the ability of the i^{th} order singular value to approximate the original matrix, the following separability index

$$\alpha_{ki} = \frac{\sigma_{ki}^2}{\sum_{j=1}^{n} \sigma_{kj}^2}, \tag{2.45}$$

is put forward to precisely indicate the nature of its separability [WRR03].

In the TCM field, the application of SVD lies commonly on the purpose of data reduction for already obtained features. Zhou et al. [Zho+09] used the SVD to perform dominant feature identification from 16 features calculated by the measured force data. The selected sets of dominant features were then passed through a regression model for mechanical monitoring in the industry.

Samraj et al. [Sam+11] proposed an online turning measurement system using emitted sound as data sources. The research employed the fuzzy clustering algorithm to classify the oriented energy obtained from SVD to monitor the tool wear. Cempel [Cem09] applies generalized SVD in symptom observation matrices to discuss machine monitoring, using rolling bearings and diesel engines as examples. These methods are all based on observing similarities in machine wear processes but are still limited to using external objects as a reference for comparison.

To the authors' knowledge, there is no similar research using SVD or PCA to explore inter-insert correlation in the angular domain for TCM. The proposed method is original and innovative. The specific physical meaning corresponding to the three obtained parts $\mathbb{U}, \mathbb{\Sigma}, \mathbb{V}^\top$ will be explained in detail in Chapter 5.

2.6 Conclusion

The main findings of the literature review, which covered many aspects of TCM systems, are listed below.

Review shows that lateral wear is the most dominant type of wear on end mills. After the initial wear, flank wear increases at a fairly constant rate for the majority of its service life. Finally, it reaches an exponentially accelerated wear zone, which marks the end of the tool's operational life. Combining the above-mentioned tool life characteristics with the model of cutting forces in case of wear proposed after the chip forming analysis, the interaction between the tool teeth was captured as the basis for inter-insert correlation.

After considering the cost-effectiveness and applications of the available sensors, as well as the availability of equipment in the laboratory, the cutting forces were selected as the target signal for the subsequent analysis. Based on the characteristics of rotating mechanisms, the advantage of the angular signal is exploited to reduce instability due to speed variations and to perform better tooth-based segmentation of signal. Thereby the concept of tool monitoring in the angular domain using inter-insert correlations was presented.

Finally, after the study based on correlation and multivariate analysis with a deepening discussion of PCA, SVD was identified as the specific algorithm for TCM based on inter-insert correlation.

Chapter 3

Modeling of the rotational machinery behavior

Summary

3.1 Introduction 66
3.2 Required signal features for inter-insert correlation 66
3.3 Trajectory change and unification of the angle 68
3.4 General modeling of rotational machinery behavior 70
3.4.1 Segmentation 71
3.4.2 In case of milling force 73
3.4.3 In case of instantaneous angular speed (IAS) 74
3.5 Correlation strategies 77
3.6 Conclusion 81

3.1 Introduction

After reading the literature and identifying the inter-insert correlation as the research direction, this chapter focuses on the applicability of the proposed method. The characteristics of the processing-oriented signal are outlined in Section 3.2 and a correction of the trajectory angle is introduced in Section 3.3 to optimize the problem of path variation in the milling process.

A general model is formulated in Section 3.4 to facilitate the expansion of the method for future applications. The cutting force model proposed in the previous chapter is incorporated into this general process as a theoretical basis for experimental validation. Meanwhile, the instantaneous angular velocity is presented as a more convenient simulation signal for the preliminary feasibility test. On this basis, specific strategies for performing inter-insert correlation analysis are discussed in Section 3.5.

3.2 Required signal features for inter-insert correlation

The methodology of obtaining the state of the studied object by constructing the correlations between the signal segments is theoretically versatile for different practical cases, especially for mechanical structures with rotational periodicity. Rotating mechanical structures with periodic movements are particularly suitable for this method. In this thesis, the subject is directed at the monitoring of milling tools, while the same principle can be applied to the diagnosis of mechanical parts such as gears and bearings. In addition to the versatility of the objects under monitoring, the signal sources associated with them are also diverse, as in the examples given by Section 2.4.1. In order to define the application scope of the inter-insert correlation method, several features that the applicable signal needs to be equipped with are summarized here as follows:

(i) **Recurrence of events**

The entire diagnostic method of inter-insert correlation has a cornerstone, which

is the recurrence of events. It is certainly possible to pick a particular point in time to analyze an individual event. But if one wants to see the global trend over the timeline, the signal being processed should contain multiple consecutive events.

The definition of the event is based on the object for which the correlation analysis is performed. For example, in this thesis, each rotation of the milling tool can be considered as one event, or the entry-exit of the material by each tooth can be considered as one event. Regardless of the choice, however, it is worth emphasizing that the recurrence of events is not equivalent to a periodic signal. During the continuous repetition of events, intentional artificially set variations and effects due to changes in the state of the detected object are allowed to occur. Therefore, the signal does not have to be cyclical in the strict sense of the word, but it needs to have a physically continuous working regime.

(ii) **Segmentability and matchability**

The second requirement is that the signal needs to possess the properties of segmentability and matchability.

Segmentability means that the signal consists of discrete data and can be segmented into equal-length observation objects based on recurring events. Matchability, on the other hand, refers to the fact that the segmented signal pieces can correspond well to the customized events in a physical sense.

Both two characteristics are aimed at improving the accuracy of multivariate correlation analysis between the segments.

(iii) **Similarity and interaction between the segments**

Another important prerequisite for inter-insert correlation is the similarity between the neighboring segments. The principle of this method is to distinguish anomalies from events that are supposed to be in the same condition. If in an ideal condition (e.g., using a brand new tool without any wear), several segments for correlation analysis already have a large difference, and the upper limit of the indicator will be below 1. In such a case, the analysis of the condition of the workpiece purely from the index will lose a standard reference state, and therefore the use of this method is not recommended.

It is also worth noting that in comparison to the continuous recurrence of the events, similarity refers rather to the short term. During the overall period, it is possible that the form of the signal may change gradually. Therefore, a signal with both recurrence and similarity is not necessarily a cyclostationary signal.

On the basis of similarity, if there are extra interactions between segments. For example, when the previous tooth wears or breaks, the cutting conditions of the corresponding process often tend to be modified. The next insert will be subjected to compensatory overload. Due to this compensatory work, the data fluctuations on the correlation indicators will be more pronounced in case of anomalies. The most intuitive change is between two consecutive teeth, but it may also affect a third or other subsequent teeth.

The above properties are the criteria to determine whether the signal can be processed by the inter-insert correlation method discussed in this research. From a practical point of view, this method is well suited for a rotating mechanism with cyclic behavior. It has very promising development prospects and application extensions.

3.3 Trajectory change and unification of the angle

In most cases of milling operations, the cutting speed and feed rate are generally set to certain constant values. However, the milling trajectory is not always as simple as a straight line. Since the research is carried out in the angular domain, changes in the trajectory will naturally introduce phase changes to the measured signal. Therefore, before proposing a general model to describe the system, it is necessary to introduce the concept of the trajectory change and the corresponding unification of the angle.

The spindle rotation behavior and the trajectory change behavior are parameterized respectively into θ and Θ. The geometric relationship is used to establish the unified angle ϑ, which expects to combine the two rotational behaviors under the same frame of reference.

It is assumed here that the preset trajectory is a straight line followed by a cir-

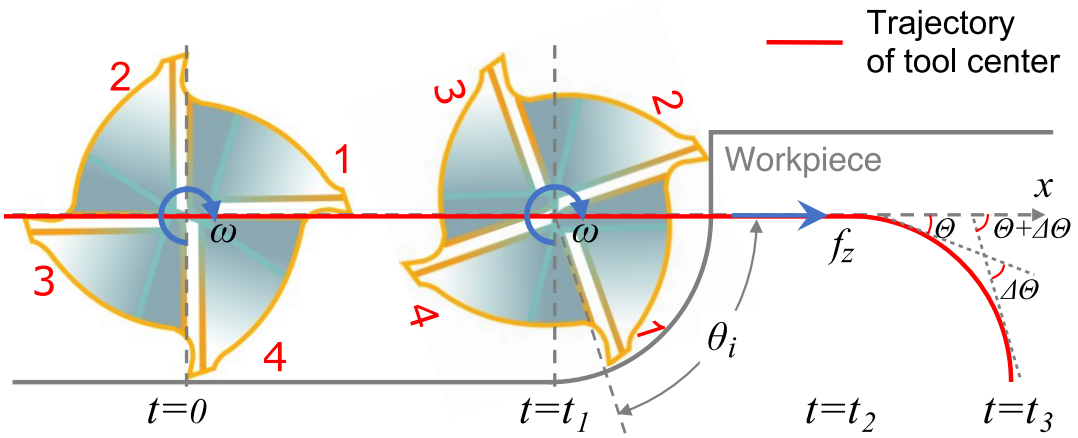

Fig. 3.1: End milling preset trajectory model

cular arc as illustrated in Figure 3.1, which presents respectively the cyclostationary and cyclo-non-stationary cases. The milling path in actual production may be more complicated, but the principle remains unchanged.

When the tool rotates, the instantaneous immersion angle θ, defined in Equation 2.7, increases along with the rotational frequency ω. Taking clockwise rotation as the positive direction, the angle of trajectory Θ is superposed on this basis. The unified angle ϑ is given by

$$\vartheta_i(t) = \theta_i(t) + \Theta(t) = \int_0^{t_3} \omega(t)dt - \frac{2\pi}{n_z} \cdot (i-1) + \Theta(t), \tag{3.1}$$

where Θ is the angle that the tangent of the path makes with the axis $\boldsymbol{x}$ and is continuously updated by superposing the variable $\Delta\Theta$ multiple times during milling process as indicated in Figure 3.1. The trajectory change angle Θ can be obtained from the information recorded by the axis encoder or can be extracted from the initial program input to the CNC machine-tool.

3.4 General modeling of rotational machinery behavior

As mentioned earlier, although the research in this thesis is targeted at the condition monitoring of end mills, the proposed method has the potential to be adapted to a broader frame of rotating machinery maintenance. Any signal that satisfies the three characteristics presented in Section 3.2, including that the signal of the cutting operation, can be regarded as a superposition of the analyzable general event and external interferences. With description of the angular parameters defined above, it can be considered that the actual collected signal is decomposed into

$$d(\theta, \Theta, t) = S(\theta) + D(\theta, \Theta, t) + I(\theta, \Theta, t) + \eta(\theta), \tag{3.2}$$

where the decomposition components are:

- $S(\theta)$: The interference driven by the motors, bearings, and joints in the spindle. Within the reference of the main shaft, therefore, the function S is linked with θ. It is considered can generally be corrected by comparing it to the idling condition. In normal working states, the interference is so small that it can be ignored after correction.

- $D(\theta, \Theta, t)$: The influence of the resistance generated by the material removal, which is the main component that interests the analysis. It not only depends on θ but also associates with the deterministic trajectory Θ. The unified angle ϑ might be used to summarize the total phase changes. The nature of this component relies upon the shape of the trajectory. In most milling cases, the cutting path is very variable depending on the manufacturing requirements. Hence, this component is always included in the analysis of the cyclo-non-stationarity category.

- $I(\theta, \Theta, t)$: The vibration impulse response in relation to time frequencies and machine-tool mode. According to [Lam+14], the chatter generated by rotating machinery is deterministic and can be summarized with second-order cyclostationarity (CS2).

- $\eta(\theta)$: The residual part due to different sources of noise, such as lubrication impact and chip evacuation, etc., which could be refined to a great extent by the filters.

Depending on the actual experimental environment and the condition of collected signals, one can choose filtering, CS2, and correction with idling rotation according to the need to reduce respectively the effects of η, I, S. In general, it is rational to consider that η, I and S are so small that overwhelmed by the valuable component D and can be appropriately ignored. The rest term D is the purest reflection of the state of the end mill.

In the following Section 3.4.2 and Section 3.4.3 of this chapter, the cutting force, and the instantaneous angular speed are used as two practical cases to represent the general model, respectively.

3.4.1 Segmentation

The purpose of segmentation is to extract relevant samples of the continuous sensor signal data set for further processing. Since the object of study is the angular signal, it avoids the sampling irregularity caused by velocity variation, satisfying the second feature required in Section 3.2. An appropriate segmentation can significantly improve the resolution of fault diagnosis [RSJ06].

In this research, each revolution of the tool is considered as a sequence of n_z events. For example, Figure 3.2(a) shows a revolution of data divided into $n_z = 4$ equal segments, where the part between the two red dashed lines includes the mechanism of the present tooth entering and then leaving the material, followed by an empty gap until the next tooth enters again. It can be seen that these segments share a similar waveform trend, which corresponds to the third feature required in Section 3.2.

It is worth emphasizing that the corresponding radial depth of cut a_e of the signal shown in Figure 3.2(a) has been controlled to ensure that only one tooth is in contact with the material at a time to clearly illustrate the processing results. However, it is envisioned that, under the good condition of the tool, even if more

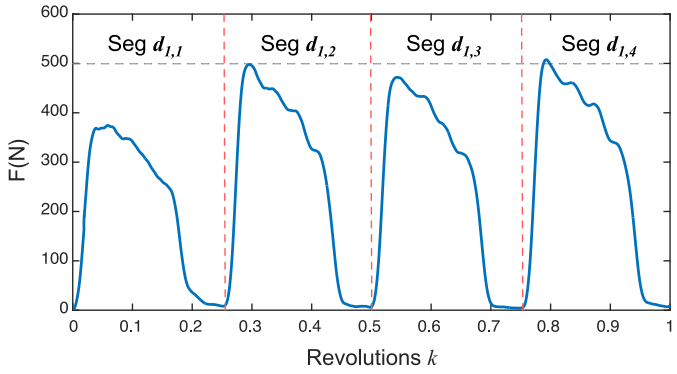

(a)

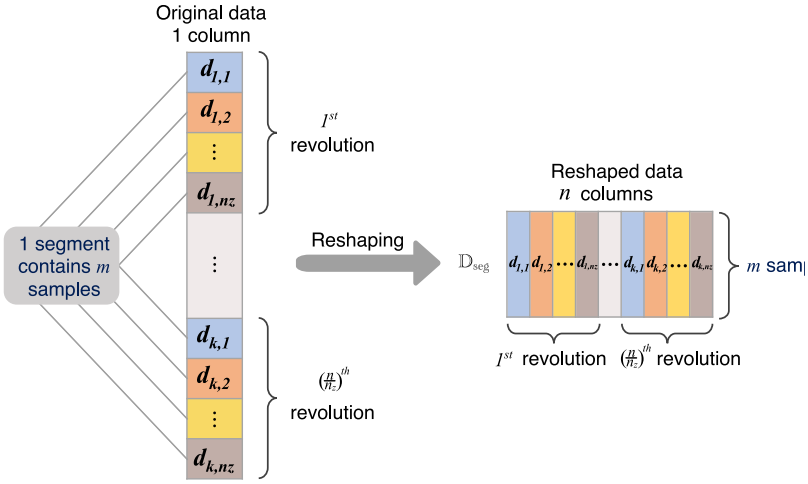

(b)

Fig. 3.2: Segmentation of signal: (a) the signal of the force divided by two red dotted lines corresponds to a segment; (b) illustration of the reshaping process.

than one tooth is in contact with the material at the same time, the consecutive n_z segments will also be identical and correlated. Because the periodicity of the signal still exists, and one revolution always contains n_z segments.

The original one-column data sequence is reshaped into a matrix

$$\mathbb{D}_{\text{seg}} = \begin{bmatrix} | & | & & | & & | \\ \boldsymbol{d_{1,1}} & \boldsymbol{d_{1,2}} & \cdots & \boldsymbol{d_{k,i}} & \cdots & \boldsymbol{d_{\frac{n}{n_z},n_z}} \\ | & | & & | & & | \end{bmatrix} \in \mathbb{R}^{m \times n}, \tag{3.3}$$

where n is a constant presenting the number of total segments, k is the subscript indicating the revolution counts ($k = 1, 2, ..., \frac{n}{n_z}$) and i is the subscript indicating the tooth counts ($i = 1, 2, ..., n_z$). The visualization of this step is illustrated in Figure 3.2(b). Each column corresponds to a segment, and $\boldsymbol{d_{k,i}}$ presents the i^{th} ($i = 1, 2...n_z$) segment sequence in the k^{th} revolution. n_z consecutive segments contains the data collected in one complete revolution.

After separating the finer component D, the signal will be split into segments corresponding to customized events for subsequent correlation analysis. This process of segmentation could be programmed by the user with the milling preset parameters in the CNC machine tool [McL16].

3.4.2 In case of milling force

Combining the general model of rotating machinery in Section 3.4 and the expression (Equation 2.27) for the cutting force in Section 2.3.5, the column vector $\boldsymbol{d_{k,i}}$ in the matrix $\mathbb{D}_{\text{seg}}$ can be further expressed as

$$\boldsymbol{d_{k,i}} = \overline{d_{k,i}} \cdot \mathbf{1}_{m,1} + \boldsymbol{\Psi_{F_{k,i}}} + \boldsymbol{\Delta F_{k,i}}, \tag{3.4}$$

where $\overline{d_{k,i}}$ is the average value corresponding to the i^{th} segment in k^{th} revolution $\boldsymbol{d_{k,i}}$, and $\mathbf{1}_{m,1}$ is an all-ones vector with dimension $m \times 1$. The term $\boldsymbol{\Psi_{F_{k,i}}}$ corresponds to the representative (theoretical) standardized waveform of the zero-centered cutting force. The term $\boldsymbol{\Delta F_{k,i}}$ presents the cut thickness characteristic due to the individual tooth condition.

When the n_z teeth have ideally the same state, the sequences possess remarkably close signal signatures and can be seen as identical. Hence, the average values of different segments $\overline{d_{k,i}}$ are equal to each other and the ideal segmentation matrix $\mathbb{D}_{\text{seg}}$ can be written as

$$Ideal \;\; \mathbb{D}_{\text{seg}} = \overline{d_{k,i}} \cdot \mathbb{1}_{m,n} + \left(\boldsymbol{\Psi_{F_{k,i}}} + \boldsymbol{\Delta F_{k,i}}\right) \cdot \mathbb{1}_{1,n}. \tag{3.5}$$

However, with the real-world external disturbances that are difficult to exclude, the segments cannot be exactly the same. At this time, the revolution matrix $\mathbb{D}_{\mathbb{k}}$ will

perform differently as

$$\begin{aligned} \mathbb{D}_{\mathbb{seg}} &= \overline{D_{seg}} \cdot \mathbb{1}_{m,n} + (\boldsymbol{\Psi}_{\boldsymbol{F_k}} + \boldsymbol{\Delta F_k}) \cdot \mathbb{1}_{1,n} \\ &= \overline{D_{seg}} \cdot \mathbb{J} + \Psi_F + \mathbb{\Delta} F, \end{aligned} \tag{3.6}$$

where $\mathbb{J} = \mathbb{1}_{m,n}$. The average value $\overline{D_{seg}}$ equals to $\overline{d_{k,i}}$ only in ideal situation. The theoretical shape $\boldsymbol{\Psi_F}$ and the remaining individual residual $\boldsymbol{\Delta F}$ extracted based on $\mathbb{D}_{\mathbb{seg}}$ are also different from $\boldsymbol{\Psi_F}$ and $\boldsymbol{\Delta F}$. Certainly, the outcomes derived from $\mathbb{D}_{\mathbb{seg}}$ and $\boldsymbol{d_{k,i}}$ should be very similar (within a certain error) during the operation in good condition. When the teeth gradually show wear, the difference between them increases significantly. Considering that the cut thickness characteristic due to individual tooth condition $\mathbb{\Delta} F$ is relatively much smaller than the original value of the data, if removing $\overline{D_{seg}}\mathbb{J}$ to reach zero-centering, then the contribution of $\mathbb{\Delta} F$ will be more prominent, and the subsequent analysis results will be more obvious.

3.4.3 In case of instantaneous angular speed (IAS)

Before the experimental data are available, the preliminary feasibility analysis of the proposed method is based on simulated data. Since the physical behavior of the cutting edge entering and exiting the material naturally makes the cutting forces intermittent and numerically complex (Figure 3.2(a)), the simulated signals are built based on the instantaneous angular speed (IAS).

IAS is also a signal parameter that is related to the tool state and at the same time fits the applicable range presented in Section 3.2. It always runs around the set cutting speed with small fluctuations, which facilitates the simulation and at the same time demonstrates side-by-side that the method can be applied to a wide range of signals generated by rotating machinery.

Straight-line simulation signal

The dynamic behavior of such a continuous and stable rotational mechanism has a law of cyclic motion that is consistent with the physical meaning implied by the trigonometric function. Therefore, using a sine or cosine function multiplied by a reasonable amplitude value K can be used to simulate the milling IAS signal, which

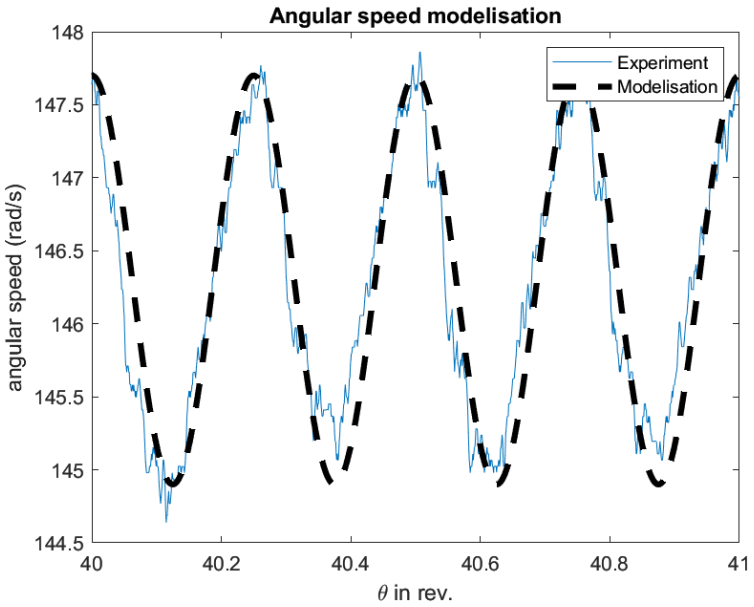

Fig. 3.3: Simulation result comparison

is much simpler than simulating the cutting force.

The object of the research D in the case of IAS can be written as

$$D = K \cdot \cos\left(n_z \cdot \omega t\right) + D_0, \tag{3.7}$$

which presents the fluctuation around setting value D_0. The comparison of the simulation result and the experimental data is shown in Figure 3.3, where the trends of the two curves matched up nicely.

Curve-line simulation signal

On the basis of straight cutting, the cutting curvature can be taken into account to simulate a cyclo-non-stationary case, with a curved trajectory. In this paper, it is assumed that the depth of the cut remains stable, only the direction changes in the curved path. For the simulated signal, that is to say, the amplitude stays steady while the phase undergoes a corresponding change.

Suppose the milling path is as shown in Figure 3.4, the tool first mills a straight line along the y-axis ($f_x = 0, f_y = const$) at the speed of ω, and then rotates an arc of angle Θ. During this process, the feed rate in the x-direction increases slowly

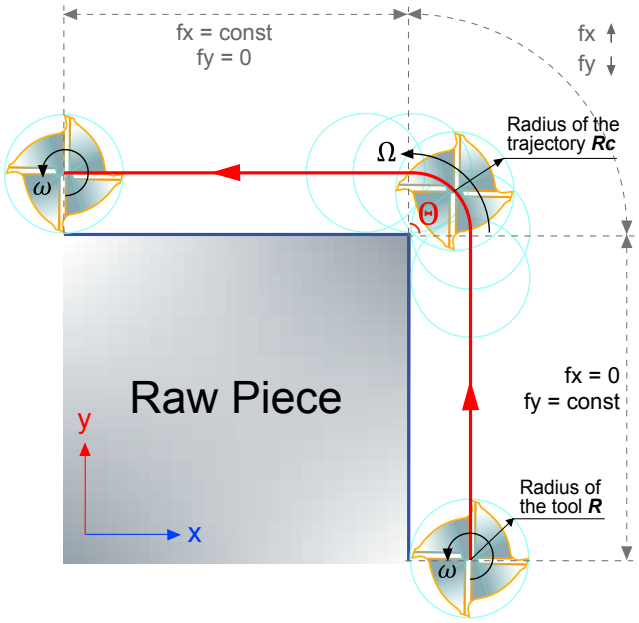

Fig. 3.4: Example diagram of curved path milling (top view)

while the one in the y-direction decreases gradually, which is usually self-adapted by the machine, rather than artificially set. After that, f_y totally becomes zero, and transverse milling is performed.

The rotational speed passing the curve is defined as Ω. It can be expressed using the rotation speed of the tool ω, the number of teeth n_z, the feed f_z, and the radius of curvature R_c of the cutting curve. The expression is

$$\Omega = \frac{\Theta}{t_{curve}} = \frac{\Theta}{\frac{2\pi R_c \cdot \frac{\Theta}{2\pi}}{f_z \cdot n_z} \cdot \frac{2\pi}{\omega}} = \frac{n_z \cdot f_z \cdot \omega}{2 \cdot \pi \cdot R_c} = \frac{\omega}{a}, \tag{3.8}$$

where

$$a = \frac{2 \cdot \pi \cdot R_c}{f_z \cdot n_z}, \tag{3.9}$$

is the number of revolutions required to pass through the curved trajectory with R_c as the radius.

On the basis of Equation (3.7), combined with the geometrical modeling of milling, the curve cutting part can be defined as

$$D = K \cdot \cos\left(n_z \cdot \omega t + \Omega \cdot (t - t')\right) + D_0 \tag{3.10}$$

where t' is the time point of entering the curve. Here, 30 revolutions for the curved path are inserted in time point t' after 30 revolutions of the straight-line cutting. Bringing reasonable parameters selected based on experience into Equation 3.8, the simulation results with segmentation by the revolution in case of IAS are presented in Figure 3.5. From $k = 1$ to $k = 30$, the yellow stripes (peak value of the signal) appear vertical, while from $k = 31$ until the end, the yellow stripes gradually tilt to the left side. This is exactly the phase shift that naturally occurs due to the trajectory angle Θ when the tool passes the corner at a constant feeding speed.

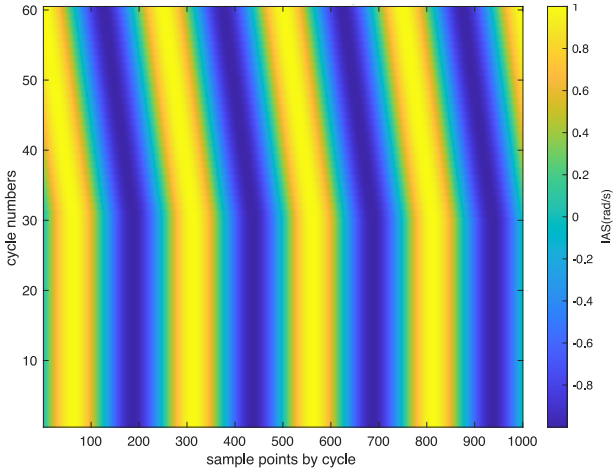

Fig. 3.5: Curve-line simulation signal

In Section 5.2, this set of simulated data is employed to explore the physical significance of the corresponding SVD decomposition components.

3.5 Correlation strategies

The signal that has been reshaped in Section 3.4.1 is presented as a matrix $\mathbb{D}_{\text{seg}}$. But for further correlation analysis, the specific strategies need to be discussed. That is to say, the principle is the same, always comparing the segments corresponding to different events, but which segments are selected to form the initial input matrix is still open to negotiation. Different strategies can be adopted by extracting different segments for the object of the correlation analysis.

Several attempts have been proposed here for discussion, listed as follows:

(A) **Correlation analysis in unit of all segments**

The first proposal is to analyze the data as a whole. In other words, the matrix $\mathbb{D}_{\mathtt{seg}}$ is directly used as the object matrix

$$\mathbb{D}_{\mathtt{e}} = \mathbb{D}_{\mathtt{seg}} = \begin{bmatrix} | & | & & | & & | \\ \boldsymbol{d_{1,1}} & \boldsymbol{d_{1,2}} & \cdots & \boldsymbol{d_{k,i}} & \cdots & \boldsymbol{d_{\frac{n}{n_z},n_z}} \\ | & | & & | & & | \end{bmatrix}. \tag{3.11}$$

It does not actually require the extraction step, hence, the extraction number $e = 1$.

As a matter of fact, such an initial input matrix is relatively simple, which requires only a single treatment of SVD to process the entire data. Consequently, this strategy is applied in Section 5.2 as a way to display the results of signal processing. The downside, however, is that it has no way of tracking the dynamic changes of the tool in real-time. Since segments of normal operating conditions constitute the majority of the data, the first hints of signal changes due to tool wear are easily drowned out, resulting in insignificant changes of the indicator value. Even if the results of the correlation analysis indicate that the tool is in a defective condition, it is hard to locate the exact time when the tool was worn. If all data from the start to the present during processing is used as the input matrix, then in practice, the amount of data will increase over time and the load on the SVD calculation will eventually exceed expectations.

(B) **Correlation analysis in the unit of individual tooth**

The second conception is to extract the segments corresponding to each tooth. For example, the object matrix of the first tooth is

$$\mathbb{D}_{\mathtt{e}} = \mathbb{D}_{\mathtt{k},1} = \begin{bmatrix} | & | & | & & | \\ \boldsymbol{d_{1,1}} & \boldsymbol{d_{2,1}} & \boldsymbol{d_{3,1}} & \cdots & \boldsymbol{d_{\frac{n}{n_z},1}} \\ | & | & | & & | \end{bmatrix}. \tag{3.12}$$

The data within $\mathbb{D}_{\mathtt{seg}}$ can form n_z object matrices $\mathbb{D}_{\mathtt{k},i}$ $(i = 1, 2, ..., n_z)$ for the subsequent correlation analysis.

The original intent of this analysis is to allow only the signal of an individual tooth to be compared with its changes in the time domain by controlling other

variables. However, the behavior of the teeth affects each other. When one tooth wears out, the rest of the teeth do compensatory work for it to varying degrees. Therefore, even if the correlation result of the object matrix for an individual tooth fluctuated, it does not necessarily mean that the corresponding tooth is in bad condition.

This attempt produces less clear results while increasing the computational load by n_z times. In addition, such a method has the same problem as case (A) and cannot achieve the target of real-time monitoring. Consequently, this strategy was negated.

(C) **Correlation analysis in unit of revolution**

Dong et al. [Don+06] pointed out that in order to reduce the effect of runout, it is better to analyze a signal within a spindle rotation range rather than a tooth period. Therefore, on the basis of above thoughts, the case (C) tends to comply with the need for real-time monitoring and tries to decompose the data in a more dynamic way. The idea is to extract the segments belonging to one revolution as the object matrix

$$\mathbb{D}_{\mathbb{e}} = \mathbb{D}_{\mathbb{k}} = \begin{bmatrix} | & | & & | & & | \\ \boldsymbol{d_{k,1}} & \boldsymbol{d_{k,2}} & \cdots & \boldsymbol{d_{k,i}} & \cdots & \boldsymbol{d_{k,n_z}} \\ | & | & & | & & | \end{bmatrix}, \tag{3.13}$$

where the extraction number $e = k = 1, 2, ..., \frac{n}{n_z}$. In other words, this matrix will be updated by each revolution continuously, and it always contains the relevant data to differentiate and compare multiple teeth passes of each cycle. The process will be repeated $\frac{n}{n_z}$ times from the beginning until the end of the machining.

The advantage of such a strategy is that the target of each analysis is fixed to n_z segments, which could make the presentation of results more concise. At the same time, it is capable of taking into account both the periodic change of the rotational angle θ of the tool and the deterioration process of the tool state over time, which enables a better correspondence between the angular domain and the time domain.

In actual production, the data of consecutive multiple revolutions can be selected as the object matrix according to the specific situation. For the same

machining operation, this processing can reduce the number of calculations e. Certainly, while reducing the computational burden, such an approach also lowers the system's refresh rate for real-time tracking feedback of the tool state. If the physical equipment enables it, what should be done is to select a parameter with a higher update ratio to better monitor the condition of the cutting tool.

In addition to these three cases, it is of course possible to choose another extraction to form the study unit $\mathbb{D}_{\mathfrak{e}}$. But regardless of the combination, the segments in $\mathbb{D}_{\mathfrak{e}}$ always share similar (and perhaps not completely identical) characteristics. Similar to Equation 3.6, $\mathbb{D}_{\mathfrak{e}}$ can be further expressed in a unified way with the weight under the identity unit as

$$\mathbb{D}_{\mathfrak{e}} = \overline{D_e} \cdot \mathbb{J} + \mathbb{K} \cdot \mathbb{W} + \mathfrak{c}, \tag{3.14}$$

where the $\mathbb{W}$ summarized the basic waveform of the segments, $\mathbb{K}$ is the amplitude corresponding to each segment superimposed on $\mathbb{W}$, $\overline{D_e}$ is the average value, and $\mathfrak{c}$ refined the individualized fluctuations for each data point (in response to the standard line shape), as illustrated in Figure 3.6. Such standardized expressions facilitate finding potential internal connections among segments.

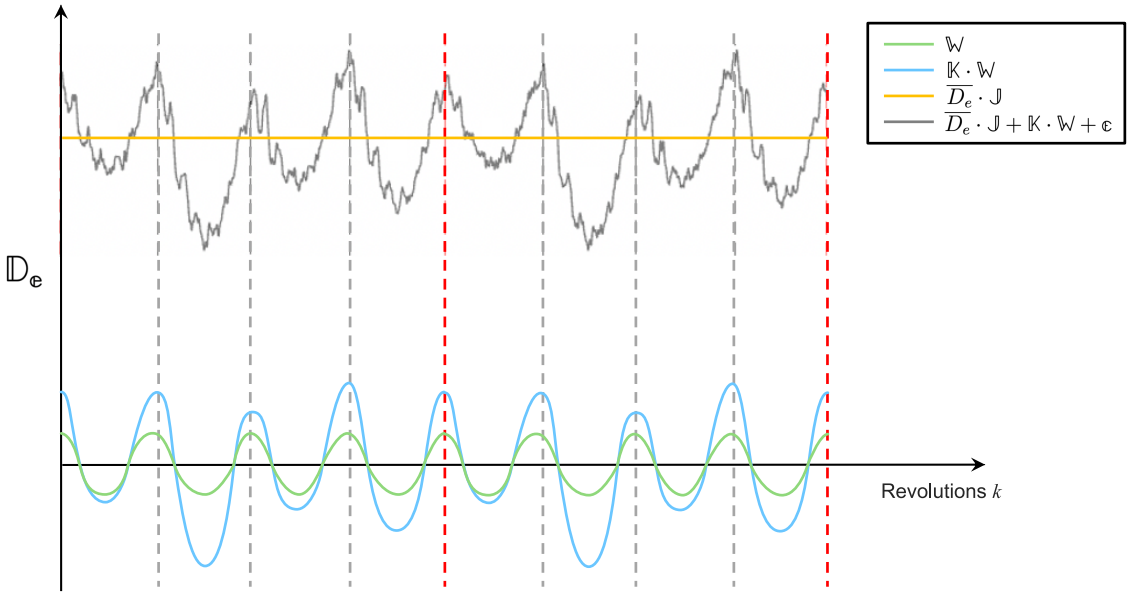

Fig. 3.6: Re-expression of components of $\mathbb{D}_{\mathfrak{e}}$

In summary, among the above three options, it is better to use correlation anal-

ysis based on the revolution (case (C)) to diagnose the real-time cutting data. If the current equipment has a problem adapting the calculation speed, the multi-revolutions extraction method can be appropriately selected according to the situation. In all the results presented hereafter, if there is no special indication, the case (C) is used, and the selected object matrix always contains n_z consecutive segments belonging to one revolution.

3.6 Conclusion

Chapter 3 begins with a summary of the applicable scope of the inter-insert correlation method for condition monitoring. Three characteristics of the oriented signal are recurrence of events, segmentability & matchability, and similarity & interaction between these segments. Based on these, a general model is developed for the future application expansion of the methodology.

Regarding the end milling process studied in this case, a trajectory angle was introduced to rectify the issue of path variation during non-stationary machining tasks in order to better accommodate this general model. The previously mentioned milling force model was adapted to the general process as a theoretical basis for subsequent experimental validation. Meanwhile, the instantaneous angular velocity is included as a more convenient simulation signal for the preliminary feasibility analysis. It is consistent with the above-mentioned three required characteristics and demonstrates from the side that inter-insert correlation can be widely employed for signals generated by rotating machines.

On the other hand, signal segmentation, as an important pre-step of inter-insert correlation, is presented in detail. On this basis, the strategy of how to perform the correlation analysis among the signal segments is specifically discussed. Three methods, including the overall-based, tooth-based, and revolution-based extraction, were analyzed. Considering the effectiveness of the update rate for online monitoring and the volume of data calculated in real-time, the target matrix was determined to be generated by the revolution-based method.

Chapter 4

Experiment design and data pre-processing

Summary

4.1 Introduction 84
4.2 Experimental setup 84
4.3 Milling parameters and trajectories 87
4.3.1 Different trajectories cases 88
4.4 Data pre-processing 92
4.4.1 Hilbert transformation 93
4.4.2 Resampling 94
4.4.3 Milling direction correction 96
4.4.4 Truncation & Segmentation & Zero-centering 97
4.5 Conclusion 98

4.1 Introduction

Within the framework of the study of tool conditions, this chapter will describe the acquisition and pre-processing of experimental signals, organized in three sections.

Section 4.2 describes the experimental devices used to perform the machining tests and the acquisition of the signals, including the setup and the measurement output. These setups, combined with different parameter settings, were used to study several cases of the milling tasks in Section 4.3. Section 4.4 explains the pre-processing steps before the inter-insert correlation analysis, including resampling, path correction, segmentation, etc.

The purpose of this chapter is to describe the setup and the intrinsic principles involved in the acquisition of experimental data in order to facilitate subsequent validation experiments. At the same time, it extends the range of applications for detecting tool wear or breakage under different cutting conditions.

4.2 Experimental setup

The DECKEL MAHO DMC 635 V milling machine was used for the experimental tests. By using the 4 holes in the bottom plate and matching types of screws-nuts, a Kistler 9257A 3-axes dynamometer could be tightened on the operation bench. It is worth noting that the support surface must be cleaned before installation (e.g. residual chips). Otherwise, the uneven supporting surface may set up internal stresses, which will impose severe additional loads on the individual measuring elements and may also increase cross talk [Kisa].

To avoid drilling holes in the workpiece, a compact self-centering vise V75100 is installed on the dynamometer, which serves to hold the workpiece and acts as a bridge to transfer the milling forces from the block to the dynamometer. After coupling with Kistler 5015B charge amplifiers, the cutting forces are measured in three orthogonal directions $(\vec{x}, \vec{y}, \vec{z})$. Simultaneously, two axis encoders for $\vec{x}, \vec{y}$ directions integrated into the bench and the rotational encoder combined in the spindle were linked to

4.2 Experimental setup

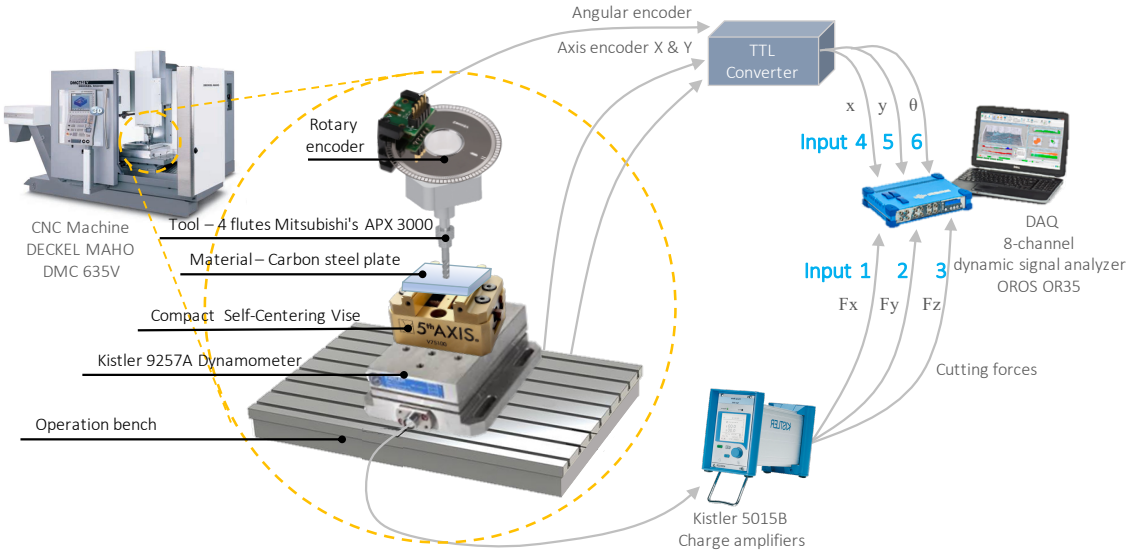

Fig. 4.1: Experimental setup

an output signals converter. The cutting force signal and encoder information are acquired synchronously, and all data converge into the Oros R35 8-channel dynamic signal analyzer. Figure 4.1 shows a general schematic of the experimental setup on which the milling tests are performed.

All inputs are handled simultaneously in parallel analysis mode by OROS. The six channels occupied during experiments are summarized in Table 4.1.

	Source	Physical meaning	
Input 1	Kistler 9257A dynamometer + Kistler 5015B Charge amplifier (Appendix A (B))	Cutting force in direction ...	x
Input 2			y
Input 3			z
Input 4	Axis sensors in operation bench of CNC machine center (Appendix A (A))	Displacement in direction...	x
Input 5			y
Input 6	Angular encoder (Appendix A (C))	Spindle rotational information	θ

Table 4.1: OROS OR35 analyzer input data recording

The workpiece used for milling was a C45 medium carbon steel plate with a

dimension of 20 × 100×100 mm. The cutting speed of 140 m/min and the sampling frequency of 50 kHz allows collecting 8–9 sample points for each sine cycle of the spindle encoder signal. The tool used in the experiment comes from Mitsubishi's APX 3000 series with four flutes. After the mounting of the VP15TF coated inserts, the operating diameter reaches 32 mm.

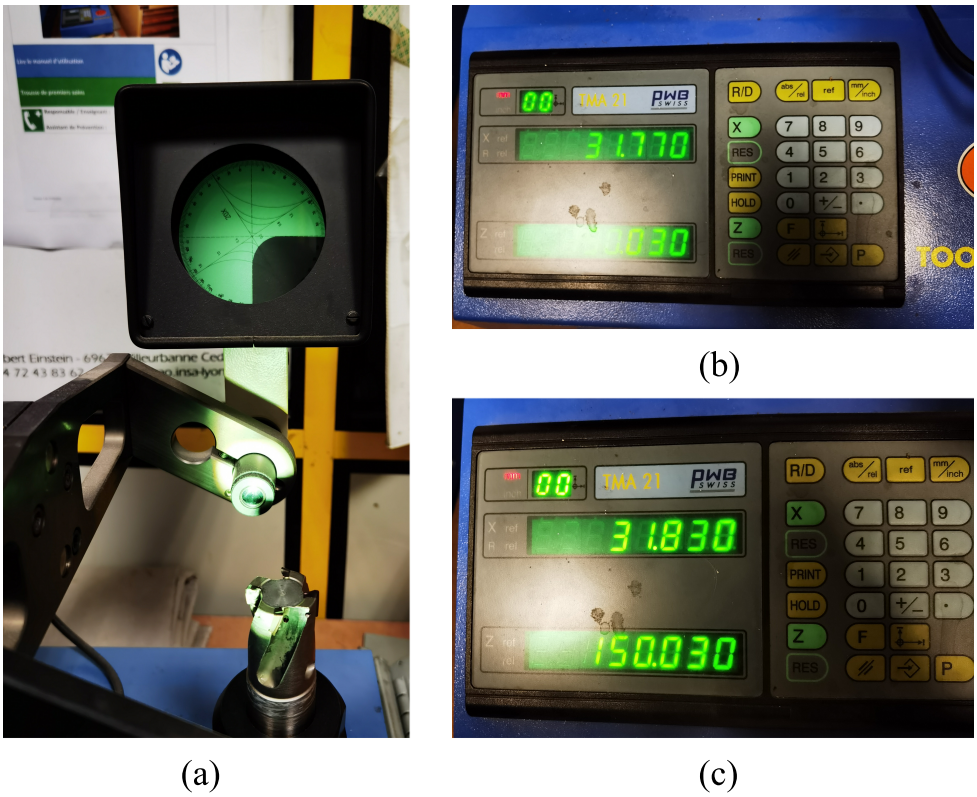

Fig. 4.2: Tool initial condition: (a) end mill inspection display; (b) the tool diameter including 1^{st}, 3^{rd} or 4^{th} tooth is 31.770 mm; (c) the tool diameter including 2^{nd} tooth is 31.830 mm.

It should be noted that the inserts used for the experiment were not brand new due to the limitations of the conditions, and one of the teeth was 0.06 mm larger than the others, as shown in Figure 4.2.

The specific parameters of the experimental materials can be found in Appendix A. The following machining tests used the same series of device setups.

4.3 Milling parameters and trajectories

In most circumstances, for a given machining operation, the cutting speed V_c will be set to an appropriate constant to complete the entire machining step at a theoretical unchanging cutting speed. For the inter-insert correlation studies, the variation of preset cutting speed has a uniform effect on all the teeth due to the integral nature of the tool. Therefore, this experiment does not make multiple comparisons of the preset spindle frequency. The cutting speed is always set to 140 m/min. The depth of milling a_p is kept at 3 mm.

The general parameters are summarized in Table 4.2.

Notation	Parameter	Value
n_z	Number of inserts	4
ω (rad/s)	Instantaneous angular speed	145.83
N (rpm)	Spindle frequency	1392.61
V_c (m/min)	Cutting speed	140
f_z (mm/tooth)	Feed per tooth	0.1
a_e (mm)	Radial depth of cut	Determined by different experimental cases
a_p (mm)	Axial depth of cut	3
R (mm)	Radius of the tool	16

Table 4.2: General parameters of milling experiments

Although theoretically, the cutting speed is always constant, in reality, the spindle speed is subject to fluctuations as the tool advances over the surface of the workpiece, especially when the operation involves machining a continuously varying diameter.

The focus of the study is to demonstrate that the proposed inter-insert correlation indicator is only related to the state of the tool itself. In other words, their correlation remained at a high level even though each tooth was subjected to non-stationary external influences as the tool passed through the non-linear trajectories. Multiple running trajectories were tested in Section 4.3.1 to demonstrate that the proposed method is equally diagnostic for cyclo-non-stationary working conditions.

4.3.1 Different trajectories cases

The experiment has proposed five different cutting trajectories to verify the subject mentioned above.

The tests are performed layer by layer on the same workpiece. At the end of each layer of the milling process, there must be some leftover materials with different shapes. Therefore, a surface milling of $a_p = 1\,\text{mm}$ is carried out after each test to ensure that the initial conditions for the next test remain the same as before. At the beginning of each cut, a reference cut of $a_e = 3.2\,\text{mm}$ is first conducted to verify and validate the initial cutting condition. The milling mode is always down-milling.

(A) **Contour of square**

Each contour of the square contains four straight-line cuts, which is the most basic milling trajectory. The radial depths of the three cuts are 3.2 mm (Test #1_3), 8 mm (Test #1_4) and 16 mm (Test #1_5), respectively. The starting point for tool entry into the material is at the bottom left. The tool follows the path shown in Figure 4.3, contouring around the workpiece and returning to the starting point again.

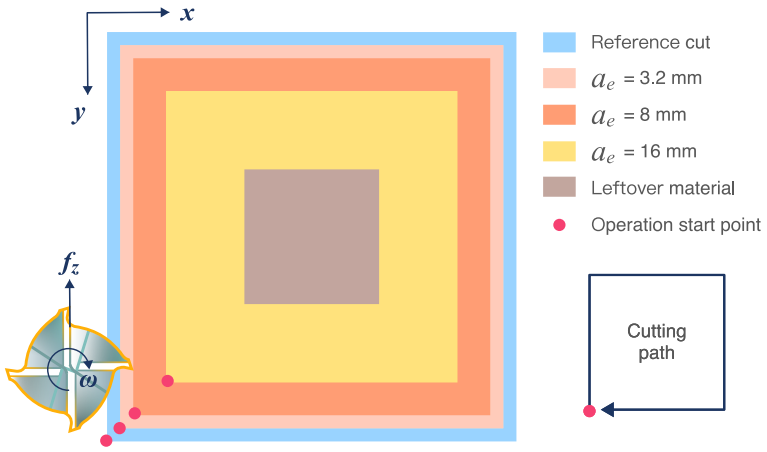

Fig. 4.3: Trajectory display for contour of square

As the tool did not show significant wear due to the experiment, the results of

these three tests $a_e = 3.2$, 8, 12 mm are similar. In the later data analysis, the results corresponding to $a_e = 3.2$ mm are used as a demonstration.

(B) **Contour of rhombus**

The cutting path of a rhombus shares a close resemblance to that of a square. They both contain straight paths on 4 sides. The difference, however, is that the square contour acts in one direction at a time ($\boldsymbol{x}$ or $\boldsymbol{y}$ axis), while the rhombus contour makes demands on both the $\boldsymbol{x}$ and $\boldsymbol{y}$ directions. According to the advice of experienced professionals, this is one of the factors to be considered in actual production.

After the reference cut, the excess material is removed in the pre-cut step, thereby obtaining a rhombus-shaped outline. The starting point is always at the bottom. The tool is milled from a clockwise direction around the workpiece, experiencing the four stages in that order: the decreasing of both $\boldsymbol{x}$ and $\boldsymbol{y}$; the increasing of $\boldsymbol{x}$ while the decreasing of $\boldsymbol{y}$; the increasing for both $\boldsymbol{x}$ and $\boldsymbol{y}$; the decreasing of $\boldsymbol{x}$ while the increasing of $\boldsymbol{y}$. With the limitations of the size of the workpiece, only two tests were planned, whose radial engagements are 3.2 mm (Test #1_17) and 8 mm (Test #1_18), correspondingly, as illustrated in Figure 4.4.

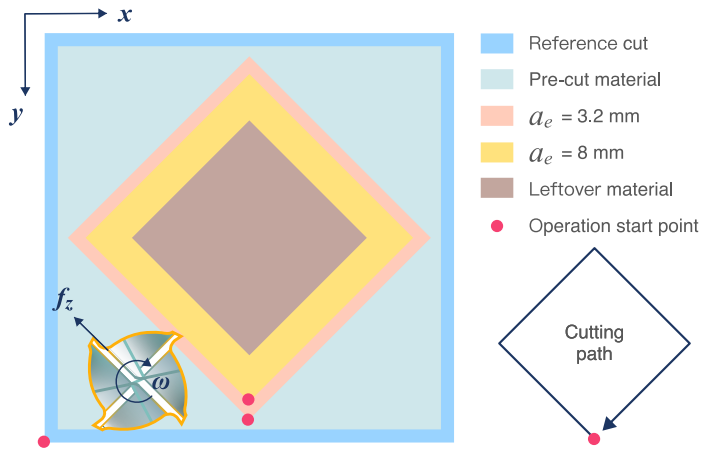

Fig. 4.4: Trajectory display for contour of square

The purpose of this designed contour is to verify that the proposed method (implemented in the angular domain with the polar coordinate system) can

be integrated with the working standard of the CNC machining center (Cartesian coordinates). The experimental set with $a_e = 3.2\,\text{mm}$ was chosen as a representative of the same type of test.

(C) **Contour of rounded square**

The rounded square milling path is generated by separating four quarters of a circle and connecting their loose ends with straight lines. Following a reference cut (starting point at the lower-left corner) and a pre-cut, the infeed for the three tests is at the lower end of the straight section on the left side of the workpiece, as shown in Figure 4.5. The radial depths of the three cuts are 3.2 mm (Test #1_10), 8 mm (Test #1_11), and 12 mm (Test #1_12). The center of their circular segments is at the same point. The outer radius of the circular is 28 mm, 24.8 mm and 16.8 mm, respectively.

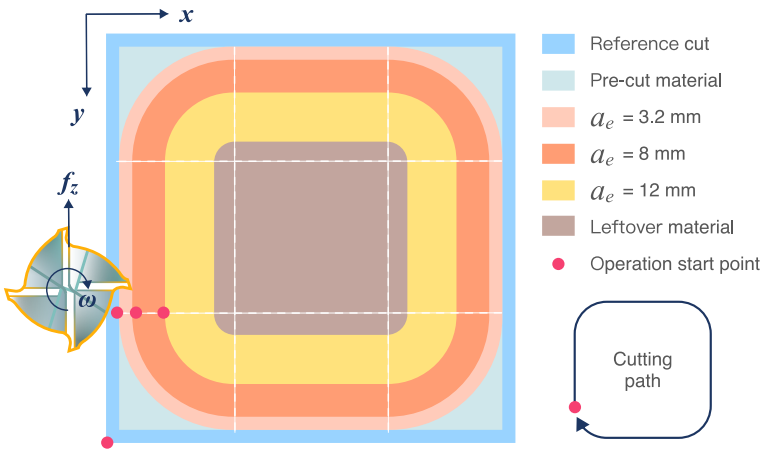

Fig. 4.5: Trajectory display for contour of rounded square

The rounded square contour shows the gradual transition of the tool from a straight line through a circular arc. During this phase, the angle of the tool immersed in the material is in a varying state. In other words, there may be inconsistencies in the material cut by each tooth at this point. Therefore, this designed contour is to examine whether the proposed method is executable in curved trajectories (cyclo-non-stationary). Since in practice, end milling operations are often accompanied by a cycloidal path, this verification, thus, is of great interest. Three tests gave similar results, where the test with $a_e =$

3.2 mm was employed as the presentation of the subsequent treatments.

(D) Contour of designed curve

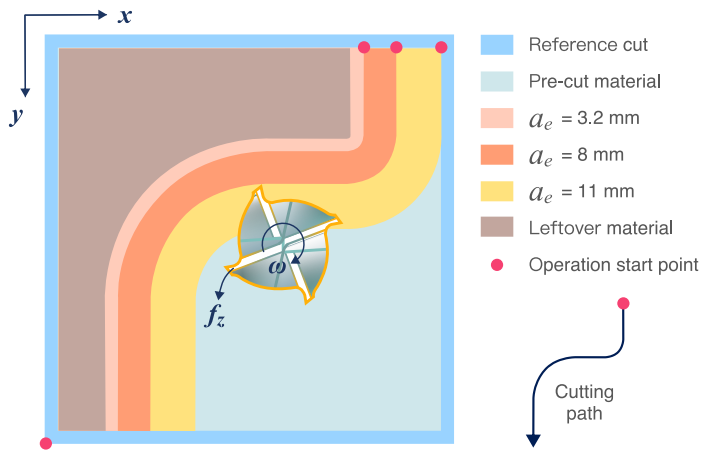

Fig. 4.6: Trajectory display for contour of designed curve

The curve of this designed path has some similarity to the rounded square, consisting of the straight line and the quartered arc as the base elements. Their loose ends are connected as shown in Figure 4.6. The difference is that all four corners of the rounded square are milled for the outer contour, while the contrast is introduced here for the inner and outer contour milling.

The start point of infeed is always at the upper edge of the workpiece. The tool first proceeds along a straight segment and passes through an outer quarter arc. The outer quarter arc is linked to an inner quarter arc whose radius is greater than the radius of the tool. And then, the tool finally enters the second straight section to finish the test. The radial depth of the cut is $a_e = 11$ mm (Test #2_6), 8 mm (Test #2_7), and 3.2 mm (Test #2_8), respectively.

Compared to outer contour milling, the material has a stronger tendency to enclose the tool when milling the inner contour. For comparison with other trajectory cases, the test with $a_e = 3.2$ mm has been selected for the subsequent interpretation.

(E) Contour of designed curve with holes

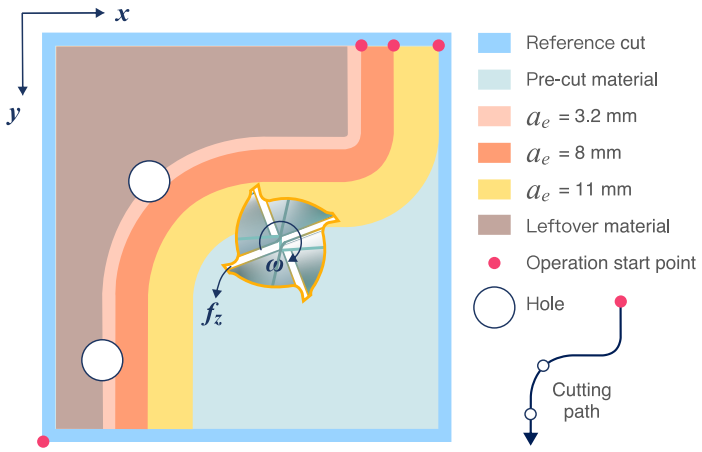

Fig. 4.7: Trajectory display for contour of designed curve with holes

In this design, the tool runs on exactly the same trajectory as in case (D). The only difference is that prior to the experiment, holes were drilled in the workpiece at the locations shown in Figure 4.7, whose diameter is 10 mm.

The position of the hole and the cutting trajectory are partially overlapped. This is considered as an unexpected event during the operation and is used to evaluate whether the proposed correlation method can cope with sudden changes. The operation with $a_e = 3.2\,\text{mm}$ (Test #3_19) is considered as the representative to display the results for the subsequent sections.

4.4 Data pre-processing

The study proposes a methodology for assessing the tool condition by exploiting the correlation between teeth signatures. Useful information, hidden fairly deep in the raw signal, includes the preceding and following idle rotations of the end-mill at the settled spindle speed. The key steps of the signal pre-processing are described in the following sections.

The data of Test #1_10 from case (C) is employed here to show the processing results.

4.4.1 Hilbert transformation

The spindle signal received from Input 6 needs to be detuned to obtain an intuitive angular signal. The Hilbert transform is served as a demodulator here.

Hilbert transform imposes an important role in signal processing. Its physical meaning is to impart a phase shift of ± 90° to every frequency component of a signal, constructing the analytic representation of the initial real data sequence. The analytic signal x can be described as

$$x = x_r + jx_i. \tag{4.1}$$

The sign of the shift depends on the sign of the frequency ω, that is:

$$\mathcal{F}(x_i(\omega)) = \begin{cases} e^{+\frac{i\pi}{2}} \cdot \mathcal{F}(x_r(\omega)) & \text{for } \omega < 0, \\ 0 & \text{for } \omega = 0, \\ e^{-\frac{i\pi}{2}} \cdot \mathcal{F}(x_r(\omega)) & \text{for } \omega > 0. \end{cases} \tag{4.2}$$

By introducing the imaginary part of the signal, the Hilbert transform returns a helical sequence, including the phase information that depends on the phase of the original, as illustrated in Figure 4.8(a).

The projection of the analytic signal on a plane consisted by the real-imaginary axes can be thought of as a vector that rotates over time (Figure 4.8(b)). The instantaneous phase

$$\theta = \arctan \frac{x_i}{x_r} \tag{4.3}$$

corresponds to the intuitive angular information of the rotational spindle, and the instantaneous amplitude

$$|x| = \sqrt{{x_r}^2 + {x_i}^2} \tag{4.4}$$

is the envelope of the signal.

Consequently, using the `hilbert` and `angle` commands in Matlab, the angular

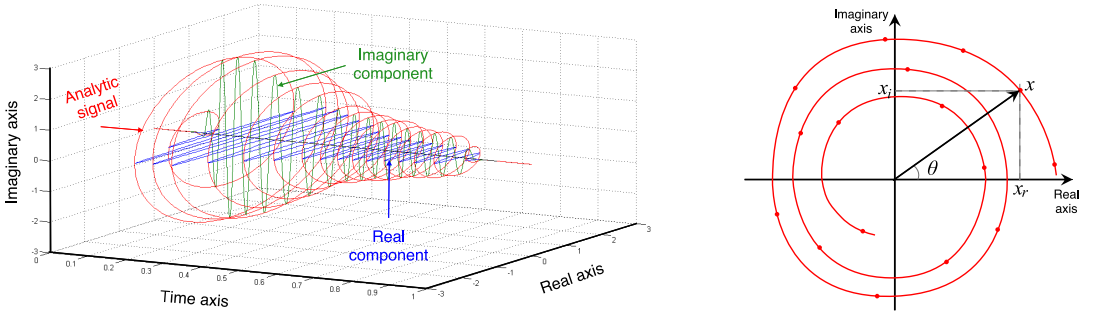

(a) (b)

Fig. 4.8: Demonstration of Hilbert transformation: (a) composition of the analytic signal; (b) representation of phase information corresponding to the rotational angle of the spindle.

information of the experimental process can be extracted from the spindle signal for subsequent resampling treatment (Section 4.4.2), and the instantaneous angular speed (IAS) can be derived as

$$\omega = \frac{\mathrm{d}\theta}{\mathrm{d}t}. \tag{4.5}$$

4.4.2 Resampling

Since all kinematic variables in the operation of rotating machinery are related to certain angles of rotation, the acquisition signals associated with mechanisms behave as angular cyclostationary rather than temporal cyclostationary [Ant+04]. Therefore, sampling the signals concerning an angular variable rather than a time variable allows better preservation of the cyclostationary property.

From a macro point of view, the cutting speed has been set at a fixed value, but as a matter of fact, due to cutting force/torque change and servo control, the milling speed changes constantly and slightly. This leads to differences in the number of sampling points within the same time length, making it difficult to later divide the signal into segments corresponding to each tooth.

In this work, the dynamometer under the workpiece records the force change over time, while the rotary encoder gives the information of the corresponding angle domain. Resampling is adopted as the means to achieve converting the time signal

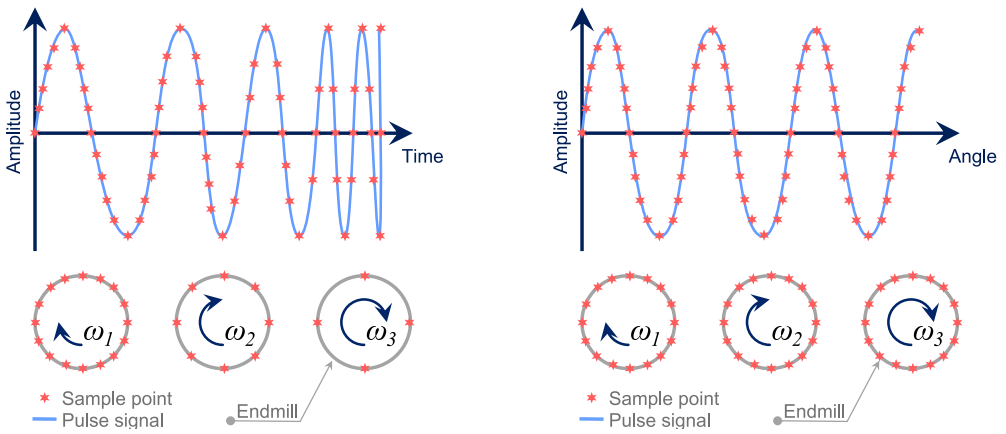

(a) (b)

Fig. 4.9: Schematic diagram for data acquisition under different domains with variable rotational speed ($\omega_1 < \omega_2 < \omega_3$): (a) the number of samples collected per revolution varies with the rotational speed if sampling in time domain; (b) the number of samples collected per revolution is evenly distributed regardless of rotational speed if sampling in angular domain.

to the angular domain.

Compared with the time sampling in Figure 4.9(a), the resampling in the angular domain can stabilize the number of samples per revolution, regardless of the rotation speed (Figure 4.9(b)). That is to say, no matter how the cutting speed changes ($\omega_1 < \omega_2 < \omega_3$), a constant number of sampling points will be recorded for each revolution.

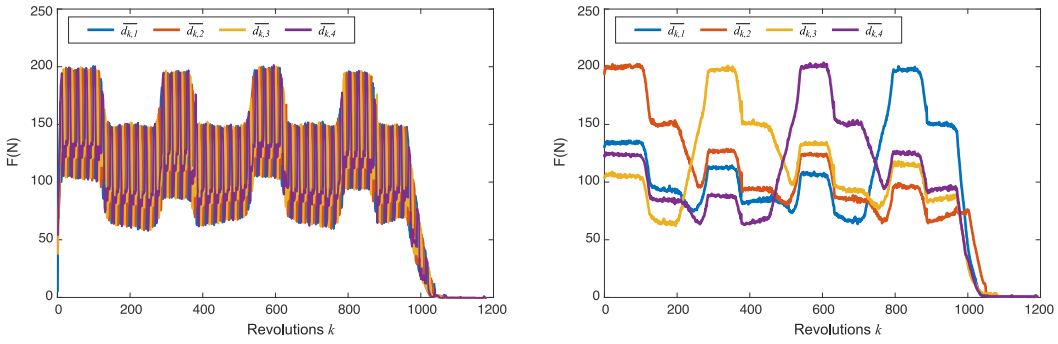

(a) (b)

Fig. 4.10: Comparison before and after resampling in angular domain of the average value of each segment $\overline{d_{k,i}}$: (a) sampling in time domain; (b) resampling in angular domain (θ)

The average value of the segment $\overline{d_{k,i}}$, as defined in Section 3.4.2, can be used to roughly represent the general state of the segment. By connecting $\overline{d_{k,i}}$ with the same segment i in series, the results provide a principal tendency to observe briefly whether the subsequent optimization process is effective before the introduction of correlation analysis.

As shown in Figure 4.10, the data with the same subscript i are plotted as one line with the rotation cycles as the abscissa. The results before and after resampling are strongly affected by whether the signal is considered in the time or in the angular domain.

4.4.3 Milling direction correction

This work ensures that the force signal is correctly synchronized with the tooth signatures. When cutting in a straight line, only angular interpolation is needed to achieve this goal. However, changing the cutting path will naturally introduce a phase shift, which affects the distribution of the signal to the cutting edge. Fortunately, the trajectory change can be simply corrected through the combination of the tool rotation angle θ and the trajectory change angle Θ as mentioned in Section 3.3.

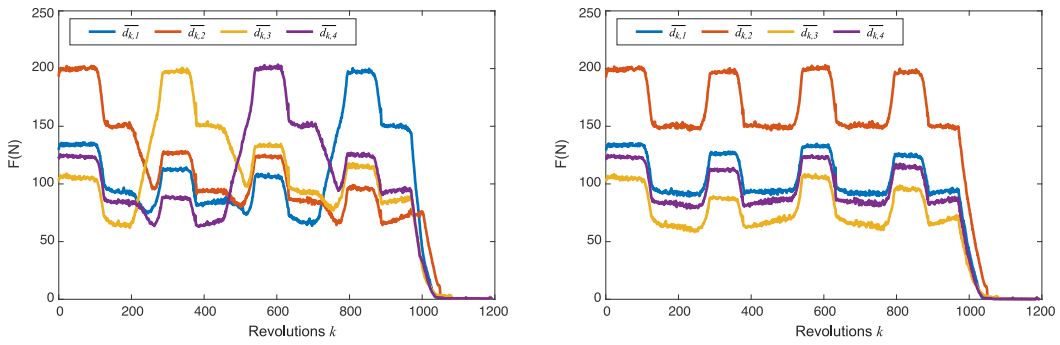

(a) (b)

Fig. 4.11: Comparison before and after trajectory correction by average value of each segment $\overline{d_{k,i}}$: (a) angle of reference (θ) without correction; (b) angle of reference ($\theta + \Theta$) with correction.

After the correction, the signal is shifted to the position corresponding to the correct segment. The cutting force is stable at a high value during the straight cutting section and drops to a low point when entering the arc. The cycle repeats four

times along the trajectory (Figure 4.11). In traditional monitoring, similar parameter changes are likely to cause false alarms, whereas, in the proposed method, the impact resulting from trajectory changes can be minimized after correlation analysis because the segments have undergone identical milling changes almost simultaneously. Due to the limitations of experimental circumstances, the tools used are not brand new. As mentioned in Section (D), the second tooth is about 0.06 mm longer than the other teeth at the beginning of the experiment. Therefore, every time it cuts into the material, the force it receives is about 50 N stronger than the other teeth. This difference is within the allowable range of machining accuracy.

4.4.4 Truncation & Segmentation & Zero-centering

The idling component of the signal (before the tool enters the material and after the tool exits the material) is of no value for identifying the signal signature corresponding to each segment. Hence, this part is truncated by manual selection.

This process also serves to round up the acquired data by revolutions. When one of the teeth cuts into the material, the resistance suddenly increases (matching the rising edge) and the angular velocity decreases. During the cutting process of one insert, the resistance gradually drops off with the formation of the chips and finally reduces to approximately zero when this insert leaves the material. The process of the previous tooth entering and then quitting the material until the next tooth enters again is called a single tooth-cut. Repeating this process n_z times is a complete rotatory cycle of the tool. Figure 4.12 illustrates the tooth-cut with dotted lines, using the cutting force signal and corresponding cutting speed signal (instantaneous angular speed (IAS) and average angular speed (AAS)).

At the same time, by truncating the incomplete head and tail, the rest of the data is rounded well according to the rotational period, as shown in Figure 4.12 below.

The remaining signal is segmented and reshaped as described in Section 3.4.1. The original one-column data sequence is folded into k object matrices for further analysis, each of which has n_z columns containing m points.

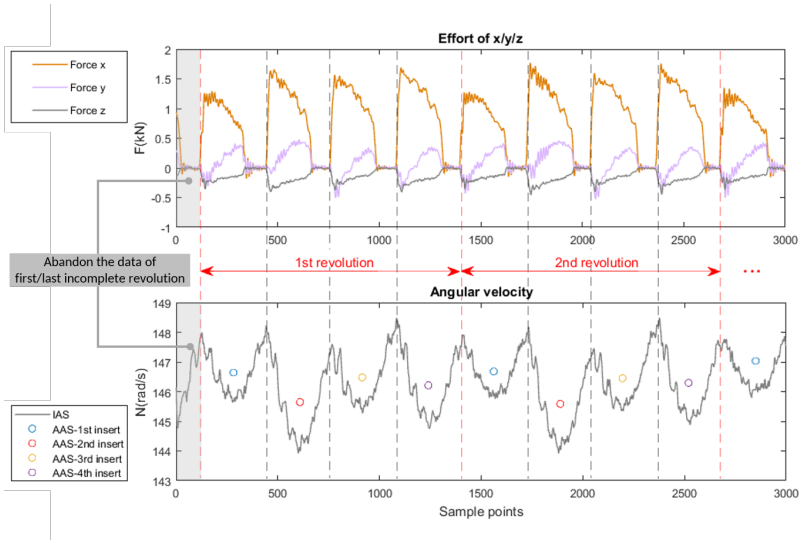

Fig. 4.12: Truncation

As mentioned in Section 3.4.2 and derived in Equation 3.6, the milling model is composed of three parts: the average value and the mean shape of the standard cutting force are determined by the original tool state and the superimposed force $\mathbb{\Delta}F_k$ (increased or decreased) due to the condition of the edge. The resulting change is very small compared to the original value; it needs to be centralized before correlation analysis. Zero-centering refers to the matrix $(\mathbb{D}_{\mathbb{k}} - \overline{D_k}\mathbb{J})$. In this way, the performance of relevance will be emphasized, and this method can be applied to map the different risk factors to each insert to realize higher-precision monitoring. The experimental results show that zero-centering can also remove the random effects in the shutdown process.

4.5 Conclusion

Chapter 4 mainly covers the acquisition and pre-processing of experimental data.

A force measurement experiment was set up with the Kistler 9257A 3-axis dynamometer as the centerpiece. In conjunction with the rotary encoder integrated into the spindle and the displacement sensors on the bench, a total of six channels of signals were gathered and saved in the OROS analyzer.

4.5 Conclusion

After determining the cutting condition parameters for the milling operation, four different milling trajectories were designed. The square contour contains four straight line cuts and is used to establish the basic stationary working condition. The rhombus-shaped path is aimed at verifying the compatibility of the angular coordinates used in the proposed method and the Cartesian coordinates from the CNC working system. The rounded square trajectory contains curved paths, i.e. for the testing of non-stationary regimes. The design curve intends to observe how the inter-insert correlation is affected by the wrapping of the material around the tool when the cutter passes through the inner and outer contours respectively. On this basis, adding holes to the path is used to test how the tool behaves when it encounters such a sudden change.

Pre-processing prior to inter-insert correlation includes signal resampling in angular domain, milling direction correction, truncation, segmentation, zero-centering, etc. The results obtained from the pre-processing of the experimental data demonstrate that the steps of angular domain resampling and direction correction effectively clarify the signal components corresponding to each tooth, which enhances the operability of the segmentation and provides a promising basis for the inter-insert correlation.

Chapter 5

Characterization of tool state by SVD

Summary

5.1 Introduction . . . 102
5.2 SVD components . . . 102
5.2.1 Straight-line simulation signal . . . 107
5.2.2 Curve-line simulation signal . . . 108
5.3 Analysis of results . . . 112
5.3.1 Validity verification of SVD analysis with experimental data . 113
5.3.2 Fundamental verification . . . 115
5.3.2.1 Compatibility of the angular domain-based approach with the Cartesian coordinate system . . . 115
5.3.2.2 Effectiveness of zero-centering . . . 117
5.3.2.3 Variation in radial depth of cut . . . 118
5.3.3 Sensitivity analysis . . . 119
5.3.3.1 Bootstrap . . . 120
5.3.3.2 Window shift . . . 125
5.4 Fault detection . . . 127
5.4.1 TCM based on separability index $\alpha_{k,1}$ . . . 128
5.4.2 TCM based on sensitivity range Δ_{WS} . . . 131
5.4.3 Summary and evaluation . . . 131
5.5 Limitation . . . 134
5.6 Conclusion . . . 137

5.1 Introduction

After the pre-processing steps described in Chapter 4, the signals obtained under different cutting conditions are ready for inter-insert correlation analysis. After the literature review (Section 2.5.3), the singular value decomposition is considered a suitable and effective means to implement inter-insert correlation.

In Section 5.2, the simulated signal of the IAS constructed in Section 3.4.3 is used as the data source for the preliminary feasibility analysis. The physical significance of the SVD decomposed components is interpreted in both straight and curved milling cases. After the ideal numerical simulations yielded optimistic results, the same algorithm was applied to the collected experimental data. Section 5.3 shows the processing results for different experimental groups and validates the previous conjectures. Following a sensitivity analysis, Section 5.4 describes in detail the two metrics based on the separability index and the window shift. After analyzing the tools in good condition, the signals of worn tools are presented to assess the feasibility of the proposed indicators. In the end, a brief evaluation is made using ROC curves. The limitations faced by the method are commented in Section 5.5.

5.2 SVD components

The signal that has been reshaped by pre-processing in Chapter 4 is presented as a matrix and ready for correlation analysis. In theory, SVD can extract the main components of the data with an underlying correlated analysis algorithm (Section 2.5.3) and determine the status of the tool. In the following section, the decomposition components of SVD will be introduced first to facilitate the presentation of the results with experimental data.

In order to understand the nature of SVD, the proposed method is first pushed to the extreme to see how the ideal situation looks like, which can help to enhance the grasp of the problem. After that, the real conditions can be added step by step.

Therefore, the IAS simulation model mentioned earlier in Section 3.4.3 is used

here to serve for the demonstration. To make the results more concise, this part of the study was performed based on the strategy of correlation analysis in the unit of all segments (case (A) in Section 3.5) and only one SVD was performed.

In the simulation, the signal contains a total of 120 segments, i.e. 30 revolutions, and the amount of data for each segment is designed to be 250 points. The amplitudes of the four segments corresponding to one revolution are set to $K = [5, 5, 10, 1]$, as illustrated in Figure 5.1(a). It is used to imitate the situation where the first and second teeth work normally, the third tooth is in worn condition, and the fourth tooth performs compensated work with lower speed.

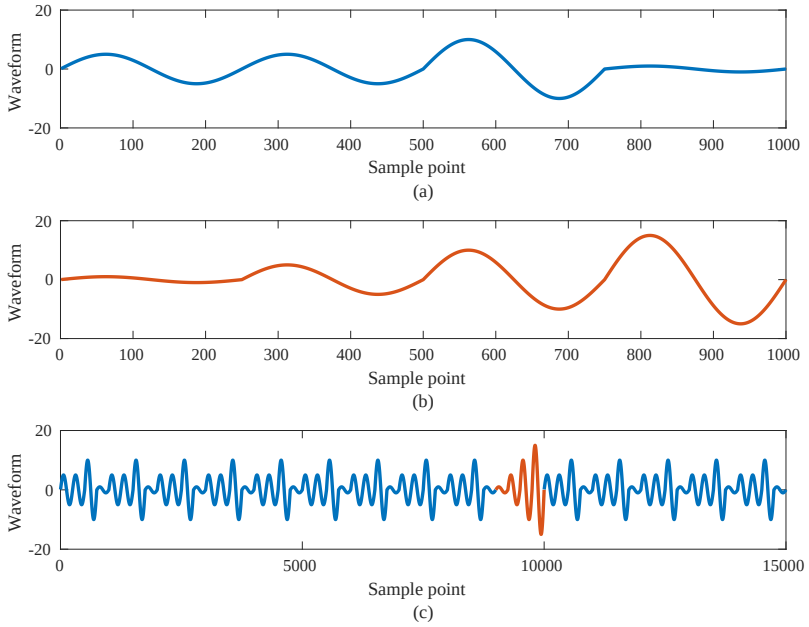

Fig. 5.1: Simulation signal for SVD components demonstration: (a) the simulated amplitudes $K = [5, 5, 10, 1]$ correspond respectively to segments of each normal revolution cycle; (b) the simulated amplitudes $K_{change} = [1, 5, 10, 15]$ correspond respectively to segments of the tenth revolution with sudden change caused by the tooth wear; (c) a full view of the simulated signal.

In order to simulate the sudden change of the signal caused by the tool damage, the signal amplitude of the tenth revolution is intentionally modulated to $K_{change} = [1, 5, 10, 15]$, as displayed in Figure 5.1(b). Such an abrupt change can be seen as the fourth tooth being overwhelmed by the hard condition of work and also undergoing wear. At the same time, the workload of compensating cuts falls on the first tooth.

The specific simulation parameters correspond to Equation 3.7 for MATLAB code are listed in Table 5.1. The complete simulation signal is shown in Figure 5.1(c).

Parameter	Value
Number of inserts n_z	4
Rotational frequency ω (rad/s)	50π
Samples for one segment m	250
Total segments n	60
Altitudes set for segments K	[5,5,10,1]

Table 5.1: Parameters for straight-time simulation signal

The result of reshaping the above-mentioned simulated signal in the manner described in Section is denoted as $\mathbb{D}_{\mathtt{seg}}$. After SVD processing, $\mathbb{D}_{\mathtt{seg}}$ can be decomposed into three matrices $\mathbb{U}$, $\mathbb{\Sigma}$ and $\mathbb{V}$. As mentioned in Section 2.5.3, SVD can grab the main components of the data by taking advantage of the underlying correlation principle. Accordingly, the information in the matrices $\mathbb{U}$, $\mathbb{\Sigma}$ and $\mathbb{V}$ are hierarchically arranged in order, based on the criteria of the importance possessed by the decomposed components.

The three parts are plotted separately in Figure 5.2. The blue line represents the 1st order component, which is the most dominant component, while the orange lines depict the components from the second to the last order. The aim is trying to connect these three components with the physical meaning in reality.

Evidently, as can be observed from Figure 5.2(a), the plotting shares the curvilinear features of trigonometric functions for both first-order and higher-order data. In comparison with Figure 5.1(c), it can be seen that the left singular matrix $\mathbb{U}$ extracts the normalized shared waveform from the segments of the original simulated signal.

Figure 5.2(b) represents the ordered singular matrix $\mathbb{\Sigma}$. It is a matrix with real, non-negative entries on the diagonal and zeros off the diagonal. Therefore, only the values on the diagonal are plotted in the diagram. The results shown in the figure indicate that the first-order value is 50, which is much larger than the other orders.

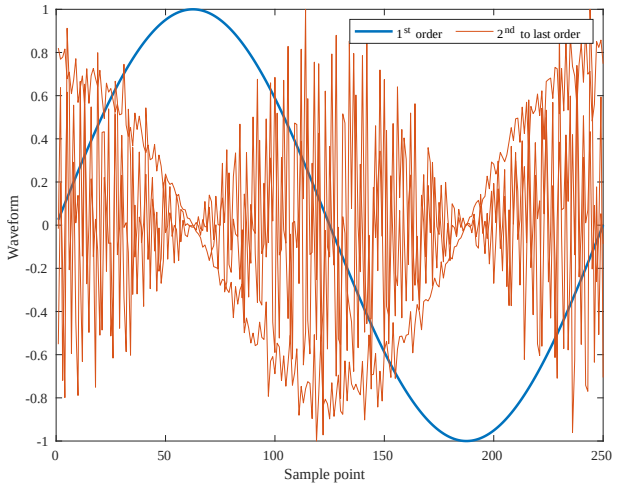

(a)

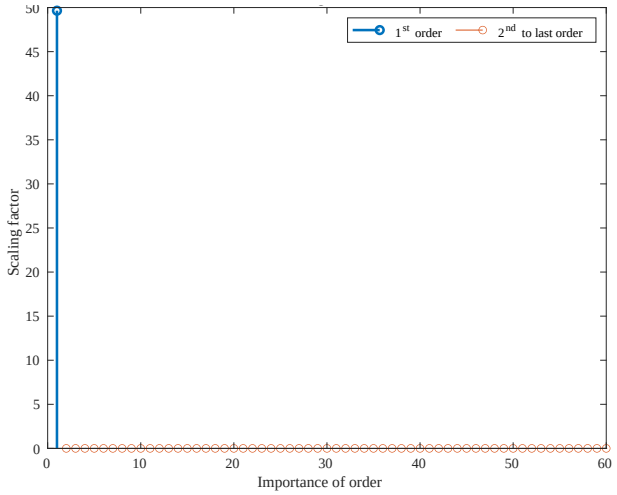

(b)

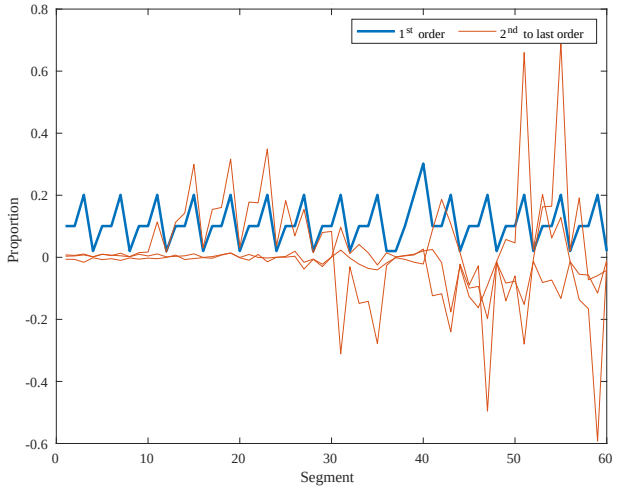

(c)

Fig. 5.2: Demonstration of decomposed components by SVD: (a) left singular matrix $\mathbb{U}$; (b) ordered singular matrix $\mathbb{\Sigma}$; (c) right singular matrix $\mathbb{V}$.

As mentioned earlier, the order represents the importance of each component and its approximation to the original signal. Therefore, $\mathbb{\Sigma}$ can be considered as a scaling factor matrix to determine the contribution of the decomposition sequences to the original signal.

As for $\mathbb{V}$, each decomposed order contains information on the amplitudes proportion. Since the previous paragraph has already concluded that the first-order component is dominant, it is reasonable to focus on the line traced by the first-order vector $\boldsymbol{v_1}$ (the blue line in Figure 5.2(c)). The amplitudes of most of the segments are repeated in cycles of [0.1, 0.1, 0.2, 0.02]. From the 37^{th} to 40^{th} segments (corresponding to the tenth revolution), the amplitude value undergoes a change.

Although the amplitudes of $\boldsymbol{v_1}$ do not exactly match the value of the given amplitude K, the result shows that the ratio between the amplitudes in $\boldsymbol{v_1}$ is consistent with the original signal. At the position of the tenth revolution, the sudden change shows up as the preset control.

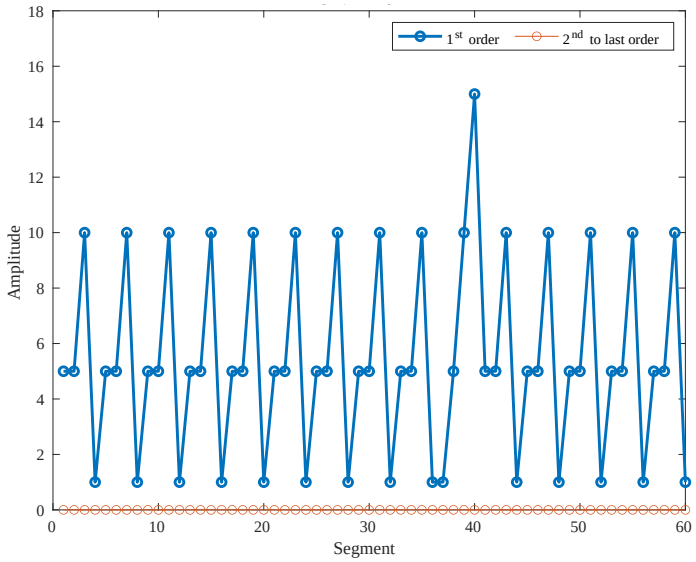

Fig. 5.3: The result of combined decomposed components $\mathbb{\Sigma V}^\top$ represents the amplitude of the signal being processed.

That is to say, the matrix $\mathbb{V}$ consists in providing a series of pulses with the correct amplitude proportions, while the matrix $\mathbb{\Sigma}$ operates with a distribution of importance, scaling up or down the pulses of the corresponding order. As a result, when plotting $\mathbb{\Sigma V}^\top$, it can be observed that the previous cluttered overlapping curves

from the second to the last order (the orange lines in Figure 5.2(c)) are multiplied by a very small factor and approach 0, while the first-order curve is enlarged. For the sake of brevity, $\mathbb{\Sigma}$ and $\mathbb{V}$ will be analyzed as a whole $\mathbb{\Sigma}\mathbb{V}^\top$ if there are no special circumstances in the following text.

It is worth noting that this is a very ideal result. Because the signal processed here is a simple straight-line simulation signal. When this method is applied to the analysis of real signals, it is often not enough to describe it by relying on only the first order, and the second, third and even higher orders also have certain reference significance. This process is like drawing. When the described object is more complex, there is a need to gradually add more details to the basic content.

5.2.1 Straight-line simulation signal

After the physical meaning of the SVD decomposition components is clear, the simulated signal of the straight cutting is subjected to SVD once again but with the object matrix in the unit of revolution (case (C) in Section 3.5). Since there are multiple extractions and calculations, the results are represented with 3D images, as demonstrated in Figure 5.4.

The abscissa in Figure 5.4(a) represents the sample size of the segments being analyzed; the ordinate corresponds to the times of extractions, i.e., the number of rotations in this case; and the applicate represents the value of the extracted waveform. In Figure 5.4(b), the horizontal coordinate indicates the number of extractions, the longitudinal coordinate stands for the respective number of teeth, and the vertical axis presents the factor for scaling the waveform.

If looking purely from the aspect of the images, Figure 5.4 appears to be a simple split of Figure 5.2. As a matter of fact, however, Figure 5.2 is the result of a decomposition of the reshaping matrix $\mathbb{D}_{\text{seg}}$, while Figure 5.4 is the result of a decomposition of the revolution-by-revolution matrix $\mathbb{D}_{\mathbb{k}}$. When dealing with more complex realistic signals, the decomposition of $\mathbb{D}_{\mathbb{k}}$ will give greater accuracy and more diagnostic advantages.

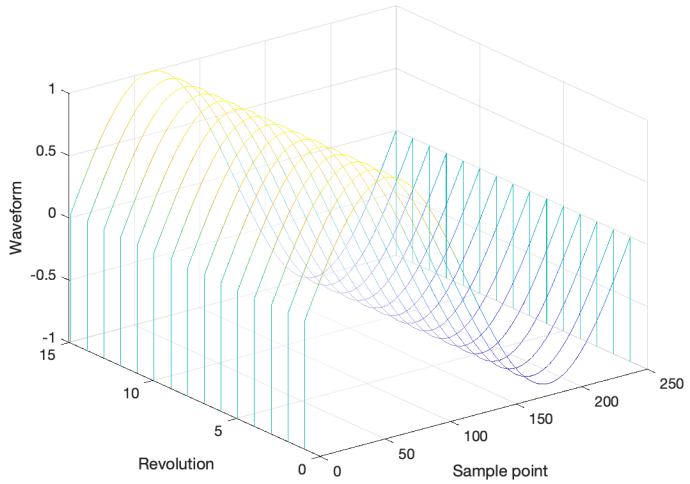

(a)

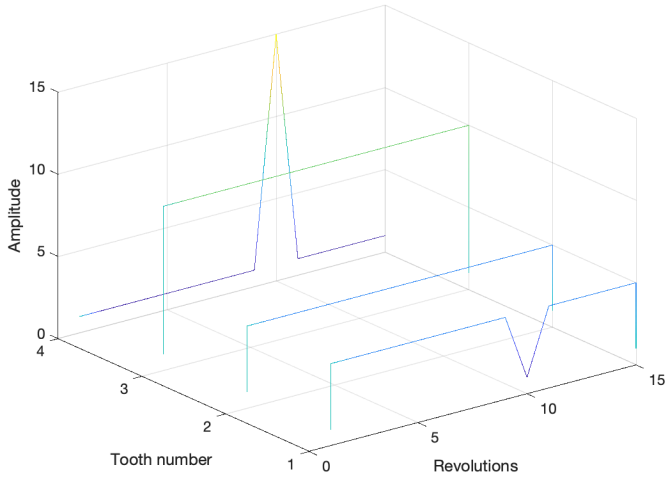

(b)

Fig. 5.4: SVD analysis by revolution for straight-line simulation signal: (a) the extracted waveforms for revolutions (the 1^{st}-order of $\mathbb{U}$); (b) the extracted amplitudes for revolutions (the 1^{st}-order of $\mathbb{\Sigma V}^{\top}$).

5.2.2 Curve-line simulation signal

Since the ultimate goal of this research is to be applied to practical machining, which must involve the cyclo-non-stationary working environment. Therefore, the simulated curve-line signal described in Section 3.4.3 is also been tested to verify the above-mentioned method (case (C) in Section 3.5). The corresponding simulation parameters for Equation 3.10 are listed in Table 5.2.

Parameter	Value
Number of inserts n_z	4
Rotational frequency ω (rad/s)	46π
Samples for one segment m	250
Total segments n	240 (half for straight-line; half for curve-line)
Altitudes set for segments K	1
Turning speed through the curve Ω (rad/s)	$\frac{5}{12\pi}$
IAS setting value D_0 (rad/s)	146

Table 5.2: Parameters for curve-time simulation signal

The signal is set to 30-revolution straight-line milling, followed by a 30-revolution curve path cutting. Together with the number of teeth $n_z = 4$, there are 240 segments. Conducting the SVD analysis by each revolution to the simulated signal, and the results are shown in Figure 5.5.

As can be seen in the 1^{st}-order subplot of Figure 5.5(a), the curve shows a consistent sine waveform from revolution counts $k = 1$ to $k = 30$, and gradually indicates a phase shift from $k = 31$ until the end. This is exactly the kind of performance of the signal when the tool goes through the curve trajectory. At the same time, from the 2^{nd}-order subplot, it is obvious that $k = 30$ is a conspicuous demarcation point. Before this, the waveform shows a mixed noise shape, and after this point, there is a clear and smooth waveform as a supplement to compensate for the insufficiency of information in the 1^{st}-order. It can be concluded that the phase of the signal does shift according to the turning angle of the trajectory Θ as the tool passes through the curve. In this case, the SVD can still produce a valid decomposition for n_z consecutive segments of a given revolution. The extracted waveform contains the overall-considered phase offset of multiple segments in the object matrix.

Similarly, in Figure 5.5 (b), the value of $\mathbb{\Sigma V}^\top$ fluctuates after the critical point of k=30. This illustrates that each tooth will experience a slightly different cutting process when the tool is under cyclo-non-stationary operations. Therefore, if conditions permit, it is advisable not to omit the prior correction of the milling direction

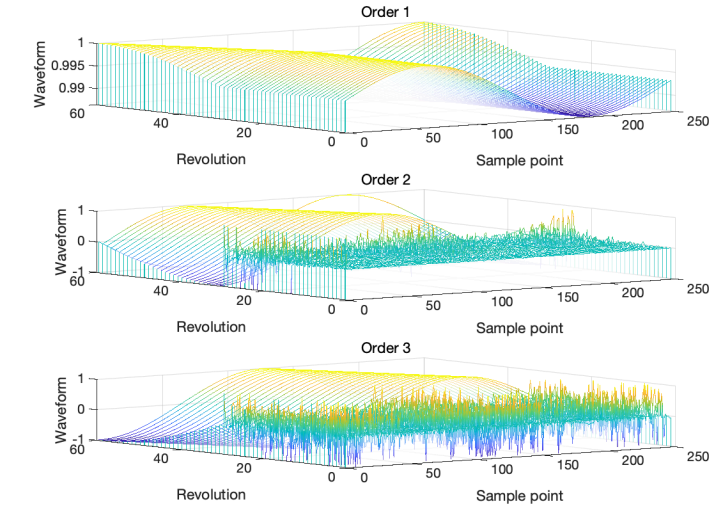

(a)

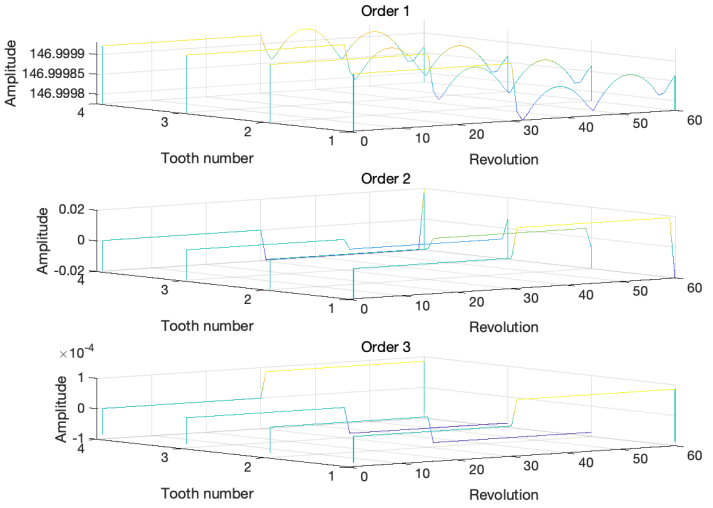

(b)

Fig. 5.5: SVD analysis by revolution for curve-line simulation signal: (a) the extracted waveforms for revolutions (the 1^{st}-order to 3^{nd}-order of $\mathbb{U}$); (b) the extracted amplitudes for revolutions (the 1^{st}-order to 3^{nd}-order of $\mathbb{\Sigma V}^{\top}$).

described in Section 4.4.3, which contributes to the stability of the diagnosis.

The corresponding 1^{st}-order to 3^{rd}-order separability indexes are shown in Figure 5.6. The index of the first-order similarly has a cliff-shape drop at the demarcation point $k = 30$. But unlike in Figure 5.5(a), where the waveform keeps shifting in

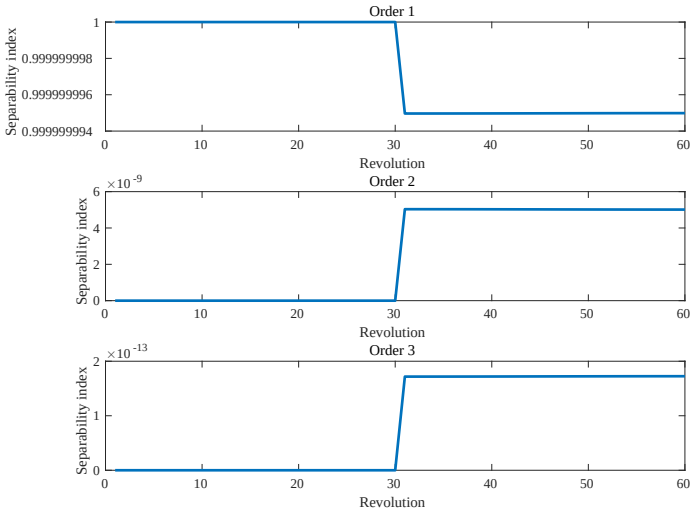

Fig. 5.6: Separability index of the curve-line simulation signal

phase with the trajectory angle Θ (the process continues from $k = 31$ to $k = 60$), the fluctuation of the separability index only appears at the point of change ($k = 30$ to $k = 31$). For both the pre- and post-change periods, the 1^{st}-order separability indexes are dominant, constant, and always remain higher than 99%.

The above results reflect two fundamental viewpoints:

- The method is sensitive to changes within the signal and has the capacity to conclude intuitive feedback.

- The fluctuation in the separability index is very small. Due to the fact that the feed rate of the tool through the curve is much lower than the tool rotation speed, the external influences for n_z segments of the same revolution can be considered to be very similar in general. Theoretically, only the state of the tool affects the separability index significantly, so false alarms triggered by external factors can be minimized.

These two foundations make the method possible to create a related indicator for tool state monitoring.

It is worth noting that although the second-order complements the first-order (Figure 5.5), the separability index of the first-order and second-order (Figure 5.6) have nine orders of magnitude (10^{-9}) differences in their values. This is due to the

fact that the zero-centering step is skipped for the simulation signals, resulting in a value of the original parameter that is much larger than its fluctuating amount.

5.3 Analysis of results

Because the tool condition is almost the same before and after the experiment (no wear was observed) and the results of multiple experiments for the same cutting path case (described in Section 4.3.1) are similar, in this section, one set of data corresponding to each milling trajectory is taken as typical objects for analysis. At the same time, in order to verify the performance of the proposed methodology under the worn tool situation, a milling data set is borrowed from F. Girardin et al. [GRR10] for experimental validation of failure detection.

The relevant information of all involved experimental datasets are summarized in Table 5.3.

Data number	Milling trajectory	Sample points per segment m	Radial depth of cut ae (mm)	Total revolutions n
Test #1_4	Contour of square	512	8	1070
Test #1_18	Contour of rhombus	512	8	845
Test #1_10	Contour of rounded square	512	3.2	1200
Test #1_12	Contour of rounded square	512	12	910
Test #2_6	Contour of designed curve	512	11	450
Test #2_8	Contour of designed curve	512	3.2	440
Test #3_19	Contour of designed curve with holes	512	3.2	450
FG #120915	Straight line	320	10	234

Table 5.3: Experimental parameters of the data sets involved in the following analysis

5.3.1 Validity verification of SVD analysis with experimental data

Test #1_10 is taken as an example to be the main object of analysis. In the case of the rounded square contour, the results can prove that the correlation analysis based on the SVD is more than sufficient to provide valid information. The tool is under good working condition and the SVD is performed on each revolution of the data, as shown in Figure 5.7.

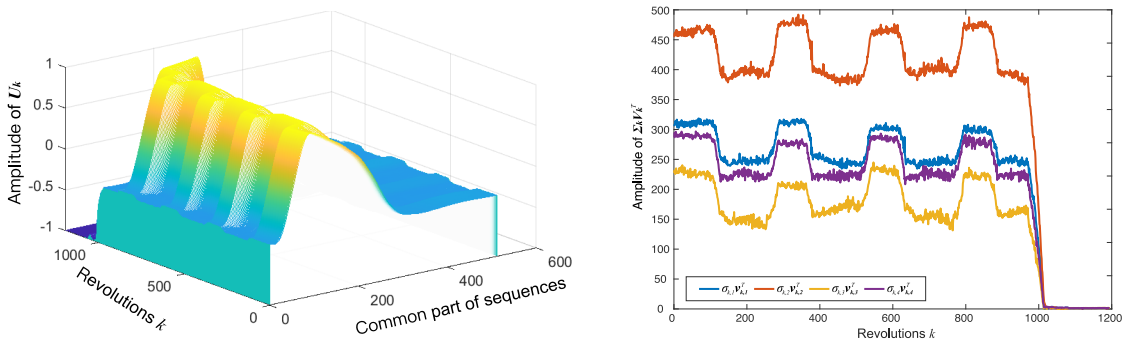

(a) (b)

Fig. 5.7: SVD results for healthy tool: (a) left singular vector $\boldsymbol{u_k}$ of SVD as a function of revolutions presents a basic waveform of signal; (b) ordered singular value σ_k times transposed right singular vector $\boldsymbol{v_k}^\top$ presents the corresponding value of force.

Combining Equation 5.1 and Equation 3.6, SVD can decompose the input matrix $(\mathbb{D}_{\mathbb{k}} - \overline{D_k}\mathbb{J})$ as

$$\mathbb{D}_{\mathbb{k}} - \overline{D_k}\mathbb{J} = \sigma_{k1}\boldsymbol{u_{k1}}\boldsymbol{v_{k1}}^\top + \sigma_{k2}\boldsymbol{u_{k2}}\boldsymbol{v_{k2}}^\top + \ldots + \sigma_{kn_z}\boldsymbol{u_{kn_z}}\boldsymbol{v_{kn_z}}^\top. \tag{5.1}$$

The left singular vector $\boldsymbol{u_k}$ extracts the common part contributed mainly by Ψ_{F_k} (defined in Equation (3.6)) for each input matrix $(\mathbb{D}_{\mathbb{k}} - \overline{D_k}\mathbb{J})$. It can be seen from Figure 5.7(a) that the first-order result of a single revolution is displayed with 512 sample points that form a basic waveform of k^{th} revolution. Throughout the milling process, the waveform remains unchanged, but there is a slight phase shift towards the right when the cutter passes through the corner. This is the phase shift that is naturally introduced by the cutting path mentioned in Section 4.4.3. The milling direction correction in signal processing has greatly improved the situation of phase

change, but a residue remains.

The right singular vector $\boldsymbol{v_k}$ contains the amplitude ratio corresponding to the n_z segments within $(\mathbb{D}_\Bbbk - \overline{D_k}\mathbb{J})$, which reflects the influence of $\boldsymbol{\Delta F_k}$. The ordered singular value σ_k is the amplification factor. The combination of the above two terms $\sigma_k \boldsymbol{v_k}^\top$ represents the characteristic amplitude value for the corresponding force of each insert after zero-centering.

One needs to pay attention to the difference between Figure 5.7(b) and Figure 4.11(b). Figure 4.11(b) simply reports the speed sequence of each segment into a single average value $\overline{d_{k,i}}$, while Figure 5.7(b) presents the characteristic amplitude extracted from the matrix $(\mathbb{D}_\Bbbk - \overline{D_k}\mathbb{J})$, which can preserve the signal information as much as possible by combination with the left singular vector $\boldsymbol{u_k}$.

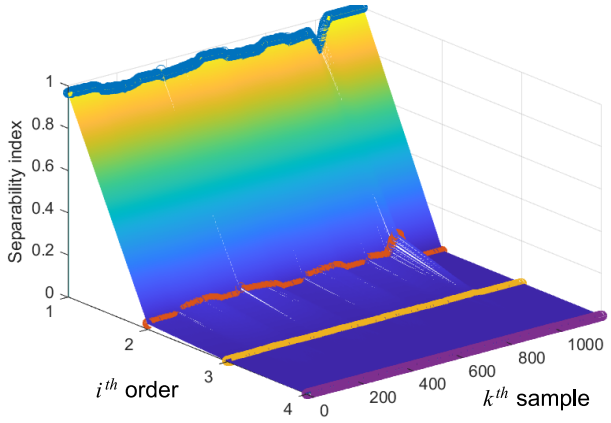

Fig. 5.8: Separability index for each order with respect to samples

The proposed separability index (Equation 2.45) can measure the proportion of the i^{th} order component to the set of all components in the decomposition process. In current case, the 1^{st}-order of the separability index α_{k1} remains above 90 % or more (Figure 5.8), whereas the 2^{nd}-, 3^{rd}-, and 4^{th}- orders are not dominant. This means that the cutting conditions of the four teeth have a fairly high similarity throughout the whole operation process, and the decomposed 1^{st}-order component represents most of the information. This state is quite stable. During the trajectory change, the index slightly fluctuates, corresponding to milling condition adjustments, except that there is a small falling gap during the shutdown process. This is a reasonable adjustment caused by the withdrawal of the tool. When the workpiece completely leaves the material, the subsequent idling part has no cutting resistance, so the

separability index α_{k1} is closer to 1 than during milling operation. Note that in the input matrix, the subscript i stands for the column number, whereas after SVD, the subscript i represents the order of the hierarchical decomposition.

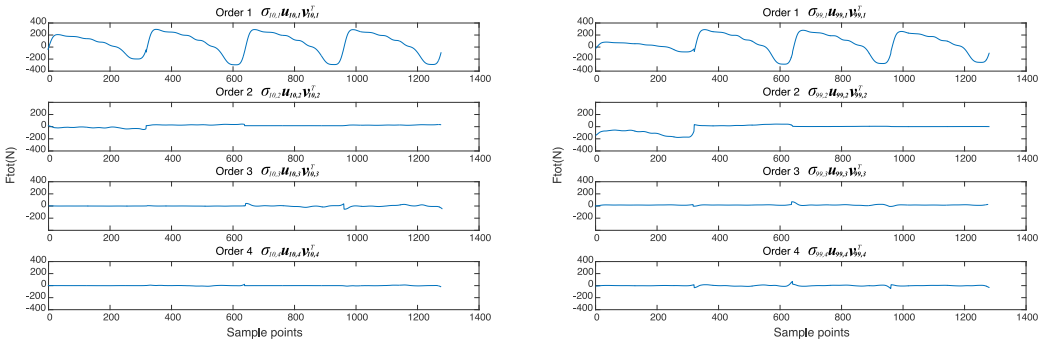

(a) (b)

Fig. 5.9: Hierarchical presentation of signal by order: (a) the 1^{st}-order component occupied dominant contribution at the beginning of tool wear; (b) when a tooth is severely worn, the 1^{st}-order is not enough to express the signal signature, thereby the proportion of the 2^{nd}-order increases.

SVD provides hierarchical results from the 1^{st}-order to the ${n_z}^{th}$-order (Equation (5.1)), which reserves more information for detailed analysis. Using the data set from Girardin et al. as an example, the 1^{st}-order shown in Figure 5.9 is the closest in the mean-square sense to the signals, and the 2^{nd}-order or higher order can supplement the remaining details on this basis. Figure 5.9(a) presents the tool state of the 10^{th} revolution where tool wear begins, whereas Figure 5.9(b) indicates the behavior in the 99^{th} revolution where the first tooth is completely worn.

5.3.2 Fundamental verification

5.3.2.1 Compatibility of the angular domain-based approach with the Cartesian coordinate system

Here in Figure 5.10, the results of **Test #1_4** and **Test #1_18** are firstly listed to verify whether the above theory is stable and valid for the analysis of experimental data.

Comparing Figure 5.10(a) and 5.10(b), it can be seen that the starting positions

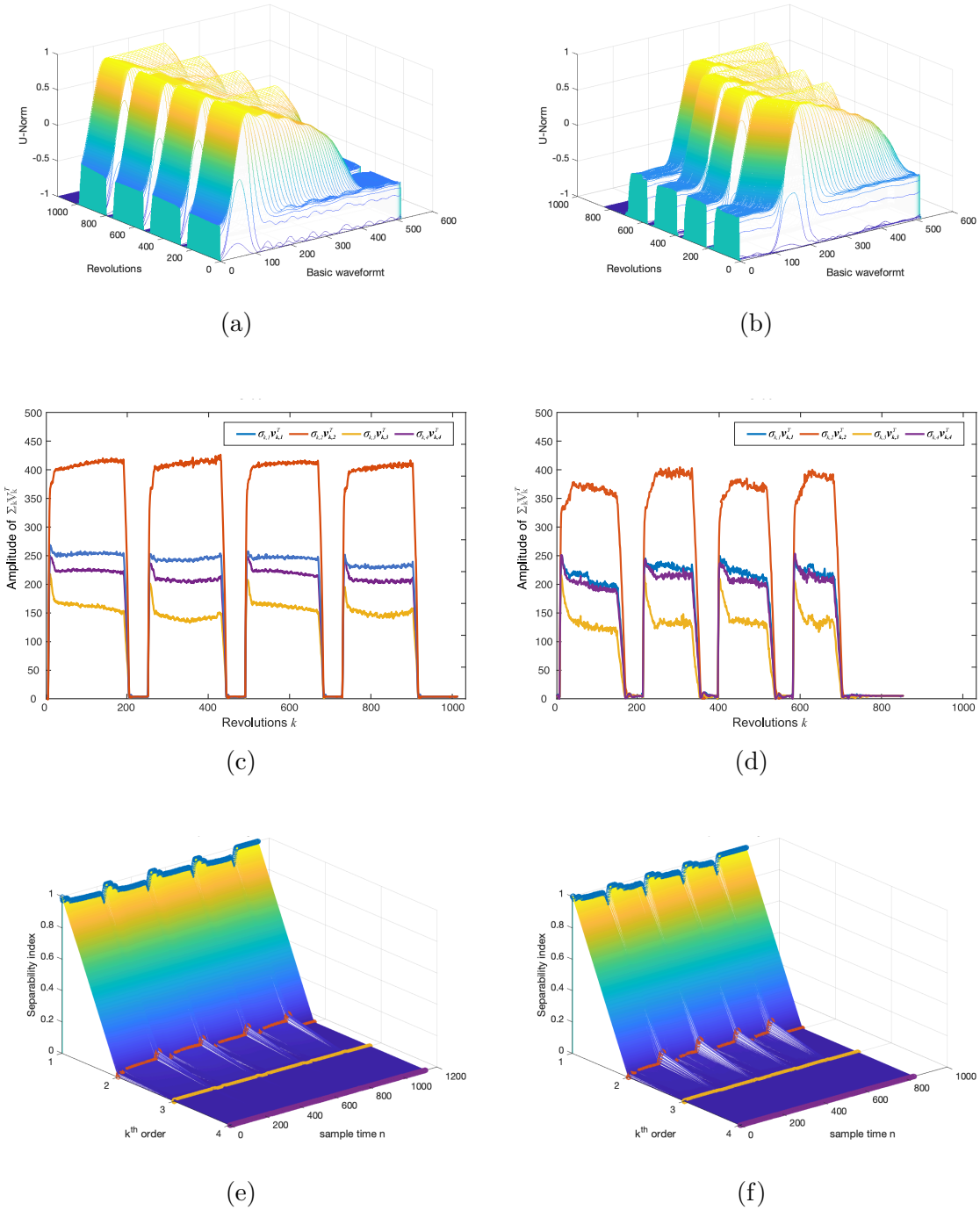

Fig. 5.10: Fundamental verification: **Contour of square** - (a) 1^{st}-order of $\mathbb{U}_{\mathbb{k}}$; (c) 1^{st}-order of $\mathbb{\Sigma V}^{\top}$; (e) Separability index; **Contour of rhombus** - (b) 1^{st}-order of $\mathbb{U}_{\mathbb{k}}$; (d) 1^{st}-order of $\mathbb{\Sigma V}^{\top}$; (f) Separability index.

of the waveforms are different, which is due to the different choice of truncation during pre-processing. This equals a certain number of sample points displaced in all segments and therefore does not affect the subsequent correlation analysis. Figure 5.10(d) shows a little more fluctuation than Figure 5.10(c), but their value and curve shape almost behave the same. The separability indices in Figure 5.10(e) and 5.10(f) are both close to 1 by a dominant margin and have the appearance of an identical trend.

The fact of similarity between the square contour milling and the rhombus contour milling confirms that the proposed SVD method can be adapted to the case where the tool acts in both $\boldsymbol{x}$ and $\boldsymbol{y}$ directions, and the algorithm compiled provides a good integration of the angular domain variation based on the polar coordinate system and the working standard of the CNC machining center based on Cartesian coordinates.

5.3.2.2 Effectiveness of zero-centering

Secondly, using the data from **Test #1_10** as a basis, the results of the first-order separability index with and without the zero-centering step are made, as shown in Figure 5.11.

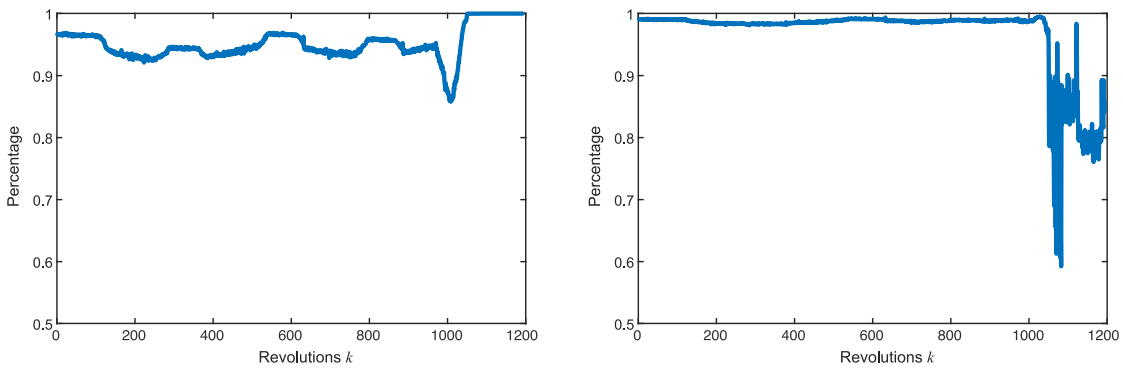

(a) (b)

Fig. 5.11: The results with and without the step zero-centering: (a) 1^{st}-order of separability index for central data; (b) 1^{st}-order of separability index for original data.

Figure 5.11(a) presents clearly the corresponding change due to the rounded square milling trajectory, whereas Figure 5.11(b) has no obvious trend change from

the overall graph. That is because the change volume is too small compared to the absolute value and zero-centering can compensate to a certain extent for the influence of the excessive value itself, highlighting the amount of change. Furthermore, during the stoppage phase, it is also worth noting that centrally processed data has shown a much more optimized characteristic.

The significant differences provided by the figures confirm that the zero-centering treatment is of great significance and therefore cannot be omitted.

5.3.2.3 Variation in radial depth of cut

Thirdly, **Test #1_10** and **Test #1_12** are compared here in Figure 5.12 to verify if the variation in radial depth of cut will cause the influence on the proposed method.

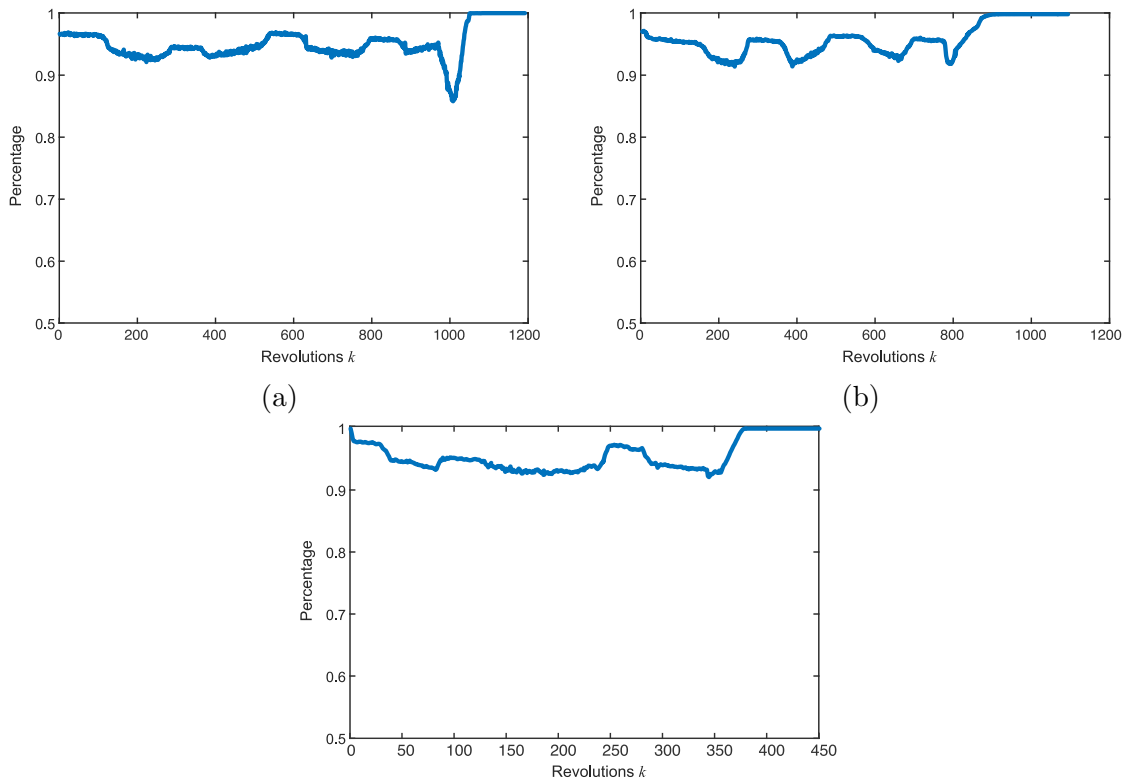

Fig. 5.12: The influence of the tool's radial engagement: (a) **Test #1_10** with a_e =3.2 mm; (b) **Test #1_12** with a_e =12 mm; (c) **Test #2_6** with a_e =11 mm.

Figure 5.12(a) presents the separability index of cut width a_e =3.2 mm and Figure 5.12(b) shows the behavior of one test with a_e =12 mm. The two lines follow more or less the same trend, except for the milling distance shortened by the change in path length (recall the rounded square trajectory in Figure 4.5).

For cases where the width of cut is too great, resulting in more than one tooth cutting the material at the same time, are covered in **Test #2_6**. Although the designed width of cut for **Test #2_6** is only 11 mm, the material wraps around the tool beyond the normal setting when milling through the inner contour (second corner). At this point, the separability index behaves logically and remains within a reasonable range of values, as shown in Figure 5.12(c).

Basically, it can be assumed that changing the radial engagement within a certain range will not affect the stability of the proposed method, as long as there are no drastic abrupt changes affecting the balanced cutting contribution of the segments within a certain revolution.

These above facts provide a solid foundation to proceed to the next level of analysis.

5.3.3 Sensitivity analysis

After confirming the compatibility of the algorithm for both Cartesian and angular coordinates and the effectiveness of the proposed method independent of the external factors, sensitivity analysis was further introduced for a systematic review of the model. It is dedicated to investigating the impact of the inputs on the output of the model.

The choice of sensitivity analysis method is guided by the constraints of the problem. In the present case, two constraints are analyzed and developed in the following paragraphs:

- The effect of the input order of the teeth and the change of the cutter teeth state — performed using bootstrap.
- The effect of the starting point of signal segmentation, as it can be fortuity

retained — performed using window shift.

5.3.3.1 Bootstrap

Bootstrapping uses a large number of random replacement observation data sets to construct resampling from the approximate distribution for establishing hypothesis testing. When parameter inference cannot be performed or complex formulas are required to calculate errors, it is usually used as an alternative to statistical inference based on parametric model assumptions.

A great advantage of bootstrap is its simplicity. It is a straightforward way to derive estimates of standard errors and confidence intervals for complex estimators of the distribution, such as percentile points, proportions, odds ratio, and correlation coefficients. Bootstrap is also an appropriate way to control and check the stability of the results. Although for most problems it is impossible to know the true confidence interval, bootstrap is asymptotically more accurate than the standard intervals obtained using sample variance and assumptions of normality [DE96]. Bootstrapping is also a convenient method that avoids the cost of repeating the experiment to get other groups of sample data.

In this section, the bootstrap method will be applied to the input matrix of the SVD algorithm to estimate the confidence interval. That is, taking each column of the input matrix as a unit, randomly select 4 columns (with or without repeat) among them and arrange those 4 columns as a new input matrix for SVD calculation.

From the mathematical definition, the random sampling methods can be clearly divided into the following four types:

- C (Combination): When only considering the combination without repeated data, there is one and only one input matrix obtained, which is the original data itself.
- P (Permutation): When it comes to the pure permutation without repeated data, the total data composition of the original matrix remains unchanged, whereas the focus is on the arrangement order between columns. For a case of $n_z = 4$, there are 24 different arrangement orders.

CR			
1st	2nd	3rd	4th
1	1	1	1
1	1	1	2
1	1	1	3
1	1	1	4
1	1	2	2
1	1	2	3
1	1	2	4
1	1	3	3
1	1	3	4
1	1	4	4
1	2	2	2
1	2	2	3
1	2	2	4
1	2	3	3
1	2	3	4
1	2	4	4
1	3	3	3
1	3	3	4
1	3	4	4
1	4	4	4
2	2	2	2
2	2	2	3
2	2	2	4
2	2	3	3
2	2	3	4
2	2	4	4
2	3	3	3
2	3	3	4
2	3	4	4
2	4	4	4
3	3	3	3
3	3	3	4
3	3	4	4
3	4	4	4
4	4	4	4

(a) Random selection CR

P			
1st	2nd	3rd	4th
4	3	2	1
4	3	1	2
4	2	3	1
4	2	1	3
4	1	2	3
4	1	3	2
3	4	2	1
3	4	1	2
3	2	4	1
3	2	1	4
3	1	2	4
3	1	4	2
2	3	4	1
2	3	1	4
2	4	3	1
2	4	1	3
2	1	4	3
2	1	3	4
1	3	2	4
1	3	4	2
1	2	3	4
1	2	4	3
1	4	2	3
1	4	3	2

(b) Random selection P

Fig. 5.13: Types of Bootstrapping

- CR (Combination with Repeat): Contrary to P, this case only focuses on changes in the composition of the data and does not focus on the sequence between columns. If repeated data is included, the possibility of combinations increases greatly from 1 to 35.

- PR (Permutation with Repeat): The last category considers all possibilities, not only focusing on the data content, but also on the data sorting. At this time, the number of situations that need to be considered surges to 125.

Here the data of the **Test #1_10** has been selected as an illustration.

Taking the data of the 250^{th} revolution as an example, it can be seen in Figure 5.14 that in the case of arbitrarily changing the data arrangement, the decomposed

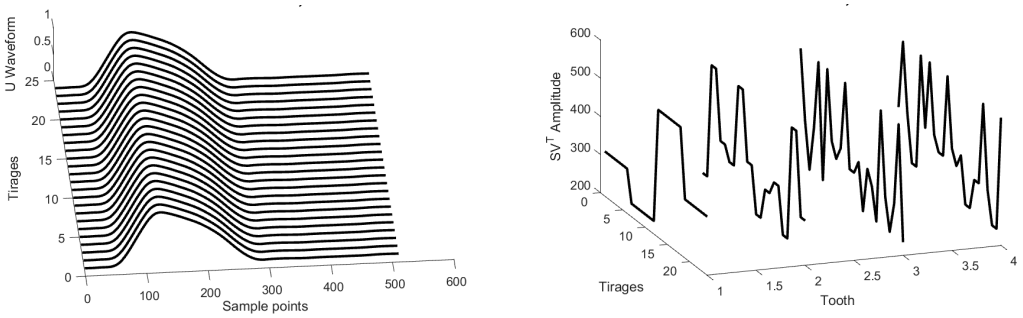

(a) $\mathbb{U}$ for random selection P (b) $\mathbb{\Sigma V}^\top$ for random selection P

Fig. 5.14: Decomposition for random selection P

waveforms are exactly the same, and the term $\mathbb{\Sigma V}^\top$ is also consistent with the corresponding data amplitude after resampling. This keeps pace with the mathematical derivation of singular value decomposition. In a physical sense, based on the correlation comparison between the four teeth, it really does not have much to do with the arrangement order. Figure 5.15 shows that the separability index for bootstrapping P completely overlaps and does not play a role in calculating the confidence interval.

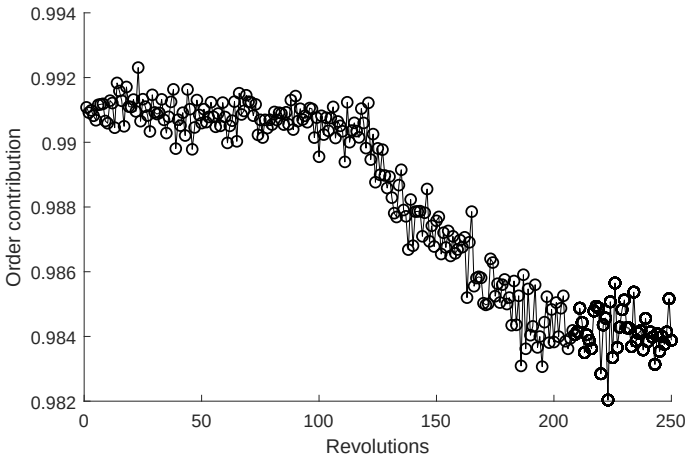

Fig. 5.15: Separability index for random selection P

In this way, it can be foreseen that there is no need to calculate the bootstrapping type PR, which also included the consideration for data sorting. Therefore, only type CR is the focus of the moment.

From Figure 5.16, the waveform is gradually and slightly changing with the modification of data content. With the comparison of Figure 5.16 and Figure 5.13(a), it is easy to find that the first waveform corresponds to the data of the first tooth

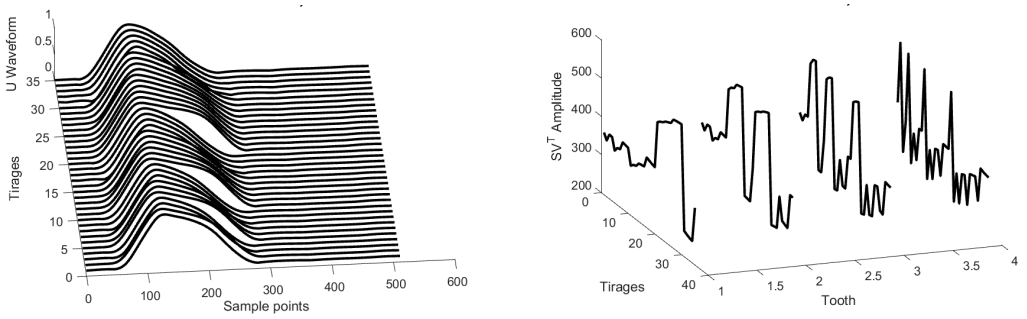

(a) $\mathbb{U}^\top$ for random selection CR (b) $\mathbb{\Sigma V}^\top$ for random selection CR

Fig. 5.16: Decomposition for random selection CR

in all four columns, so the principal component waveform is the normalized original waveform. From the second to fourth curves, the data of the first tooth occupies three-quarters, and the remaining data occupies one-quarter, therefore the principal component waveform gradually changes. As the amount of data occupied by the first tooth decreases, the principal component waveform is more and more deviated from the original first waveform, presenting comprehensive feedback of the whole input matrix.

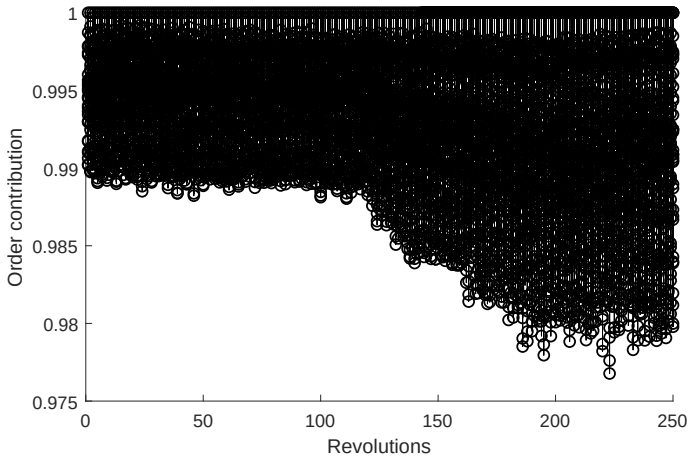

Fig. 5.17: Separability index for random selection CR

As a result, the separation index is constantly changing under different combinations, forming an interval like Figure 5.17. From the beginning to the 120^{th} revolution, the cutter cuts in a straight line, so the operation of the four teeth is basically the same. After the 120^{th} revolution, the tool entered an arc-shaped trajectory, and the cutting condition of the four teeth appeared subtle differences. Therefore, the proportion of the separability index for the first order decreased, but it was very

slight and did not trigger the alarm.

For simplicity of drawing, only the maximum and minimum values are taken. It is worth noting that when the data columns are exactly the same in the bootstrap method, 1 is obtained because the degree of identicalness reaches the ideal state. At this time, this value is of no help for actual production, so the next largest value is taken.

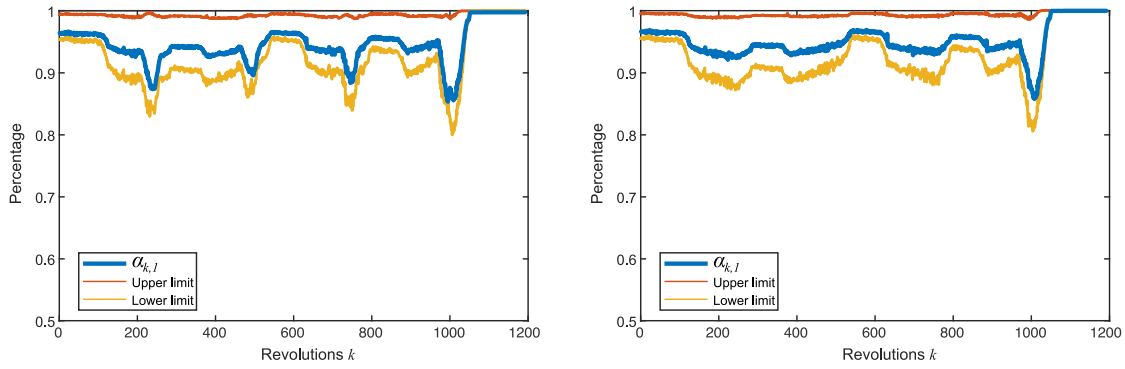

(a) (b)

Fig. 5.18: Sensitivity analysis based on bootstrap before and after trajectory correction: (a) angle of reference (θ) without correction; (b) angle of reference ($\theta + \Theta$) with correction.

Therefore, the interval calculated by bootstrap CR can be defined as all numbers in between the minimum and maximum values (other than 1) of the separability index. These upper and lower limits are obtained from testing each combination of n_z column vectors (including repeats) within the input matrix at the current moment.

In the case of changing only the ordering of the column vector in the input matrix (P), the separability index remained stable at all times. This is consistent with the expectation of multivariate correlation analysis. With the addition of repeated combinations in random sampling (CR), the separability index had a fluctuation interval. When there are multiple vectors of the same data in the input matrix, the separability index increases in response to the rising correlation. So far, no unintended input-output relationships have been observed by bootstrap, proving the basic stability of the proposed method.

However, from Figure 5.18, the interval calculated by bootstrap CR will be influenced by the pre-processing of milling direction correction. The bootstrap method

will enumerate many combinations that are close to the ideal situation, and thus the upper limit will always approach 1. To a certain extent, the upper limit calculated by bootstrap is not able to reflect the state of the tool. At the same time, the lower limit has more distinguishing features than the upper limit. However, after processing multiple sets of experimental data, the variation of the lower limit does not bring any additional useful information. It only records the worst-case scenario for the current combination of segments, and the pattern of its variation depends heavily on the external conditions encountered by the tool.

As such, the sensitivity analysis was rethought, and this time it targeted window shift.

5.3.3.2 Window shift

In the above-mentioned signal processing, the preceding idling part is truncated to accurately select the starting point of the segmentation (Section 4.4.4). This step ensures that each tooth signature corresponds to the segment, rather than one continuous signature being divided into two segments. However, it is a relatively ideal situation achieved by manual choice. The data length of the idling part is variable when the proposed method is implemented in real-time monitoring with different milling items. Therefore, it is not realistic to expect an accurate and automatic division of the signal at the starting position of the cutting force every time. The concept of window shift sensitivity range Δ_{WS} is introduced to proceed with sensitivity analysis and include this uncertainty in the input.

As named, it is assumed to be a shifted window of size m sliding backward from the beginning of the original one-column data sequence to capture the sample set corresponding to the first segment $\boldsymbol{d_{1,1}}$, which can be expressed as

$$\boldsymbol{d_{1,1}} = \begin{bmatrix} d_{1+(m-l)(L-1)} \\ d_{2+(m-l)(L-1)} \\ \vdots \\ d_{m+(m-l)(L-1)} \end{bmatrix}, \tag{5.2}$$

where

$$L = \left\lceil \frac{m}{m-l} \right\rceil. \tag{5.3}$$

The scalar d represents a sample point, and the subscript shows the row number of the sample in the original one-column data set. l ($l \in \mathbb{N}$) is the overlap number in the shifting process. L is the execution number of the shift defined by the ceiling function of $\frac{m}{m-l}$. Once the first segment is chosen, the following data points will fold into input matrices and proceed with correlation analysis as normal steps for each shift. The process of element shifting for the general segment is described as

$$\boldsymbol{d_{k,i}} = \begin{bmatrix} d_{m(ki-1)+1+(m-l)(L-1)} \\ d_{m(ki-1)+2+(m-l)(L-1)} \\ \vdots \\ d_{mki+(m-l)(L-1)} \end{bmatrix}. \tag{5.4}$$

By presetting the overlap points l, the means of the window shift can achieve approximate ergodicity ($l > 95\,\%m$). The separability indexes of multiple processes corresponding to different start points will form the value range Δ_{WS}. This indicator reflects how the separability index is affected by the choice of the starting point of the data.

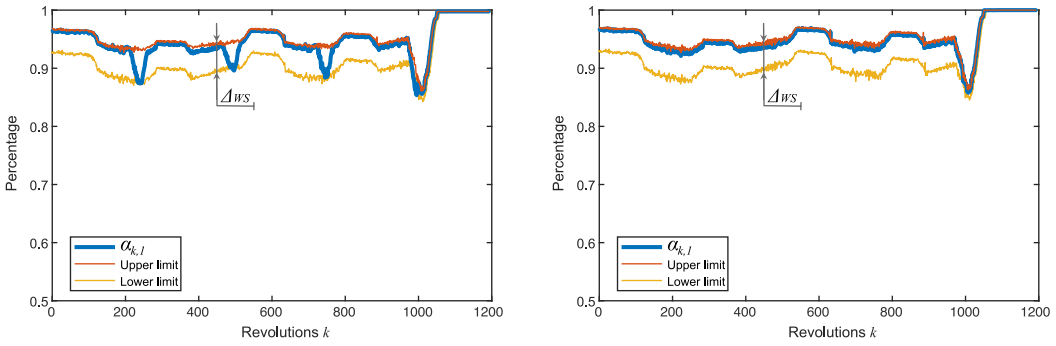

Fig. 5.19: Sensitivity analysis Δ_{WS} of separability index α_{k1} before and after trajectory correction are almost the same: (a) angle of reference (θ) without correction; (b) angle of reference ($\theta + \Theta$) with correction.

In the previous text (Equation (3.1)), the behavior of the signal is defined as a function of the rotational angle corrected with trajectory angle ($\theta + \Theta$). The

separability index α_1 is greatly influenced by the combined angle. It can be seen that the data without trajectory correction have jitters during each passage of corner (Figure 5.19(a)), whereas the lines become smoother after correction (Figure 5.19(b)). When performing the sensitivity analysis, each shift will introduce an additional angle θ_c, which varies according to the sliding window position. After θ_c goes from 0 to $\frac{2\pi}{n_z}$, $(\theta + (\Theta + \theta_c))$ can be seen as a set that contains all the possible gyration angles including the trajectory angle Θ. Thereby the separability index must be included in the sensitivity range Δ_{WS} regardless of the trajectory correction (Figure 5.19). Note that the upper and the lower limits of the sensitivity range Δ_{WS} possess a very similar tendency, and the value of Δ_{WS} is nearly constant. That means that the possible results obtained from all gyration angles are consistent for each revolution, indicating that no tool condition problem interfered during the operation. After comparing multiple sets of data, Δ_{WS} will fluctuate to a certain extent according to different cutting parameters, but the value of Δ_{WS} can be considered constant under the same cutting conditions (the error between Figure 5.19(a) and Figure 5.19(b) is about 0.0047 ± 0.001). If the starting point is well selected, the separability index basically coincides with the upper limit of Δ_{WS}.

Although the separability index fluctuates up and down due to the signal segmentation bias, the resulting sensitivity range remains stable and the value of Δ_{WS} is not affected by the trajectory direction correction. This provides an opportunity for model simplification.

The indifference of the window shift for external influences (angular corrections, etc.) is exploited in Section 5.4.2, as a strategy to diagnose the tool alongside the separability index. It has the advantage of being stable and simplifying the trajectory correction steps.

5.4 Fault detection

Based on the above results, two methods are derived for assessing the status of the tool:

5.4.1 TCM based on separability index $\alpha_{k,1}$

The judgment directly made by the performance of the separability coefficient is clear and intuitive. Under normal operating conditions, the 1^{st}-order main components can already explain more than 90 % of the information. In the event of abnormal wear, the signal will deviate from the typical waveform, and the 1^{st} order will no longer be sufficient to describe the signal, while the 2^{nd}- or 3^{rd}-order contribution of SVD will increase rapidly.

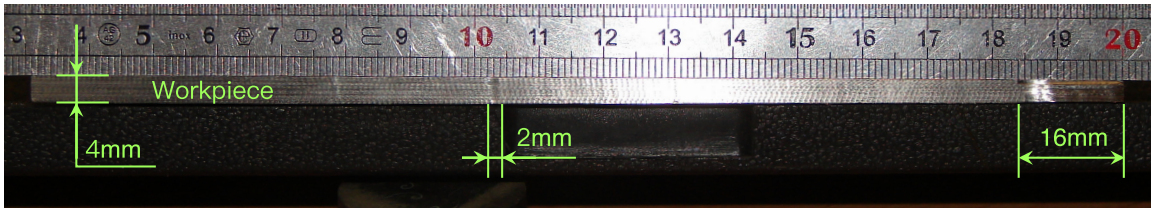

(a)

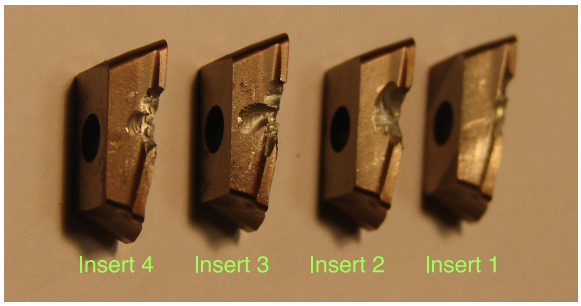

(b)

Fig. 5.20: Status information of the data used for validation: (a) surface condition of machined workpiece; (b) final condition of inserts.

The milling data borrowed from Girardin et al. [GRR10] consist of tool state information. Although the initial image of the breaking of the insert was not captured due to the high speed of the tool rotation, the surface of the machined workpiece revealed traces of the accident, which can be used as supporting evidence of tool state change. Figure 5.20(a) shows two defects in the machined workpiece. One in the middle and the other at the end, with a length of about 2 mm and 16 mm, respectively. Girardin et al. [GRR10] therefore make the inference that at around the 94^{th} revolution, one of the teeth partially broke, and at about the 193^{rd} revolution, all the teeth may break. The final state of the inserts after the stoppage was registered as in Figure 5.20(b).

5.4 Fault detection

If the results obtained are consistent with the known tool state after processing this set of data according to the steps mentioned in the above sections, the effectiveness of the proposed method can be verified.

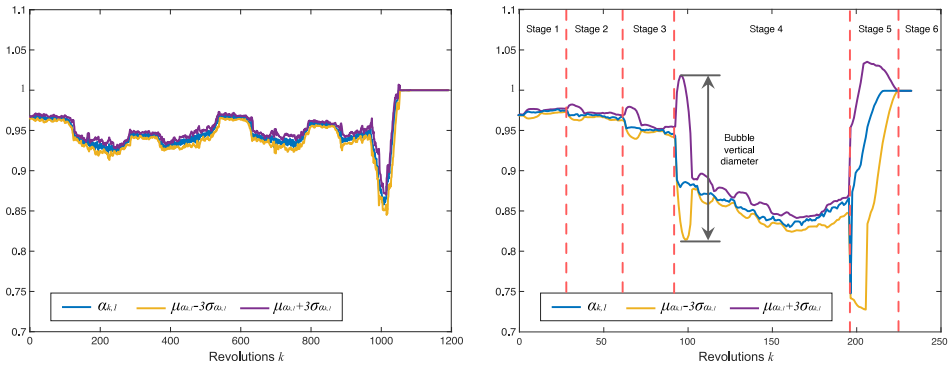

(a) (b)

Fig. 5.21: Fault detection based on separability index α_{k1} (blue line) with upper (purple line) and lower (yellow line) limit of 3-sigma interval: (a) tool in good condition; (b) tool in worn condition.

For tools in good condition, the separability index is always above 0.9 before the stoppage, whereas the separability index has an obvious decline near the 100^{th} revolution on the curve for the worn tool (Figure 5.21 (b)). Periodic wear gradually occurs at stages 1, 2, and 3. The longer tooth cuts more material and is more stressed, which causes and aggravates different levels of wear between teeth. From the perspective of the separability index, the correlation continues to decrease and becomes more and more severe. At the start of stage 4, the indicator drops dramatically. It corresponds to the situation where the wear increases exponentially until the tool is completely damaged, which might damage the spindle. After a certain reaction time, the tool was stopped manually (S5), completely withdrew from the material, and reached the idling state (S6).

As mentioned in Section 5.3.3, the separability index α_{k1} and sensitivity range Δ_{WS} will fluctuate slightly with different machining conditions. Using Figure 5.21 (b) as an example, even if the tool continues to wear in the S1, S2, and S3 stages, the values corresponding to the separability index are all above 0.95 due to its simple rectilinear cutting condition. Therefore, it is difficult to use this value to clearly define the wear status of tools with high precision.

The empirical rule is chosen as the definition of the threshold to solve this prob-

lem. The three-sigma interval encompasses 99.7 % of the values under the assumption of a Gaussian distribution [UC14]. Supposing the operation runs to the q^{th} revolution, the previous separability indexes from $(q-p)^{th}$ to q^{th} revolutions are considered as a cluster to present the current tool state. Their average value μ_{qp} and standard deviation σ_{qp} are calculated as

$$\mu_{qp} = \frac{1}{p+1} \sum_{k=q-p}^{q} \alpha_{k1}, \tag{5.5}$$

and

$$\sigma_{qp} = \sqrt{\frac{1}{p} \sum_{k=q-p}^{q} |\alpha_{k1} - \mu_{qp}|^2}. \tag{5.6}$$

The value of p can be adjusted to control the response speed of the TCM system. In the studied case, $p = 9$, and the thresholds are set at $\mu_{qp} \pm 3\sigma_{qp}$.

The interval formed by $\mu_{qp} \pm 3\sigma_{qp}$ for the tool in good condition is very close to the separability index (Figure 5.21 (a)). The standard deviation σ_{qp} emphasizes the variation of the separation index for the worn tool, so regardless of its own value, when α_{k1} shows a downward trend, $\mu_{qp} \pm 3\sigma_{qp}$ will form a raised area in both the up and down limit, named the bubble effect.

The vertical diameter of the first bubble in Figure 5.21 (b) is 0.01196, and then the diameter gradually increases. In the second and third stages, the values are 0.01898 and 0.03785, and the fourth stage shows an order of magnitude change at 0.2011. According to the different accuracy requirements, an alarm threshold can be set corresponding to a suitable bubble diameter to monitor the tool state. For the current case, the milling process ideally should be stopped at S2 or S3 to avoid subsequent catastrophic failure. At this time, the tool is no longer in a steady-state, which means that at least one of the teeth is entering the rapid wear phase. The result of the verification is in full agreement with the acknowledged tool status.

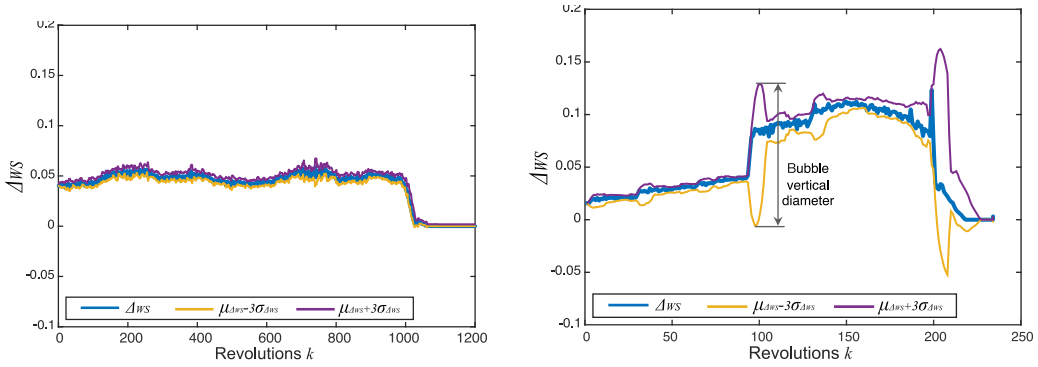

(a) (b)

Fig. 5.22: Fault detection based on sensitivity range Δ_{WS} (blue line) with upper (purple line) and lower (yellow line) limit of 3-sigma interval: (a) tool in good condition; (b) tool in worn condition.

5.4.2 TCM based on sensitivity range Δ_{WS}

The assessment based on the sensitivity range has the advantage of skipping the step of milling direction correction (Section 4.4.3). During regular milling conditions, Δ_{WS} remains stable with a standard deviation of approximately 0.005. Once tool wear is detected, the sensitivity range varies greatly due to the decline of the correlation between segments. The bubble appears in the same position as with the previous method.

5.4.3 Summary and evaluation

The above two judgments are actually two expressions of the same phenomenon. The first one simply relies on the separability index. Only current revolution data need to be included when calculating real-time monitoring, which is fast and efficient. However, the trajectory angle and the spindle angle must be synchronized to achieve higher accuracy. The second method uses the traversal mode, which has the advantage of not requiring a trajectory correction but needs a longer running time to process a larger amount of calculations for the window shift. Depending on the available equipment, it provides different monitoring strategies to suit variable machining conditions. The general workflow for tool state diagnosis based on the inter-insert correlation method by SVD is illustrated in Figure 5.23.

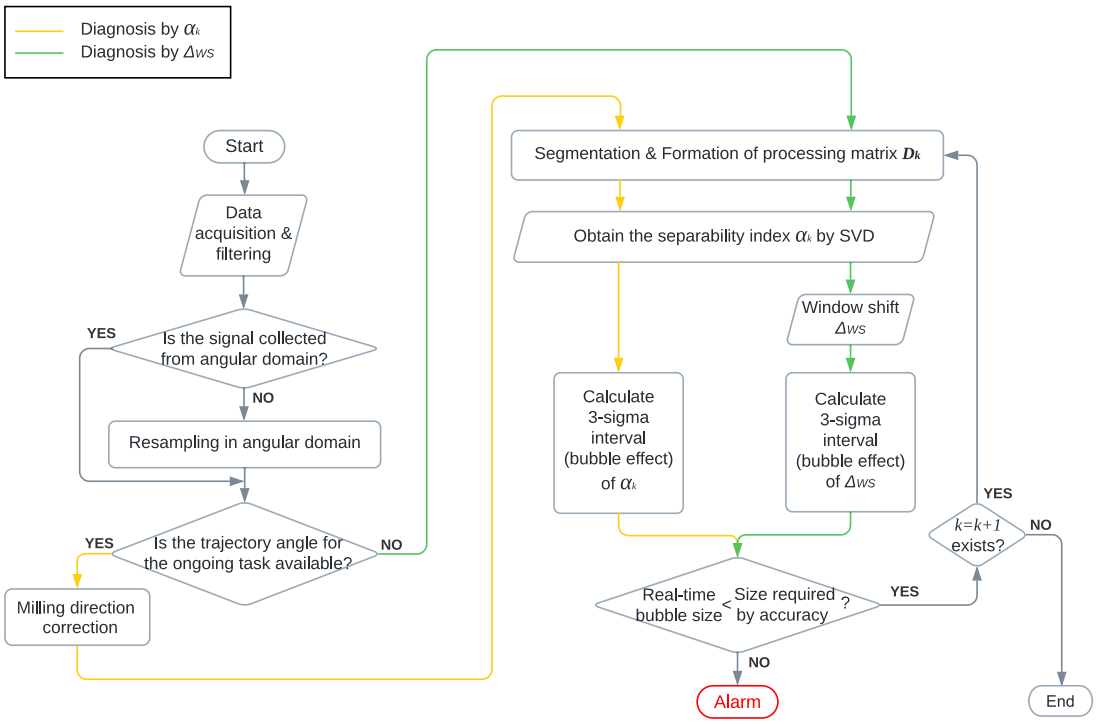

Fig. 5.23: General flowchart of TCM system based on the inter-insert correlation using SVD

No single method can guarantee that the right decision will be made all the time. The notion of false alarm is considered in a statistical sense for tool condition monitoring. The threshold establishes a balance between the probability of good detection and the probability of false alarm. As described in Section 2.4.3, the ROC curve is introduced in Figure 5.24 to determine the optimal threshold setting and the corresponding accuracy.

According to the information given by Girardin et al., the 94^{th} revolution is chosen as the turning point for the validation signal, before which the data are labeled as **good condition** and after which the data are labeled as **worn condition**. With the comparison of the given true labels and diagnosed states, the ROC curve shows the relationship between the true positive (TP) rate for the model and the false positive (FP) rate. When the threshold is adjusted, the resulting classifications will also change based on the value of this threshold. The curve shown in Figure 5.24 is obtained when all thresholds have been tried. The area under the curve (AUC) provides

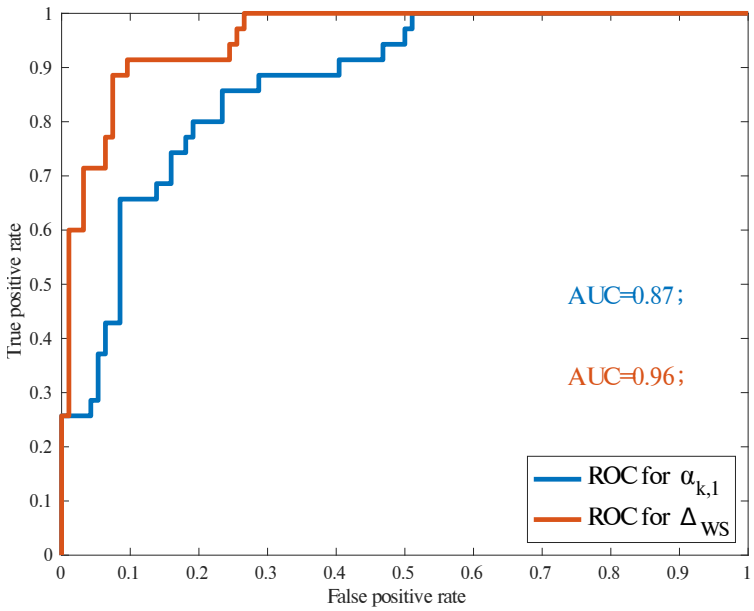

Fig. 5.24: Receiver operating characteristic curves of proposed two TCM methods

an aggregate measure of performance across all possible classification thresholds. It appears that, according to the auto calculation, the indicator based on Δ_{WS} indicated the accuracy of 0.96 with a threshold = 0.017; while $\alpha_{k,1}$-based indicator gave out the accuracy of 0.87 with a threshold = 0.021. It does not necessarily mean the Δ_{WS}-based indicator performs better than $\alpha_{k,1}$-based one. Because the manual set state labels may have errors corresponding to the real tool condition.

Note that the bubble size could cross the threshold during stoppage, due to a really fast drop in width of cut. There is still room for optimization at this stage. The current strategy adopted is to cooperate with the milling program to indicate the finish point of product processing. After the product processing is completed, the monitoring is stopped while the tool is withdrawn (no chips are generated).

In summary, this method provides effective and stable feedback on the condition of the tool, which is very promising for TCM system construction.

5.5 Limitation

In the above results, the proposed indicators provide effective feedback on the state of the tool. However, some of the limitations of the method are shown in the findings from the comparison between **Test #2_8** and **Test #3_19**.

Both tests contain the base path as shown in Figure 5.25, consisting of the following stages:

- **S1**: straight cut along the positive direction of the y-axis;
- **S2**: external contour milling with a 90° corner;
- **S3**: straight cut along the negative direction of the x-axis;
- **S4**: inside contour milling with a 90° corner;
- **S5**: straight cut along the positive direction of the y-axis again;
- **S6**: stoppage.

Figure 5.26(a), (c), and (e) show the results corresponding to the basic designed curve, including respectively the decomposition components $\mathbb{\Sigma V}^\top$ and the bubble effects around α_{k1} and Δ_{WS}. Correspondingly, the subplots (b), (d), and (f) of Figure 5.26 demonstrate the counterparts of the results with the addition of two extra holes in the S4 and S5 accordingly.

It is clear from the amplitude extraction given by the first-order $\mathbb{\Sigma V}^\top$ (Figure 5.26(a), (b)) that there are three value drops before the stoppage. The first drop occurs in the S2, where the radius of the outer profile milling is too small compared to the tool radius, thus resulting in a different amount of cut distribution for each tooth. The second and third value falls happen in S4 and S5, respectively. Obviously, when the tool passes over the holes, the material to be cut suddenly decreases, so the cutting force will be definitely reduced significantly at this instant. These two sharp valleys raised challenges for the TCM system. Both the separability index α_{k1} based, and the sensitivity range Δ_{WS} based diagnostic approaches exhibited fluctuations when the tool passed over the holes.

The right column images in Figure 5.26 actually show a similar trend, but the

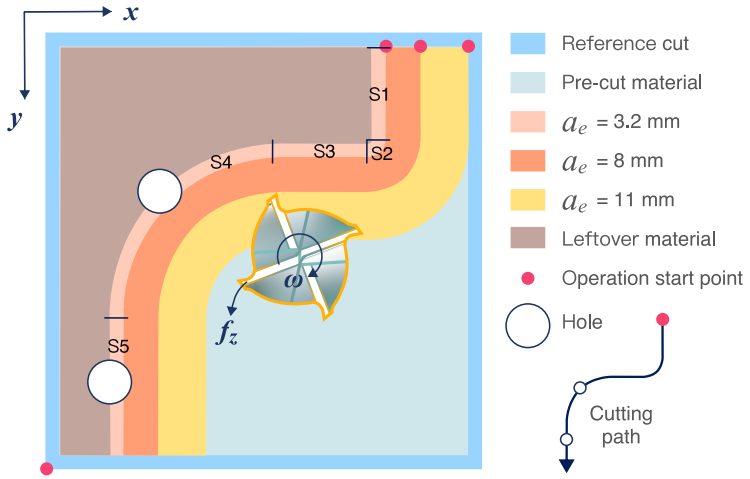

Fig. 5.25: Demonstration of the milling trajectory and corresponding stages of tool states

reasons for the decline are not the same. When look closer, the trough of S4 in Figure 5.26(b) arrives at the 214^{th} revolution, while the corresponding troughs in Figure 5.26(d) and (f) begin at the 211^{th} revolution. This is because the values drop in Figure 5.26(b) is due to the reduction of cutting forces as mentioned before, while the decrease in Figure 5.26(d) and (f) are the consequence of inter-tooth correlation analysis. Therefore, the valleys in Figure 5.26(d) and (f) correspond to the time when the tool has just touched the hole area. At that time, the teeth of the tool experience very different states within the same revolution, and the value of SVT in Figure 5.26(b) did not reach the bottom yet. The fluctuation of values in S2 and S5 can be explained by the same principle.

The cause of the fluctuations is logical, but the fact is that the separability index (the blue line in Figure 5.26(d)) falls below 90% in S2, S4, and S5, especially when the tool passes over the hole, where the minimum value can be less than 80%. For S2, the bubble based on the separability index is about 0.06, and the bubble size based on the sensitivity range is close to 0.025. This is still in a tolerable range if the same accuracy requirement in Section 5.4 is used as a reference. But for the two cases passing over the hole, the bubble based on the separability index is quite large, up to 0.37, while the bubble based on the sensitivity range is around 0.15. This has reached the threshold for triggering an alarm.

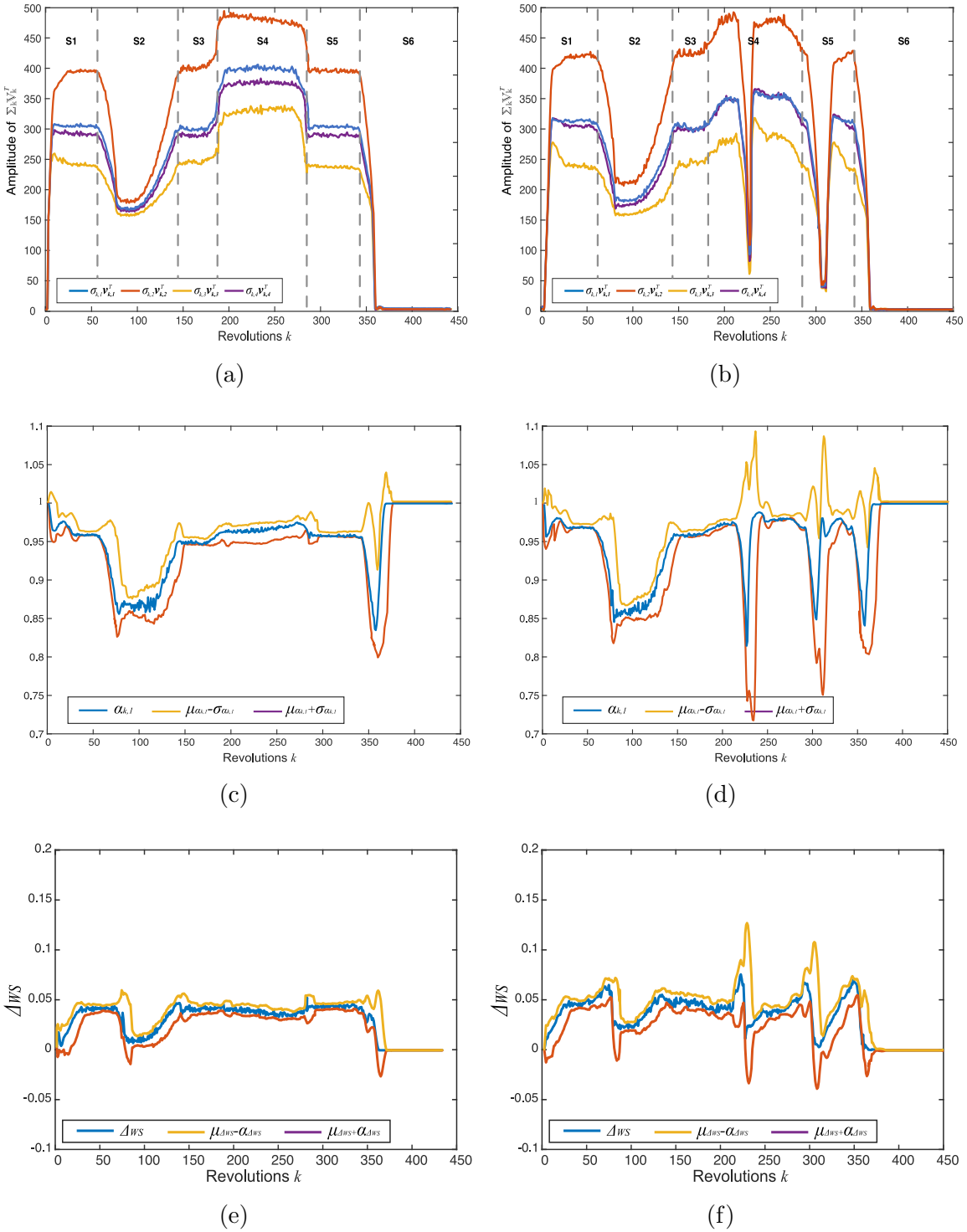

Fig. 5.26: Limitation: **Contour of designed curve** - (a) 1^{st}-order of $\mathbb{\Sigma V}^\top$; (c) fault detection based on separability index α_{k1}; (e) Fault detection based on sensitivity range Δ_{WS}; **Contour of designed curve with holes** - (b) 1^{st}-order of $\mathbb{\Sigma V}^\top$; (d) fault detection based on separability index α_{k1}; (f) Fault detection based on sensitivity range Δ_{WS}.

Based on the above analysis, the proposed method is hard to maintain a steady state when encountering certain situations that would create an imbalance in the cutting amount between the inserts, such as passing over a hole, and milling the outer contour with a tiny radius, etc. Consequently, for projects with these special scenarios and high accuracy requirements, it is necessary to pre-mark the sudden changes in advance with the help of 3D machining design software to reduce the unnecessary false alarm. A more appropriate and targeted application of this method is intelligent planning machining, which is recently emerged. For example, Esprit has proposed ProfitMilling, which automatically plans and optimizes the milling paths mainly using basic geometries such as linear, spiral, and trochoidal motions [Mita].

5.6 Conclusion

Chapter 5 details the processing results from SVD algorithms for target revolution-based matrices, which is the core content of the inter-insert correlation for TCM.

The simple and idealized IAS simulation signal was first taken as the data source for the SVD, and the physical significance of the corresponding components was explored in both straight and curved scenarios. The left singular matrix $\mathbb{U}$ extracts the normalized shared waveform from the segments with preservation of the phase shift due to the curved trajectory; the singular value matrix $\mathbb{\Sigma}$ can be considered as the scaling factor determining the contribution of the decomposition sequences to the original signal; the right singular matrix $\mathbb{V}$ contains the proportional evolution in segments.

Afterward, the SVD method is applied to the experimental data to verify that the results are consistent with the simulated signal. The outcomes show that the inter-insert correlation successfully copes with the more complex real data. Meanwhile, the comparison between the different experimental groups reveals that the method has good compatibility with angular and Cartesian coordinates and is independent of the radial depth of cut. A sensitivity analysis was then carried out, which derives two indicators based on the separability index $\alpha_{k,1}$ and the sensitivity range Δ_{WS}, respectively. These two indicators are in fact two expressions of the same principle. The indicator $\alpha_{k,1}$ has the advantage of a fast response and ease of calculation, but

the path direction correction is necessary to achieve greater accuracy. The indicator Δ_{WS}, on the other hand, does not require prior correction of the trajectory but has a greater computational burden. Depending on equipment availability, a suitable strategy can be selected flexibly. The signal from the worn tool was employed to test these two indicators. Finally, the ROC curves give AUC of 0.87 and 0.96 respectively.

The inter-insert correlation for TCM can effectively reduce the influence of external factors on the analysis process and is therefore independent of changes in width of cut and trajectory changes. This reference-free method partially fills the gap for tool monitoring in small-batch customized production. Amidst the promising prospects, some limitations are also identified. The proposed method has difficulty in maintaining a steady state when encountering certain situations that may cause an imbalance in the cutting amount between inserts, such as passing over a hole, milling a tiny radius outer contour, etc. This poses a new challenge for future developments.

Chapter 6

General conclusion

Summary

6.1 Conclusion 140
6.2 Principal contributions 142
6.3 Further works 143

6.1 Conclusion

The condition monitoring system is an important factor to ensure part quality and production safety in the emerging flexible manufacturing of Industry 4.0. In which the tool, as the terminal executive part of the machining process, contacts directly with the workpiece, so TCM is extremely important. However, at the same time, it is a challenging task due to the complex working environment. Therefore, the work carried out in this thesis aims to propose a solution that allows real-time condition monitoring of end mills in both stationary and non-stationary regimes, especially to meet the monitoring needs for customized small batch production.

In the literature review (Chapter 2), we first investigated the characteristics of milling operations, mainly concerning operating parameters, tool wear types, tool service life, and chip forming process under normal and wear conditions of the tool, and milling force analysis. On this basis, sensorial perception, feature extraction, and decision making, these three elements for building the TCM system were explored in depth. Combined with the sensor performance, the indirect signals that can reasonably describe the machining process are identified. Feature extraction is further discussed in the time and frequency domains as well as in the emerging angular domain.

After extensive literature reading, we found that most extant methods perform detection by TCM teach-in method with a pre-established reference. Such methods either require trial cuts or big data learning, which makes it difficult to adjust quickly to changes in trajectory and velocity. This prompted us to propose a new concept: TCM using correlation analysis between multiple teeth of the tool, i.e. inter-insert correlation. While treating the tool as a whole, the concept also strives to consider multiple inserts as interacting individuals. The correlation analysis among them can eliminate as much as possible the external non-stationary factors and gather the focus on the condition of the tool. When the cutter undergoes variation in speed, all the inserts can be seen as being similarly affected. At the same time, the operating mode of high rotational speed with low feed rate makes the trajectory changes experienced by individual cutting edges tend to be similar. Especially the high-speed machining can better approximate the external working environment of each tooth as quasi-

equivalent, thus contributing to more accurate correlation results.

For this concept, correlation and multivariate analysis were investigated. Eventually, the study settled on the SVD algorithm, which decomposes the signal with underlying correlation-based analysis and gives a comprehensive indicator for assessing the tool condition.

It is worth emphasizing that this work is seen as part of a broader framework for monitoring and maintaining rotating machinery. Although the application in this thesis is restricted to signals generated by end mills (mainly milling forces and spindle speed), the applicability of the developed method is intended to cover a wide range of mechanical signals. Theoretically, it could also potentially be applied to condition monitoring of other mechanical components with a rotating nature, such as gears, bearings, etc. Therefore, in Chapter 3, we establish the criteria for applicable signals and a general model of rotating machinery behavior. Under this model, the IAS signals are simulated for preliminary validation of the proposed approach and the specific strategies for the correlation analysis are discussed.

After the numerical simulations yielded promising results, representative cutting paths were designed and experiments were conducted. The experimental setup and data pre-processing are shown in Chapter 4.

In Chapter 5, the obtained experimental data are used to verify the effectiveness of inter-insert correlation for TCM. The corresponding decomposed components of SVD are interpreted in terms of their physical significance. Based on sensitivity analysis, the separability index $\alpha_{k,1}$ and the difference between the upper and the lower limits obtained by window shift Δ_{WS} were derived as the two indicators of detection. These are actually two expressions of the same phenomenon. The first one simply relies on the separability index. Only current revolution data need to be included when calculating real-time monitoring, which is fast and efficient. However, the trajectory angle and the spindle angle must be synchronized to achieve higher accuracy. The second method uses the traversal mode, which has the advantage of not requiring a trajectory correction but needs a longer running time to process a larger amount of calculations for the window shift. Depending on the available equipment, it provides different monitoring strategies to suit variable machining conditions. A simple evaluation of these two indicators based on the ROC curve is given, as well

as the workflow of the method.

The above work answers the objectives of the study proposed in Chapter 1. The obtained results partially fill the gap of tool monitoring demand in flexible manufacturing for customized small batch production. It is promising to be further extended to monitoring and maintenance of other rotating machinery.

Certainly, there were some setbacks that were also summarized during the research. The proposed method has difficulty in maintaining a steady state when encountering certain situations that may cause an imbalance in the cutting amount between inserts, such as passing over a hole, milling a tiny radius outer contour, etc. This is a more specific challenge that can be a direction for future improvements.

6.2 Principal contributions

The main contributions of this research can be concluded as follows:

- The behavior of the rotational signals is further explored in the angular domain, which creates a steady base for the segmentation of the signals corresponding to each insert of the tool.
- The concept of exploiting the inter-insert correlation to monitor the tool state is proposed. Both theoretical derivation and experimental analysis are preliminarily justified with very promising results.
- Among the many methods of correlation, a specific treatment employing SVD is identified. Each of its decomposition components has a corresponding physical meaning, meanwhile, it also possesses computational efficiency. On this basis, the order separability index for assessing the current operating state of the tool is introduced and two derived strategies for fault detection are proposed.
- Compared to the decision-making by *Teach-in & Comparison* used in the most monitoring system, the method proposed in this paper has the advantages of convenience, intuitiveness, and flexibility to adapt to the different milling trajectories (cyclostationary and cyclo-non-stationary conditions). As it does

not require any trial runs or big data training to obtain a standard threshold reference for each milling task, it is very friendly to customize on-demand in production as well as in small-batch production.

6.3 Further works

This thesis proposes a method based on correlation analysis for the monitoring of tool conditions during milling processes. In view of the fact that there is only a small number of publications in the same direction, there are still many techniques and algorithms that can be further discussed in addition to the implementation presented in this work. In order to advance future related research, some of the outlooks on the topic are described below.

- The purposefulness of both roughing and finishing operations should be further considered: roughing places more emphasis on the issue of allowing full productivity, whereas finishing is more about guaranteeing the quality of the workpieces. This requires a more precise correspondence between the accuracy requirements and the suggested indicator to determine in different scenarios whether a tool with minor damage is still suitable for further machining. It will require a series of experiments to determine the specific criteria to be applied, but it only concerns the characteristics of the tool (material, helix angle, etc.), independent of the cutting conditions.

- As described in Section 5.5, when encountering certain situations such as passing over a hole, etc., the proposed indicator will fluctuate due to the imbalanced cutting amount between inserts. Consideration could be given to optimizing this instability digitally by combining it with a pre-implanted milling program, or by taking multiple sensor signal signatures together, to enhance the monitoring stability.

- In this study, the cutting force was taken as the object, but dynamometers are mostly used in the laboratory and it would be appropriate to follow up with a signal source from the real production to validate the indicator. The addition of signal sources could also be accompanied by a diversification of the parameters

set during the milling process.

- As its working principle is based on the correlation analysis of repeated events on the revolution-base, it can be seen as part of a broader framework for monitoring and maintaining rotating machinery. Hence, another direction that can be expected is to explore the potential in the diagnosis of other periodic structures, such as gears and bearings.

Appendix A

Experimental equipment

(A) **Machine center**

Fig. A.1: Display of DECKEL MAHO DMC 635 V machine center

The DECKEL MAHO DMC 635 V machine center is employed to conduct experimental tests. It is a 3-axis vertical milling machine equipped with an operation panel and a rinsing gun. The look and characteristics concerned are shown in Figure A.1 and Table A.1 [Too05].

It has two axis sensors integrated in the operating bench, measuring the displacements in the x and y directions during the milling process.

Name of machine	DECKEL MAHO DMC 635 V
Type of machine	Vertical Machining Center
Tool holder	SK 40 - DN 69871 A
Table dimensions	790 mm × 560 mm
Displacement	X - 635 mm; Y - 510 mm; Z - 460 mm
Max. rotational speed	8000 rpm
Max. torque (40% DC)	83 N m
Magazine places	20 pieces
Rapid traverse	30 m/min
Feed speed	Infinitely variable; 20 000 mm/min

Table A.1: The characteristics of DECKEL MAHO DMC 635 V machine center

(B) **Dynamometer plate**

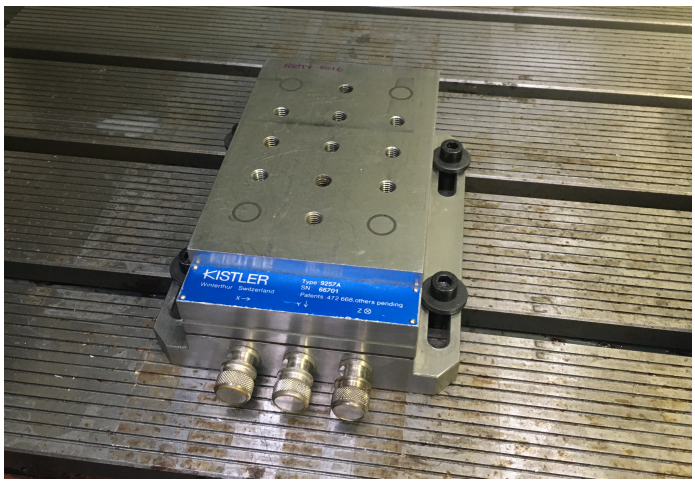

Fig. A.2: Display of Kistler 9257A dynamometer

To measure the cutting force during the milling process, a Kistler 9257A 3-axes dynamometer is used in the experiment. It contains 4 force sensors fitted under high preload. Each sensor has 3 pairs of quartz plates: one sensitive to pressure in the z direction and the other two responding to shear in the x and y directions respectively. The force occurring is exported in real-time by proportional load signals through 3 ports corresponding to the forces in three orthogonal directions. The frequency range is up to 100 kHz.

As shown in Figure A.2, there are eleven M8 × 1.25 mm threaded holes in the top plate for workpiece mounting. Meanwhile, the top plate is covered with a special insulation layer, which is against the penetration by coolant fluid (IP 67) and the temperature fluctuation in the working environment [Kisa]. The measuring range and the sensitivity of the dynamometer are detailed in Table A.2. In conjunction with the Kistler 5015B charge amplifiers [Kisc], it enables accurate measurements of small dynamic changes in the context of large cutting forces.

Measuring range (N)	F_x	0 – 5000
	F_y	0 – 5000
	F_z	0 – 10000
Sensitivity (pC/N)	F_x	-7.93
	F_y	-7.99
	F_z	-3.73

Table A.2: The characteristics of Kistler 9257A dynamometer

(C) **Encoder**

The sinusoidal signal from the sensor is in phase with the light passing through the slit. The hardware parameters of the encoder indicate that for each revolution of the spindle, it emits 1 rotational reference signal named R and two quadrature signals with 256 electrical periods, noted as sine A and cosine B (Figure A.3 (a)).

The three analog signals are converted to digital signals through a TTL converter. In parallel, a high-frequency clock provides an $f_c = 80$ MHz counting pulses. Each rising edge of the encoder digital signal triggers one recording. The number of pulses between two rising edges combined with the counting frequency f_c determines the time between two consecutive events [Li+05] (Figure A.3 (b)).

As opposed to sampling using a constant time step, this system measures the elapsed time based on the occurrence of the event, or to say in this case, on the rotational position of the spindle. It uses the dynamic event as a function

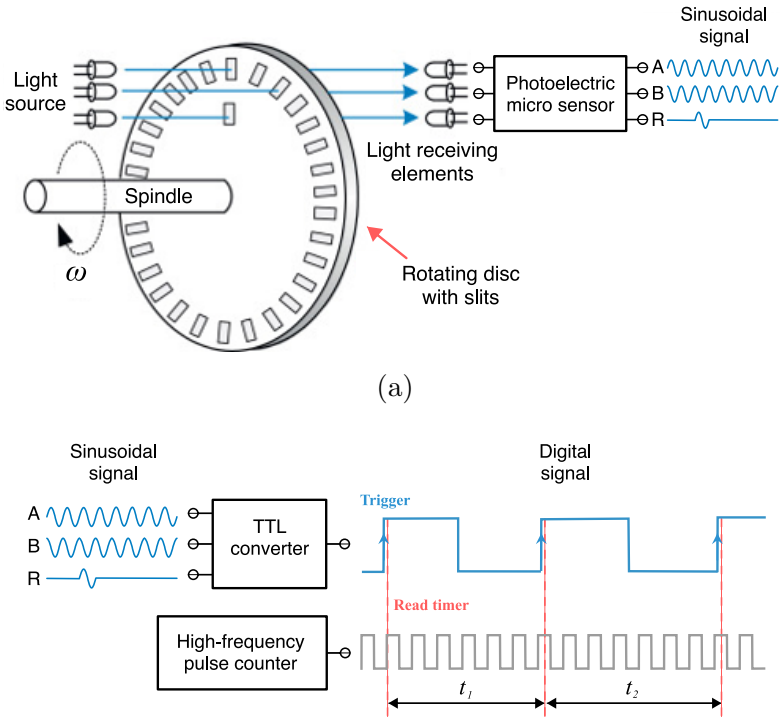

Fig. A.3: Working principle of the rotary encoder: (a) for each revolution, the photosensitive sensor receives the light information passing through the slits, and then produces a reference signal and two sinusoidal analogue signals with a phase difference of 90°; (b) the three signals from the rotary encoder are converted into a TTL signal, which triggers one acquisition of the high-frequency pulse clock for each of its rising edges.

of the variable to stimulate the acquisition processes. It is known as angular sampling, which can better express the signature of the event and as well as offer the potential to synchronize other signals (e.g., the cutting force signal measured from the dynamometer plate) into the angular domain.

(D) Tool and workpiece

The tool used to perform the experiment operations comes from Mitsubishi's APX 3000 series with four flutes. The specific technical parameters can be referred to [Mitc]. To extend the service life, the milling tips of the tool are four screw-tightened replaceable coated inserts (parts marked in yellow in Figure A.4).

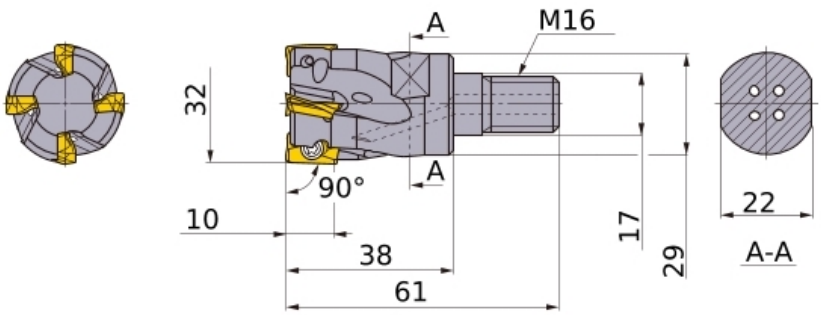

Fig. A.4: The characteristics of APX3000R325M16A end mill

The workpiece used for milling was a C45 medium carbon steel plate (AFNOR standard, equal to AISI/SAE 1045) with a dimension of 20 mm × 100 mm × 100 mm. According to the material and corresponding cutting conditions recommended in the manual, Miracle VP15TF coated insert is selected, and cutting speed is set at 140 m/min [Mitc; Mitb]. After the mounting of the VP15TF coated inserts, the tool operating diameter reaches 32 mm.

(E) **Signal analyzer**

All the real-time measurement information and data points from the experiments are recorded in the OROS OR35 analyzer. It has eight input channels and the maximum sampling frequency is 102.4 kHz (Table A.3). NVGate 11.0 acquisition software was developed specifically for the OR35 analyzer to proceed online supervision and recording of the studied signals.

OROS OR35 V1.1	
Input	8
Input range	± 100 mV — ± 40 V
Output	2
Onboard software	NVGate V11.0
Accuracy	Phase ± 0.02°; Amplitude ± 0.02 dB; Dynamic >140 dB
Sampling capacity	2 kHz — 102.4 kHz

Table A.3: The characteristics of OROS OR35 Analyzer

In this experiment, a cutting speed of about 140 m/min (1392.61 rpm) was chosen, and it was desired that about 8 acquisition points per electrical period

could be obtained to characterize the signal. Therefore, the required sampling frequency can be derived from Equation A.1. According to the calculation result, the sampling frequency is chosen to be 51.2 kHz for the experiments.

$$f_{sampling} = \frac{8 \times 1392.61 \times 256}{60} \approx 47\,534.27\,\text{Hz} \tag{A.1}$$

(F) **FFT of spindle**

The Fourier analysis of the initial spindle signal is shown in Figure A.5(a). The filtering step was done with a zero-phase filter (`Filtfilt` in Matlab). The cut-off frequency is settled as 1.5 times the main frequency according to experiences.

The spectral representation of the signal after filtering are shown in Figure A.5(b). The SNR obtained is about 33-35 dB.

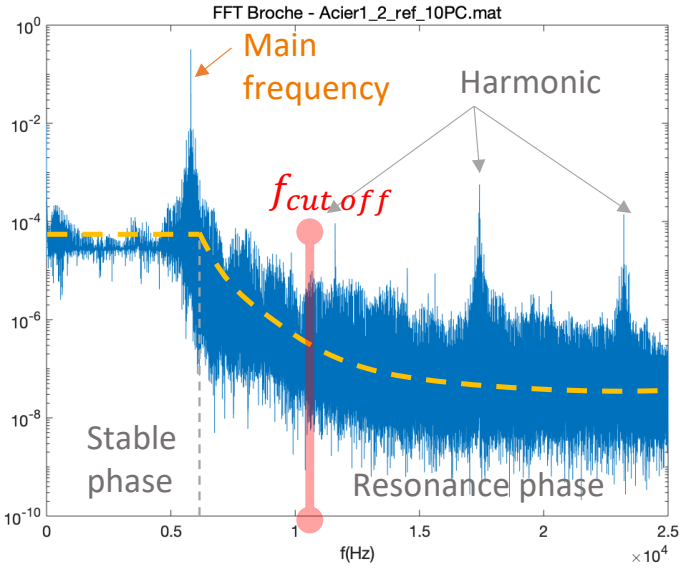

(a)

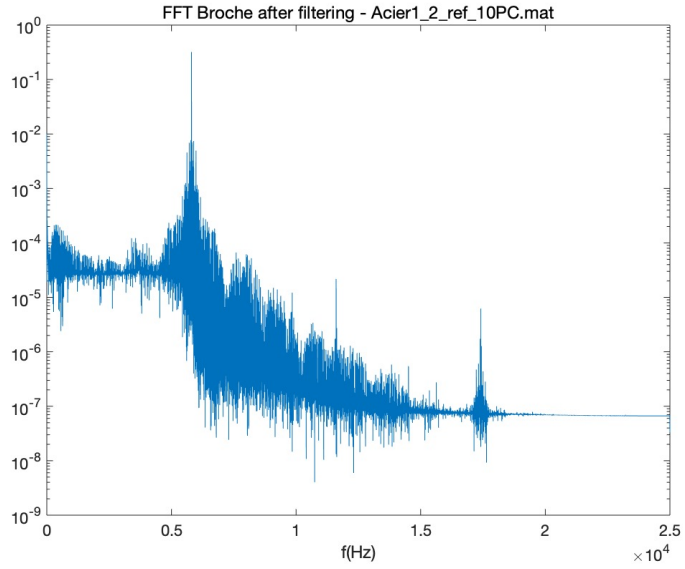

(b)

Fig. A.5: FFT of spindle: (a) spectral representation of initial signal; (b) spectral representation after filtering.

Appendix B

Two attempts of correlation-based TCM

Two attempts based on the simple correlation algorithm that were developed at the beginning of the research are presented in this appendix. As their constructions were fairly simple, these two methods were employed as probes to feel out of feasibility when the idea of diagnosing tool state with correlation was first proposed. Their limitations are also summarized to provide assistance in the next phase of the indicator design ideas.

The data from **Test #1_10** and **FG #120915** are used as examples to demonstrate the analysis results.

Expansion of Pearson correlation coefficient

PCC for correlation analysis of two continuous variables, as discussed in Section 2.5.1, is the first attempt object. The anticipation is to extend the defining equation of PCC to accommodate the application of inter-insert correlation for n_z teeth.

Equation (2.33) can be alternatively expressed as below:

$$R(\boldsymbol{A}, \boldsymbol{B}) = \frac{\sum_{j=1}^{m} (A_j - \mu_A)(B_j - \mu_B)}{\left\{ \sum_{j=1}^{m} (A_j - \mu_A)^2 \sum_{j=1}^{m} (B_j - \mu_B)^2 \right\}^{1/2}}, \tag{B.1}$$

where μ_A and μ_B are the mean of $\boldsymbol{A}$ and $\boldsymbol{B}$.

The object matrix $\mathbb{D}_{\mathbb{k}}$ is obtained by the revolution-based extraction (3.5), and k successive analyses will be done in real-time. Each column vector in Equation 3.13 is seen as one variable. By the analogy of the PCC formula, the comprehensive equation of the inter-insert correlation is deduced as

$$R_{tot,k} = \frac{\sum_{j=1}^{m} \prod_{i=1}^{n_z} \left(\boldsymbol{d}_{k,i,j} - \overline{\boldsymbol{d}_{k,i,j}} \right)}{\left\{ \prod_{i=1}^{n_z} \sum_{j=1}^{m} \left(\boldsymbol{d}_{k,i,j} - \overline{\boldsymbol{d}_{k,i,j}} \right)^{n_z} \right\}^{1/n_z}}, \tag{B.2}$$

where k is the subscript indicating the revolution counts, i is the subscript indicating the tooth counts, and j is the subscript indicating the sample counts.

For the ideal case, where each tooth has the same behavior, the result of $R_{tot,k}$ in a calculation is equal to 1. The safe test is carried out using data from **Test #1_10** as shown in Figure B.1(a). Except for the stoppage period, the indicator $R_{tot,k}$ has a quite stable action. The average of $R_{tot,k}$ is 0.954 with a standard deviation of 0.0089. The data from **FG #120915** is taken to test the validity of $R_{tot,k}$. From the trend of the curves in Figure B.1(b), it is clear that $R_{tot,k}$ has corresponding feedback for the different stages of known wear.

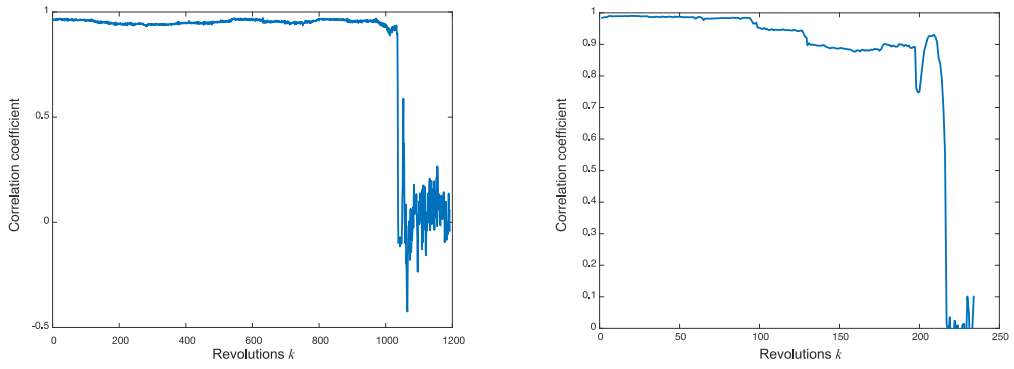

(a) (b)

Fig. B.1: The result of traditional correlation analysis by expansion of PCC: (a) **Test #1_10**; (b) **FG #120915**.

From the above diagram alone, $R_{tot,k}$ looks very promising. However, during the verification phase, the vulnerabilities were quickly discovered. When the teeth number of the tool n_z is odd, even if the behaviors of all the inserts are consistent, it

often causes a negative result due to the parameter points may be smaller than the average value when performing the operation. The tool with n_z=4 is always used due to the limitations of the experimental conditions, and therefore this issue was neglected at the beginning of the study.

But this is not pointless. The result curves obtained in the case, where the number of teeth n_z is even, are a good encouragement to use inter-insert correlation to diagnose the tool state. What should be done is to stick to the principle but find a more appropriate way to handle the data.

Correlation between each pair of the inserts

The second attempt returns to the most original conception of the idea of inter-insert correlation, as described in Section 2.5.1.

The n_z column vectors in $\mathbb{D}_{\mathbb{k}}$ are paired with permutation to proceed correlation. All pair-based correlation coefficients calculated according Equation (2.33) are arranged in the following matrix as

$$\mathbb{R}_{\mathbb{k}} = \begin{bmatrix} R_{1,1} & R_{1,2} & \cdots & R_{1,n_z} \\ R_{2,1} & R_{2,2} & \cdots & R_{2,n_z} \\ \vdots & \vdots & \ddots & \vdots \\ R_{n_z,1} & R_{n_z,2} & \cdots & R_{n_z,n_z} \end{bmatrix}. \tag{B.3}$$

Obviously, the $\mathbb{R}_{\mathbb{k}}$ is a symmetric matrix and the elements of the diagonal are all equal to 1. Therefore, for the case of **FG #120915**, 6 valuable curves are drawn in Figure B.2(a).

After about the 90^{th} revolution, the curves undergo a visible bifurcation. It is clear that the $R_{1,2}$ continues to fall, indicating a significant divergence in the state trends between the first and second insert. $R_{3,4}$ has always been fluctuating at a position close to 1, indicating that those two are pretty similar. The rest of the curves fluctuate up and down around the value of 0.8 and behave without any significant characteristics. Since the number of curves analyzed by pair equals the combination $C_2^{n_z}$, many curves will be generated simultaneously for a tool with multiple teeth.

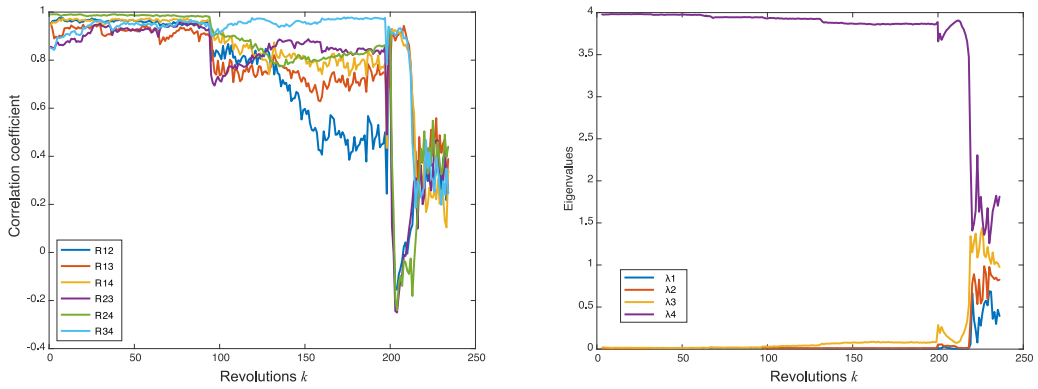

(a) (b)

Fig. B.2: Correlation between each pair of the inserts: (a) Upper triangular part of the matrix $\mathbb{R}_{\mathbb{k}}$; (b) Eigenvalues of the matrix $\mathbb{R}_{\mathbb{k}}$.

This makes the results insufficiently concise and overwhelming to produce intuitive judgments during the analysis.

For a more succinct representation, the eigenvalues of the $\mathbb{R}_{\mathbb{k}}$ matrix λ_1, λ_2, λ_3, λ_4 are calculated and plotted in Figure B.2(b). Compared to figure (a), the graph with eigenvalues is obviously much more concise. From lambda1 it can be seen that the curve has a stair-step descent and that the drop points all coincide with the known locations of the tool wear stage. But these eigenvalues have no superior recognition in the corresponding physical meaning. In addition to this, the value of the eigenvalue varies with the content of $\mathbb{R}_{\mathbb{k}}$. It is not fixed in a definite interval. Hence, the threshold for diagnostic alarms will also be difficult to determine.

Both of these attempts above are failed cases, but they are very inspiring for the following studies. The inter-insert correlation analysis with SVD for the diagnosis of the tool status in Chapter 5 is built on their basis.

Appendix C

Relevant results

Due to the high degree of similarity, out of multiple sets of similar experimental data, we processed only a few of them. The following figures show the results of several relevant tests that are not presented in the main text.

☐ Square #1-4:

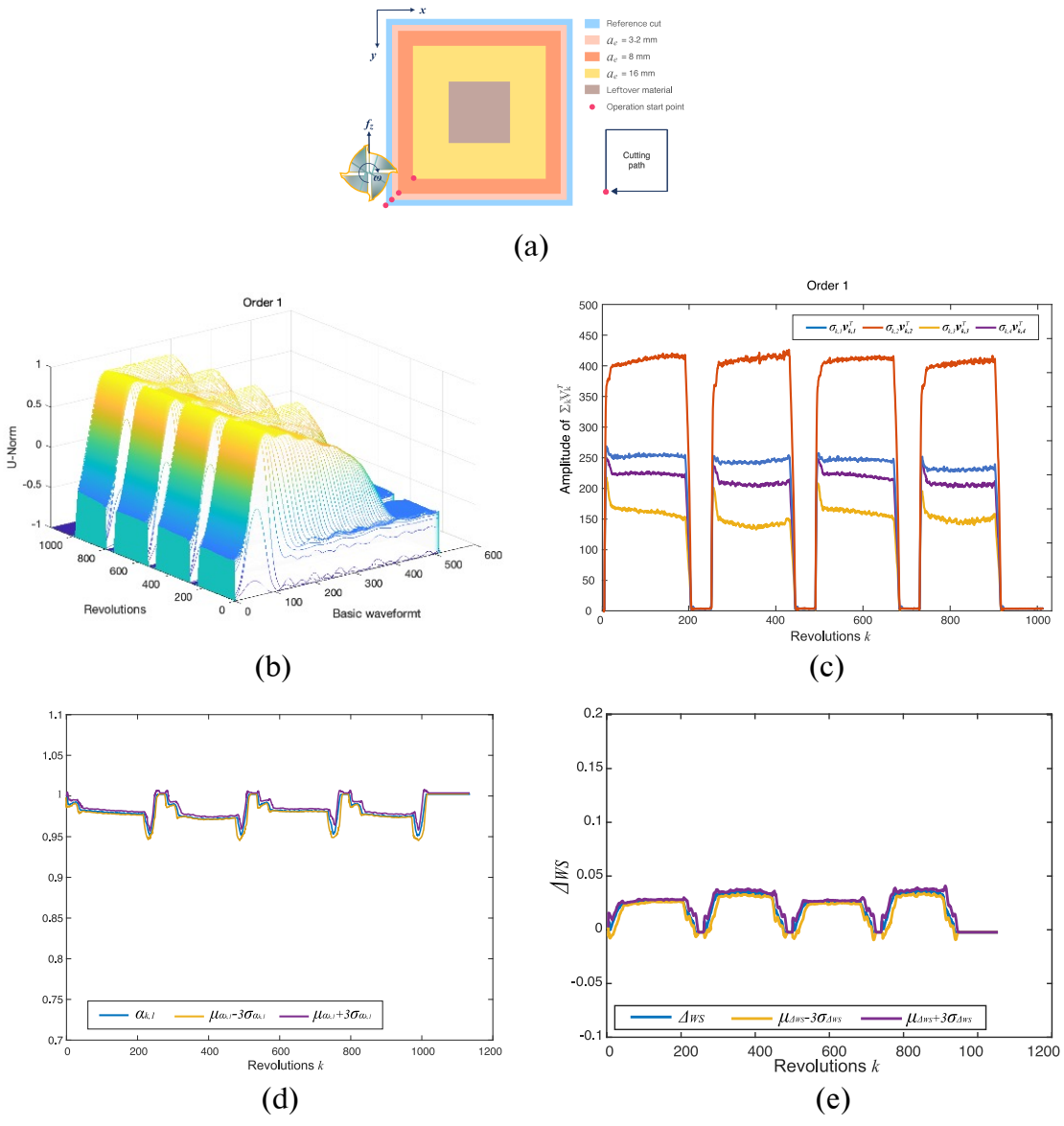

Fig. C.1: **Results of square contour Test #1_4** ($a_e = 8mm$) - (a) illustration of the cut; (b) 1^{st}-order of $\mathbb{U}$; (c) 1^{st}-order of $\mathbb{\Sigma V}^\top$; (d) fault detection based on separability index α_{k1}; (e) Fault detection based on sensitivity range Δ_{WS}.

☐ Rhombus #1-18:

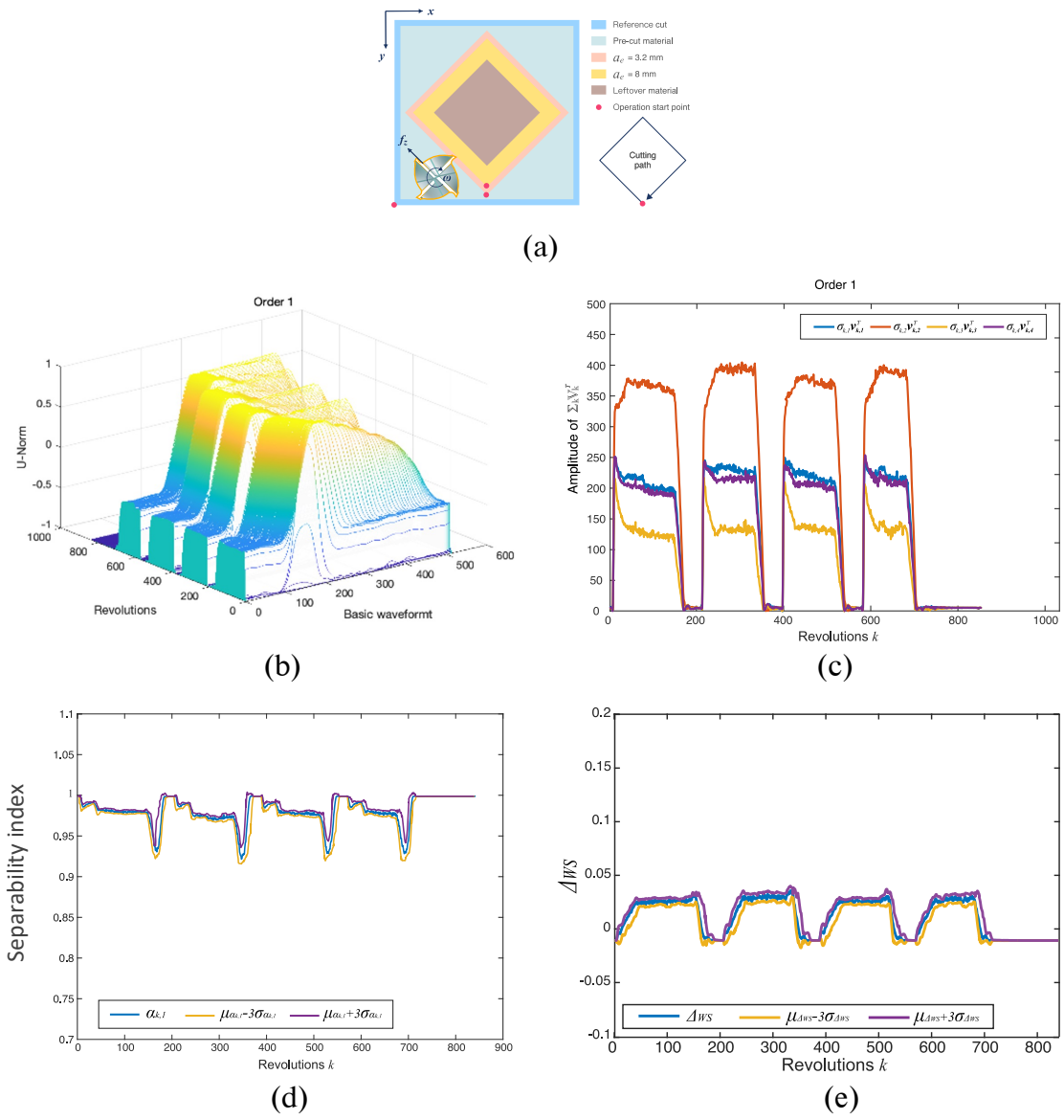

Fig. C.2: **Results of rhombus contour Test #1_18** ($a_e = 8mm$) - (a) illustration of the cut; (b) 1^{st}-order of $\mathbb{U}$; (c) 1^{st}-order of $\mathbb{\Sigma V}^\top$; (d) fault detection based on separability index α_{k1}; (e) Fault detection based on sensitivity range Δ_{WS}.

☐ Designed curve #2-8:

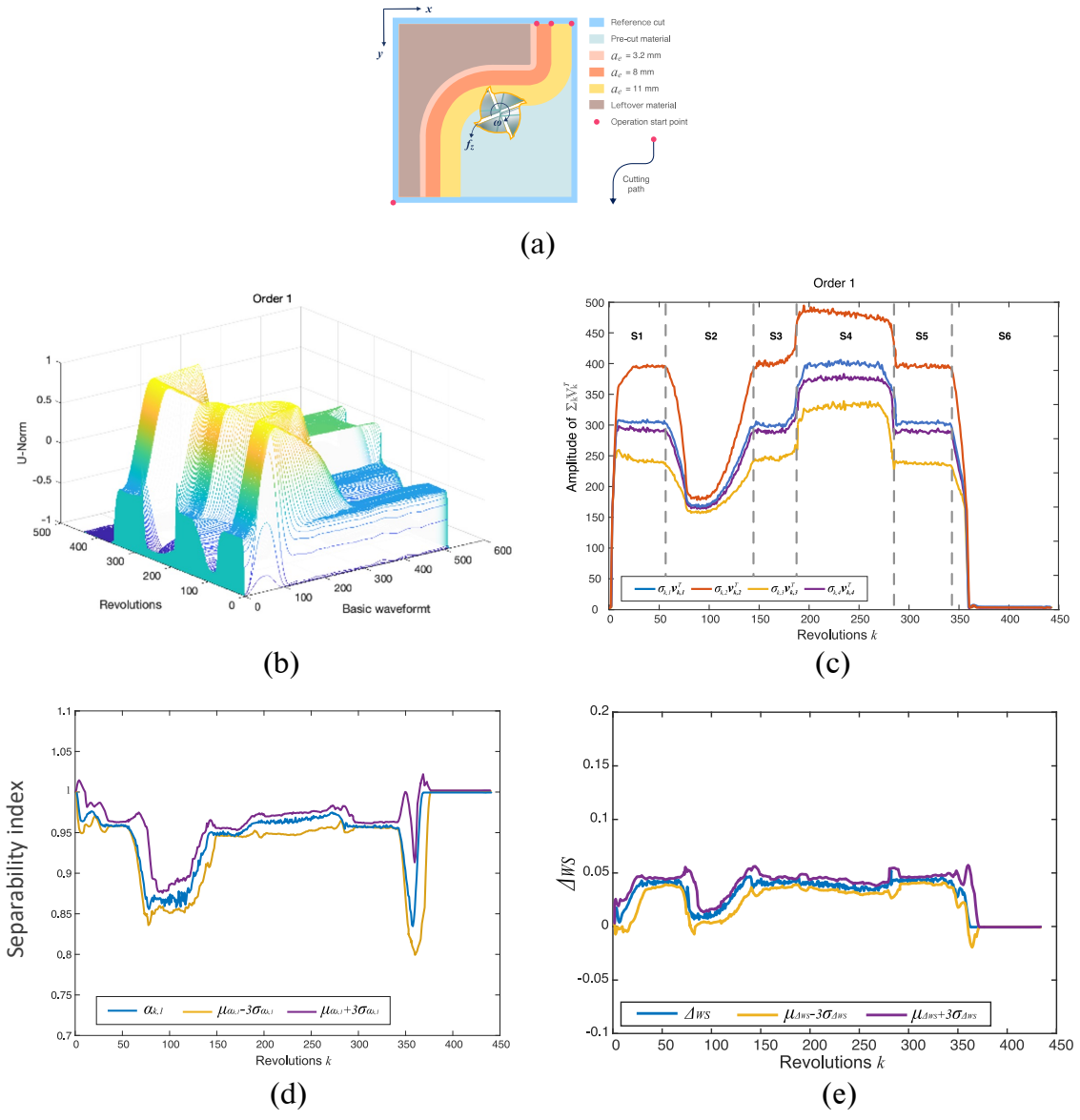

Fig. C.3: **Results of designed curve Test #2_8** ($a_e = 3.2mm$) - (a) illustration of the cut; (b) 1^{st}-order of $\mathbb{U}$; (c) 1^{st}-order of $\mathbb{\Sigma V}^\top$; (d) fault detection based on separability index α_{k1}; (e) Fault detection based on sensitivity range Δ_{WS}.

Bibliography

[AAB14] Jérôme Antoni, Dany Abboud, and Sophie Baudin. "Time-angle periodically correlated processes". In: *Cyclostationarity: theory and methods*. Springer, 2014, pp. 3–14.

[AAX16] J Antoni, D Abboud, and G Xin. "Cyclostationarity in condition monitoring: 10 years after". In: *Proceedings of ISMA*. 2016, pp. 2365–2375.

[Abb+15] Dany Abboud et al. "Angle\time cyclostationarity for the analysis of rolling element bearing vibrations". In: *Measurement* 75 (2015), pp. 29–39.

[Abb+16a] Dany Abboud et al. "Deterministic-random separation in nonstationary regime". In: *Journal of Sound and Vibration* 362 (2016), pp. 305–326.

[Abb+16b] Dany Abboud et al. "The spectral analysis of cyclo-non-stationary signals". In: *Mechanical Systems and Signal Processing* 75 (2016), pp. 280–300.

[ABB00] Sofiane Achiche, Marek Balazinski, and Luc Baron. "Génération automatique par un algorithme génétique de bases de connaissances pour un systèmes d'aide à la décision". In: (2000).

[Ach+02] Sofiane Achiche et al. "Tool wear monitoring using genetically-generated fuzzy knowledge bases". In: *Engineering Applications of Artificial Intelligence* 15.3-4 (2002), pp. 303–314.

[ADG02] J Antoni, J Daniere, and F Guillet. "Effective vibration analysis of IC engines using cyclostationarity. Part IA methodology for condition monitoring". In: *Journal of sound and vibration* 257.5 (2002), pp. 815–837.

[AFN16] AFNOR. "Maintenance industrielle - Fonction maintenance". In: *NF X60-000, Association française de normalisation* (Avril 2016). URL: https://www.boutique.afnor.org/norme/nf-x60-000/maintenance-industrielle-fonction-maintenance/article/856912/fa063074.

[Alt12] Yusuf Altintas. *Manufacturing Automation: Metal Cutting Mechanics, Machine Tool Vibrations, and CNC Design*. 2nd ed. Cambridge University Press, 2012. DOI: 10.1017/CBO9780511843723.

[And+10] Hugo André et al. "Comparison between angular sampling and angular resampling methods applied on the vibration monitoring of a gear meshing in non stationary conditions". In: *Proceedings of ISMA2010 including USD2010* (2010), pp. 2727–2736.

[Ano17] Anon. "Condition monitoring and diagnostics of machines". In: *ISO 13374, International Standards Institution* (LAST REVIEWED AND CONFIRMED IN 2017). DOI: https://doi.org/10.3403/BSISO13374.

[Ano89] Anon. "Tool life testing in machining — Part 2". In: *ISO 8688-2, International Standards Institution* (1989).

[Ant+04] J. Antoni et al. "Cyclostationary modelling of rotating machine vibration signals". In: *Mechanical Systems and Signal Processing* 18.6 (2004), pp. 1285–1314. ISSN: 0888-3270. DOI: https://doi.org/10.1016/S0888-3270(03)00088-8. URL: http://www.sciencedirect.com/science/article/pii/S0888327003000888.

[Ant09] Jérôme Antoni. "Cyclostationarity by examples". In: *Mechanical Systems and Signal Processing* 23.4 (2009), pp. 987–1036.

[AR02] Jerome Antoni and RB Randall. "Differential diagnosis of gear and bearing faults". In: *J. Vib. Acoust.* 124.2 (2002), pp. 165–171.

[AR10] Jose Vicente Abellan-Nebot and Fernando Romero Subirón. "A review of machining monitoring systems based on artificial intelligence process models". In: *The International Journal of Advanced Manufacturing Technology* 47.1 (2010), pp. 237–257.

[ASG06] A. G. Asuero, A. Sayago, and A. G. González. "The Correlation Coefficient: An Overview". In: *Critical Reviews in Analytical Chemistry* 36 (2006), pp. 41–59.

[Ayk+07] Şeref Aykut et al. "Experimental observation of tool wear, cutting forces and chip morphology in face milling of cobalt based super-alloy with physical vapour deposition coated and uncoated tool". In: *Materials & Design* 28.6 (2007), pp. 1880–1888. ISSN: 0261-3069. DOI: https://doi.org/10.1016/j.matdes.2006.04.014. URL: https://www.sciencedirect.com/science/article/pii/S0261306906001129.

[Bin+09] Sultan Binsaeid et al. "Machine ensemble approach for simultaneous detection of transient and gradual abnormalities in end milling using multisensor fusion". In: *Journal of Materials Processing Technology* 209.10 (2009), pp. 4728–4738.

[Bis+12] Claudiu Florinel Bisu et al. "Envelope dynamic analysis: a new approach for milling process monitoring". In: *The International Journal of Advanced Manufacturing Technology* 62.5 (2012), pp. 471–486.

[BK19] S. L. Brunton and J. N. Kutz. *Data-Driven Science and Engineering: Machine Learning, Dynamical Systems, and Control*. Cambridge University Press, 2019.

[BM85] N. G. Bilalis and A. G. Mamalis. "The flexible manufacturing systems (FMS) in metal removal processing: An overview". In: *Journal of Applied Metalworking* (Jan. 1985), pp. 400–409. DOI: 10.1007/BF02833662. URL: https://doi.org/10.1007/BF02833662.

[BSM07] P. Bhattacharyya, D. Sengupta, and S. Mukhopadhyay. "Cutting force-based real-time estimation of tool wear in face milling using a combination of signal processing techniques". In: *Mechanical Systems and Signal Processing* 21.6 (2007), pp. 2665–2683. ISSN: 0888-3270. DOI: https://doi.org/10.1016/j.ymssp.2007.01.004. URL: https://www.sciencedirect.com/science/article/pii/S0888327007000088.

[Byr+95] G. Byrne et al. "Tool Condition Monitoring (TCM) — The Status of Research and Industrial Application". In: *CIRP Annals* 44.2 (1995), pp. 541–567. ISSN: 0007-8506. DOI: https://doi.org/10.1016/S0007-8506(07)60503-4. URL: https://www.sciencedirect.com/science/article/pii/S0007850607605034.

[Cas+18] Paolo Casoli et al. "A methodology based on cyclostationary analysis for fault detection of hydraulic axial piston pumps". In: *energies* 11.7 (2018), p. 1874.

[CBA10] Sohyung Cho, Sultan Binsaeid, and Shihab Asfour. "Design of multisensor fusion-based tool condition monitoring system in end milling". In: *The International Journal of Advanced Manufacturing Technology* 46.5 (2010), pp. 681–694.

[CC13] Jean-Pierre Cordebois and Michel Colombié. *Fabrication par usinage*. DUNOD, 2013. URL: https://www.dunod.com/sciences-techniques/fabrication-par-usinage.

[CC18] Christopher Chatfield and Alexander J Collins. *Introduction to multivariate analysis*. Routledge, 2018.

[Cem09] Czeslaw Cempel. "Generalized singular value decomposition in multidimensional condition monitoring of machines—a proposal of comparative diagnostics". In: *Mechanical Systems and Signal Processing* 23.3 (2009), pp. 701–711.

[Che+15] Wei Cheng et al. "Acoustical source tracing using independent component analysis and correlation analysis". In: *Shock and Vibration* 2015 (2015).

[Chi+00] Thomas HC Childs et al. *Metal machining: theory and applications*. Butterworth-Heinemann, 2000.

[CJV08] H Chelladurai, VK Jain, and NS Vyas. "Development of a cutting tool condition monitoring system for high speed turning operation by vibration and strain analysis". In: *The International Journal of Advanced Manufacturing Technology* 37.5 (2008), pp. 471–485.

[CK17] Besmir Cuka and Dong-Won Kim. "Fuzzy logic based tool condition monitoring for end-milling". In: *Robotics and Computer-Integrated Manufacturing* 47.C (2017), pp. 22–36.

[Com19] Ford Motor Company. *Ford T Series Manual*. Ford Motor Company, Detroit, Michigan, USA, 1919, pp. 9–11. URL: https://manualzz.com/doc/59037179/ford-t-series-manual.

[CRI13] European Commission, Directorate-General for Research, and Innovation. *Factories of the future : multi-annual roadmap for the contractual PPP under Horizon 2020*. Publications Office, 2013. DOI: doi/10.2777/29815.

[CST18] Alessandra Caggiano, Tiziana Segreto, and Roberto Teti. "Cloud Manufacturing On-demand Services for Holistic Quality Assurance of Manufactured Components". In: *Procedia CIRP* 67 (2018). 11th CIRP Conference on Intelligent Computation in Manufacturing Engineering, 19-21 July 2017, Gulf of Naples, Italy, pp. 144–149. ISSN: 2212-8271. DOI: https://doi.org/10.1016/j.procir.2017.12.191. URL: https://www.sciencedirect.com/science/article/pii/S2212827117311356.

[DBP18] Simone Delvecchio, Paolo Bonfiglio, and Francesco Pompoli. "Vibro-acoustic condition monitoring of Internal Combustion Engines: A critical review of existing techniques". In: *Mechanical Systems and Signal Processing* 99 (2018), pp. 661–683.

[DE96] Thomas J. DiCiccio and Bradley Efron. "Bootstrap confidence intervals". In: *Statistical Science* 11.3 (1996), pp. 189–228. DOI: 10.1214/ss/1032280214. URL: https://doi.org/10.1214/ss/1032280214.

[Dim02] D. E. Dimla Snr. "The Correlation of Vibration Signal Features to Cutting Tool Wear in a Metal Turning Operation". In: *The International Journal of Advanced Manufacturing Technology* 19.10 (June 2002), pp. 705–713. ISSN: 1433-3015. DOI: 10.1007/s001700200080. URL: https://doi.org/10.1007/s001700200080.

[Don+06] Jianfei Dong et al. "Bayesian-inference-based neural networks for tool wear estimation". In: *The International Journal of Advanced Manufacturing Technology* 30.9 (2006), pp. 797–807.

[DPS16] Samik Dutta, Surjya Pal, and Ranjan Sen. "Progressive tool condition monitoring of end milling from machined surface images". In: *Proceedings of the Institution of Mechanical Engineers, Part B: Journal of Engineering Manufacture* 232 (Apr. 2016). DOI: 10.1177/0954405416640417.

[Dut+13a] S Dutta et al. "Correlation study of tool flank wear with machined surface texture in end milling". In: *Measurement* 46.10 (2013), pp. 4249–4260.

[Dut+13b] S. Dutta et al. "Correlation study of tool flank wear with machined surface texture in end milling". In: *Measurement* 46.10 (2013), pp. 4249–4260. ISSN: 0263-2241. DOI: https://doi.org/10.1016/j.measurement.2013.07.015. URL: https://www.sciencedirect.com/science/article/pii/S026322411300314X.

[EI15] Research European Commission and Innovation. *Advanced monitoring technology to track tool wear*. Last viewed Oct 2021. EU Publications Office, 2015. URL: https://cordis.europa.eu/article/id/170358-advanced-monitoring-technology-to-track-tool-wear.

[EI20] Research European Commission and Innovation. *Call for Factories of the Future*. Last viewed Oct 2021. 2020. URL: https://ec.europa.eu/programmes/horizon2020/en/news/call-factories-future.

[EKT03] Yalcin M Ertekin, Yongjin Kwon, and Tzu-Liang Bill Tseng. "Identification of common sensory features for the control of CNC milling operations under varying cutting conditions". In: *International Journal of Machine Tools and Manufacture* 43.9 (2003), pp. 897–904.

[FDK84] H. J. Fu, R. E. DeVor, and S. G. Kapoor. "A Mechanistic Model for the Prediction of the Force System in Face Milling Operations". In: *Journal of Engineering for Industry* 106.1 (Feb. 1984), pp. 81–88. ISSN: 0022-0817. DOI: 10.1115/1.3185915. eprint: https://asmedigitalcollection.asme.org/manufacturingscience/article-pdf/106/1/81/6505529/81_1.pdf. URL: https://doi.org/10.1115/1.3185915.

[Fen+21] Ke Feng et al. "Use of cyclostationary properties of vibration signals to identify gear wear mechanisms and track wear evolution". In: *Mechanical Systems and Signal Processing* 150 (2021), p. 107258.

[Fon+21] Ka Mun Fong et al. "Investigation on universal tool wear measurement technique using image-based cross-correlation analysis". In: *Measurement* 169 (2021), p. 108489.

[For11] W.E. Forsthoffer. "11 - Preventive and Predictive Maintenance Best Practices". In: *Forsthoffer's Best Practice Handbook for Rotating Machinery*. Ed. by W.E. Forsthoffer. Boston: Butterworth-Heinemann, 2011, pp. 563–576. ISBN: 978-0-08-096676-2. DOI: https://doi.org/10.

1016/B978-0-08-096676-2.10011-6. URL: http://www.sciencedirect.com/science/article/pii/B9780080966762100116.

[Gar+13] E Garcia-Plaza et al. "Surface finish monitoring in taper turning CNC using artificial neural network and multiple regression methods". In: *Procedia Engineering* 63 (2013), pp. 599–607.

[Gar86] William A Gardner. "Introduction to random processes with applications to signals and systems((Book))". In: *New York, MacMillan Co., 1986, 447* (1986).

[Gha+11] JA Ghani et al. "Monitoring online cutting tool wear using low-cost technique and user-friendly GUI". In: *Wear* 271.9-10 (2011), pp. 2619–2624.

[Gho+07] N Ghosh et al. "Estimation of tool wear during CNC milling using neural network-based sensor fusion". In: *Mechanical Systems and Signal Processing* 21.1 (2007), pp. 466–479.

[GNP06] William A Gardner, Antonio Napolitano, and Luigi Paura. "Cyclostationarity: Half a century of research". In: *Signal processing* 86.4 (2006), pp. 639–697.

[Gro10] M.P. Groover. *Fundamentals of Modern Manufacturing: Materials, Processes, and Systems*. John Wiley & Sons, 2010. ISBN: 9780470467008. URL: https://books.google.fr/books?id=QU-Qvud3OvoC.

[GRR10] François Girardin, Didier Rémond, and Jean-François Rigal. "Tool wear detection in milling—An original approach with a non-dedicated sensor". In: *Mechanical Systems and Signal Processing* 24.6 (2010), pp. 1907–1920.

[HA03] Rodolfo E Haber and A Alique. "Intelligent process supervision for predicting tool wear in machining processes". In: *Mechatronics* 13.8-9 (2003), pp. 825–849.

[Han01] Robin Hanson. "Long-term growth as a sequence of exponential modes". In: *ICES Brown Bag Lectures* (Jan. 2001).

[HLC12] Wan-Hao Hsieh, Ming-Chyuan Lu, and Shean-Juinn Chiou. "Application of backpropagation neural network for spindle vibration-based tool wear monitoring in micro-milling". In: *The International Journal of Advanced Manufacturing Technology* 61.1 (2012), pp. 53–61.

[HMK15] PoTsang B Huang, Cheng-Chieh Ma, and Chia-Hao Kuo. "A PNN self-learning tool breakage detection system in end milling operations". In: *Applied Soft Computing* 37 (2015), pp. 114–124.

[Hon+16] Young-Sun Hong et al. "Tool-wear monitoring during micro-end milling using wavelet packet transform and Fisher's linear discriminant". In: *International Journal of Precision Engineering and Manufacturing* 17.7 (2016), pp. 845–855.

[HWG17] Ramin M Hasani, Guodong Wang, and Radu Grosu. "An automated auto-encoder correlation-based health-monitoring and prognostic method for machine bearings". In: *arXiv preprint arXiv:1703.06272* (2017).

[Int85] U.S. Department of Commerce International Trade Administration. *A Competitive assessment of the U.S. flexible manufacturing systems industry*. Office of Capital Goods and International Construction Sector Group, Washington, D.C., USA, 1985. URL: https://www.worldcat.org/title/competitive-assessment-of-the-us-flexible-manufacturing-systems-industry/oclc/1225666834.

[Jem00] Krzysztof Jemielniak. "Some aspects of AE application in tool condition monitoring". In: *Ultrasonics* 38.1-8 (2000), pp. 604–608.

[JM+60] Pierre Jolicoeur, James E Mosimann, et al. "Size and shape variation in the painted turtle. A principal component analysis". In: *Growth* 24.4 (1960), pp. 339–354.

[Kar07] Sedat Karabay. "Design criteria for electro-mechanical transducers and arrangement for measurement of strains due to metal cutting forces acting on dynamometers". In: *Materials & Design* 28.2 (Jan. 2007), pp. 496–506. ISSN: 0261-3069. DOI: 10.1016/J.MATDES.2005.08.014. URL: https://www.sciencedirect.com/science/article/pii/S026130690500244X.

[KDK19] Pradeep Kundu, Ashish K Darpe, and Makarand S Kulkarni. "A correlation coefficient based vibration indicator for detecting natural pitting progression in spur gears". In: *Mechanical Systems and Signal Processing* 129 (2019), pp. 741–763.

[KDL82] W.A. Kline, R.E. DeVor, and J.R. Lindberg. "The prediction of cutting forces in end milling with application to cornering cuts". In: *International Journal of Machine Tool Design and Research* 22.1 (1982), pp. 7–22. ISSN: 0020-7357.

[Kisa] Kistler. *3-axes Dynamometer - Type 9257A*. Operating and service instructions.

[Kisb] Kistler. *Brochure: Cutting Force Measurements*. Last viewed March 2022. Documents marketing. URL: https://www.kistler.com/files/download/960-002e.pdf.

[Kisc] Kistler. *Charge Meter - Type 5015*. Last viewed Oct 2021. Operating and service instructions. URL: https://www.kistler.com/fr/produit/type-5015a/.

[KK97] Jeong-Du Kim and Dong-Sik Kim. "Development of a combined-type tool dynamometer with a piezo-film accelerometer for an ultra-precision lathe". In: *Journal of materials processing technology* 71.3 (1997), pp. 360–366.

[Kos+21] Philip Kosky et al. "Chapter 12 - Manufacturing Engineering". In: *Exploring Engineering*. Ed. by Philip Kosky et al. Fifth. Academic Press, 2021, pp. 259–291. ISBN: 978-0-12-815073-3. DOI: https://doi.org/10.1016/B978-0-12-815073-3.00012-0. URL: https://www.sciencedirect.com/science/article/pii/B9780128150733000120.

[KS17] Thomas Kärcher and Gernot Schullerus. "Correlation-based condition monitoring of a roller chain". In: *Proceeding - World Congress on Condition Monitoring (WCCM)* (2017).

[KST08] E Kuljanic, Marco Sortino, and G Totis. "Multisensor approaches for chatter detection in milling". In: *Journal of Sound and Vibration* 312.4-5 (2008), pp. 672–693.

[Kwa06] Jae-Seob Kwak. "Application of wavelet transform technique to detect tool failure in turning operations". In: *The International Journal of Advanced Manufacturing Technology* 28.11 (2006), pp. 1078–1083.

[KZ13] Y.H. Kang and C.M. Zheng. "Mathematical modelling of chip thickness in micro-end- milling: A Fourier modelling". In: *Applied Mathematical Modelling* 37.6 (2013), pp. 4208–4223. ISSN: 0307-904X. DOI: https://doi.org/10.1016/j.apm.2012.09.011. URL: https://www.sciencedirect.com/science/article/pii/S0307904X12005082.

[Lam+14] M. Lamraoui et al. "Indicators for monitoring chatter in milling based on instantaneous angular speeds". In: *Mechanical Systems and Signal Processing* 44.1-2 (2014), pp. 72–85. ISSN: 08883270. DOI: 10.1016/j.ymssp.2013.05.002. URL: http://dx.doi.org/10.1016/j.ymssp.2013.05.002.

[Lau+13] C. Lauro et al. "Monitoring the temperature of the milling process using infrared camera". In: *Scientific Research and Essays* 7 (2013), pp. 1112–1120.

[Lau+14] CH Lauro et al. "Monitoring and processing signal applied in machining processes–A review". In: *Measurement* 58 (2014), pp. 73–86.

[Lee99] B. Lee. "Application of the Discrete Wavelet Transform to the Monitoring of Tool Failure in End Milling Using the Spindle Motor Current". In: *The International Journal of Advanced Manufacturing Technology* 15 (1999), pp. 238–243.

[LHL04] Steven Y Liang, Rogelio L Hecker, and Robert G Landers. "Machining process monitoring and control: the state-of-the-art". In: *J. Manuf. Sci. Eng.* 126.2 (2004), pp. 297–310.

[Li+05] Yuhua Li et al. "The measurement of instantaneous angular speed". In: *Mechanical Systems and Signal Processing* 19 (July 2005), pp. 786–805. DOI: 10.1016/j.ymssp.2004.04.003.

[Li02] Xiaoli Li. "A brief review: acoustic emission method for tool wear monitoring during turning". In: *International Journal of Machine Tools and Manufacture* 42.2 (2002), pp. 157–165.

[LK02] Ming-Chyuan Lu and Elijah Kannatey-Asibu Jr. "Analysis of sound signal generation due to flank wear in turning". In: *J. Manuf. Sci. Eng.* 124.4 (2002), pp. 799–808.

[LLM16] David C Lay, Steven R Lay, and Judi J McDonald. *Linear algebra and its applications*. Pearson, 2016.

[LTB14] M. Lamraoui, M. Thomas, and M. El Badaoui. "Cyclostationarity approach for monitoring chatter and tool wear in high speed milling". In: *Mechanical Systems and Signal Processing* 44.1 (2014). Special Issue on Instantaneous Angular Speed (IAS) Processing and Angular Applications, pp. 177–198. ISSN: 0888-3270. DOI: https://doi.org/10.1016/j.ymssp.2013.05.001. URL: http://www.sciencedirect.com/science/article/pii/S0888327013001994.

[Lu08] Chen Lu. "Study on prediction of surface quality in machining process". In: *Journal of materials processing technology* 205.1-3 (2008), pp. 439–450.

[MA08] Iulian Marinescu and Dragos A Axinte. "A critical analysis of effectiveness of acoustic emission signals to detect tool and workpiece malfunctions in milling operations". In: *International Journal of Machine Tools and Manufacture* 48.10 (2008), pp. 1148–1160.

[MAR41] ME. MARTELLOTTI. "An analysis of the milling process". In: *Trans ASME* 63 (1941), p. 677. URL: https://ci.nii.ac.jp/naid/10020378228/en/.

[MAR45] ME. MARTELLOTTI. "An analysis of the milling process. Part II : down milling". In: *Trans ASME* 67 (1945), p. 233. URL: https://ci.nii.ac.jp/naid/10020378229/en/.

[MAT22] MATLAB. *Evaluate the performance of machine learning classification models*. Last viewed April 2022. 2022. URL: https://www.mathworks.com/discovery/roc-curve.html.

[McL16] Thomas E McLeay. "Unsupervised monitoring of machining processes". PhD thesis. University of Sheffield, 2016.

[Mer45] M. Eugene Merchant. "Mechanics of the Metal Cutting Process. II. Plasticity Conditions in Orthogonal Cutting". In: *Journal of Applied Physics* 16 (1945), pp. 318–324.

[Mita] Mitsubishi. *High-Speed Machining with ESPRIT's patented ProfitMilling®*. Last viewed Dec 2021. URL: https://www.espritcam.com/fr-fr/product/high-speed-machining.

[Mitb] Mitsubishi. *Miracle VP15TF coated grade for milling machining*. Last viewed Oct 2021. Technical catalog. URL: http://www.mitsubishicarbide.com/application/files/7214/4643/8968/b034g.pdf.

[Mitc] Mitsubishi. *Multifunctional end mill APX3000R325M16A*. Last viewed Oct 2021. Technical catalog. URL: http://www.mitsubishicarbide.net/mhg/fr/end_mills/10000403/20067643.

[MIT04] The Institute Archives of MIT Libraries. *The History of the MIT Servomechanisms Laboratory*. Last viewed September 2021. MASSACHUSETTS INSTITUTE OF TECHNOLOGY, Boston, US, Sept. 2004. URL: https://libraries.mit.edu/mithistory/research/labs/mit-servomechanisms-laboratory/.

[MKV76] G. F. Micheletti, W. Koenig, and H. R. Victor. "In Process Tool Wear Sensors for Cutting Operations". In: *Annals of CIRP* 25-2 (1976), pp. 483–496.

[Moh+19] Thangamuthu Mohanraj et al. "Tool condition monitoring in the milling process with vegetable based cutting fluids using vibration signatures". In: *Materials Testing* 61.3 (2019), pp. 282–288.

[Moh+20] T Mohanraj et al. "Tool condition monitoring techniques in milling process—a review". In: *Journal of Materials Research and Technology* 9.1 (2020), pp. 1032–1042.

[Niu+21] Peng Niu et al. "Sensitivity analysis of machining accuracy reliability considering partial correlation of geometric errors for Horizontal Machining Center". In: *Proceedings of the Institution of Mechanical Engineers, Part B: Journal of Engineering Manufacture* 235.3 (2021), pp. 455–465. DOI: 10.1177/0954405420958843. URL: https://doi.org/10.1177/0954405420958843.

[NL19] Jinqiang Ning and Steven Y. Liang. "Predictive Modeling of Machining Temperatures with Force–Temperature Correlation Using Cutting Mechanics and Constitutive Relation". In: *Materials* 12.2 (2019). ISSN:

1996-1944. DOI: 10.3390/ma12020284. URL: https://www.mdpi.com/1996-1944/12/2/284.

[Nou+15] Mehdi Nouri et al. "Real-time tool wear monitoring in milling using a cutting condition independent method". In: *International Journal of Machine Tools and Manufacture* 89 (2015), pp. 1–13.

[OC01] D. O'Sullivan and M. Cotterell. "Temperature measurement in single point turning". In: *Journal of Materials Processing Technology* 118.1 (2001). PART 1: CONTAINING PAPERS PRESENTED AT INTERNATIONAL CONFERENCE ON ADVANCES IN MATERIALS PROCESSING TECHNOLOGY, pp. 301–308. ISSN: 0924-0136. DOI: https://doi.org/10.1016/S0924-0136(01)00853-6. URL: http://www.sciencedirect.com/science/article/pii/S0924013601008536.

[PA04] Simon S Park and Yusuf Altintas. "Dynamic compensation of spindle integrated force sensors with kalman filter". In: *J. Dyn. Sys., Meas., Control* 126.3 (2004), pp. 443–452.

[PB17] Balla Srinivasa Prasad and M Prakash Babu. "Correlation between vibration amplitude and tool wear in turning: Numerical and experimental analysis". In: *Engineering Science and Technology, an International Journal* 20.1 (2017), pp. 197–211.

[PNR13] M. Prabhuswamy, P. Nagesh, and K. Ravikumar. "Statistical Analysis and Reliability Estimation of Total Productive Maintenance". In: *The IUP Journal of Operations Management* 12 (Apr. 2013), pp. 7–22. URL: https://papers.ssrn.com/sol3/papers.cfm?abstract_id=2246601.

[PŽB19] Peter Poor, David Ženíšek, and Josef Basl. "Historical Overview of Maintenance Management Strategies: Development from Breakdown Maintenance to Predictive Maintenance in Accordance with Four Industrial Revolutions". In: *Proceedings of the International Conference on Industrial Engineering and Operations Management, Pilsen, Czech Republic, July 23-26, 2019* (Aug. 2019).

[Rei91] J. Francis Reintjes. "Numerical control: making a new technology". In: *Technology and Culture* 33 (1991), p. 841.

[Ren+10] Laurence Renaudin et al. “Natural roller bearing fault detection by angular measurement of true instantaneous angular speed”. In: *Mechanical Systems and Signal Processing* 24.7 (2010), pp. 1998–2011.

[Ren+14] Qun Ren et al. “Type-2 fuzzy tool condition monitoring system based on acoustic emission in micromilling”. In: *Information Sciences* 255 (Jan. 2014), pp. 121–134. DOI: 10.1016/j.ins.2013.06.010.

[Rit+14] Mathieu Ritou et al. “Angular approach combined to mechanical model for tool breakage detection by eddy current sensors”. In: *Mechanical Systems and Signal Processing* 44.1-2 (Feb. 2014), pp. 211–220. DOI: 10.1016/j.ymssp.2013.02.004. URL: https://hal.archives-ouvertes.fr/hal-00862232.

[RJO05] Adam G Rehorn, Jin Jiang, and Peter E Orban. “State-of-the-art methods and results in tool condition monitoring: a review”. In: *The International Journal of Advanced Manufacturing Technology* 26.7 (2005), pp. 693–710.

[RM05] Didier Remond and Jarir Mahfoud. “From Transmission Error Measurements to Angular Sampling in Rotating Machines with Discrete Geometry”. In: *Shock and Vibration* 12 (Jan. 2005), pp. 149–161. DOI: 10.1155/2005/205291.

[RMK98] Oleg Ryabov, Kazuo Mori, and Nagayoshi Kasashima. “Laser displacement meter application for milling diagnostics”. In: *Optics and Lasers in Engineering* 30.3 (1998), pp. 251–263. ISSN: 0143-8166. DOI: https://doi.org/10.1016/S0143-8166(98)00032-3. URL: https://www.sciencedirect.com/science/article/pii/S0143816698000323.

[RN88] J. Lee Rodgers and W. Alan Nicewander. “Thirteen Ways to Look at the Correlation Coefficient”. In: *The American Statistician* 42(1) (1988), pp. 59–66. DOI: 10.2307/2685263.

[Roe16] J.W. Roe. *English and American Tool Builders*. Yale University Press, 1916. URL: https://books.google.fr/books?id=X-EJAAAAIAAJ.

[RSJ06] Adam G. Rehorn, Ervin Sejdić, and Jin Jiang. “Fault diagnosis in machine tools using selective regional correlation”. In: *Mechanical Systems and Signal Processing* 20.5 (2006), pp. 1221–1238. ISSN: 0888-3270. DOI: https://doi.org/10.1016/j.ymssp.2005.01.010.

URL: https://www.sciencedirect.com/science/article/pii/S0888327005000154.

[RST08] Eva Rubio, T. Segreto, and R. Teti. "A Review of Tool Condition Monitoring Literature Data Base 1996 - 2006". In: (May 2008).

[Sam+11] A Samraj et al. "Dynamic clustering estimation of tool flank wear in turning process using SVD models of the emitted sound signals". In: *International Journal of Industrial and Manufacturing Engineering* 5.8 (2011), pp. 1644–1648.

[Sen+12] Johanna Senatore et al. "Correlation between machining direction, cutter geometry and step-over distance in 3-axis milling: Application to milling by zones". In: *Computer-Aided Design* 44.12 (2012), pp. 1151–1160. ISSN: 0010-4485. DOI: https://doi.org/10.1016/j.cad.2012.06.008. URL: https://www.sciencedirect.com/science/article/pii/S0010448512001376.

[Ser+05] Erchin Serpedin et al. "Bibliography on cyclostationarity". In: *Signal processing* 85.12 (2005), pp. 2233–2303.

[Sev+11] P.Y. Sevilla-Camacho et al. "Tool breakage detection in CNC high-speed milling based in feed-motor current signals". In: *The International Journal of Advanced Manufacturing Technology* 53 (Apr. 2011), pp. 1141–1148. DOI: 10.1007/s00170-010-2907-9.

[Sev+15] PY Sevilla-Camacho et al. "Tool failure detection method for high-speed milling using vibration signal and reconfigurable bandpass digital filtering". In: *The International Journal of Advanced Manufacturing Technology* 81.5 (2015), pp. 1187–1194.

[SH05] CJ Stander and PS Heyns. "Instantaneous angular speed monitoring of gearboxes under non-cyclic stationary load conditions". In: *Mechanical systems and signal processing* 19.4 (2005), pp. 817–835.

[SH06] CJ Stander and PS Heyns. "Transmission path phase compensation for gear monitoring under fluctuating load conditions". In: *Mechanical systems and signal processing* 20.7 (2006), pp. 1511–1522.

[Shi88] M Shiraishi. "Scope of in-process measurement, monitoring and control techniques in machining processes—Part 1: In-process techniques for tools". In: *Precision engineering* 10.4 (1988), pp. 179–189.

[SJ07] Ervin Sejdic and Jin Jiang. "Selective Regional Correlation for Pattern Recognition". In: *IEEE Transactions on Systems, Man, and Cybernetics - Part A: Systems and Humans* 37.1 (Jan. 2007), pp. 82–93. ISSN: 1558-2426. DOI: 10.1109/TSMCA.2006.886333.

[SMP19] S Shankar, T Mohanraj, and A Pramanik. "Tool condition monitoring while using vegetable based cutting fluids during milling of inconel 625". In: *Journal of Advanced Manufacturing Systems* 18.04 (2019), pp. 563–581.

[SMR19] Subramaniam Shankar, T Mohanraj, and R Rajasekar. "Prediction of cutting tool wear during milling process using artificial intelligence techniques". In: *International Journal of Computer Integrated Manufacturing* 32.2 (2019), pp. 174–182.

[SÖ16] Aydin Salimiasl and Ahmet Özdemir. "Analyzing the performance of artificial neural network (ANN)-, fuzzy logic (FL)-, and least square (LS)-based models for online tool condition monitoring". In: *The International Journal of Advanced Manufacturing Technology* 87.1 (2016), pp. 1145–1158.

[SS12] P.S. Sivasakthivel and R. Sudhakaran. "Optimization of machining parameters on temperature rise in end milling of Al 6063 using response surface methodology and genetic algorithm". In: *The International Journal of Advanced Manufacturing Technology* 67 (Aug. 2012). DOI: 10.1007/s00170-012-4652-8.

[Sta+16] P Stavropoulos et al. "Tool wear predictability estimation in milling based on multi-sensorial data". In: *The International Journal of Advanced Manufacturing Technology* 82.1 (2016), pp. 509–521.

[Str93] Gilbert Strang. "The fundamental theorem of linear algebra". In: *The American Mathematical Monthly* 100.9 (1993), pp. 848–855.

[Tan+00] IN Tansel et al. "Tool wear estimation in micro-machining.: Part I: tool usage–cutting force relationship". In: *International Journal of Machine Tools and Manufacture* 40.4 (2000), pp. 599–608.

[Tan+93] Ibrahim Nur Tansel et al. "Monitoring drill conditions with wavelet based encoding and neural networks". In: *International Journal of Machine Tools and Manufacture* 33.4 (1993), pp. 559–575.

[Tet+10] R. Teti et al. "Advanced monitoring of machining operations". In: *CIRP Annals* 59.2 (2010), pp. 717–739. ISSN: 0007-8506. DOI: https://doi.org/10.1016/j.cirp.2010.05.010. URL: https://www.sciencedirect.com/science/article/pii/S0007850610001976.

[TG08] Kourosh Tatar and Per Gren. "Measurement of milling tool vibrations during cutting using laser vibrometry". In: *International Journal of Machine Tools and Manufacture* 48.3 (2008), pp. 380–387. ISSN: 0890-6955. DOI: https://doi.org/10.1016/j.ijmachtools.2007.09.009. URL: https://www.sciencedirect.com/science/article/pii/S0890695507001988.

[Tol09] Tullio Tolio. *Design of Flexible Production Systems: Methodologies and Tools*. Springer-Verlag Berlin Heidelberg, Jan. 2009. ISBN: 978-3-540-85413-5. DOI: 10.1007/978-3-540-85414-2.

[Too05] Kistner Machine Tools. *Manuals for DECKEL MAHO DMC 635 Vertical machining center*. Last viewed Oct 2021. 2005. URL: https://www.maschinen-kistner.de/files/Produkte/Bearbeitungszentren/DECKEL_MAHO_DMC_635_V/PDF_Englisch/DECKEL_MAHO_DMC_635_V_EN.pdf.

[TTV09] Walter Terkaj, Tullio Tolio, and Anna Valente. "A Review on Manufacturing Flexibility". In: *Design of Flexible Production Systems: Methodologies and Tools*. Ed. by Tullio Tolio. Berlin, Heidelberg: Springer Berlin Heidelberg, 2009, pp. 41–61. ISBN: 978-3-540-85414-2. DOI: 10.1007/978-3-540-85414-2_3. URL: https://doi.org/10.1007/978-3-540-85414-2_3.

[UC14] Graham Upton and Ian Cook. *A dictionary of statistics 3e*. Oxford university press, 2014.

[UKE18] UKEssays. *The History of CNC Machines*. Last viewed September 2021. Nottingham, UK, Nov. 2018. URL: https://www.ukessays.com/essays/information-technology/examining-the-history-of-cnc-machines-information-technology-essay.php?vref=1.

[Ver+09] A Verl et al. "Sensorless automated condition monitoring for the control of the predictive maintenance of machine tools". In: *CIRP annals* 58.1 (2009), pp. 375–378.

[Wan+05] PC Wanigarathne et al. “Progressive tool-wear in machining with coated grooved tools and its correlation with cutting temperature”. In: *Wear* 259.7-12 (2005), pp. 1215–1224.

[Wan+14] GF Wang et al. “Vibration sensor based tool condition monitoring using ν support vector machine and locality preserving projection”. In: *Sensors and Actuators A: Physical* 209 (2014), pp. 24–32.

[Wan+19] Tianyang Wang et al. “Vibration based condition monitoring and fault diagnosis of wind turbine planetary gearbox: A review”. In: *Mechanical Systems and Signal Processing* 126 (2019), pp. 662–685.

[WEC+80] M. WECK et al. “Concept of integrated data processing in computer controlled manufacturing systems (FMS)”. In: *International Journal of Production Research* 18.3 (1980), pp. 295–306. DOI: 10.1080/00207548008919669. URL: https://doi.org/10.1080/00207548008919669.

[WGY13] Guofeng Wang, Zhiwei Guo, and Yinwei Yang. “Force sensor based online tool wear monitoring using distributed Gaussian ARTMAP network”. In: *Sensors and Actuators A: Physical* 192 (2013), pp. 111–118.

[WRR03] Michael E. Wall, Andreas Rechtsteiner, and Luis M. Rocha. “Singular Value Decomposition and Principal Component Analysis”. In: *A Practical Approach to Microarray Data Analysis*. Ed. by Daniel P. Berrar, Werner Dubitzky, and Martin Granzow. Boston, MA: Springer US, 2003, pp. 91–109. ISBN: 978-0-306-47815-4. DOI: 10.1007/0-306-47815-3_5. URL: https://doi.org/10.1007/0-306-47815-3_5.

[Yuq+15] Zhou Yuqing et al. “An online damage identification approach for numerical control machine tools based on data fusion using vibration signals”. In: *Journal of Vibration and Control* 21 (2015), pp. 2925–2936.

[Zha+13] Xiaomin Zhao et al. “Diagnosis of artificially created surface damage levels of planet gear teeth using ordinal ranking”. In: *Measurement* 46.1 (2013), pp. 132–144.

[Zho+09] Jun-Hong Zhou et al. “Intelligent diagnosis and prognosis of tool wear using dominant feature identification”. In: *IEEE transactions on Industrial Informatics* 5.4 (2009), pp. 454–464.

[Zho+22] Yuqing Zhou et al. "A new tool wear condition monitoring method based on deep learning under small samples". In: *Measurement* 189 (2022), p. 110622.

[Zhu+21] Qinsong Zhu et al. "Sample augmentation for intelligent milling tool wear condition monitoring using numerical simulation and generative adversarial network". In: *IEEE Transactions on Instrumentation and Measurement* 70 (2021), pp. 1–10.

[ZSH09] Kunpeng Zhu, Yoke San Wong, and Geok Soon Hong. "Wavelet analysis of sensor signals for tool condition monitoring: A review and some new results". In: *International Journal of Machine Tools and Manufacture* 49.7-8 (2009), pp. 537–553.

[ZV14] Kunpeng Zhu and Birgit Vogel-Heuser. "Sparse representation and its applications in micro-milling condition monitoring: noise separation and tool condition monitoring". In: *The International Journal of Advanced Manufacturing Technology* 70.1 (2014), pp. 185–199.

[ZX18] Yuqing Zhou and Wei Xue. "Review of tool condition monitoring methods in milling processes". In: *The International Journal of Advanced Manufacturing Technology* 96.5 (2018), pp. 2509–2523.

[ZYN15] Kai-feng Zhang, Hui-qun Yuan, and Peng Nie. "A method for tool condition monitoring based on sensor fusion". In: *Journal of Intelligent Manufacturing* 26.5 (2015), pp. 1011–1026.

[ZZW13] ZW Zhong, J-H Zhou, and Ye Nyi Win. "Correlation analysis of cutting force and acoustic emission signals for tool condition monitoring". In: *2013 9th Asian Control Conference (ASCC)*. IEEE. 2013, pp. 1–6.

FOLIO ADMINISTRATIF

THESE DE L'INSA LYON, MEMBRE DE L'UNIVERSITE DE LYON

NOM : ZHU

DATE de SOUTENANCE : 19/09/2022

Prénoms : Xiaowen

TITRE : A reference-free mill monitoring method based on the inter-insert periodic correlation in angular domain

NATURE : Doctorat

Numéro d'ordre : 2022ISAL0078

Ecole doctorale : ED 162 MEGA

Spécialité : Génie Mécanique

RESUME : Based on the tendency of Industry 4.0, this thesis targets the tool condition monitoring (TCM), which is the terminal process of flexible production. The aim is to detect abnormal tool behavior as early as possible to improve the surface quality of workpieces and to prevent subsequent losses from serious tool failures.

In this context, a methodology for monitoring the wear of end mills in real-time production based on the inter-insert correlation is presented. The approach takes advantage of the angular domain characteristics to segment the signal into periodic cycles of the same angular duration, which are then amenable to correlation analysis. Under high rotational speeds, the external working environment experienced by the individual teeth can be considered quasi-equivalent. Through the correlation analysis, the impact of the non-stationary operation on the monitored signal is effectively reduced. From a wide range of correlation algorithms, singular value decomposition (SVD) is selected to proceed with the analysis, and an ordered separability index with latent correlation characteristics is extracted to assess the current condition of the tool. The feasibility of the proposed indicator was valid and evaluated via the simulated signal and a series of experimental data collected by designed milling patterns.

The results demonstrate the promising development of this method in forming an efficient TCM system. The proposed approach is more independent of the cutting conditions (changes in speed or direction) than the traditional teach-in method and does not require a trial run. It partially fills the gap of tool monitoring demand in flexible manufacturing for customized small batch production. At the same time, inter-insert correlation is also seen as part of a broader framework for monitoring and maintaining rotating machinery. It has great potential to be applied to the analysis of different signals generated by other mechanical components with a rotating nature.

MOTS-CLÉS : Tool condition monitoring (TCM), milling, wear, correlation, SVD.

Laboratoire (s) de recherche : Laboratoire Vibrations Acoustique
EA677 – INSA de Lyon
20 Avenue Albert Einstein
69621 Villeurbanne Cedex FRANCE

Directeur de thèse: Professeur ANTONI Jérôme

Président de jury : M. FROMENTIN Guillaume

Composition du jury : M. RITOU Mathieu
MME CHANAL Hélène
MME KAFTANDJIAN-DOUDET Valérie
M. GIRARDIN François
M. SERRA Roger
M. GUILLET François
M. ANTONI Jérôme